AD-A092 712 ARMY ENGINEER WATERWAYS EXPERIMENT STATION VICKSBURG--ETC F/G 8/3
EROSION CONTROL OF SCOUR DURING CONSTRUCTION: REPORT 3. EXPERIM--ETC(U)
SEP 80 L Z HALES

UNCLASSIFIED WES/TR/HL-80-3-3 NL

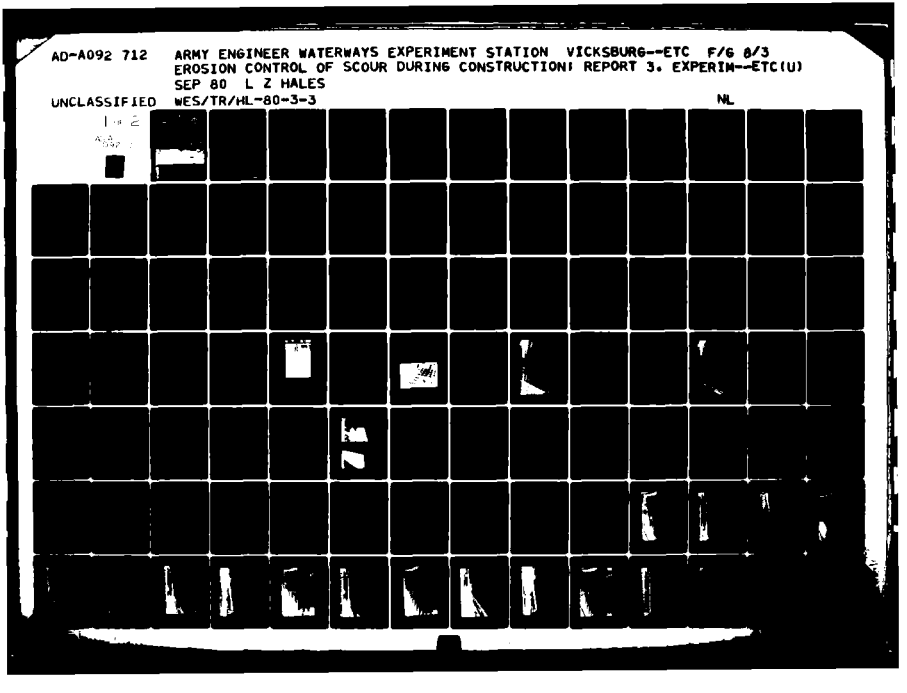

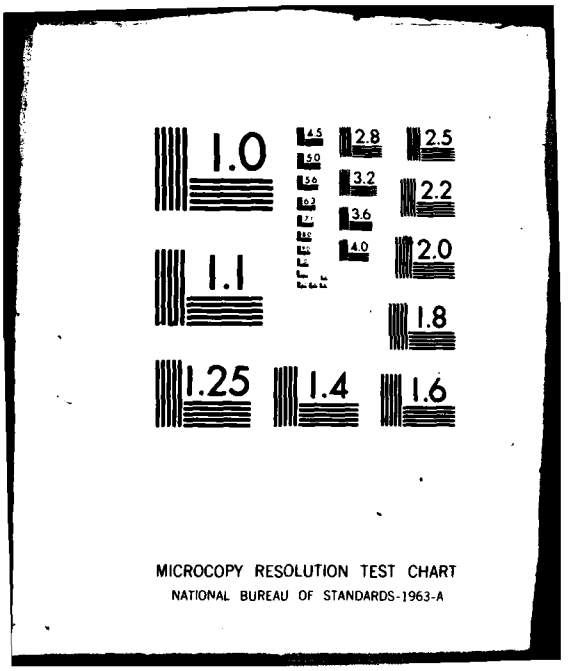
1.0
1.1
1.25
1.4
1.6
1.8
2.0
2.2
2.5
2.8
3.2
3.6
4.0
4.5
5.0
5.6
6.3
7.1
8.0
9.0
MICROCOPY RESOLUTION TEST CHART
NATIONAL BUREAU OF STANDARDS-1963-A

TECHNICAL REPORT HL-80-3

EROSION CONTROL OF SCOUR DURING CONSTRUCTION

Report 3

EXPERIMENTAL MEASUREMENTS OF REFRACTION DIFFRACTION, AND CURRENT PATTERNS NEAR JETTIES

by

Lyndell Z. Hales

Hydraulics Laboratory
U. S. Army Engineer Waterways Experiment Station
P. O. Box 631, Vicksburg, Miss. 39180

September 1980
Report 3 of a Series

Prepared for Office, Chief of Engineers, U. S. Army
Washington, D. C. 20314

Destroy this report when no longer needed. Do not return it to the originator.

The findings in this report are not to be construed as an official Department of the Army position unless so designated by other authorized documents.

The contents of this report are not to be used for advertising, publication, or promotional purposes. Citation of trade names does not constitute an official endorsement or approval of the use of such commercial products.

(14) WES/TR/HL-80-3-3

Unclassified

SECURITY CLASSIFICATION OF THIS PAGE (When Data Entered)

(9) **REPORT DOCUMENTATION PAGE**

READ INSTRUCTIONS BEFORE COMPLETING FORM

1. REPORT NUMBER: Technical Report HL-80-3 / AD-A092 712	3. RECIPIENT'S CATALOG NUMBER
(6) 4. TITLE (and Subtitle): EROSION CONTROL OF SCOUR DURING CONSTRUCTION; Report 3, EXPERIMENTAL MEASUREMENTS OF REFRACTION, DIFFRACTION, AND CURRENT PATTERNS NEAR JETTIES.	5. TYPE OF REPORT & PERIOD COVERED: Report 3 of a series
	6. PERFORMING ORG. REPORT NUMBER
(10) 7. AUTHOR(s): Lyndell Z. Hales	8. CONTRACT OR GRANT NUMBER(s)
9. PERFORMING ORGANIZATION NAME AND ADDRESS: U. S. Army Engineer Waterways Experiment Station, Hydraulics Laboratory, P. O. Box 631, Vicksburg, Miss. 39180	10. PROGRAM ELEMENT, PROJECT, TASK AREA & WORK UNIT NUMBERS (11)
11. CONTROLLING OFFICE NAME AND ADDRESS: Office, Chief of Engineers, U. S. Army, Washington, D. C. 20314	12. REPORT DATE: Sept[illegible]980
	13. NUMBER OF PAGES: 150
14. MONITORING AGENCY NAME & ADDRESS (if different from Controlling Office) (12) 54	15. SECURITY CLASS. (of this report): Unclassified
	15a. DECLASSIFICATION/DOWNGRADING SCHEDULE

16. DISTRIBUTION STATEMENT (of this Report)

Approved for public release; distribution unlimited.

17. DISTRIBUTION STATEMENT (of the abstract entered in Block 20, if different from Report)

18. SUPPLEMENTARY NOTES

19. KEY WORDS (Continue on reverse side if necessary and identify by block number)

Construction practices
Erosion control
Harbor structures
Scour

20. ABSTRACT (Continue on reverse side if necessary and identify by block number)

(4) Effective, comprehensive, and low cost procedures do not exist for eliminating scour during construction in the nearshore environment. Determination of potential alternative procedures is seriously hampered by the inability to predict the extent of potential scour. The objectives of this research program are to develop techniques to minimize and control scour during nearshore construction and to predict the probable magnitude of

(Continued)

DD FORM 1 JAN 73 1473 EDITION OF 1 NOV 65 IS OBSOLETE

Unclassified

SECURITY CLASSIFICATION OF THIS PAGE (When Data Entered)

411389 (1) 61

20. ABSTRACT (Continued)

scour that may result as a function of currents and wave climate. One phase of the research effort is the development of numerical techniques (incorporating both refraction and diffraction effects near the structure) for computing wave-induced velocities and tidal currents in the vicinity of structures and applying these results to determine sediment transport of the bottom material at the particular site.

The purpose of this study was to obtain detailed and precise experimental data regarding wave-height variations and currents (patterns and magnitudes) downwave from a shore-connected breakwater or jetty under the simultaneous effects of refraction and diffraction. This information provides insight into the phenomenon of combined wave refraction and diffraction and can be used to verify numerical models that simulate this phenomenon. The experimental investigation was conducted in a wave basin that was molded in cement mortar and consisted of an area 50 ft x 60 ft with a water depth of 1 ft in the open-ocean region. A vertical, impermeable breakwater (shore-connected) extending perpendicularly from the shoreline was installed on a beach slope of 1V on 20H.

In the neighborhood of the breakwater, currents existed that affected the wave heights. The magnitude of these wave-induced return currents is a function of incident wave characteristics. The effect of varying the incident wave height on the wave-height amplification factor, H/H_o, was investigated and it was determined that the greatest variation in H/H_o occurred in the deep shadow zone near the breakwater and shore region where the currents are the strongest. This nonlinear effect diminishes rapidly away from the structure, and at a distance of 5 ft (model dimensions) downwave appears to be relatively insignificant except for the extreme shadow region at acute angles of incidence. The establishment of a counterclockwise circulation cell approximately 4 ft wide adjacent to the downwave side of the breakwater results in a seaward flowing current all along the breakwater. The bottom current is especially intense approximately 40 percent of the breakwater length from the shoreline and decreases seaward along the structure. The physical model sidewall boundary was responsible for a clockwise circulation cell which developed as a result of mass transport downcoast by the nearshore current. Based on these experiments, any numerical techniques for describing scour and erosion near structures should account for wave-induced currents and circulation cells near the structure as well as tidal or other currents that may exist in the near region.

PREFACE

The study reported herein was authorized as a part of the Civil Works Research and Development Program by the Office, Chief of Engineers (OCE). This particular work unit, Erosion Control of Scour During Construction, is part of the Improvement of Operations and Maintenance Techniques (IOMT) Program. Mr. William Godwin was the OCE Technical Monitor for the IOMT Program during preparation and publication of this report.

This study was conducted during the period 1 March 1979 through 30 April 1980 by personnel of the Hydraulics Laboratory of the U. S. Army Engineer Waterways Experiment Station (WES) under the general supervision of Messrs. H. B. Simmons, Chief of the Hydraulics Laboratory; F. A. Herrmann, Jr., Assistant Chief of the Hydraulics Laboratory; R. A. Sager, Chief of the Estuaries Division and IOMT Program Coordinator; Dr. R. W. Whalin, Chief of the Wave Dynamics Division; Mr. D. D. Davidson, Chief of the Wave Research Branch; and Dr. J. R. Houston, Research Engineer and Principal Investigator for the Erosion Control of Scour During Construction work unit. Dr. L. Z. Hales, Research Hydraulic Engineer, Mr. K. A. Turner, Computer Specialist, Ms. M. L. Hampton, Computer Technician, Mr. R. E. Ankeny, Computer Technician, and Mr. K. M. Strausbaugh, Civil Engineering Technician, performed the study described herein. Dr. Hales prepared this report.

Commanders and Directors of WES during the conduct of this investigation and the preparation and publication of this report were COL John L. Cannon, CE, and COL Nelson P. Conover, CE. Technical Director was Mr. F. R. Brown.

CONTENTS

CONVERSION FACTORS, U. S. CUSTOMARY TO METRIC (SI) UNITS OF MEASUREMENT

U. S. customary units of measurement used in this report can be converted to metric (SI) units as follows:

Multiply	By	To Obtain
feet	0.3048	metres
feet per second	0.3048	metres per second
feet per second per second	0.3048	metres per second per second
foot-pounds per foot per foot	148.8164434	kilogram-centimetre per metre per metre
foot-pounds per second	13825.5	gram-centimetre per second
inches	25.4	millimetres
pounds per foot per foot	4.8824276	kilogram per metre per metre
pounds-second per foot per foot	4.8824276	kilogram-second per metre per metre
pounds-second-second per foot per foot per foot per foot	52.5540137	kilogram-second-second per metre per metre per metre per metre
square feet	0.09290304	square metres

EROSION CONTROL OF SCOUR DURING CONSTRUCTION

EFFECT OF SIMULTANEOUS REFRACTION AND DIFFRACTION ON WAVE HEIGHTS AND CURRENT PATTERNS

PART I: INTRODUCTION

Statement of the Problem

1. When major structures are erected in the coastal zone, they alter currents that are in a dynamic equilibrium with the existing bathymetry. These altered currents may change the existing bathymetry. In addition, waves breaking on the new structure will cause bottom material to be suspended and transported from the region by longshore or other currents. This removal of material from around structures is often not compensated by an influx of additional material; the result is scour, or erosion, that usually develops along the toe of the structure. In order to ensure structural stability, the scour area must be filled with nonerodible material (sufficiently stable to withstand the environmental forces to which it will be subjected). This may result in additional quantities of material being required during construction that can potentially be very costly. To minimize potential cost increases due to scour during construction, it is necessary to quantify the probability and ultimate extent of potential scour during the scheduled construction period.

2. Effective, comprehensive, and low cost procedures do not exist for eliminating scour during construction in the nearshore environment. Determination of potential alternative procedures is seriously hampered by the inability to predict the extent of potential scour. Objectives of this research effort are to develop techniques to minimize and control scour during nearshore construction and to predict the probable magnitude of scour that may result as a function of currents and wave climate. One phase of the research program is development of numerical techniques (incorporating both refraction and diffraction effects near the

structure) for computing wave-induced velocities and tidal currents in the vicinity of structures and applying these results to determine sediment transport of the bottom material at the particular site. This will result in an accounting of the flux of material around the structure, and thus knowledge of the extent of erosion or accretion to be expected as a function of wave climate, currents, local bathymetry, and structure design.

Purpose of the Study

3. The present state of nearshore current and wave theories has reached the point where detailed experimental investigations are required for the verification of analytical developments and numerical models. To provide a firm foundation for further advancements, a simple beach profile consisting of straight, uniform contours parallel with the shoreline was physically modeled. A shore-connected vertical, impermeable barrier (breakwater) was installed perpendicular to the shoreline to simulate the usual prototype jetties and breakwaters commonly occurring along many coasts. This single jetty (shore-connected breakwater) simplifies the experiment, facilitates direct comparisons with numerical model results, and provides greater understanding and insight into the phenomena of wave-height variations and current circulation patterns downwave of a jetty or breakwater. Analytical models of this physical arrangement have been developed (for example, Liu and Mei 1975) that extrapolate the small amplitude wave theory to calculate the radiation stress distribution. Such analytical developments regarding practical cases involving both refraction and diffraction have not been verified for either wave-height distribution or currents (magnitude and direction) in the near-vicinity of the structure. Knowledge of these important phenomena will be used as the basis for advanced studies of sediment movement around major structures under combined effects of wave refraction and diffraction.

4. The purpose of this study was to obtain quantitative and detailed laboratory measurements of combined refraction and diffraction in

the lee of a jetty or shore-connected breakwater. These measurements include both the wave-height distribution downwave of the structure, and the associated wave-induced current field and circulation patterns, and can be used to verify numerical models that simulate the phenomena.

PART II: LITERATURE REVIEW

5. The approximate solution of water wave refraction caused by a variable bathymetry is well known and can be derived by assuming that bottom reflections are negligible or by the more rigorous Wentzel-Kramers-Brillouin (WKB) approximation. The exact solution for the diffraction of surface waves by vertical barriers of simple cross section in water of constant depth also is well known (being analogous to classical problems of physics). An analytical theory for the practical case of combined refraction and diffraction has not been completely developed. The present engineering practice for determining wave heights under this condition is a stepwise procedure (Dunham 1951; Liu and Mei 1976a; U. S. Army Engineer Coastal Engineering Research Center, CERC 1977). The procedure involves the following steps: (a) calculate refraction effects up to the barrier (jetty or shore-connected breakwater), (b) calculate for a "few" wavelengths the effects of diffraction assuming a constant water depth, and (c) beyond this region calculate the refraction effects only. This procedure is obviously imprecise, and Mobarek (1962) indicates that the method is suitable only for intermediate water depths. In addition, it can be stated that this procedure is only valid for small refraction effects as demonstrated by Whalin (1972).

6. In addition to wave-height variation, scour and erosion around structures are also influenced significantly by current magnitudes and circulation patterns. These phenomena can develop differently under the simultaneous effects of refraction and diffraction. Many studies, theoretical and laboratory, have investigated the uniform longshore current on a long beach of straight, parallel contours, since this particular current is many times the most important of littoral transport mechanisms. Early analytical work considered the longshore component of the momentum flux to be the net driving force to be balanced by bottom friction (proportional to the square of the longshore velocity). This resulted in an indication of the magnitude of the longshore current. The advances of Longuet-Higgins and Stewart (1960, 1961, 1964), Longuet-Higgins (1970a, 1970b), and Lundgren (1962) were important because of

the introduction of the radiation stress. This stress is induced by wave fluctuations and is the time average of the local horizontal momentum flux integrated over the depth. Away from the surf zone, these stresses have a sound theoretical basis. In the surf zone, where turbulence due to breaking conditions exists, theories for describing either the oscillatory wave motion or radiation stress have not been fully developed. Hence, the relationships between radiation stress and mean flow velocities have been hypothesized only by empiricism and plausible reasoning.

7. Theories have been developed by Longuet-Higgins (1970a, 1970b) and Thornton (1970) for describing longshore currents on a straight beach with parallel contours which rely on the radiation stress concept. Empirical reasoning regarding lateral turbulence and bottom friction allows reasonable velocity distributions to be obtained for the longshore current. Liu and Mei (1975, 1976b) have investigated analytically the combined effects of refraction and diffraction on both wave heights and currents due to a jetty or shore-connected breakwater on a sloping beach by ignoring convective inertia and lateral turbulent diffusion. The resulting equations are solved by finite difference techniques and, in addition to the displacement of the longshore current, a cell develops in the shadow zone. Vorticity arguments indicate that the radiation stress establishes a mean sea level gradient which drives the longshore current.

Refraction and Shoaling

8. In intermediate and shallow water, the phase speed of a surface gravity wave depends on water depth. Since wave celerity decreases as depth decreases, the wavelength must also decrease for the period to remain constant. Phase velocity varies along the crest of a wave propagating at an angle to underwater contours because that part of the wave in deeper water moves faster than that part in shallower water. This variation causes the wave crest to bend toward alignment with the contours. This bending effect due to changes in bottom topography, called refraction, depends on the relation of water depth to wavelength and is

analogous to refraction of other types of waves such as light. A basic assumption in wave refraction theory is the conservation of energy between wave orthogonals (i.e., no diffraction of energy along wave crests).

9. As waves propagate from deep water into shallow water, changes other than refraction occur. These changes, called shoaling, are investigated under the assumption that there is no loss of wave energy and negligible reflection. The power being transmitted by the wave train in water of any depth is equal to the power being transmitted by the wave system in deep water. The wave period remains constant regardless of the water depth, whereas the wavelength, velocity, and height vary.

10. Refraction and shoaling effects are important for several reasons. These phenomena determine the wave height in many locations for a given set of incident deepwater wave conditions; i.e., wave height, period, and direction of propagation in deep water. Refraction and shoaling, therefore, have a significant influence on the distribution of wave energy along the coast. The change in wave direction of different parts of the wave results in convergence or divergence of wave energy and materially affects the forces exerted by waves on structures and of the capacity of waves to transport sand either alongshore or onshore/offshore.

Waves on water of variable depth

11. Procedures for the computation of refraction of surface gravity waves on water of nonuniform depth involve the assumption that a wave with a curved crest pattern and variable amplitude along the crest behaves locally as a straight-crested wave of constant amplitude. Rayleigh (1877) appears to have been the first to use the approximations of geometrical optics in this analysis, and theoretical results have been developed with respect to energy flux and phase speed. As expressed by Keller (1958), the geometrical optics theory defines a propagation velocity at each point on the water surface, with this velocity being exactly that which waves of given period would have in water of uniform depth at all points. By employing Fermat's principle of optics, wave rays are defined and surface waves are assumed to propagate along these

rays. The variation of the amplitude along the rays is determined by the use of the principle of conservation of energy. This principle (in its optical form) states that the flux of energy is the same at all cross sections between two adjacent wave rays. The energy flux is proportional to the square of the amplitude of the waves and to the distance between the rays, and hence the wave-height variation along the ray is available.

12. Keller's (1958) derivation is based upon an asymptotic solution of the equations of the exact linear theory for periodic waves in water of arbitrary nonuniform depth. The solution is asymptotic in the sense that the depth and wavelength are small compared with the horizontal scale of the bottom contours. The first term of the solution agrees exactly with the asymptotic form of the solution for waves in water with a uniformly sloping bottom as the bottom slope tends to zero. This solution conforms with all the principles of the geometrical optics theory of Rayleigh (1877) and thus provides a derivation of that theory. The results are not valid, however, at caustics or ray crossings.

13. In problems of linear wave propagation over mild slopes, the principle of geometrical optics has been applied by Carrier (1966) as the first approximation in a systematic perturbation scheme while the bottom is considered to be locally horizontal. The depth variation was dealt with afterward by requiring the appropriate energy conservation. This was also the basic idea for the work of Koh and Le Méhauté (1966) in which the transformation of progressive waves was investigated as they travel from deep water to shore. The Stokes' theory at a fifth order of approximation was applied along with the method of conservation of energy flux. The first, third, and fifth orders of approximation were compared with each other and with experiments. The differences between the predictions of wave-height changes based on the three orders of approximation were found to be small, on the order of 5 percent. For practical purposes, the third-order theory was found to give reliable results. The third and fifth order Stokes' theories are based on a series expansion in terms of H/L where terms of the order of $(H/L)^3$ and $(H/L)^5$, respectively, are retained and higher order terms are neglected. It should be noted that this theory is based on an expansion

in term of the wave steepness, H/L, and consequently can be expected to better approximate limit steepness waves in deep water. However, it cannot be expected to do a very good job of approximating waves in shallow water since water depth is not a parameter in the series expansion. It also is assumed that the wave is simply harmonic in time. This theory could be considered as a finite amplitude deepwater wave theory.

14. In cases of limiting shallow water, the wave conditions are nearly independent of wavelength, and the important parameters are water depth and the ratio of wave height to water depth. Mathematical arguments show that Stokes waves are most nearly valid in water deeper than about $d/L > 1/8$ to $1/10$ (Keulegan 1950). In shallower water, the theory for a wave type known as cnoidal appears to be more satisfactory, and Masch (1964) investigated the problem of wave shoaling using cnoidal wave theory with the formulas developed by Keulegan and Patterson (1940). Masch (1964) assumed hydrostatic pressure distribution and neglected the convective inertia term in his expression for the energy flux. The third and fifth order cnoidal theories are based on a series expansion in terms of H/d, where terms of the order of $(H/d)^3$ and $(H/d)^5$, respectively, are retained and higher order terms neglected. It should be noted that this theory is based on an expansion of the relative wave height (H/d) and can be expected to better approximate the wave form in shallow water. However, it cannot be expected to do a very good job of approximating the wave form for limiting steepness waves in deep water. In that case, water depth is unimportant and wavelength is crucial. This theory could be considered a finite amplitude intermediate and shallow-water theory.

15. A technique of asymptotic expansion was applied by Mei, Tlapa, and Eagleson (1968) to water wave propagation over an uneven bottom that has straight and parallel contours. Attention was focused on the establishment of a rigorous scheme of successive approximation for higher order corrections. The bottom depth was assumed to vary slowly within a wavelength. By introducing a compressed coordinate in the direction normal to the contours and by assuming an expansion of the WKB type, the weakness of the depth variation in the normal direction was incorporated

in the mathematical formulation. The conventional linearized theory of wave refraction was obtained as the first-order solution without the explicit assumption of Snell's law. In the second order, a steady-state depression of the mean water surface was found for the general case where the incident wave approaches the contours obliquely. To the first order, this development was the same as the classical theory of Rayleigh (1877). At higher order some differences existed from the usual adaptation of the Stokes' theory for a horizontal bottom. The source of the difference is the explicit appearance of the variation of the bottom boundary conditions for the first harmonic at second and higher orders. The theory is expected to hold up to the neighborhood where the wave breaks, except at the shoreline where a singularity exists for all orders.

16. The refraction of surface gravity waves propagating in an ideal fluid was investigated by Battjes (1968) with amplitudes small so that linear theory was applicable and harmonic in time. It was known a priori that the velocity of propagation of a wave crest (to third order and greater) is a function of the wave height. In zones of convergence or divergence of wave energy, gradients in wave height will exist along sections of the wave crest. The regions of greater wave height will propagate faster than the regions of lesser wave height and this will, in turn, create bending of the wave crest (in addition to that bending caused by the bottom topography, called refraction). This supplemental bending is not usually accounted for by refraction analysis. Battjes (1968) developed an expression for this local correction to the wave speed because of wave-height variations along the crest from an exact derivation of the wave number, k. It was determined that the magnitude of the exact wave number equals k plus corrections which depend on the second derivative of the wave amplitude. This correction of the wave number implies, in turn, a correction to the phase speed c, which was found to be:

$$c = (g/k \tanh kd)^{1/2}\left(1 + \frac{a_{xx} + a_{yy}}{k^2 a}\right)^{-1/2} \qquad (1)$$

where

g = gravitational constant, 32.174 ft/sec^2*

k = wave number, $2\pi/L$, 1/ft

d = local water depth, ft

a = local wave amplitude, ft

The second derivative of the wave amplitude in the horizontal plane is given by a_{xx} or a_{yy}. The rate of power transmission P, or energy flux, was determined to be:

$$P\Delta b = (1/2\ \rho g a^2 n \frac{\omega}{k} \Delta b)\left(1 + \frac{a_{xx} + a_{yy}}{k^2 a}\right)^{1/2} \qquad (2)$$

where

Δb = wave ray spacing, ft

ρ = fluid density, lb-sec^2/ft^4

n = ratio of group velocity c_g, to phase velocity c, dimensionless

ω = angular frequency, $2\pi/T$, 1/sec

Define:
$$\delta = \left(\frac{a_{xx} + a_{yy}}{k^2 a}\right) \qquad (3)$$

The commonly used existing procedures (Dunham 1951, Liu and Mei 1976a, CERC 1977), for construction or computation of refraction diagrams utilize phase speeds that are obtained by neglecting δ.

17. Battjes (1968) examined the omission of δ from a qualitative standpoint. In an area of strong local convergence, omission of δ from Equation 1 results in underestimating the local phase speed. The result is that in Equation 2 the ray separation Δb will be underestimated. Thus, there are generally two contributions to the error which results in the computed wave amplitude a. However, these two contributions are of a different nature because the effect on the wave pattern of using an incorrect value for the phase speed is cumulative,

* A table of factors for converting U. S. customary units of measurements to metric (SI) units is presented on page 3.

whereas the effect on energy flux is local. In any case, the omission of δ will generate wave heights at variance with the height inferred from refraction diagrams based on linear small amplitude wave theory which neglects the effects of wave-height gradients along the wave crest, so that it would appear that energy had been transferred across orthogonals. An estimate of the magnitude of δ has been approximated by Battjes (1968) for four distinctly different cases. For simple shoaling, the amplitude varies only in the direction of wave propagation, and for shallow water the variation was:

$$\delta = 8 \times 10^{-3} \, (L/d)^2 S^2 \tag{4}$$

where S is the bottom slope. For short-crested waves where the distance along the wave crest is two or three times the wavelength, δ = -20% or -10% , respectively. For the case of diffraction around a semi-infinite breakwater, δ was found to reach values between +10% and -10% at points a distance of one wavelength from the breakwater tip, decreasing inversely proportional to the distance from the tip. For the case of diffraction through a gap of width two times the wavelength, δ was evaluated in a few points on the center line of the gap where it was found to reach values of 25%, 7%, and 3% at distances of 1, 2, and 4 wavelengths, respectively, from the gap.

Longshore currents
due to wave breaking

18. It is well known that as sea or swell approaches a coastline at an angle, breaking waves create a mean current in the surf zone parallel to the coastline. This longshore current transports sand or other material and is of primary importance to coastal engineers. It has often been suggested that the magnitude of the longshore current is related in some way to the energy flux or momentum flux of the incoming wave train. Indeed, it appears reasonable to believe that the forces available for transporting material should be related to the available wave power in the vicinity. The approach employing momentum flux should be the more promising since momentum is conserved, whereas energy is

dissipated in the breaking process. Even so, Inman and Quinn (1952) have shown that in order to make the momentum flux theory fit prototype observations, the friction coefficient, C , would have to vary over a range of 3 to 4 orders of magnitude. The momentum flux theory which was analyzed by Inman and Quinn (1952) was that which had been developed by Putnam, Munk, and Traylor (1949) and contains the beach slope parameter.

19. Galvin and Eagleson (1965) performed experimental studies of longshore currents on a plane beach. Measurements were made of the characteristics of breaking waves and the resulting longshore currents for 34 combinations of wave height (up to 0.22 ft), period (0.90 to 1.50 sec), and breaker angle (up to 32 deg), along a 20-ft test section of a 30-ft plane, smooth concrete beach with a slope of 0.104. Observations and measurements showed that most of the fluid in the surf zone stays there, and that longshore current velocity initially increases downstream from an obstruction (jetty or shore-connected breakwater). Velocity increases along the beach because the fluid forming the breaking wave has been withdrawn from the surf zone and thus already has a longshore component of motion of the breaking wave. A differential equation for this nonuniform flow agreed qualitatively with the measured variation of velocity with breaker angle and with distance from an obstacle. The nonuniformity of the flow was also indicated by the mean water level which increased, and by the breaker position and runup limit which moved shoreward downstream from the obstruction. The energy used to maintain the flow of the longshore current was found to be a small fraction (less than 10 percent of the energy brought to the surf zone by the shoaling waves. The mean velocity of the uniform longshore current, V_{ls} , was approximately:

$$V_{ls} = gST \sin 2\alpha_b \tag{5}$$

where

S = beach slope, dimensionless

T = wave period, sec

α_b = angle breaking wave makes with the shoreline, deg

Equation 5 is one form of the conservation of mass in the surf zone.

20. By using known results of the radiation stress associated with gravity waves, Longuet-Higgins (1970a, 1970b) investigated the mechanism of obliquely incident sea waves which generate longshore currents. The total lateral thrust, F_w , per unit distance parallel to the coastline exerted by incoming waves on the beach and in the nearshore zone was shown to be:

$$F_w = 1/4\ E_o \sin 2\ \alpha_o \tag{6}$$

where

E_o = wave energy density in deep water, ft-lb/ft^2

α_o = deepwater wave approach angle, deg

The local stress, τ , per unit area exerted on the surf zone in steady conditions was shown to be:

$$\tau = D/c \sin \alpha \tag{7}$$

where

D = local rate of energy dissipation, lb/ft/sec

c = phase velocity, ft/sec

α = local angle of incidence, deg

These relations appear independent of the manner of the energy dissipation, but because breaker height is related to local depth in shallow water, it is conceivable that most of the dissipation is due to wave breaking and not to bottom friction. Under these considerations, the local mean longshore stress in the surf zone, τ_{ls} , is given as:

$$\tau_{ls} = 5/4\ \rho\ u_{max}^2\ S \sin \alpha \tag{8}$$

Here u_{max} is the maximum orbital velocity in the wave, and the other symbols have been previously defined. It was also shown that if the friction coefficient, C , on the bottom is assumed constant and if

horizontal mixing is neglected, the mean longshore component of velocity, V_{ls} , is given as:

$$V_{ls} = (5\pi/8)(S/C)\, u_{max} \sin \alpha \qquad (9)$$

This value of longshore current is proportional to the longshore component of the orbital velocity. When the horizontal mixing is taken into account the longshore currents observed in prototype situations and laboratory experiments are consistent with a dimensionless friction coefficient, C , of about 0.01.

21. The profile of the longshore current, as a function of distance from the swash line, was calculated by Longuet-Higgins (1970a, 1970b) by using the concept of radiation stress together with a horizontal eddy viscosity, μ_e , of the form:

$$\mu_e = \rho\, N\, x\, (gd)^{1/2} \qquad (10)$$

where

N = dimensionless parameter that varied between 0.000 and 0.016

x = distance offshore, ft

This development gives rise to a family of current profiles whose form depends only on a nondimensional parameter P_{L-H} :

$$P_{L-H} = \pi/2\ (SN/0.41C) \qquad (11)$$

The current profiles are of simple analytic form, having a maximum in the surf zone and tending to zero at the swash line. Comparison with the laboratory experiments of Galvin and Eagleson (1965) showed remarkably good agreement if the friction coefficient, C , is taken as 0.010. The theoretical profiles are insensitive to the exact value of P_{L-H} , but the experimental results suggest that P_{L-H} never exceeds a value of 0.016.

22. CERC (1977) has modified the Longuet-Higgins (1970a, 1970b) expression for longshore velocity, based on more recent experimental

data and prototype observations, and determined that:

$$V_{ls} = 20.7\ S\ (gH_b)^{1/2} \sin 2\alpha_b \qquad (12)$$

where H_b is the breaker height. Here again there is a direct proportionality to the beach slope, S. Komar and Inman (1970) concluded earlier that there was no dependence on S, and proposed the relationship:

$$V_{ls} = 2.7\ u_m \sin \alpha_b \cos \alpha_b \qquad (13)$$

in which

$$u_m = (2E_b/\rho d_b)^{1/2} \qquad (14)$$

where

E_b = wave energy density at breaking, ft-lb/ft^2

d_b = water depth at breaking, ft

Komar and Inman (1970) demonstrated that Equation 13 has fairly good agreement with the available longshore current data, and that it is equivalent to the theoretical longshore current relationship of Longuet-Higgins which was derived from radiation stress concepts. Komar (1979) reiterates that the inclusion of the beach slope, S, leads to a somewhat less precise degree of fit for much of the available data (prototype and laboratory) than do best-fit expressions which do not include the beach slope parameter.

Diffraction

23. Diffraction of water waves is the phenomenon by which wave energy propagates into the sheltered lee of structures even in the absence of bathymetric refraction. In these situations, wave crests bend (even in constant depth water) and gradients of wave height exist along the wave crest. This phenomenon is most visible when a

train of regular waves is interrupted by an obstruction such as a jetty or shore-connected breakwater. The theory of water wave diffraction can be explained by Huygens' principle. Each point of an advancing wave front (wave crest) may be considered as the center of a secondary circular wave which advances in all directions. The resultant shape of the crest is the envelope of all these secondary waves. In a straight-crested wave train, the envelope of the secondary waves is a straight line also. When the wave passes an obstruction, the energy intensity at a certain point is a vector combination of all the circular waves emitted by every point of the passing wave train.

24. Sommerfeld (1896) presented a solution for the diffraction of light waves past the edge of a semi-infinite screen. Penny and Price (1944) showed that this is also the solution of the water wave diffraction problem at the end of a semi-infinite obstacle such as a jetty or shore-connected breakwater. This exact solution of the surface elevations behind the breakwater is applicable only to water of constant depth and waves of small amplitude. Putman and Arthur (1948) summarized the solution of Penny and Price (1944) for the definitive sketch of Figure 1. In cylindrical coordinates, the water-surface elevation is:

$$\eta = (aikc/g)e^{ikct} \cosh kd\ F(r,\theta) \tag{15}$$

where

η = water-surface elevation, ft

a = wave amplitude, ft

c = wave celerity, ft/sec

i = square root of -1

$F(r,\theta)$ is a function which satisfies the wave equation in cylindrical coordinates:

$$\frac{\partial^2 F}{\partial r^2} + \frac{1}{r}\frac{\partial F}{\partial r} + \frac{1}{r^2}\frac{\partial^2 F}{\partial \theta^2} + k^2 F = 0 \tag{16}$$

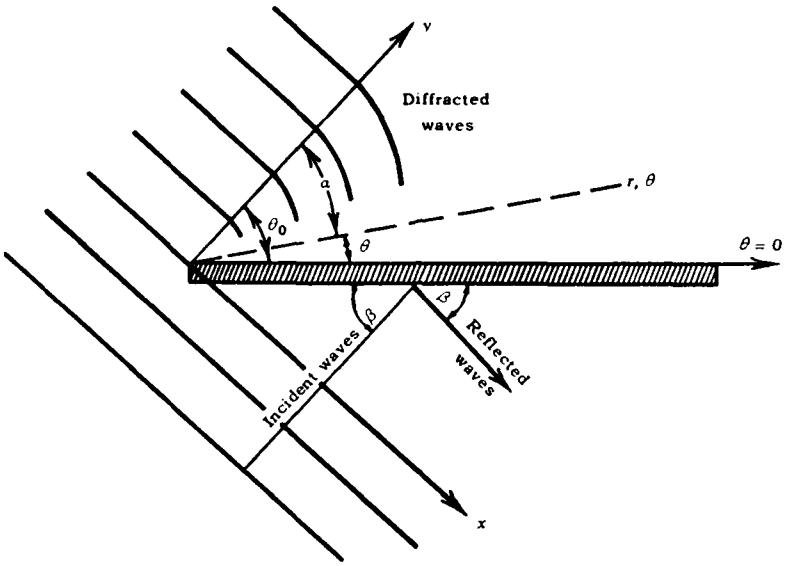

Figure 1. Definitive sketch, wave diffraction around a breakwater

In the presence of a jetty or breakwater, the boundary condition is imposed that the normal component of the fluid velocity is zero along the breakwater, leading to the solution:

$$F(r,\theta) = \frac{1}{\sqrt{2}} e^{i\left[\frac{\pi}{4} - kr\cos(\theta_o - \theta)\right]} \int_{-\infty}^{u_1} e^{-\frac{i\pi u^2}{2}} du$$

$$+ \frac{1}{\sqrt{2}} e^{i\left[\frac{\pi}{4} - kr\cos(\theta_o - \theta)\right]} \cdot \int_{-\infty}^{u_2} e^{-\frac{i\pi u^2}{2}} du \qquad (17)$$

$$u_1 = 4\sqrt{kr/\pi}\,\sin\left[\frac{1}{2}(\theta_o - \theta)\right] \qquad (18)$$

$$u_2 = -4\sqrt{kr/\pi}\ \sin\left[\frac{1}{2}\ (\theta_o + \theta)\right] \qquad (19)$$

Bretschneider (1966) has presented computational procedures for evaluating the diffraction coefficients at arbitrary points behind jetties or breakwaters.

25. Wiegel (1962) developed a graphical procedure for determining diffraction coefficients of waves passing the tip of single breakwaters. The family of diagrams shows, for uniform water depth, lines of equal wave-height reduction displayed in terms of the diffraction coefficients. The diffraction diagrams (typical example, Figure 2) are constructed in polar coordinate form centered at the structure tip. The arcs behind the breakwater are spaced one radius-wavelength unit apart so that, in application, a specific diagram must be scaled up or down so that the particular wavelength corresponds to the scale of the hydrographic area under investigation. The set of diffraction diagrams of waves passing the tip of a single breakwater were presented by CERC (1977), along with diagrams of waves entering a breakwater (typical example, Figure 3).

26. Laboratory tests were performed by Harms (1979) to investigate the distribution of wave heights in the lee of a breakwater (shore-connected) for waves normally incident upon the structure and with a horizontal bottom both in front of and in the lee of the structure. In general, satisfactory agreement was obtained between measurement and theory, but diffraction theory was not found to be conservative. At large distances in the shadow zone, measured wave heights consistently exceeded theoretical values. Close to the breakwater outside the shadow zone, the measured maximum wave height was also found to be larger than that predicted by theory. The diffraction behavior appeared to be insensitive to the intensity of wave reflections from the seaward side of the breakwater.

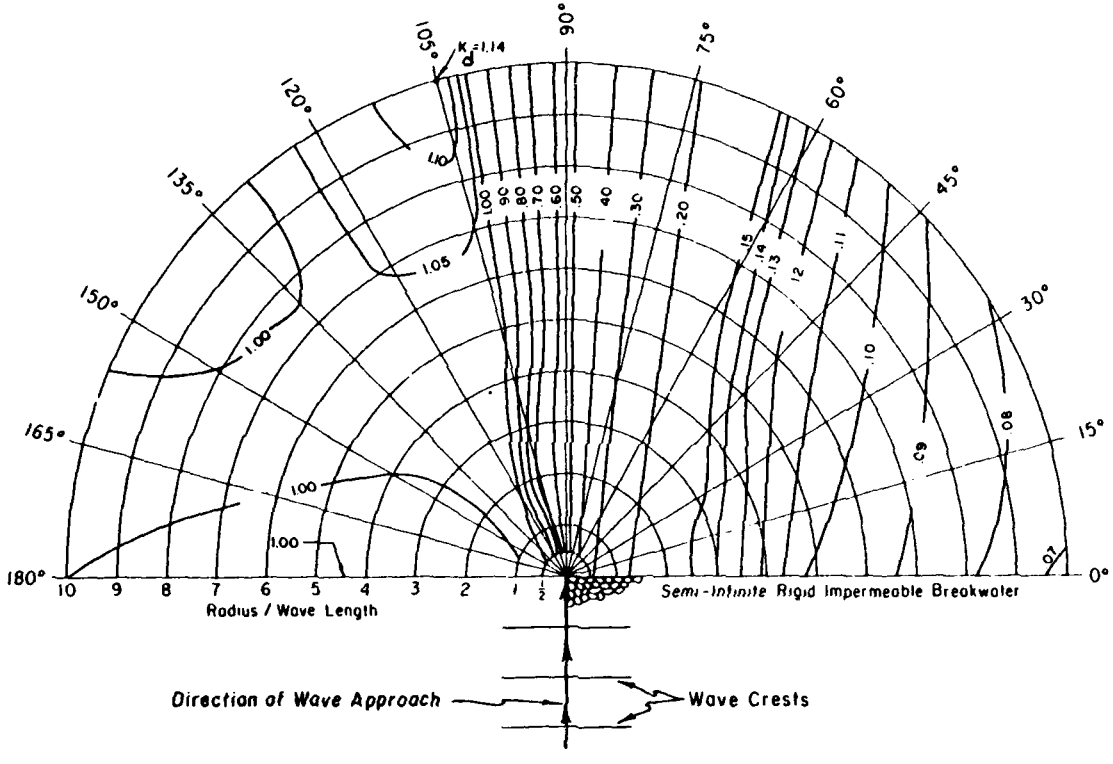

Figure 2. Typical example, wave diffraction diagram past a semi-infinite breakwater, angle of incidence equals 90 deg (after CERC 1977)

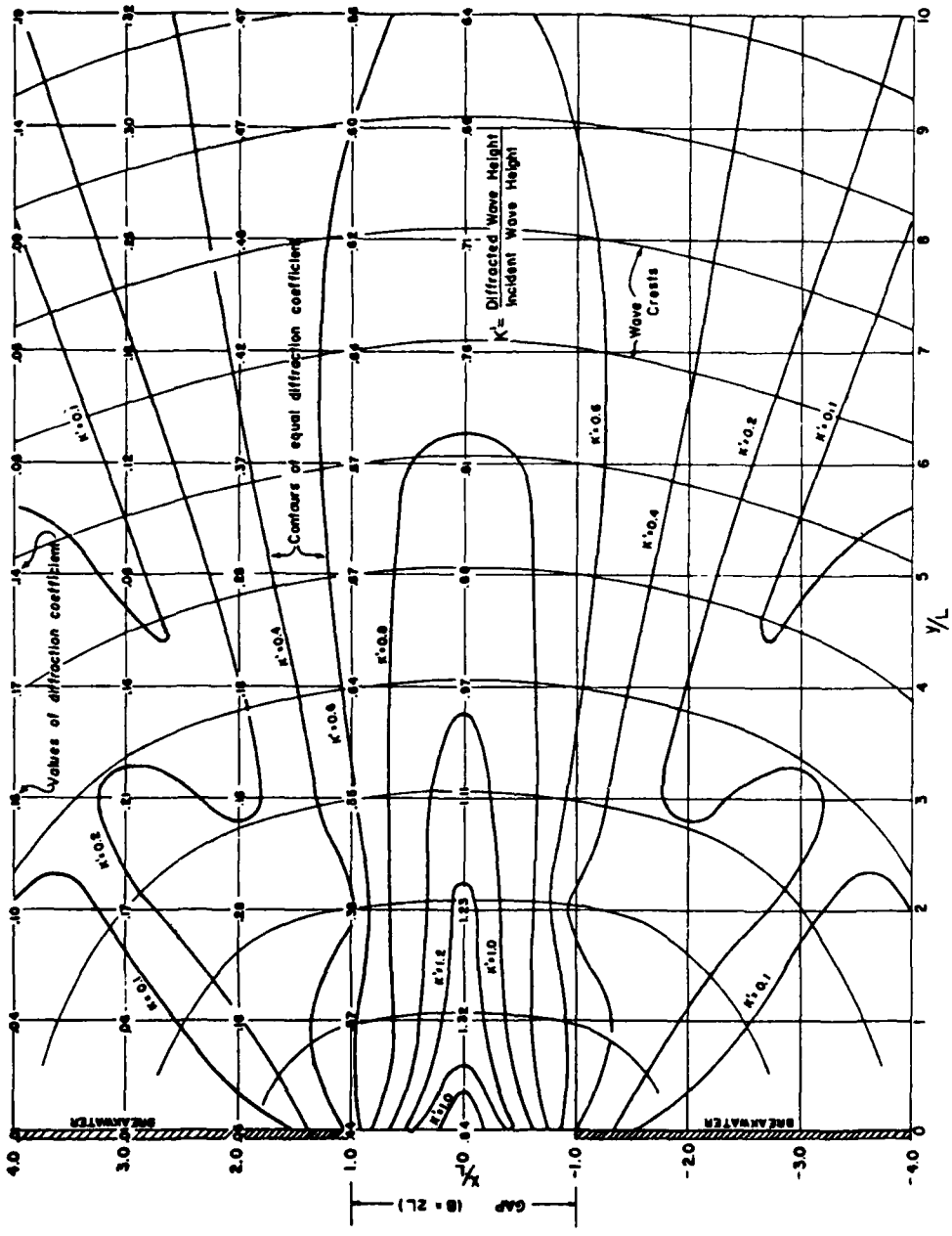

Figure 3. Generalized diffraction diagram for a breakwater gap width of two wavelengths (after CERC 1977)

Combined Refraction and Diffraction

27. The bathymetry shoreward of a jetty or breakwater usually is not flat or even uniform; hence, refraction generally occurs in addition to the diffraction effects. While a general unified analytical approach to the simultaneous solution of these two distinctly different phenomena has not been entirely developed, considerable insight has been gained through the theoretical work of Liu and Mei (1975, 1976a, 1976b), Lick (1978), Liu and Lozano (1979), and through the earlier experimental work of Mobarek (1962). The procedure usually followed by coastal engineers concerned with wave-height variation behind jetties or breakwaters is to construct refraction diagrams shoreward to the structure, then construct diffraction diagrams for three or four wavelengths shoreward of the jetty, and finally refract the last wave crest on toward the shoreline. This procedure is schematized in Figure 4, where the overall refraction diffraction coefficient, K_{r-d}, in the region behind the structure is:

$$K_{r-d} = K_r K_d \sqrt{b_1 b_2} \tag{20}$$

where

K_r = refraction coefficient at the structure, dimensionless

K_d = diffraction coefficient on last wave crest behind the structure from which additional refraction computations are performed, dimensionless

b_1 = orthogonal spacing at the last diffracted wave crest, ft

b_2 = orthogonal spacing near the shore, ft

Wave heights resulting from refraction and diffraction

28. Mobarek (1962) experimentally investigated the effect of bottom slope on wave diffraction through a gap in a breakwater normal to the incident wave direction. Also investigated was the effect of an abrupt increase or decrease in the water depth behind the breakwater. The theoretical analysis for the comparison of experimental results followed the treatment of Penny and Price (1944) restricted to the case of

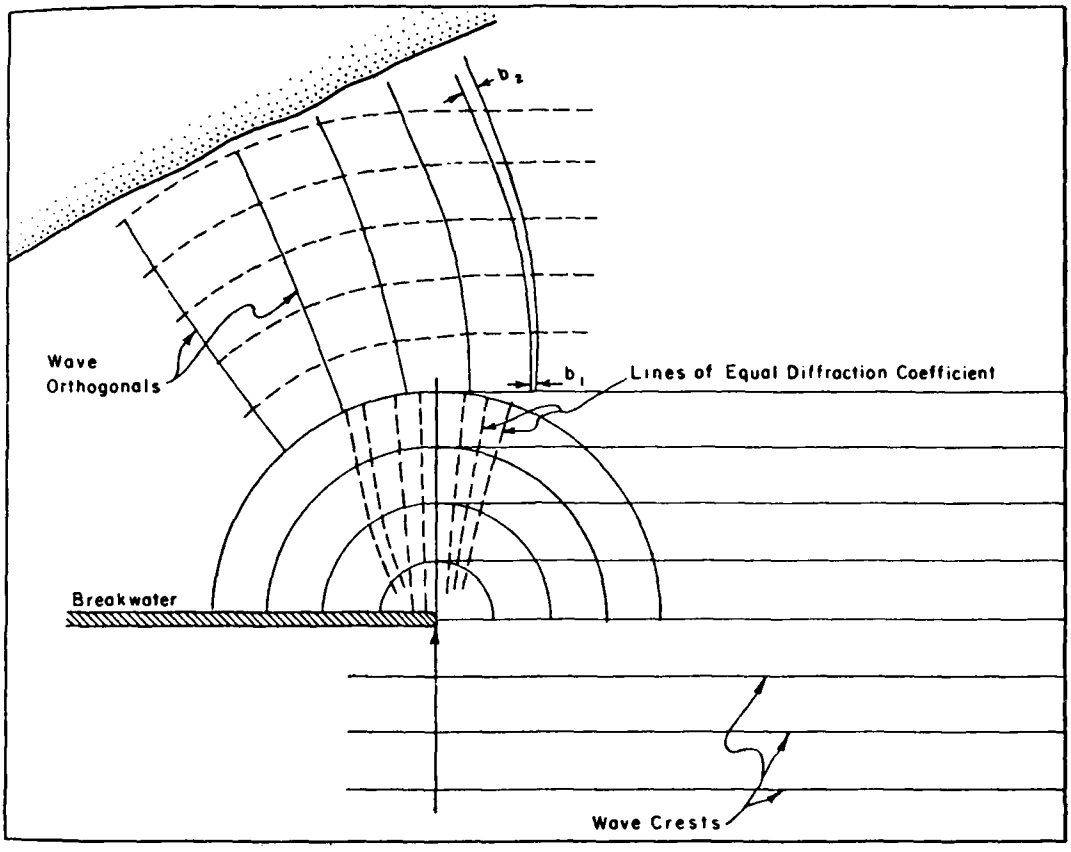

Figure 4. Graphical procedure for determining overall refraction and diffraction effects past a breakwater (after CERC 1977)

normal incidence for which the Sommerfeld (1896) solution is simplified and in the presence of a horizontal bottom. Two fundamentally different basin configurations were used in the study. The first (Figure 5) consists of a longitudinally sloping bottom with the slope commencing at the breakwater and extending to the shoreline. The second (Figure 6) was constructed with a flat bottom extending beyond the breakwater gap but sloping laterally to the shoreline.

29. Results of the Mobarek (1962) investigation for a longitudinally sloping bottom and for a laterally sloping bottom are shown in Figures 7 and 8, respectively. Taking into consideration the serious limitations of the experimental equipment (very small model, 72 sq ft), the investigation led to the conclusion that the procedure usually

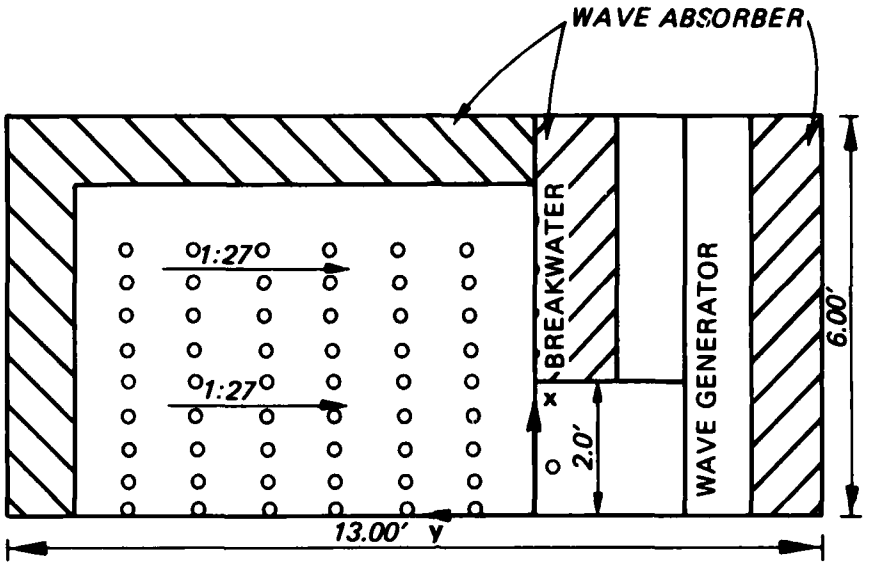

Figure 5. Experimental wave basin with longitudinal bed slope (after Mobarek 1962)

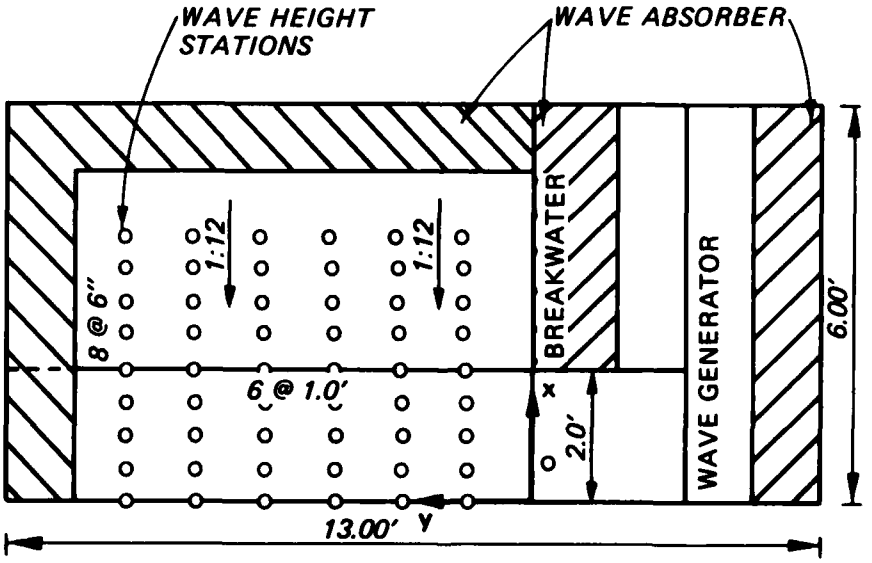

Figure 6. Experimental wave basin with lateral bed slope (after Mobarek 1962)

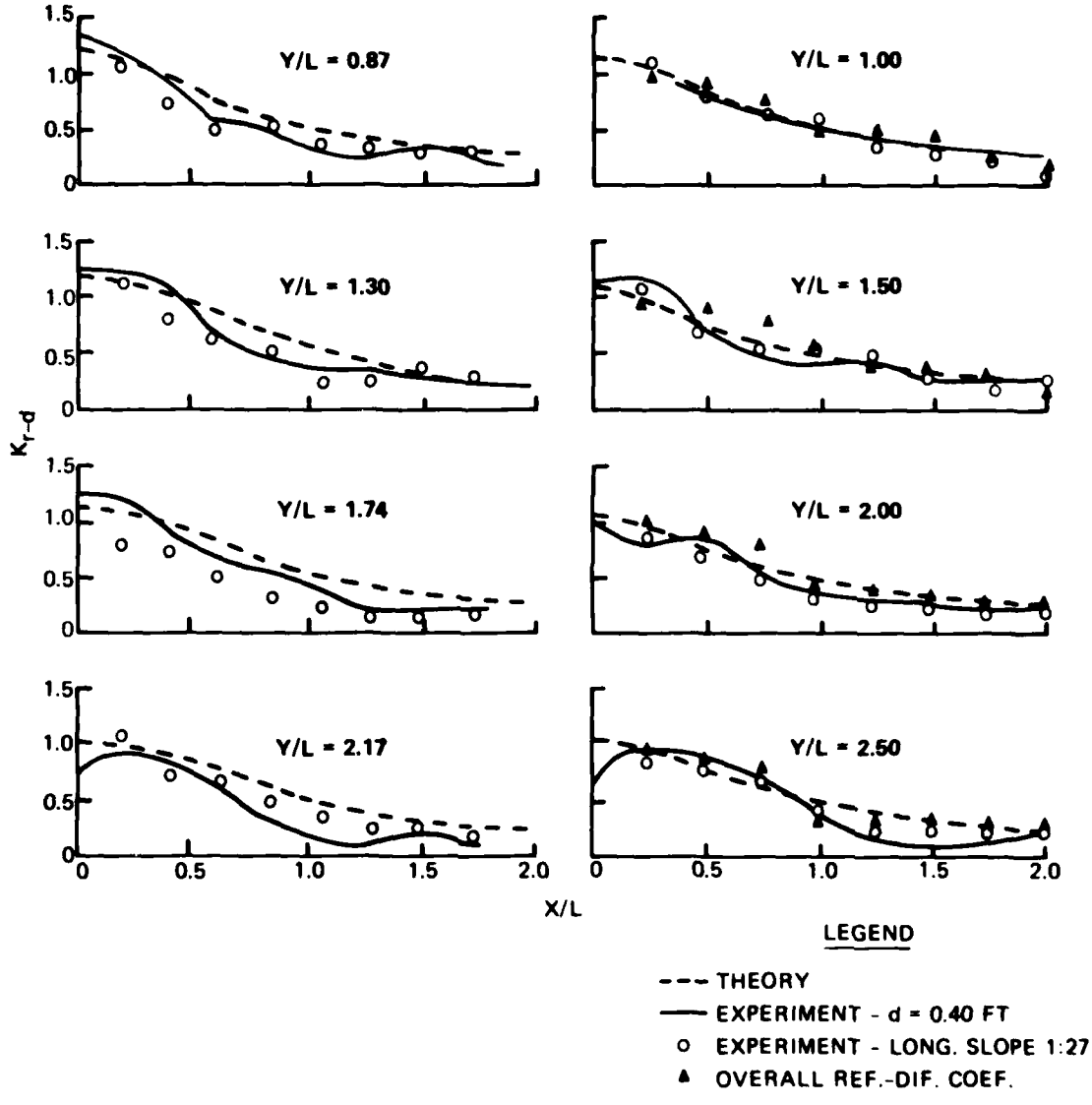

Figure 7. Combined refraction and diffraction coefficients, K_{r-d}, for longitudinal bed slope behind breakwater (after Mobarek 1962)

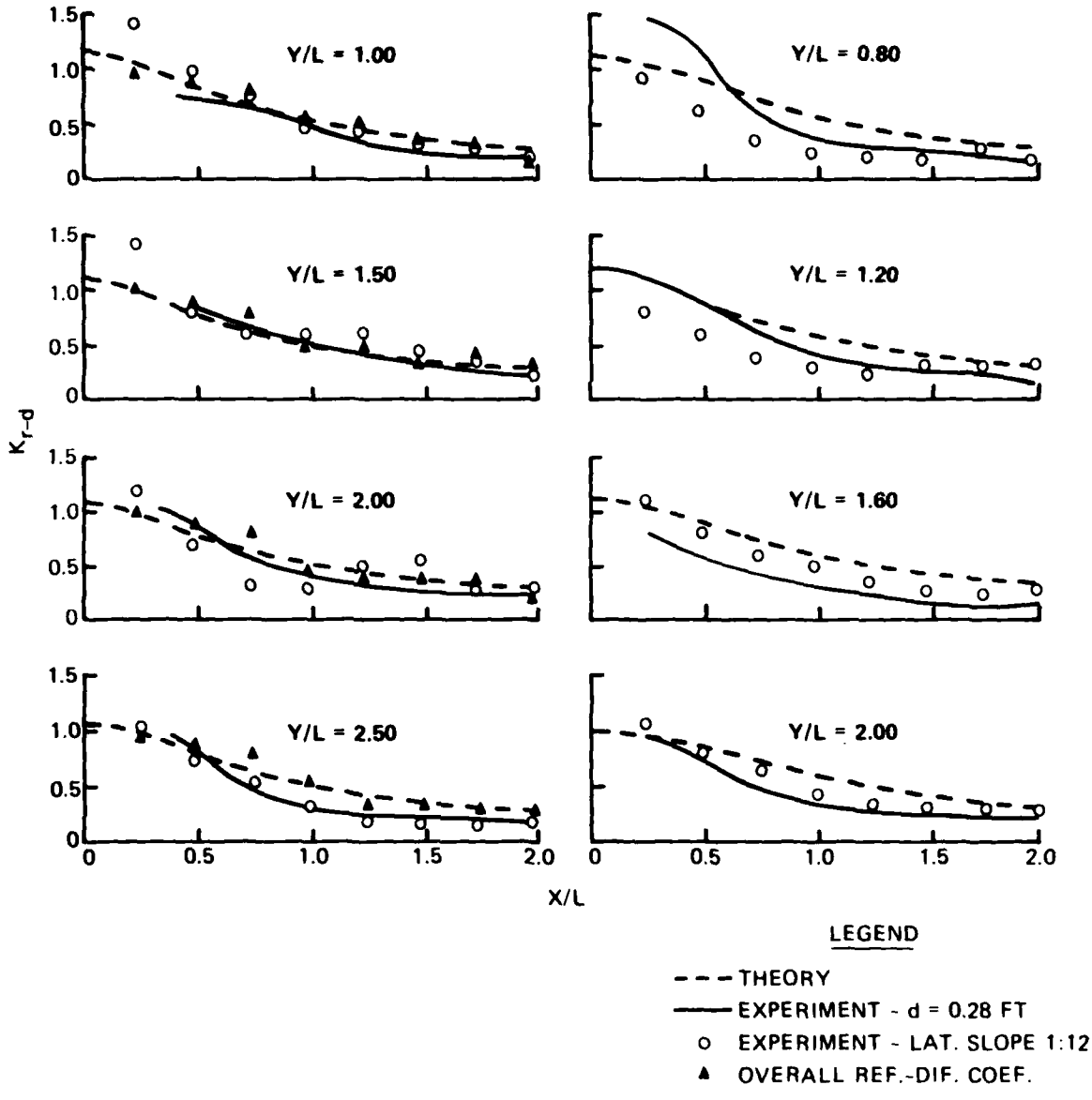

Figure 8. Combined refraction and diffraction coefficients, K_{r-d}, for lateral bed slope behind breakwater (after Mobarek 1962)

followed for estimating wave heights behind jetties or shore-connected breakwaters (Figure 4) was sufficiently good for medium period waves; but in the case of long waves, the effect of the shoaling bottom on waves should be taken into consideration. Experiments on a larger scale were highly recommended.

30. For a long shore-connected breakwater on a slowly varying bottom, an asymptotic theory has been developed by Liu and Mei (1976a) which accounts for the combined effects of refraction and Fresnel diffraction of water waves. Qualitatively, the axis of the diffraction zone downwave of the breakwater or jetty was found to be curved; and quantitatively, the diffracted wave amplitude must be modulated horizontally an amount depending on the refracted wave amplitude. The total wavefield is complex, especially near the tips of the jetty, and is caused by the interference between the incident and the reflected waves. An example solution is presented in Figure 9 for a jetty assumed to be 400 m long from the still-water shoreline. The beach slope was 0.1 for $x < 100$ m and 0.01 for $x > 100$ m. The incident wave period was 10 sec, and the initial amplitude was 0.5 m with the incidence at infinity of 45 deg. For short jetties or groins, the reflection and diffraction effects may be either too localized or too complicated by

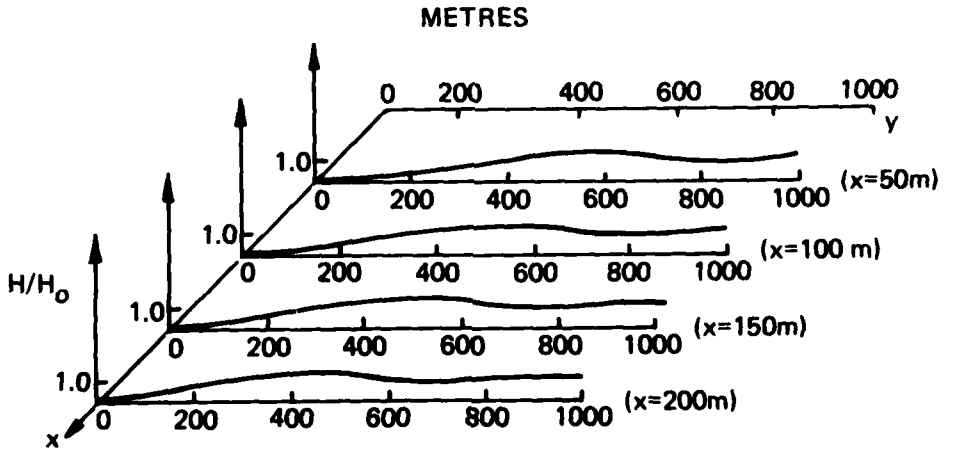

Figure 9. Variation of the diffraction factor downwave of a shore-connected breakwater, incidence angle = 45 deg (after Liu and Mei 1976a)

virtue of the dominant influence of the surf zone to be handled by this theory. The approximation is a combination of Kirchhoff's theory and geometrical optics. This permits the diffraction field near the beach to be calculated analytically and this can, in turn, be used for breaker line estimates.

31. A uniformly valid asymptotic solution for water waves has been developed by Liu and Lozano (1979) that accounts for the combined effects of refraction due to slowly varying water depth and diffraction by a long shore-connected breakwater. This solution is more general than the approximate solution developed by Liu and Mei (1976a) because this theory is valid near the edge and the tip of the breakwater. The wave behavior in the near field is of particular interest for studying the scour and erosion that may occur near the tip of a breakwater. In this analysis, recent developments in the field of formal geometrical optics have been extended to include the effects of diffraction. A numerical example is presented for a linear sloping bottom, although the theory is not restricted to this condition. The length of the breakwater is assumed to be 400 m positioned on a beach slope of 1V on 20H. The incident wave train with period of 10 sec arrives at an angle of 45 deg. Figure 10 shows dimensionless results of the wave amplitude variation downwave of the breakwater for two sections taken perpendicular

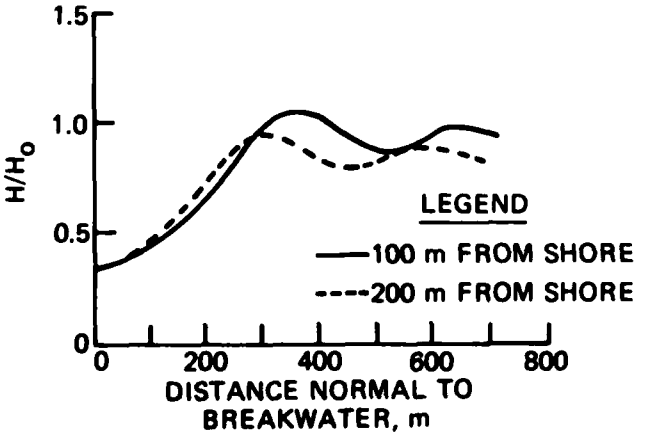

Figure 10. Dimensionless wave amplitudes perpendicular to, and downwave of, shore-connected breakwater (after Liu and Lozano 1979)

to the breakwater at distances of 100 and 200 m from the shoreline.

32. Berkoff (1972), Schonfeld (1972), and Smith and Sprinks (1975) independently derived a two-dimensional equation that governs short-wave propagation over moderately varying depths. Rewriting Berkoff's expression, Jonsson and Brink-Kjaer (1973) introduced the mild-slope wave equation:

$$\nabla \cdot (cc_g \nabla \eta) + c_g / c\omega^2 \eta = 0 \tag{21}$$

where

∇ = horizontal gradient operator, dimensionless

c = phase velocity, ft/sec

c_g = group velocity, ft/sec

ω = angular frequency, $2\pi/L$, 1/ft

η = complex wave amplitude, ft

Equation 21 can be rewritten in the form:

$$\nabla \cdot (cc_g \nabla \phi) + c_g / c\omega^2 \phi = 0 \tag{22}$$

where ϕ is a velocity potential defined by $\vec{u} = \nabla\phi$ and $\vec{u}$ is a two-dimensional vector. Equation 22 reduces to the diffraction Helmholtz equation in deep or constant-depth water. In shallow water, the equation reduces to the linear long-wave equation.

33. Houston (1980) solved Equation 22 by the use of a hybrid finite-element numerical model originally developed by Chen and Mei (1974) to solve the diffraction Helmholtz equation in a constant-depth region. The appropriate modifications, including variable depth and frequency dispersion, were incorporated by Houston (1980) and the solution of Equation 22 was applied to the geometry of the physical model (described in PARTS III and IV of this report) used in this investigation. A problem in simulating these hydraulic model tests numerically is that the waves break in the hydraulic model near the shoreline and thus dissipate their energy. No mechanism exists to dissipate energy in the numerical model. However, dissipation was simulated by allowing

waves to continue to propagate out of the problem area. The breakwater and uniform slope were modeled only to the point where breaking occurred. The depth was then increased to the depth of a semi-infinite ocean region surrounding the region of computation, and the waves were allowed to radiate away from the area of interest.

34. Figure 11 shows a typical comparison between the hydraulic

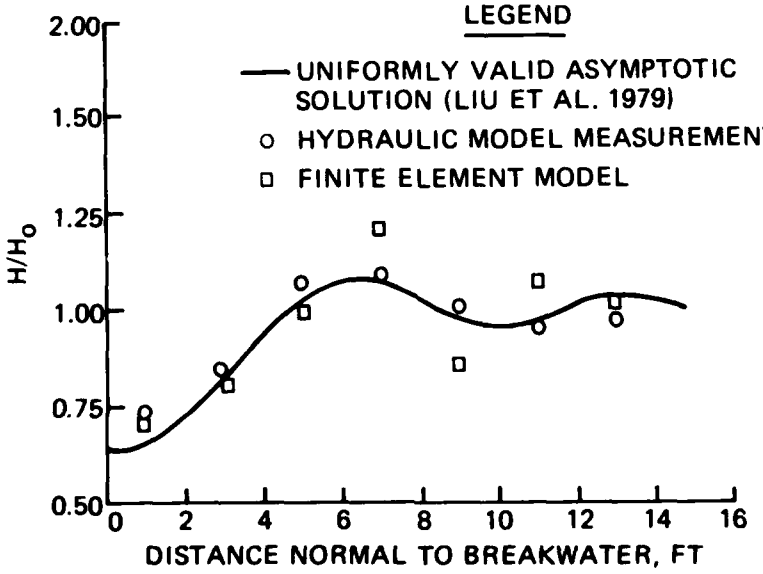

Figure 11. Comparison of asymptotic and finite-element solutions with hydraulic model measurements (after Houston 1980)

model measurements and the finite-element calculations (Houston 1980). Also shown is the uniformly valid asymptotic solution derived by Liu and Lozano (1979). The solution derived by Liu and Lozano (1979) appears to be in good agreement with the hydraulic model tests. The finite-element calculations of Houston (1980) agree quite well in the shadow zone with the hydraulic model tests. The agreement is not as good outside the shadow zone. The difference is partially attributable to the artificial increase in depth to allow the waves to radiate from the inner region. This depth transition would cause some energy to reflect back into the region of interest.

Wave-induced currents produced
by refraction and diffraction

35. The wave field near a shore-connected breakwater has been studied by Liu and Mei (1975, 1976b) for the purpose of developing the wave-induced current patterns, magnitudes, and circulation cells in the neighborhood of the breakwater. By employing an approximation which adequately describes Fresnel diffraction, the first order wave was deduced accounting for diffraction and refraction. In a natural environment, the waves and current change the bottom topography and vice versa, with the actual beach process being one of interaction. Efforts were focused on the effect of wave pattern due to reflection, refraction, and diffraction on the current, assuming the topography to be fixed and simple. The beach was considered to be immobile, infinitely long, and uniform in the longshore direction. The depth contours were straight and parallel. The walls of the breakwater were vertical, impermeable, perfectly reflecting, and of negligible thickness compared with a wavelength and extended far into the surf zone. For mathematical simplification, the assumptions were made that turbulent lateral stresses and convective inertia terms could be ignored. The bottom friction was assumed proportional to the square of the average current velocity.

36. The assumption by Liu and Mei (1975) of the law of bottom friction has been made by other researchers and the constant of proportionality (friction factor) determined by laboratory and field experiments. Longuet-Higgins (1970a) and Thornton (1970) investigated typical ranges of possible values of the friction factor based on laboratory experiments with rigid and rough bottoms. Typical values appeared to lie within the range 0.005 to 0.012. In field conditions, other factors such as sediment motion at the bottom may enter into consideration. Bretschneider (1954) reported from measurements in shallow water in the Gulf of Mexico that for wind waves the friction factor varied from 0.03 to 0.097, with an average value of 0.053. Based on laboratory and field studies, Putnam, Munk, and Traylor (1949) reported values between 0.07 and 0.385. For comparison purposes, Liu and Mei (1975) used two values, 0.01 and 0.09.

37. Sample calculations were prepared by Liu and Mei (1975), but because of the many scales involved, the results are presented in physical dimensions. A shore-connected breakwater of 400 m length was evaluated, with the incident wave being of 10-sec period and having an amplitude of 0.5 m. The angle of incidence in deep water was 45 deg. One of the more significant results of the study was the formation of cells. Whether in the diffraction zone (downwave) or in the reflection zone, these cells are associated with variations in the breaking wave height which is closely related to the variations in the breaker line position, the surf zone width, and the mean sea level. In the downwave zone, the current generally follows the breakwater and the shore. Around the point where the breaking wave is the highest, there is a large counterclockwise cell near the shore. The corresponding mean sea level shows that little disturbance is felt near the breakwater. Near the breaker line, the mean sea level is lowest. As the longshore current is approached, the mean sea level contours become parallel to the shoreline. The streamline patterns for coefficients of friction of 0.01 and 0.09 are shown in Figures 12

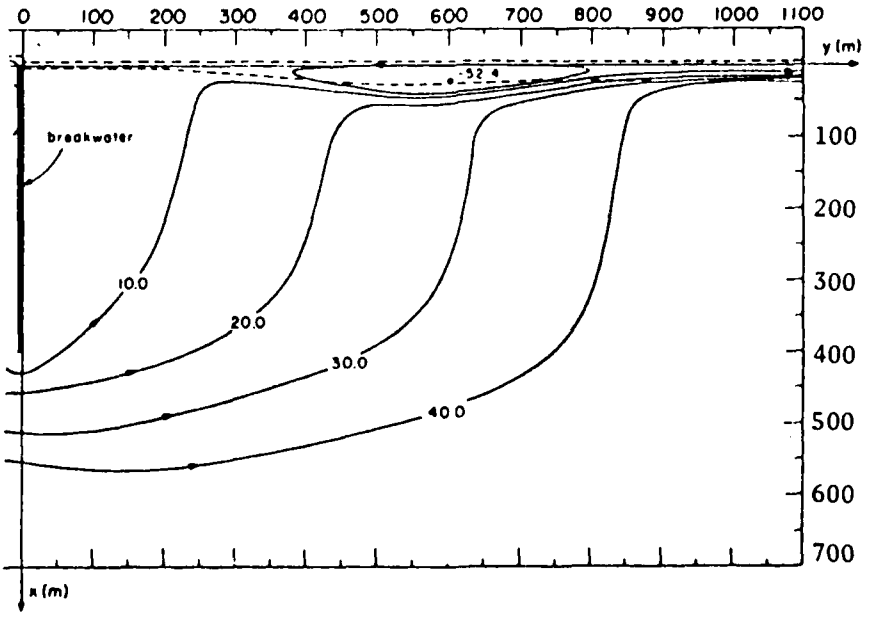

Figure 12. Streamline pattern, downwave region, C = 0.01 (after Liu and Mei 1975)

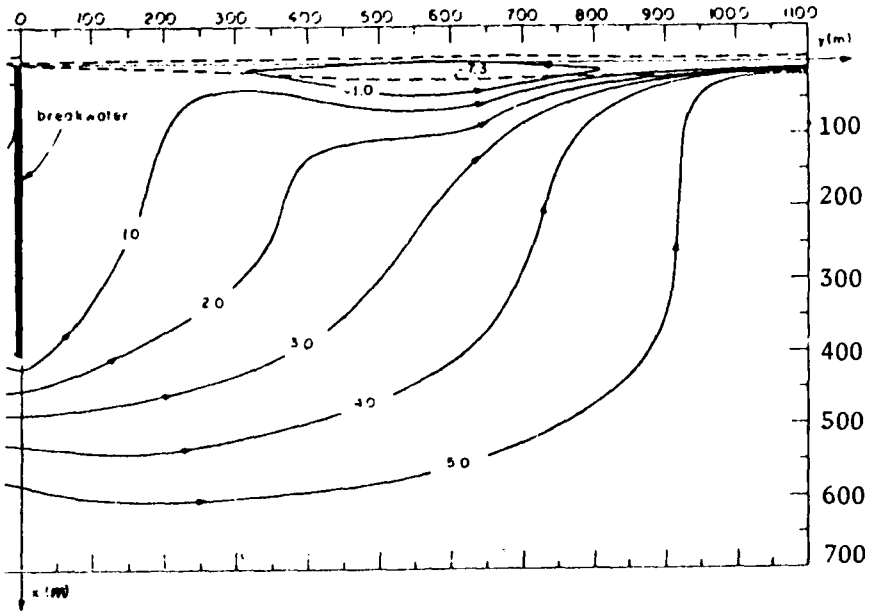

Figure 13. Streamline pattern, downwave region, C = 0.09 (after Liu and Mei 1975)

and 13, respectively, for the downwave region. Contours of mean sea level for the downwave region are shown in Figure 14.

38. Liu and Mei (1975) were not able to find any direct observation of currents comparable to the shore-connected breakwater problem which they had investigated analytically. The existing experiments at that time dealt largely with configurations of a harbor breakwater or a pair of inlet jetties. Short groins were not strictly relevant to the study of Liu and Mei (1975). For short groins, the diffraction effect could be overwhelmed by the inertial effect of the incoming longshore current which would be simply deflected seaward as a jet. Hence, cells near the shore should not be expected to form. To provide insight and gain a better understanding of the phenomena, the U. S. Army Engineer Waterways Experiment Station (WES) performed physical model investigations of a shore-connected single breakwater oriented perpendicular to the shoreline. Wave-height distributions, current magnitudes and patterns, and cell formations were determined and are described in PART IV.

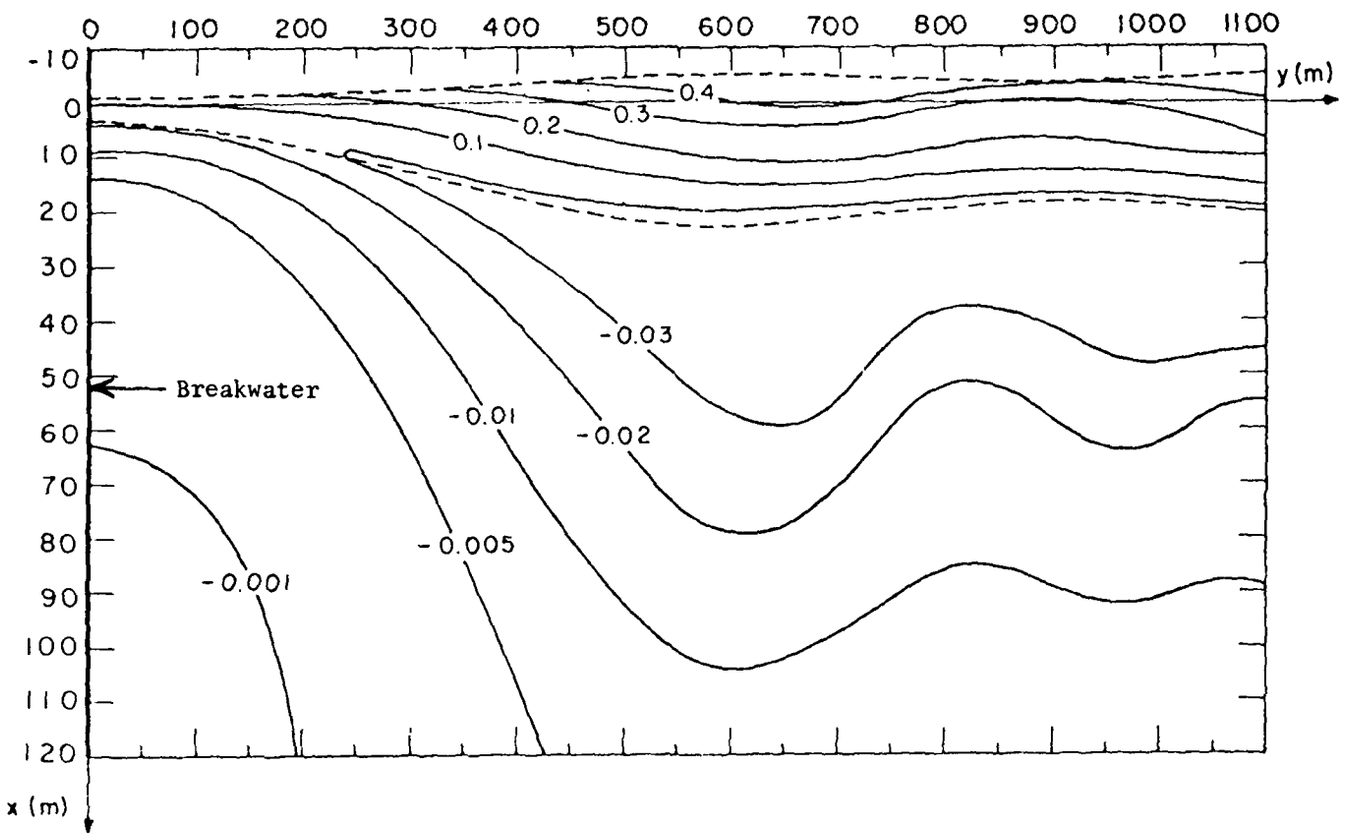

Figure 14. Contours of mean sea level, downwave region, C = 0.01
(after Liu and Mei 1975)

PART III: EXPERIMENTAL FACILITIES

Physical Model

39. This experimental investigation was conducted in the facilities of the Hydraulics Laboratory of WES. The physical model, which was molded in cement mortar, consisted of a 50- 60-ft area, with a water depth of 1 ft in the open-ocean region (Figure 15). The beach slope was 1V on 20H, with a vertical, impermeable breakwater extending perpendicularly from the shoreline for a distance of 15 ft to a point where the water depth was 0.75 ft. The uniform slope continued on to a water depth of 1 ft, beyond which the basin was horizontal to the facility walls. The wave generator was mobile, and two positions were tested (incident waves of 20 and 30 deg). Wave guides extended from the ends of the generator along wave orthogonals toward the shoreline. Orthogonals were determined by standard refraction techniques for waves propagating onto a uniform slope in the absence of the breakwater. The area of interest was downwave of the breakwater. Four sections perpendicular to the breakwater were instrumented with wave-height sensors for determination of the wave field. These sections were located 6, 8, 10, and 12 ft from the mean waterline (shoreline end of the breakwater), and are labeled "distance along the breakwater."

40. Model waves were generated by a 30-ft-long wave generator with a trapezoidal-shaped, vertical-motion plunger. The vertical movement of the plunger caused a periodic displacement of water surface. The length of stroke and the frequency of the vertical motion were variable over the range necessary to generate waves with the required characteristics. In addition, the wave generator was mounted on retractable casters which enabled it to be positioned to generate waves from the required directions. A 2-ft (horizontal) solid layer of fiber wave absorber was placed around the inside perimeter of the model to damp wave energy that might otherwise be reflected from the model walls.

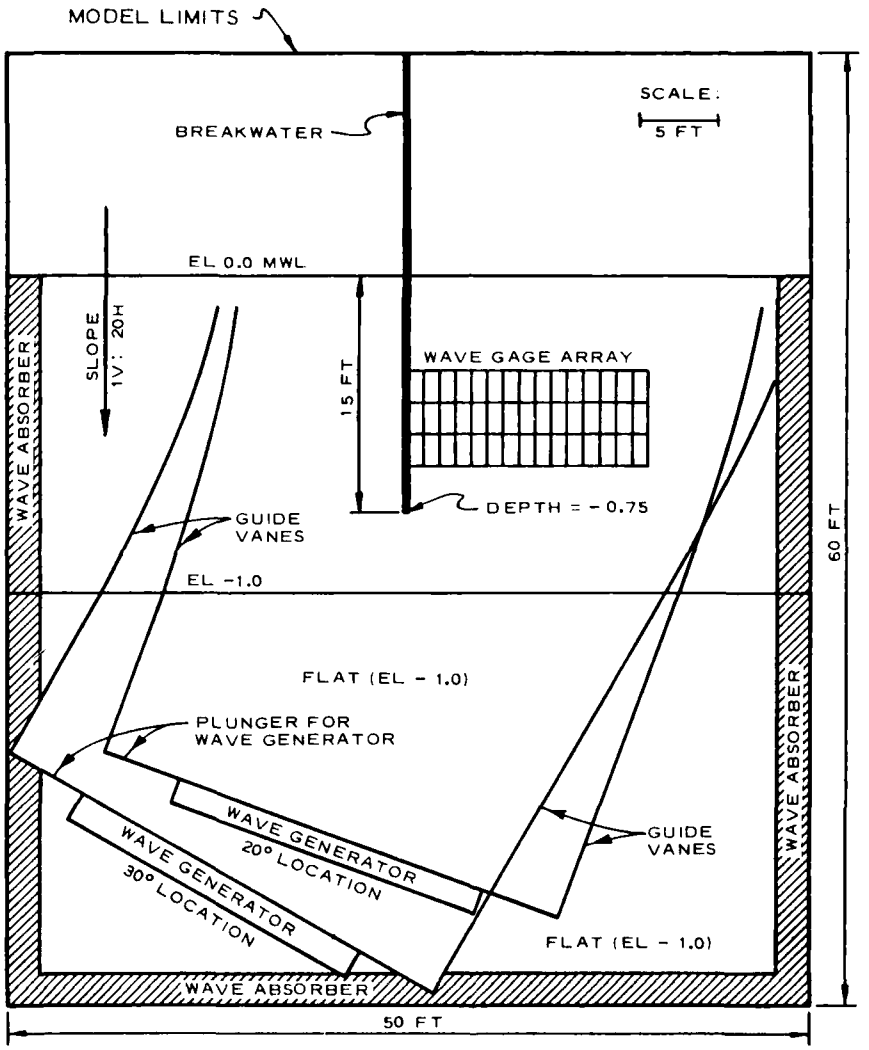

Figure 15. Experimental facility

Instrumentation for Wave-Height Determination

41. The increase in recent years in the number and complexity of wave model studies conducted by the Hydraulics Laboratory of WES and the use of such models to solve long-wave problems (requiring large model

areas) have demonstrated a need for automation of modeling procedures including operation, data collection, and data analysis (Durham and Greer 1976). Automated Data Acquisition and Control Systems (ADACS) have been designed and built at WES for the purpose of collecting wave data and controlling operations of hydraulic wave models. The computer hardware configuration for each system consists of a minicomputer with 32k 16-bit words of memory, a magnetic tape controller with two 9-track tape drives, one moving head disc controller with one removable platter and one nonremovable platter, an interval timer (1 μsec), an analog to digital 12-bit converter featuring 64 analog (±10 volts) inputs and a 45 kHz multiplexer, an ASR 33 teletype unit, 96 sense/control lines, and one matrix electrostatic printer/plotter.

42. The ADACS are capable of automatically calibrating the wave sensors, controlling wave generators, acquiring data from the sensors at a high sampling rate, and analyzing test data. Data are taken and recorded on disc or magnetic tape for direct analyses by the minicomputer system or on magnetic tape in a format compatible with a Honeywell G635 for backup analyses. Automatic calibration of wave sensors has reduced the time required to calibrate the sensors by a factor of four. In addition, several times the number of tests can be run during a day with test results analyzed at completion of model tests by minicomputer. The system configuration (Figure 16) of ADACS consists of the following subsystems: (a) digital data recording and controls, (b) analog recorders and channel selection circuits, (c) wave sensors and interfacing equipment, and (d) wave generators and control equipment.

Wave sensors

43. The data acquired from wave models are the water-surface variations about a reference water level. This information is collected at selected geographic locations within the model for specified wave conditions at the wave generator. Wave sensors are used to obtain this information at selected locations in the model. Each of the water-surface-piercing, parallel rod wave sensors is connected to a Wheatstone bridge and a transducer measures the conductance of the water between the two parallel rods which are mounted vertically

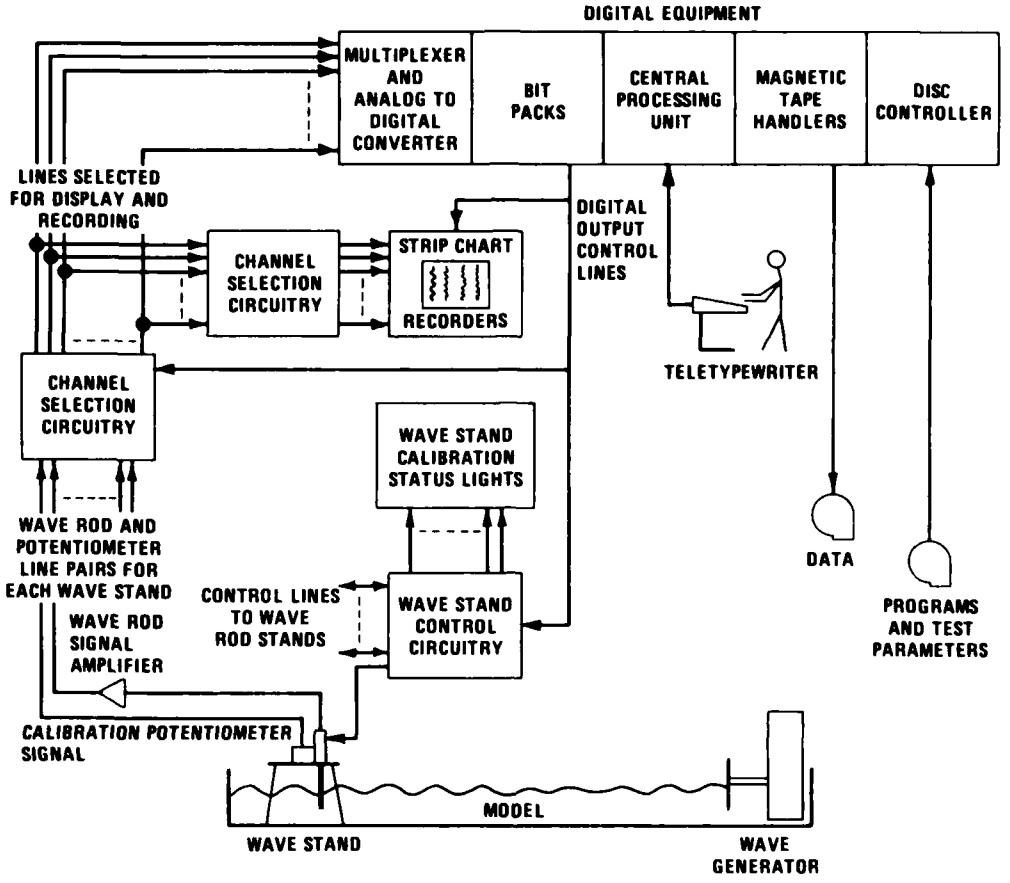

Figure 16. Schematic of components of Automated Data Acquisition and Control System (ADACS)

(Figure 17). The conductance is directly proportional to the depth of submergence of the two rods in the water. The output of each wave sensor, is routed through shielded cables to its signal conditioning equipment where it is processed for recording. The ADACS can detect changes in water-surface elevations to an accuracy of 0.001 ft. To obtain this accuracy, ultrastable power supplies and good signal-to-noise ratios are necessary. The carrier source for the wave sensor bridge maintains a variation of less than 0.025 percent.

Calibration

44. In order to convert the water-elevation data in millivolts to

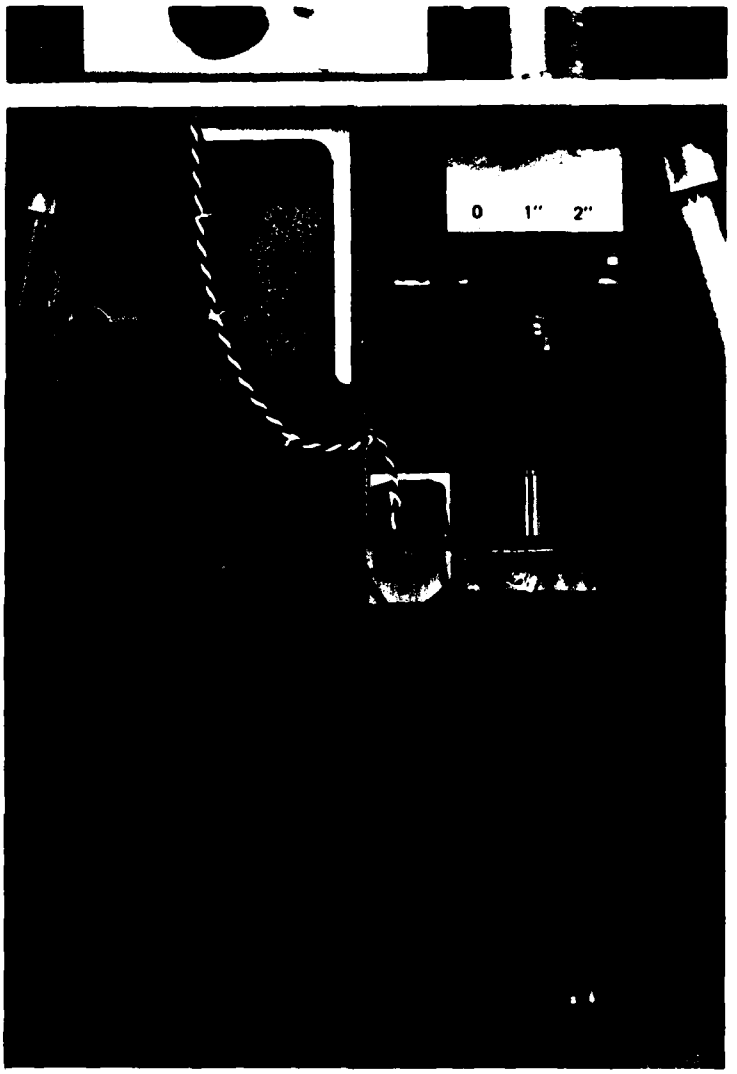

Figure 17. Parallel rod conductance-type wave sensor

water-surface elevations in feet, each wave sensor must be calibrated. The capability of automatically calibrating the wave sensors (maximum of 25 rods simultaneously) prior to collecting data is provided by ADACS. To calibrate each set of parallel rods, the voltage from the signal conditioning equipment is monitored and recorded as the parallel rods are moved vertically a known distance into or out of the water. A precision, linear-position potentiometer is located on the wave sensor stand and is coupled directly to the parallel rods by a gear train driven by electric

motor. By moving vertically the coupled wave sensor and potentiometer with the electric motor and by monitoring the output voltage from the potentiometer, the wave sensor can be moved vertically a precise distance. The electric motor for each wave sensor is controlled by a control/sense line and a relay contact. The minicomputer controls the vertical movement of each wave sensor by actuating the control/sense line. The central processing unit acts as a voltage comparator by monitoring the potentiometer voltage and comparing it with a reference voltage which is determined from desired displacement and potentiometer calibration. When the voltage comparison is satisfied, the control/sense line is reactivated, the electric motor stops, and voltage samples from the rods and potentiometers are acquired. By systematically moving each wave sensor through 11 quasi-equally spaced locations over the range of rod length used, voltage versus known displacements are obtained from which a calibration curve for each sensor can be calculated and recorded on magnetic tape or disc. After collecting the calibration data, the minicomputer analyzes these data by least-squares fitting a set of curves (linear, quadratic, or spline) to the data, determining the best order of fit, and comparing the maximum deviation of the best fit with a previously acceptable value for this maximum deviation.

Data acquisition and analysis

45. During the acquisition mode, wave data for a specified wave condition at the wave generator are collected from a maximum of 50 wave sensors, recorded on analog strip charts, digitized, and recorded on magnetic tape or disc for further analyses. The sampling scheme is flexible and can be tailored for different applications with maximum throughput rates theoretically limited by the multiplexer rate and allocatable buffer size. The sampling scheme used in this investigation was 60 discrete voltage samples equally spaced over each wave period for a predetermined number of 90 wave periods, for each of the sensor locations. The minicomputer calculated from input parameters the lag at the beginning of data acquisition by 10 wave periods after starting the generator, provided timing pulses for synchronizing and controlling the

recorders, and determined completion of the test. The determination of the height of each wave of the monochromatic wave train was performed (at each sensor location), the average of these 90 individual heights was calculated, and the standard deviation of these individual observations about the mean was computed. The value displayed as the wave height at each sensor location is this mean value plus or minus one standard deviation. The data were obtained by operating 32 wave-height sensors simultaneously for each test condition, and then repeating the same test with the sensors repositioned to allow better definition of wave-height gradients away from the breakwater. A typical arrangement of the 32 sensors near the breakwater is shown in Figure 18. Only the wave sensor probe penetrates the water surface, thereby minimizing local disturbances.

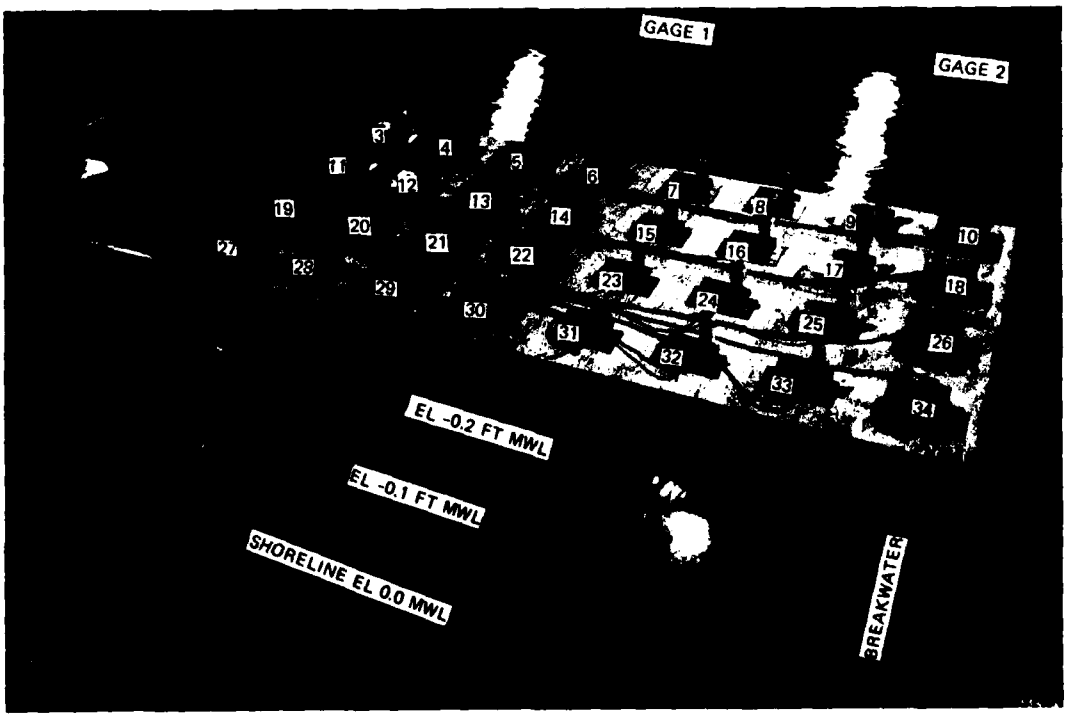

Figure 18. Wave-height sensor arrangement, grid spacing = 2 ft

Average Current Determination

46. To define the circulation patterns downwave of the breakwater, average values of wave-induced velocity were determined at those grid locations shown in Figure 19. The average values were determined at each individual station after the wave generator had been operating for 2 min so that the circulation cell immediately adjacent to the breakwater could become well established prior to measurements. After the measurement at either surface, middepth, or bottom had been obtained at each station, wave generator operation was terminated so that those fluid motions unique to the physical model (downcoast circulation cell induced by the boundary of the finite model area) would not have time to progress into the area of major interest (the immediate vicinity of the structure). It was known a priori that the existence of the downcoast boundary condition would preclude exact duplication of an infinite coastline; however, for the purpose of verifying various theories, numerical models can be formulated to represent a finite model area that includes all boundaries appropriately defined.

47. Surface current magnitudes were determined by timing a particle floating on the surface and initially positioned over the grid points. The time and direction required for each particle to traverse a distance of 1 ft was noted and recorded. Surface velocities were especially sensitive to wave orbital motions. Middepth velocities were determined by observing the movement of dye placed at one-half the still-water depth. While a measure of dispersion would tend to occur after a finite time interval, the center of the dye region could be easily ascertained; and this was the element considered in the average velocity determinations. Bottom current velocities and directions were determined by observing dye movement which had been placed essentially on the bottom of the model. Except for those regions in the breaker zone, the dye patterns on the bottom were more easily observable than those at middepth because downward dispersions were precluded. Hence, the dye region moved in a more concentrated form.

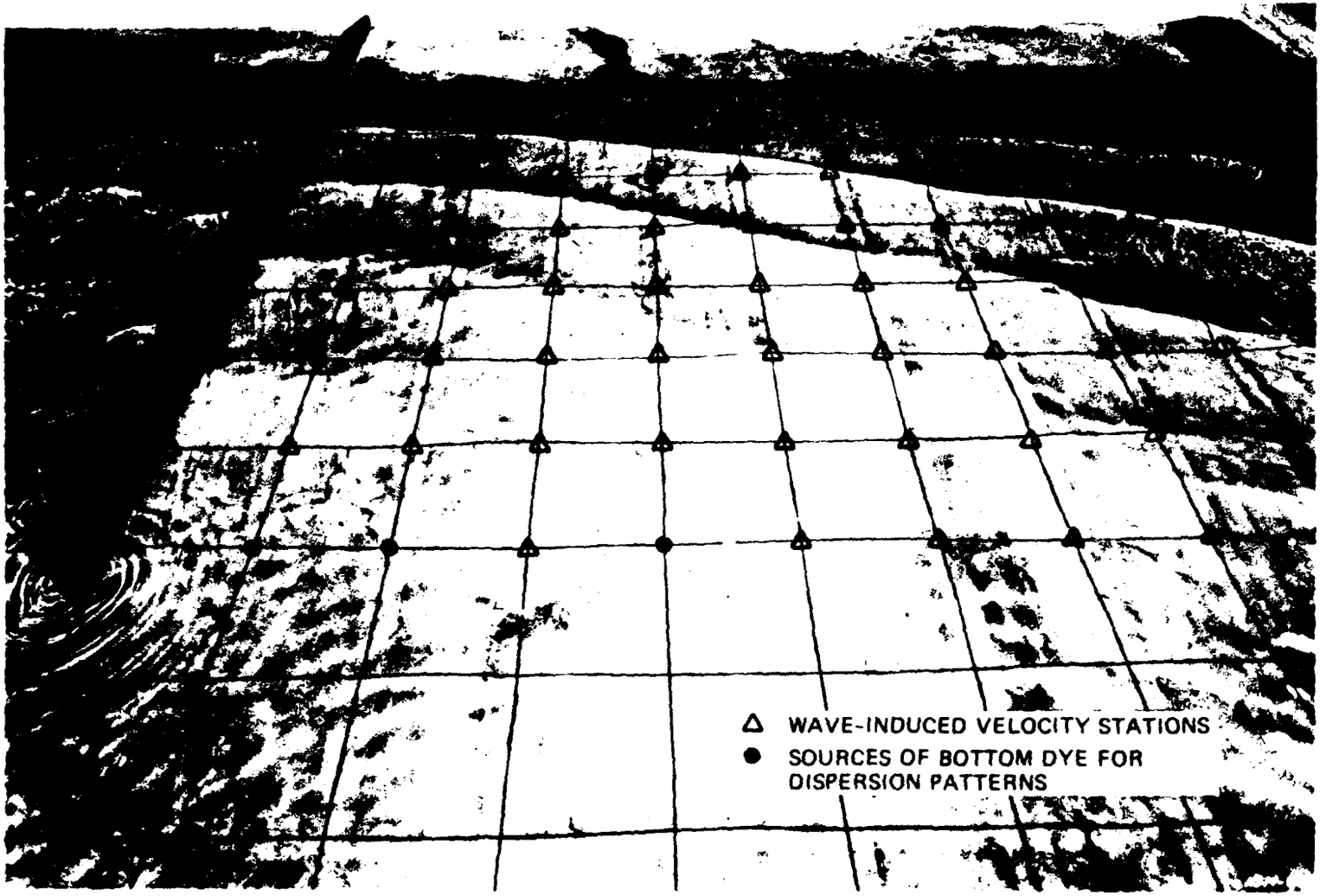

Figure 19. Stations for determining average wave-induced velocities

PART IV: RESULTS

Wave Heights

48. The experimental facility used in this study was constructed so that transition-to-shallow-water waves would exist near the breakwater (representative of prototype waves which are capable of causing scour and erosion). This requirement indicated that transition-depth waves should be generated, since physical model size and depth constraints precluded the generation of deepwater waves with required characteristics. In addition, the requirement existed that the generated wave heights should be large enough so that small changes in the heights could be detectable, and at the same time the heights should be small enough so that comparisons with linear theories could be performed. Preliminary tests indicated that for the area of major interest and for the range of wave periods considered pertinent, the specific test conditions shown in Table 1 could be experimentally investigated with height changes remaining essentially linear, thus permitting comparisons with theoretical developments.

49. Typical examples of the manner in which the wave profile transforms under the combined effects of refraction and diffraction are displayed in Figure 20 for a 1.00-sec wave approaching the breakwater from an incident direction of 20 deg. Positions of the two referenced gages are shown in Figure 21. Typical wave patterns covering the range of conditions tested from the 20 deg incident direction are shown in Photos 1-15. Wave-height amplification coefficients, H/H_o, for all conditions tested, are shown in Plates 1-48. Each plate constitutes a section perpendicular to the breakwater at distances from the shoreline of 6, 8, 10, or 12 ft, and depicts the average maximum wave height that occurred at each sensor location. The corresponding scatter of the experimental data is indicated by the error bars of plus-or-minus one standard deviation.

50. Thirty-four wave-height sensors were used to determine the wave heights along the four sections perpendicular to, and downwave of,

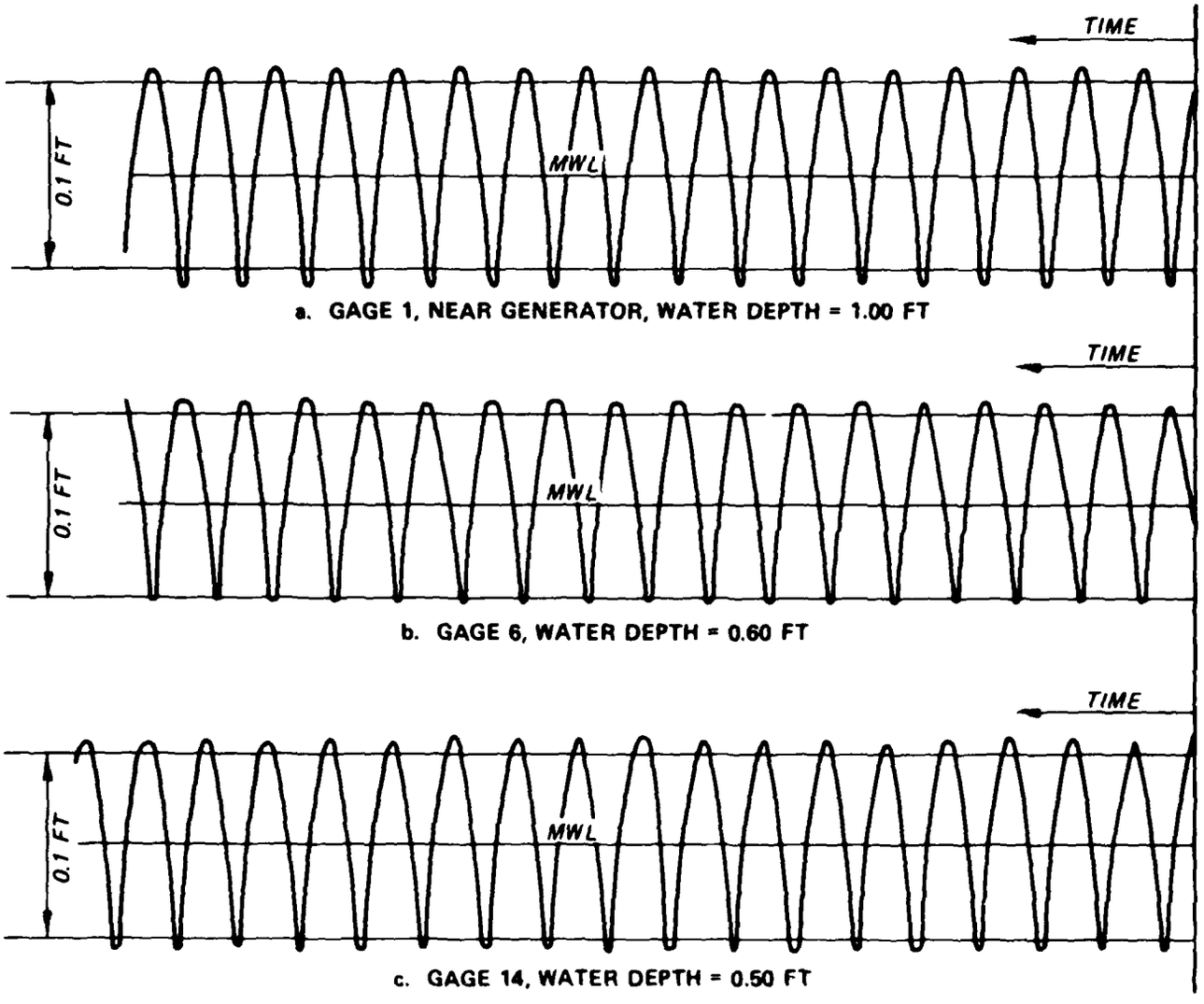

Figure 20. Typical wave form transformation after leaving generator, wave period = 1.00 sec, wave height near generator = 0.112 ft, approach angle of incidence = 20 deg

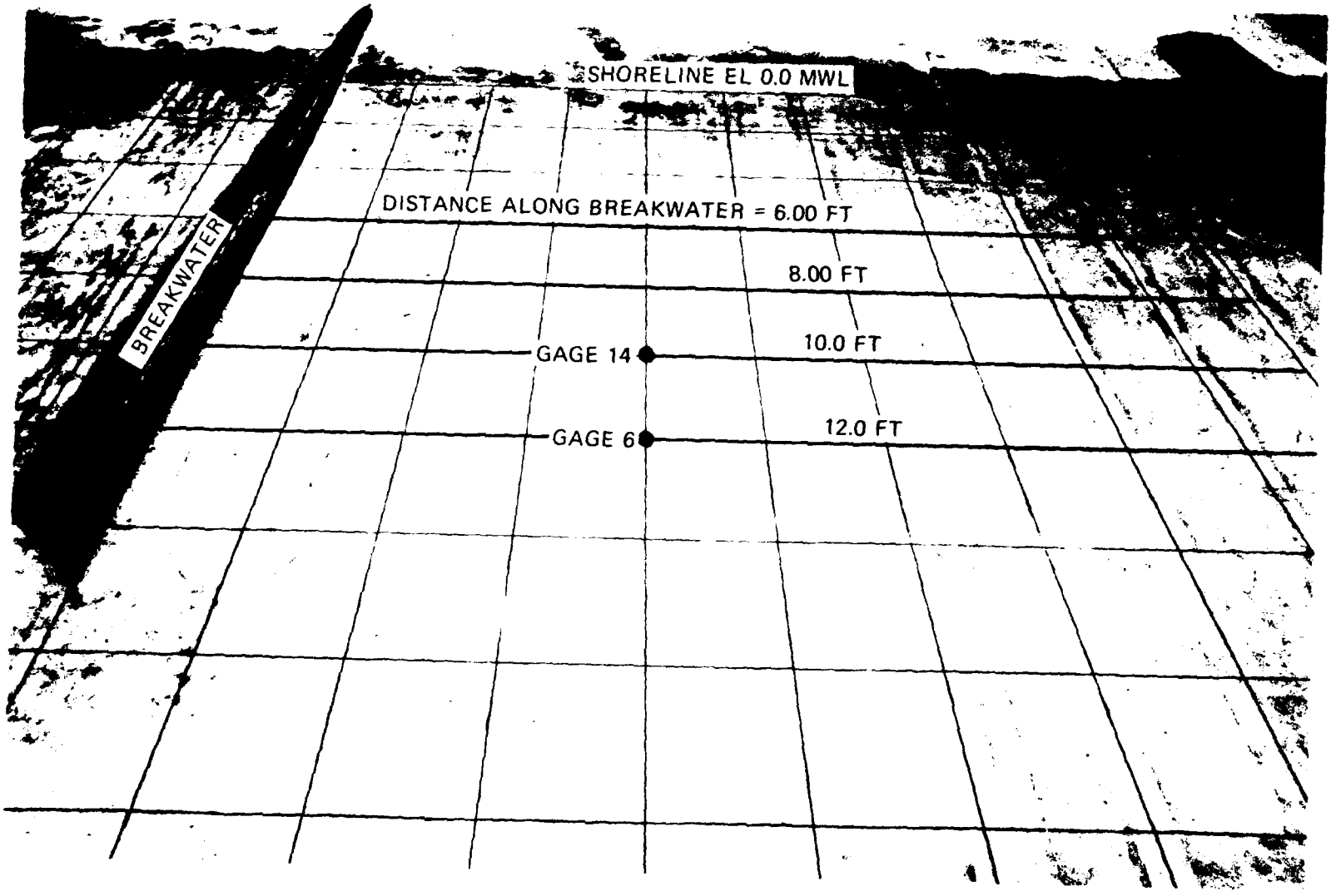

Figure 21. Location of gages 6 and 14

the vertical breakwater (eight gages along each section and two reference gages in the ocean region near the wave generator). The average of the heights recorded at the two ocean gages was selected to be the input wave height from the wave generator. The heights recorded at the remaining 32 gages were normalized to this input wave height. All 34 gages were recorded simultaneously with each individual reading at all data stations consisting of the average of 90 waves. Repeatability testing was conducted under identical test conditions to define the variability of the measurements. The numbers of replications varied from 3 to 10 and are shown in Table 2. The statistical measure of the variability was the square root of the variance, or the standard deviation. The variance is defined as the sum of the squares of the deviates of each individual observation from their average, divided by one less than the total number of deviates. The average of the ratios is displayed in Plates 1-48, with error bars showing plus or minus one standard deviation. One standard deviation is usually 2 to 3 percent of the average value of the observations. The data were originally obtained with the gages positioned at 2-ft intervals starting at the breakwater and extending to a location 14 ft from the breakwater (even number of feet from the breakwater in Table 2). To provide better definition of the wave field, the gages were repositioned at 2-ft intervals starting at a location 1 ft from the breakwater and extending to a location 15 ft from the structure (odd number of feet from the breakwater in Table 2). Also shown in Plates 1-20 are the wave heights determined by diffraction theory alone, based on the semigraphical constant depth procedure of CERC (1977). These were the only identical situations available for comparison. The fit is seen to be best at most locations for short-period waves. Agreement also is best at the seaward end of the breakwater, since refraction becomes more significant the farther the waves propagate toward the shoreline.

51. The incident wave heights generated in the model were sufficiently small such that the waves were usually linear within the measurement region shown in Figure 15. The degree of linearity is displayed in Tables 3-14 for representative replications of each different wave

characteristic (period, height, and direction of approach) tested. It was found that at the ocean gages on the average, 98.50 percent of the energy of the wave form exists at the generated period (fundamental frequency). Of the remaining 1.50 percent of the energy, 1.28 percent exists at the first harmonic. The distribution of the wave energy throughout the model for these representative experiments is displayed in Table 3-14 also. Here is seen the manner in which nonlinear effects are detectable as the wave propagates shoreward past the various gages. A portion of the energy of the wave form is redistributed from the fundamental frequency to higher harmonics, and only 95.25 percent of the energy exists (on the average) at the generated period. However, of the remaining 4.75 percent of the energy, 4.16 percent exists (on the average) at the first harmonic.

52. In the neighborhood of the breakwater, there were currents (described in the next section) that affected the wave heights. Opposing currents are known to produce significant increases in wave heights for relatively small values of current-to-wave velocity ratios. Since the magnitude of the currents is a function of the incident wave height, the ratio of measured wave height to incident wave height, H/H_o, is expected to be a function of the incident wave height wherever the current is strong. The effect of varying the incident wave height on H/H_o (defined as the amplification factor) was investigated, and it was determined that the greatest variation in H/H_o occurred in the deep shadow zone near the breakwater and shore region where currents were strongest. In both Figures 22 and 23 (for incident wave approach directions of 20 and 30 deg, respectively), the effect of initial wave height is seen to be greatest near the breakwater and at the sensor location 6 ft from the shoreline. The effect of incident angle is also apparent, with the more acute angle producing the greater degree of nonlinearity. The nonlinear effect diminishes rapidly away from the structure, and at a distance of 5 ft downwave appears to be relatively insignificant except for the extreme shadow region at acute angles of incidence.

Currents

53. The establishment of a counterclockwise circulation cell

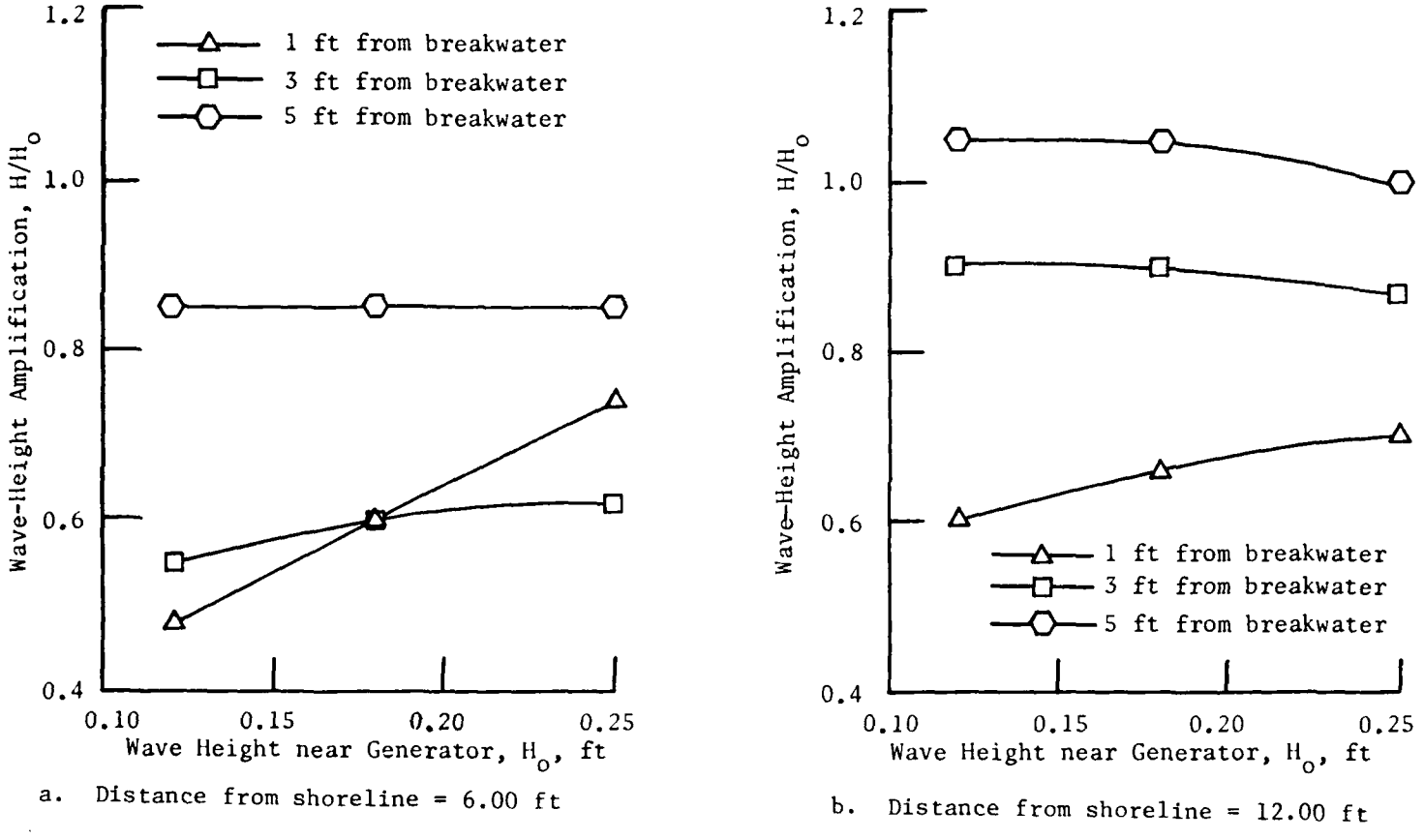

Figure 22. Effect of varying initial wave height at generator on wave-height amplification, H/H_o, at distances of 6 and 12 ft from shoreline; angle of incidence = 20 deg

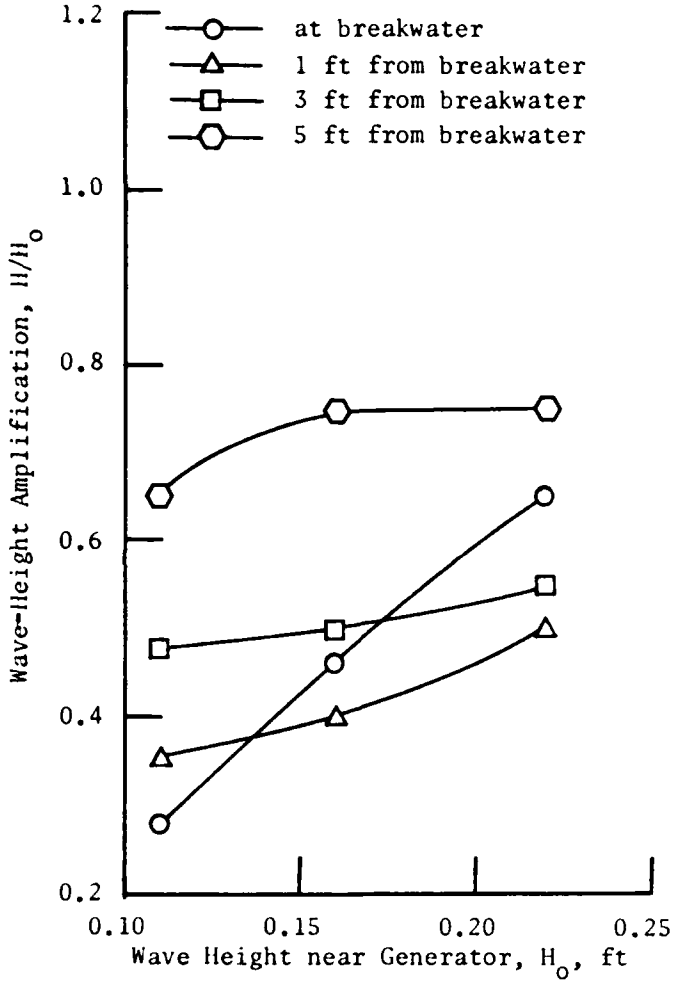

a. Distance from shoreline = 6.00 ft

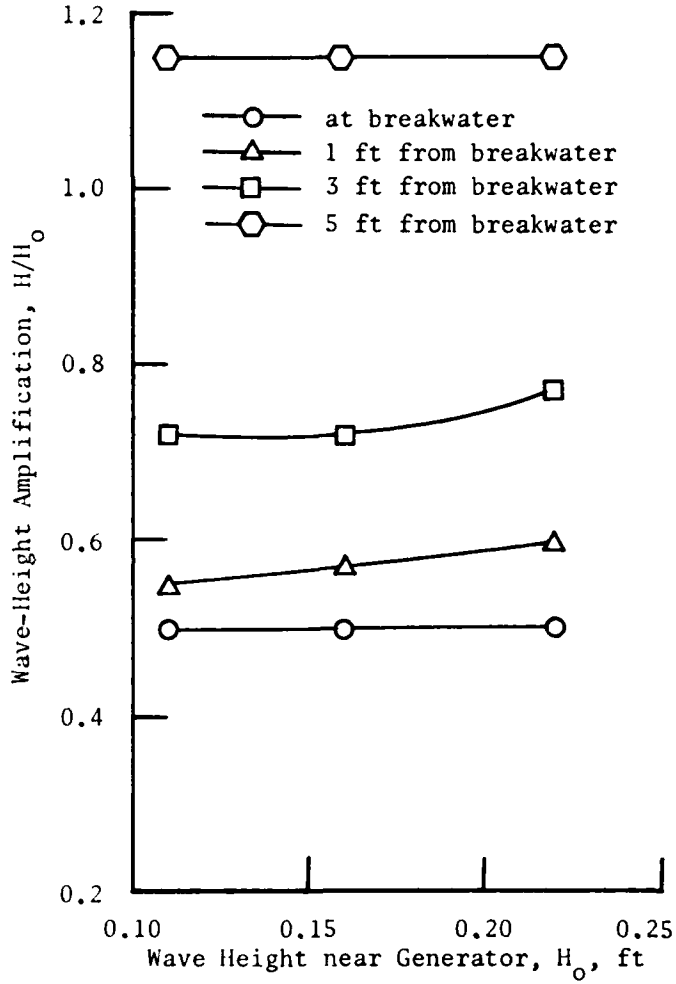

b. Distance from shoreline = 12.00 ft

Figure 23. Effect of varying initial wave height at generator on wave-height amplification, H/Ho , at distances of 6 and 12 ft from shoreline; angle of incidence = 30 deg

approximately 4 ft wide adjacent to the downwave side of the breakwater results in a seaward flowing current all along the breakwater. The bottom current is especially intense approximately 40 percent of the breakwater length from the shoreline, and decreases seaward along the structure as the water depth increases (since mass transport remains constant). Middepth velocities decrease seaward along the breakwater also, but remain approximately 35 percent of the maximum value even at the seaward end of the structure. The middepth, surface, and bottom velocity measurements are displayed in Plates 49-51, respectively. The model sidewall boundary is responsible for the creation of the clockwise circulation cell that develops as a result of mass transport downcoast by the longshore current. The numerical model of Liu and Mei (1975) considered an infinitely long coastline, and thus precluded the clockwise circulation pattern which developed in the physical model. However, the counterclockwise circulation expected, and indeed which occurred adjacent to the model breakwater, did not appear in the numerical computational procedures. A counterclockwise cell developed in the numerical model of Liu and Mei (1975) approximately a breakwater length downwave from the breakwater. At such a distance in the physical model, however, the sidewall effects begin to be encountered. Therefore, the physical model results for a finite section of beach should not be expected to be identical to numerical model results for an infinite section of beach. Numerical models can, however, be formulated that will represent the physical model boundary conditions, including the sidewall effects. The development of numerical techniques for determining wave characteristics and current magnitudes near structures is presently under way. These techniques incorporate combined refraction and diffraction, and the results of these experiments will be used to verify such numerical models. The middepth and bottom velocity profiles adjacent to the breakwater on the downwave side are shown in Figure 24 for a 1-sec wave of 0.139-ft height near the generator and approaching from an angle of incidence of 30 deg.

54. Coal tracer tests were conducted to obtain qualitative knowledge about the transport and dispersion mechanisms. A 1/2-in.-thick

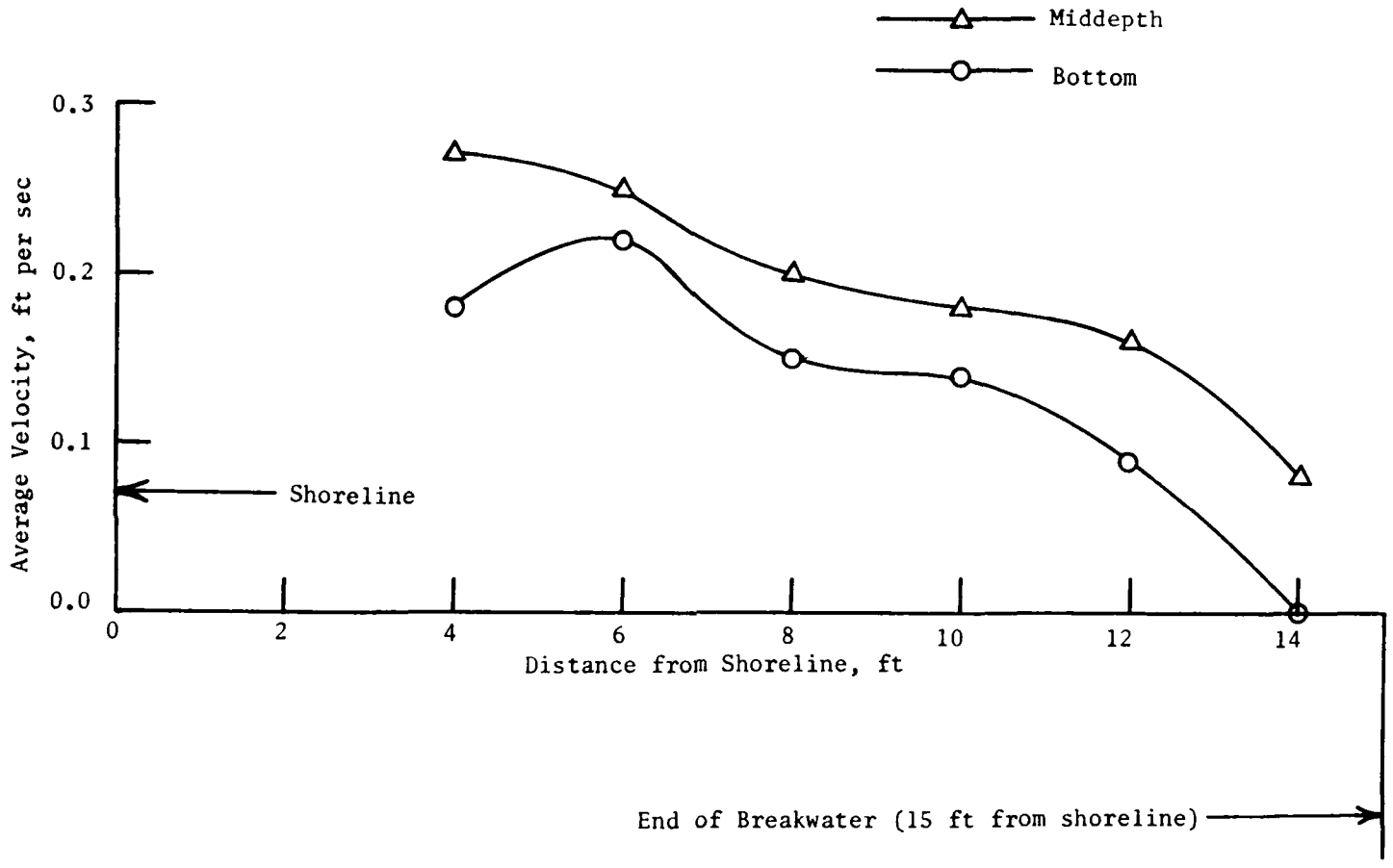

Figure 24. Middepth and bottom velocities adjacent to breakwater on downwave side, time after starting generator = 2.0 min, wave period = 1.0 sec, wave height near generator = 0.139 ft, angle of incidence = 30 deg

layer of crushed coal was placed in a 4-ft-wide section adjacent downwave and extending the length of the breakwater. The coal had a mean diameter of 1.89 mm, and varied in size from a maximum diameter of 3.35 mm to a minimum diameter of 0.43 mm. The model was operated continuously for 1 hr with a wave period of 1 sec, and the results are displayed in Figure 25. Significant movement appeared to have ceased after that time, and the dynamic balance between the incoming wave train and the return flow created by the circulation cell near the breakwater resulted in the configuration of Figure 25b.

55. Net fluid particle movement was visualized by a series of photographs of successive locations of bottom dye streaks originating from four locations on the bottom of the model. The dye placed at a distance of 4 ft laterally from the tip of the breakwater is seen in Photos 16-23 to move shoreward and become part of the development of the clockwise circulation cell associated with the downwave boundary. (A grid spacing of 2 ft is shown in these photographs.) Dye placed 2 ft laterally from the tip of the breakwater becomes part of the counterclockwise circulation cell near the breakwater. After the circulation cells had developed (Photos 21-23), dispersion of the dye upward from the bottom had had time to occur and the streaklines are less defined, although the upward dispersion is not necessarily associated with the cell formation. The dye movement patterns are in good agreement with the bottom velocity measurements shown in Plate 51. A circular wave pattern of reflected waves radiates outward from the tip of the breakwater, and is clearly evident in this series of photographs.

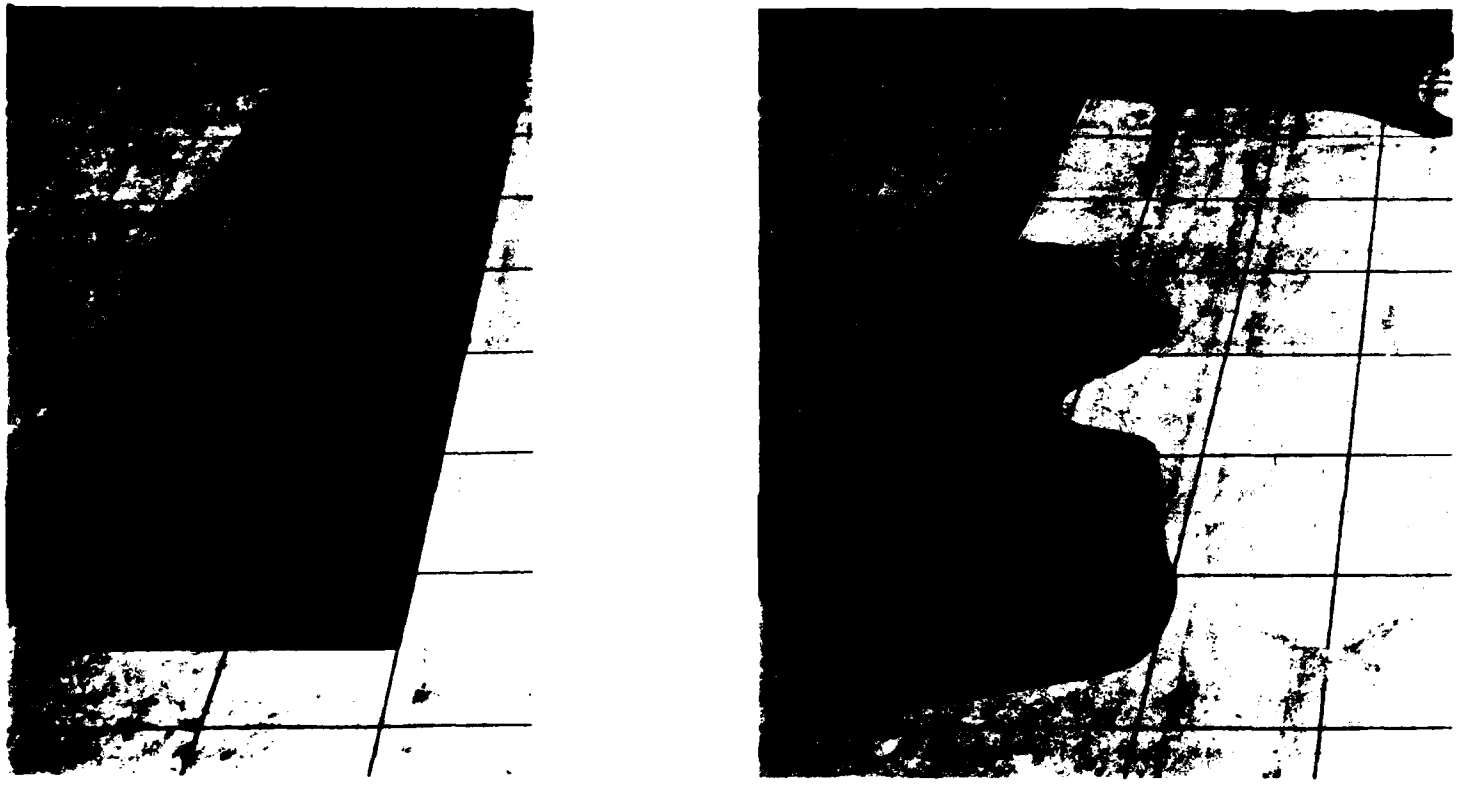

a. Before wave attack

b. After passage of 3,600 waves

Figure 25. Coal tracer tests, wave period = 1.0 sec, wave height near generator = 0.139 ft, angle of incidence = 30 deg, coal d_{50} = 1.89 mm

PART V: SUMMARY AND CONCLUSIONS

56. The purpose of this study was to obtain detailed and precise experimental data regarding wave-height variations and currents (patterns and magnitudes) downwave from a shore-connected breakwater or jetty under the simultaneous effects of refraction and diffraction. This information provides insight into the phenomenon of combined wave refraction and diffraction and can be used to verify numerical models that simulate this phenomenon. The experimental investigation was conducted in a wave basin that was molded in cement mortar and consisted of an area 50 ft x 60 ft with a water depth of 1 ft in the open-ocean region. A vertical, impermeable breakwater (shore-connected) extending perpendicularly from the shoreline was installed on a beach slope of 1V on 20H. Previous experimental studies had been conducted, for the most part, with horizontal bottoms which provided information only about the diffraction phenomenon (Blue and Johnson 1949, Wiegel 1962). One experimental study of extremely limited nature (very small model, 72 sq ft) had been conducted that propagated waves through a harbor entrance (normal angle of incidence) onto a linearly varying bathymetry. Results of that study by Mobarek (1962) indicated that as long as the incoming waves were within the transition-to-deepwater range, the rule-of-thumb procedure of refracting a wave to the structure, diffracting for a couple of wavelengths past the structure, and then refracting the diffracted wave shoreward was probably adequate for most applications. However, for long-period (shallow water) waves, the combined effects of refraction and diffraction should be considered simultaneously.

57. This experimental study used 34 wave-height sensors to ascertain the average maximum wave heights downwave of the shore-connected breakwater, with up to 10 replications of each individual experiment to quantify the experimental variability. The measurements were highly accurate with a standard deviation for repeated observations of usually 2 to 3 percent of the average value of the observations. A comparison of these experimental data of combined refraction and diffraction was made with analytical theories of diffraction alone for a shore-connected

breakwater on a horizontal bottom. As expected, the comparison was found to be best for short-period waves and for waves at the seaward end of the breakwater, since short-period waves experience less shoaling and refraction and these effects become more significant the farther the waves propagate toward the shoreline. The incident waves generated in the model were sufficiently small that the waves were usually linear within the measurement region.

58. In the neighborhood of the breakwater, currents existed that affected the wave heights. The magnitude of these wave-induced return currents is a function of incident wave characteristics. The effect of varying the incident wave height on the wave-height amplification factor, H/H_o, was investigated and it was determined that the greatest variation in H/H_o occurred in the deep shadow zone near the breakwater and shore region where the currents are the strongest. This nonlinear effect diminishes rapidly away from the structure, and at a distance of 5 ft downwave appears to be relatively insignificant except for the extreme shadow region at acute angles of incidence. The establishment of a counterclockwise circulation cell approximately 4 ft wide adjacent to the downwave side of the breakwater results in a seaward flowing current all along the breakwater. The bottom current is especially intense approximately 40 percent of the breakwater length from the shoreline and decreases seaward along the structure. The physical model sidewall boundary was responsible for a clockwise circulation cell which developed as a result of mass transport downcoast by the longshore current. Based on these experiments, any numerical techniques for describing scour and erosion near structures should account for wave-induced currents and circulation cells near the structure as well as tidal or other currents that may exist in the near region.

REFERENCES

Battjes, J. A. 1968 (Nov). "Refraction of Water Waves," Journal, Waterways and Harbors Division, American Society of Civil Engineers, Vol 94, No. WW4, pp 437-451.

Berkhoff, J. C. W. 1972 (Jul). "Computation of Combined Refraction-Diffraction," Proceedings, Thirteenth Conference on Coastal Engineering, Vol 1, pp 471-490, Vancouver, British Columbia, Canada.

Blue, F. L., Jr., and Johnson, J. W. 1949 (Oct). "Diffraction of Water Waves Passing Through a Breakwater Gap," Transactions, American Geophysical Union, Vol 30, No. 5, pp 705-718.

Bretschneider, C. L. 1954 (Sep). "Field Investigation of Wave Energy Loss in Shallow Water Ocean Waves," Technical Memorandum No. 46, U. S. Army Engineer Beach Erosion Board, Washington, D. C.

_____. 1966. "Wave Refraction, Diffraction, and Reflection," Chapter 6, Estuary and Coastline Hydrodynamics, A. T. Ippen, ed., McGraw-Hill Book Co., New York.

Carrier, G. F. 1966 (Apr). "Gravity Waves on Water of Variable Depth," Journal of Fluid Mechanics, Vol 24, Part 4, pp 641-659.

Chen, H. S., and Mei, C. C. 1974. "Oscillations and Wave Forces in an Offshore Harbor," Technical Report No. 190, Massachusetts Institute of Technology, Cambridge, Mass.

Dunham, J. W. 1951 (Oct). "Refraction and Diffraction Diagrams," Proceedings, First Conference on Coastal Engineering, Long Beach, Calif., pp 33-49.

Durham, D. L., and Greer, H. C., III. "Automated Data Acquisition and Control Systems for Hydraulic Models," Proceedings, 1976 Army Numerical Analysis and Computer Conference, St. Louis, Mo., pp 509-520.

Galvin, C. J., Jr., and Eagleson, P. S. 1965 (Jan). "Experimental Study of Longshore Currents on a Plane Beach," Technical Memorandum No. 10, U. S. Army Engineer Coastal Engineering Research Center, Washington, D. C.

Harms, V. K. 1979 (Dec). "Diffraction of Waves by Shore-Connected Breakwater," Journal, Hydraulics Division, American Society of Civil Engineers, Vol 105, No. HY12, pp 1501-1519.

Houston, J. R. 1980 (May). "Modeling of Shore Waves Using the Finite Element Method," Proceedings, Third International Conference on Finite Elements in Water Resources, Vol 2, pp 5.181-5.195, University of Mississippi, Oxford, Miss.

Inman, D. L., and Quinn, W. H. 1952 (Nov). "Currents in the Surf Zone," Proceedings, Second Conference on Coastal Engineering, Houston, Tex., pp 24-36.

Jonsson, I. G., and Brink-Kjaer, O. 1973. "A Comparison Between Two Reduced Wave Equations for Gradually Varying Depth," Technical Report No. 31, Technical University of Denmark.

Keller, J. B. 1958. "Surface Waves on Water of Non-Uniform Depth," Journal of Fluid Mechanics, Vol 4, pp 607-614.

Keulegan, G. H. 1950. "Wave Motion," Engineering Hydraulics, Wiley, New York, 1950.

Keulegan, G. H., and Patterson, G. W. 1940 (Jan). "Mathematical Theory of Irrotational Translation Waves," Journal of Research, National Bureau of Standards, Vol 24, No. 1, pp 47-101.

Koh, R. C. Y., and LeMehaute, B. 1966 (Apr). "Wave Shoaling," Journal of Geophysical Research, Vol 71, No. 8, pp 2005-2012.

Komar, P. D. 1979 (Nov). "Beach-Slope Dependence of Longshore Currents," Journal, Waterway, Port, Coastal and Ocean Division, American Society of Civil Engineers, Vol 105, No. WW4, pp 460-464.

Komar, P. D., and Inman, D. L. 1970 (Oct). "Longshore Sand Transport on Beaches," Journal of Geophysical Research, Vol 75, No. 30, pp 5914-5927.

Lick, W. 1978 (May). "Diffraction of Waves by a Wedge," Journal, Waterway, Port, Coastal and Ocean Division, American Society of Civil Engineers, Vol 104, No. WW2, pp 119-133.

Liu, P. L., and Lozano, C. J. 1979 (Mar). "Combined Wave Refraction and Diffraction," Proceedings, Coastal Structures 79, Alexandria, Va., Vol II, pp 978-997.

Liu, P. L., and Mei, C. C. 1975 (Nov). "Effects of a Breakwater on Nearshore Currents Due to Breaking Waves," Technical Memorandum No. 57, U. S. Army Engineer Coastal Engineering Research Center, Washington, D. C.

_____. 1976a (Jun). "Wave Motion on a Beach in the Presence of a Breakwater; 1, Waves," Journal of Geophysical Research, Vol 81, No. 18, pp 3079-3084.

_____. 1976b (Jun). "Wave Motion on a Beach in the Presence of a Breakwater; 2, Mean Currents," Journal of Geophysical Research, Vol 81, No. 17, pp 3085-3094.

Longuet-Higgins, M. C. 1970a (Nov). "Longshore Currents Generated by Obliquely Incident Sea Waves; 1," Journal of Geophysical Research, Vol 75, No. 33, pp 6778-6789.

_____. 1970b (Nov). "Longshore Currents Generated by Obliquely Incident Sea Waves; 2," Journal of Geophysical Research, Vol 75, No. 33, pp 6790-6801.

Longuet-Higgins, M. C., and Stewart, R. W. 1960 (Aug). "Changes in the Form of Short Gravity Waves on Long Waves and Currents," Journal of Fluid Mechanics, Vol 8, Part 4, pp 565-583.

Longuet-Higgins, M. C., and Stewart, R. W. 1961 (Jun). "The Changes in Amplitude of Short Gravity Waves on Steady Nonuniform Currents," Journal of Fluid Mechanics, Vol 10, Part 4, pp 529-549.

_____. 1964 (Nov). "Radiation Stresses in Water Waves; A Physical Discussion with Applications," Deep Sea Research, No. 11, pp 529-562.

Lundgren, H. 1962 (Jul). "The Concept of the Wave Thrust," Progress Report No. 3, Coastal Engineering Laboratory, Technical University of Denmark, pp 1-5.

Masch, F. D. 1964. "Cnoidal Waves in Shallow Water," Proceedings, Ninth Conference on Coastal Engineering, Lisbon, Portugal, pp 1-21.

Mei, C. C., Tlapa, G. A., and Eagleson, P. S. 1968 (Jul). "An Asymptotic Theory for Water Waves on Beaches of Mild Slope," Journal of Geophysical Research, Vol 73, No. 14, pp 4555-4561.

Mobarek, I. 1962 (Nov). "Effect of Bottom Slope on Wave Diffraction," Technical Report No. HEL-1-1, University of California, Berkeley, Calif.

Penny, W. G., and Price, A. T. 1944. "Diffraction of Sea Waves by Breakwaters," Technical History Report No. 26, Directorate of Miscellaneous Weapons Development, Washington, D. C.

Putnam, J. A., and Arthur, R. S. 1948. "Diffraction of Water Waves by Breakwaters," Transactions, American Geophysical Union, Vol 29, No. 4, pp 481-490.

Putnam, J. A., Munk, W. H., and Traylor, M. A. 1949. "The Prediction of Longshore Currents," Transactions, American Geophysical Union, Vol 30, pp 337-345.

Rayleigh, J. W. S. 1877. "On Progressive Waves," Proceedings, London Mathematical Society, Vol 9, pp 21-26.

Schonfeld, J. 1972. "Propagation of Two-Dimensional Short Waves," Delft University of Technology, Delft, the Netherlands.

Sommerfeld, A. 1896. "Mathematical Theory of Diffraction," Annals of Mathematics, Vol 47.

Smith, R., and Sprinks, T. 1975. "Scattering of Surface Waves by a Conical Island," Journal of Fluid Mechanics, Vol 72, pp 373-384.

Thornton, E. B. 1970 (Sep). "Variation of Longshore Currents Across the Surf Zone," Proceedings, Twelfth Conference on Coastal Engineering, Washington, D. C., pp 291-308.

U. S. Army Engineer Coastal Engineering Research Center, CE. 1977. Shore Protection Manual, Washington, D. C.

Whalin, R. W. 1972 (Jul). "Wave Refraction Theory in a Convergence Zone," Proceedings, Thirteenth Conference on Coastal Engineering, Vancouver, British Columbia, Canada, pp 451-470.

Wiegel, R. L. 1962 (Jan). "Diffraction of Waves by Semi-Infinite Breakwaters," Journal, Hydraulics Division, American Society of Civil Engineers, Vol 88, No. HY1, pp 27-44.

Table 1

Test Conditions

	Incident Wave Approach Direction				
	30-deg Direction		20-deg Direction		
Wave period, sec, =	0.75	1.00	0.75	1.00	1.50
Wavelength near generator, ft, =	2.82	4.52	2.82	4.52	7.69
d/L =	0.355	0.221	0.355	0.221	0.130
Wave height near generator, ft, = (Generator stroke = 0.50 in.)	0.111		0.122		
Wave height near generator, ft, = (Generator stroke = 0.75 in.)	0.164	0.101	0.180	0.112	
Wave height near generator, ft, = (Generator stroke = 1.00 in.)	0.221	0.139	0.245	0.154	0.077
Wave height near generator, ft, = (Generator stroke = 1.50 in.)					0.111

Table 2

Test Replications*

	Incident Wave Approach Direction				
	30-deg Direction		20-deg Direction		
Wave period, sec, =	0.75	1.00	0.75	1.00	1.50
Wavelength near generator, ft, =	2.82	4.52	2.82	4.52	7.69
d/L =	0.355	0.221	0.355	0.221	0.130
Wave height near generator, ft, =	0.111		0.122		
Gage arrangement 1**	10*				
Gage arrangement 2†	10*		5*		
Wave height near generator, ft, =	0.164	0.101	0.180	0.112	
Gage arrangement 1**	10*	10*	3*	3*	
Gage arrangement 2†	10*	10*	10*	10*	
Wave height near generator, ft, =	0.221	0.139	0.245	0.154	0.077
Gage arrangement 1**	5*	10*		3*	5*
Gage arrangement 2†	5*	10*	5*	10*	
Wave height near generator, ft, =					0.111
Gage arrangement 1**					3*
Gage arrangement 2†					

* Number of times identical tests were repeated to reduce experimental variability.

** Gages positioned 0, 2, 4, 6, 8, 10, 12, and 14 ft from (normal to) breakwater.

† Gages positioned 1, 3, 5, 7, 9, 11, 13, and 15 ft from (normal to) breakwater.

Table 3

Distribution of Wave Energy Throughout the Model, 30-deg Incident Direction, Period = 0.75 sec, Ocean Wave Height = 0.111 ft

Percent of Total Energy and Phase Angle (deg)

Gage	Fundamental Period 0.75 sec	First Harmonic 0.38 sec	Second Harmonic 0.25 sec	Third Harmonic 0.19 sec	Fourth Harmonic 0.15 sec
1*	99.91(-162)	0.08(+25)	0.01(+19)	0.00(-137)	0.00(-170)
2*	99.81(-177)	0.18(+27)	0.01(+12)	0.00(-136)	0.00(+59)
3	99.29(-151)	0.70(+60)	0.01(-87)	0.00(+103)	0.00(-64)
4	98.74(+74)	1.23(+149)	0.02(-112)	0.00(-9)	0.00(+101)
5	99.44(-57)	0.55(-108)	0.01(-102)	0.00(-167)	0.00(-32)
6	99.00(-170)	0.99(+23)	0.01(-116)	0.00(+61)	0.00(+167)
7	99.40(+67)	0.60(+140)	0.00(-53)	0.00(+147)	0.00(-50)
8	99.26(-69)	0.73(-150)	0.01(+144)	0.00(+83)	0.00(+73)
9	99.58(+159)	0.42(-19)	0.00(-158)	0.00(-154)	0.00(-44)
10	99.96(+76)	0.03(-141)	0.01(+17)	0.00(-149)	0.00(-45)
11	99.23(+94)	0.76(-171)	0.01(-59)	0.00(+40)	0.00(+121)
12	98.75(-35)	1.24(-67)	0.12(-64)	0.00(-142)	0.00(+154)
13	99.37(-165)	0.62(+41)	0.01(-95)	0.00(+3)	0.00(-178)
14	98.50(+86)	1.46(+161)	0.03(-115)	0.01(-11)	0.00(+83)
15	98.25(-60)	1.68(-112)	0.06(-152)	0.01(+170)	0.00(+165)
16	98.95(+168)	1.03(-32)	0.01(+130)	0.00(-64)	0.00(+110)
17	99.34(+65)	0.66(+137)	0.00(-23)	0.00(+113)	0.00(-154)
18	99.96(+2)	0.01(+33)	0.02(+108)	0.00(-58)	0.00(-76)
19	97.15(-12)	2.77(-25)	0.08(-35)	0.00(-28)	0.00(+75)
20	97.69(-128)	2.24(+100)	0.07(-38)	0.01(-149)	0.00(+152)
21	96.86(+115)	3.03(-134)	0.10(-17)	0.00(+118)	0.00(-40)
22	97.41(-16)	2.54(-38)	0.05(-52)	0.00(-48)	0.00(+25)
23	97.95(-156)	1.99(+44)	0.05(-109)	0.00(+119)	0.00(+11)
24	99.05(+84)	0.94(+149)	0.01(-176)	0.00(-119)	0.00(-5)
25	98.87(-9)	1.13(-24)	0.00(-48)	0.00(-149)	0.00(-148)
26	99.84(-59)	0.16(-152)	0.00(+99)	0.00(+23)	0.00(-63)
27	94.67(-68)	4.90(-146)	0.36(+140)	0.06(+87)	0.01(+61)
28	92.34(-175)	6.96(-1)	0.62(+178)	0.08(+21)	0.00(-115)
29	91.37(+45)	7.77(+76)	0.77(+119)	0.09(+176)	0.00(-129)
30	92.16(-88)	7.22(+175)	0.57(+85)	0.04(+13)	0.00(+25)
31	93.92(+136)	5.67(-96)	0.37(+38)	0.04(-174)	0.00(+12)
32	98.10(+37)	1.87(+73)	0.03(+126)	0.00(+113)	0.00(+119)
33	98.61(-54)	1.37(-120)	0.01(-145)	0.00(+93)	0.00(-0)
34	99.78(-90)	0.21(+172)	0.01(-144)	0.00(-130)	0.00(-145)

* Ocean gage.

Table 4

Distribution of Wave Energy Throughout the Model, 30-deg Incident Direction, Period = 0.75 sec, Ocean Wave Height = 0.164 ft

Percent of Total Energy and Phase Angle (deg)

Gage	Fundamental Period 0.75 sec	First Harmonic 0.38 sec	Second Harmonic 0.25 sec	Third Harmonic 0.19 sec	Fourth Harmonic 0.15 sec
1*	99.62(+67)	0.30(+158)	0.03(+23)	0.02(+128)	0.02(-156)
2*	99.93(+58)	0.03(+31)	0.00(+116)	0.03(-118)	0.00(-49)
3	98.22(-29)	1.68(-46)	0.09(-52)	0.01(-41)	0.00(+7)
4	98.64(-143)	1.32(+58)	0.03(-98)	0.01(-174)	0.00(+170)
5	97.41(+88)	2.40(-170)	0.17(-56)	0.02(+85)	0.00(-125)
6	96.87(-12)	2.91(-49)	0.20(-81)	0.02(-111)	0.00(+169)
7	96.18(-132)	3.39(+112)	0.36(+17)	0.07(-87)	0.00(+175)
8	97.62(+109)	2.15(-167)	0.21(-72)	0.02(+62)	0.00(+74)
9	99.20(+4)	0.73(-40)	0.06(-133)	0.02(-173)	0.00(-174)
10	99.03(-52)	0.78(-35)	0.17(-48)	0.02(-79)	0.00(-95)
11	96.10(-131)	3.66(+92)	0.20(-38)	0.04(-149)	0.00(+99)
12	97.84(+108)	2.10(-141)	0.05(+4)	0.01(+166)	0.00(-24)
13	94.61(-7)	4.92(-19)	0.43(-22)	0.04(-15)	0.00(-71)
14	97.26(-121)	2.63(+114)	0.09(+13)	0.01(-60)	0.00(-36)
15	94.56(+116)	4.99(-130)	0.40(-4)	0.05(+139)	0.00(+68)
16	98.09(+5)	1.79(+3)	0.11(-1)	0.01(-4)	0.00(+101)
17	98.72(-84)	1.16(+144)	0.10(+5)	0.02(-92)	0.00(+161)
18	99.96(-117)	0.04(-32)	0.00(+45)	0.00(-121)	0.00(+43)
19	96.06(+133)	3.69(-107)	0.23(+20)	0.02(-165)	0.00(+113)
20	92.96(+22)	6.43(+39)	0.57(+74)	0.04(+116)	0.00(+112)
21	94.45(-103)	5.28(+146)	0.26(+42)	0.01(-24)	0.00(+111)
22	90.03(+132)	8.89(-100)	1.00(+32)	0.07(+172)	0.01(-98)
23	95.28(+14)	4.42(+18)	0.27(+30)	0.02(+65)	0.00(-27)
24	97.22(-81)	2.63(-178)	0.14(+87)	0.01(+10)	0.00(-78)
25	98.02(-152)	1.94(+14)	0.04(-175)	0.00(+7)	0.00(-171)
26	99.64(-169)	0.31(-54)	0.04(+81)	0.01(-30)	0.00(+121)
27	87.58(+65)	10.83(+126)	1.46(-171)	0.14(-98)	0.00(-46)
28	86.90(-51)	11.26(-114)	1.65(-171)	0.16(+128)	0.04(+35)
29	80.76(+170)	15.73(+56)	2.86(+134)	0.50(-67)	0.15(+77)
30	85.36(+60)	12.47(+106)	1.95(+164)	0.19(-137)	0.03(-114)
31	89.89(-49)	9.07(-102)	0.91(-149)	0.13(-177)	0.00(+176)
32	95.04(-117)	4.67(+101)	0.26(-40)	0.03(-173)	0.00(+77)
33	97.63(+173)	2.25(-63)	0.11(+70)	0.01(+178)	0.00(-1)
34	98.69(+171)	1.30(-59)	0.01(+31)	0.01(+129)	0.00(-33)

* Ocean gage.

Table 5

Distribution of Wave Energy Throughout the Model, 30-deg Incident Direction, Period = 0.75 sec, Ocean Wave Height = 0.221 ft

Percent of Total Energy and Phase Angle (deg)

Gage	Fundamental Period 0.75 sec	First Harmonic 0.38 sec	Second Harmonic 0.25 sec	Third Harmonic 0.19 sec	Fourth Harmonic 0.15 sec
1*	98.03(-87)	1.63(-141)	0.29(-174)	0.05(+105)	0.00(+105)
2*	99.49(-73)	0.48(-179)	0.03(+32)	0.00(+103)	0.00(-39)
3	96.62(+177)	3.25(-12)	0.12(+172)	0.01(+58)	0.00(+48)
4	92.90(+41)	6.44(+77)	0.60(+123)	0.05(+165)	0.01(+163)
5	95.82(-98)	3.79(-173)	0.35(+136)	0.04(+80)	0.00(+44)
6	94.56(+151)	4.92(-73)	0.47(+65)	0.04(-155)	0.01(-43)
7	94.24(+20)	5.31(+52)	0.40(+105)	0.05(+157)	0.00(+122)
8	95.02(-102)	4.60(+148)	0.35(+53)	0.01(-46)	0.01(+150)
9	96.56(+164)	3.18(-55)	0.23(+108)	0.03(-53)	0.00(-154)
10	97.73(+118)	2.19(-112)	0.06(-5)	0.01(+128)	0.00(-72)
11	92.23(+55)	6.80(+113)	0.84(+175)	0.11(-119)	0.03(-92)
12	96.05(-76)	3.81(-146)	0.11(-178)	0.03(+173)	0.00(-100)
13	91.37(+152)	7.61(-65)	0.87(+83)	0.11(-137)	0.03(-3)
14	91.71(+27)	7.47(+56)	0.72(+103)	0.08(+143)	0.02(+128)
15	92.90(-101)	6.57(+149)	0.48(+47)	0.03(-71)	0.02(+153)
16	94.90(+154)	4.62(-70)	0.45(+78)	0.03(-120)	0.00(-41)
17	97.17(+75)	2.66(+137)	0.13(-157)	0.04(-39)	0.00(+54)
18	96.88(+48)	2.86(+117)	0.24(+179)	0.02(-120)	0.01(-60)
19	93.00(-54)	6.48(-106)	0.49(-148)	0.03(-166)	0.00(+15)
20	87.63(+174)	10.82(-27)	1.33(+137)	0.17(-72)	0.06(+84)
21	85.85(+31)	11.86(+62)	1.80(+94)	0.04(+117)	0.01(+137)
22	89.21(-88)	9.63(+170)	1.06(+74)	0.08(-32)	0.02(-159)
23	92.98(+149)	6.48(-62)	0.49(+102)	0.04(-99)	0.01(+12)
24	95.48(+74)	4.19(+122)	0.31(+171)	0.02(-84)	0.00(+7)
25	96.32(+2)	3.50(-11)	0.16(-23)	0.01(-14)	0.00(+15)
26	95.79(-3)	3.86(+13)	0.29(+34)	0.05(+46)	0.01(+51)
27	83.14(-145)	14.17(+60)	2.26(-98)	0.34(+94)	0.09(-81)
28	78.60(+81)	16.72(+142)	3.57(-159)	0.79(-111)	0.32(-67)
29	82.84(-62)	14.74(-145)	1.98(+125)	0.33(+15)	0.11(-91)
30	77.44(-168)	17.58(+9)	3.82(-171)	0.88(+2)	0.28(+167)
31	84.45(+82)	13.40(+154)	1.87(-123)	0.22(-44)	0.05(+8)
32	94.29(+26)	5.32(+54)	0.36(+99)	0.03(+156)	0.00(-91
33	94.35(-26)	5.20(-68)	0.40(-109)	0.05(-127)	0.01(-125)
34	92.11(-29)	7.36(-60)	0.44(-84)	0.08(-96)	0.01(-95)

* Ocean gage.

Table 6

Distribution of Wave Energy Throughout the Model, 30-deg Incident Direction, Period = 1.00 sec, Ocean Wave Height = 0.101 ft

Percent of Total Energy and Phase Angle (deg)

Gage	Fundamental Period 1.00 sec	First Harmonic 0.50 sec	Second Harmonic 0.33 sec	Third Harmonic 0.25 sec	Fourth Harmonic 0.20 sec
1*	98.87(+130)	0.77(+178)	0.23(-125)	0.11(-14)	0.02(+114)
2*	99.42(+134)	0.23(+174)	0.22(-145)	0.11(-18)	0.03(+105)
3	98.96(+129)	1.03(-157)	0.00(-126)	0.00(-42)	0.00(+86)
4	97.95(+49)	2.02(+127)	0.02(+167)	0.00(+95)	0.00(+178)
5	97.52(-31)	2.46(-99)	0.02(-178)	0.00(+78)	0.00(+9)
6	99.66(-111)	0.26(+147)	0.07(+159)	0.01(+58)	0.00(+2)
7	97.07(+172)	2.84(-5)	0.09(-155)	0.01(+66)	0.00(-144)
8	97.96(+88)	1.95(+160)	0.06(+144)	0.02(-164)	0.01(-85)
9	99.43(+27)	0.43(-13)	0.13(+14)	0.00(+44)	0.00(-84)
10	99.90(+4)	0.10(+115)	0.00(+110)	0.00(+157)	0.00(-178)
11	95.53(-57)	4.41(-133)	0.05(+170)	0.01(+95)	0.00(+61)
12	99.61(-139)	0.37(+54)	0.01(-159)	0.00(+52)	0.00(-21)
13	96.30(+140)	3.59(-76)	0.11(+49)	0.00(+169)	0.00(-56)
14	96.58(+60)	3.26(+89)	0.12(+109)	0.03(+133)	0.00(-178)
15	98.95(-19)	1.03(-46)	0.01(-161)	0.01(+172)	0.00(+125)
16	99.32(-97)	0.61(-174)	0.06(-169)	0.01(+119)	0.00(+65)
17	97.47(-147)	2.49(+78)	0.01(+107)	0.03(-28)	0.00(-135)
18	98.12(-160)	1.85(+12)	0.02(+167)	0.00(-134)	0.00(+69)
19	95.16(+121)	4.65(-111)	0.17(+27)	0.01(+150)	0.00(-79)
20	95.02(+51)	4.66(+70)	0.29(+111)	0.03(+154)	0.00(-144)
21	96.02(-36)	3.82(-80)	0.16(-126)	0.01(+176)	0.00(-160)
22	92.75(-116)	6.70(+117)	0.50(-7)	0.04(-142)	0.01(+119)
23	95.80(+164)	4.01(-52)	0.17(+111)	0.01(-108)	0.01(+69)
24	97.66(+90)	2.03(+145)	0.30(-130)	0.01(-44)	0.00(+20)
25	99.64(+55)	0.33(+96)	0.02(-39)	0.01(+4)	0.00(+115)
26	99.67(+45)	0.32(+114)	0.01(+20)	0.01(+31)	0.00(+110)
27	89.24(-14)	9.52(-51)	1.08(-81)	0.14(-97)	0.03(-97)
28	82.63(-96)	14.39(+142)	2.48(+33)	0.43(-74)	0.07(-171)
29	87.19(+174)	11.11(+38)	1.41(+118)	0.25(-78)	0.04(+96)
30	88.20(+92)	10.37(+168)	1.21(-109)	0.18(-23)	0.04(+83)
31	90.84(+16)	8.36(+24)	0.72(+27)	0.07(+31)	0.01(+47)
32	91.39(-32)	8.40(-78)	0.20(-138)	0.00(+142)	0.01(+85)
33	93.99(-74)	5.79(-173)	0.19(+98)	0.02(-35)	0.01(-179)
34	96.13(-85	3.75(+157)	0.12(+64)	0.00(-100)	0.00(+96)

* Ocean gage.

Table 7

Distribution of Wave Energy Throughout the Model, 30-deg Incident Direction, Period = 1.00 sec, Ocean Wave Height = 0.139 ft

Percent of Total Energy and Phase Angle (deg)

Gage	Fundamental Period 1.00 sec	First Harmonic 0.50 sec	Second Harmonic 0.33 sec	Third Harmonic 0.25 sec	Fourth Harmonic 0.20 sec
1*	99.23(+127)	0.65(+126)	0.09(+124)	0.03(-115)	0.01(+52)
2*	99.77(+126)	0.14(+31)	0.05(+22)	0.03(+141)	0.00(-41)
3	97.70(+111)	2.27(-100)	0.03(+15)	0.00(-115)	0.00(-139)
4	94.44(+35)	5.30(+53)	0.25(+60)	0.02(+76)	0.00(+134)
5	99.25(-43)	0.64(-111)	0.08(+63)	0.03(+11)	0.00(+7)
6	96.35(-120)	3.55(+133)	0.08(+61)	0.01(-4)	0.00(-86)
7	96.15(+164)	3.77(-51)	0.08(+108)	0.00(-52)	0.00(+121)
8	99.53(+76)	0.36(+123)	0.09(+43)	0.02(+140)	0.00(-148)
9	98.44(+10)	1.53(+38)	0.02(-154)	0.01(-104)	0.00(-56)
10	99.39(-14)	0.58(+3)	0.03(-53)	0.00(-25)	0.00(-86)
11	98.51(-75)	1.40(+172)	0.08(+76)	0.01(+29)	0.00(-11)
12	96.78(-157)	3.02(+68)	0.19(-84)	0.01(+160)	0.00(+7)
13	92.87(+130)	6.39(-121)	0.66(-2)	0.08(+122)	0.01(-100)
14	97.63(+49)	2.27(+84)	0.09(+98)	0.01(+146)	0.00(-86)
15	95.76(-32)	4.03(-46)	0.20(-82)	0.02(-129)	0.00(-89)
16	96.65(-111)	3.08(+125)	0.23(+28)	0.04(-75)	0.01(-162)
17	98.53(-168)	1.42(+28)	0.04(-93)	0.01(+156)	0.00(+70)
18	99.06(+178)	0.92(-15)	0.02(+129)	0.00(-113)	0.00(+105)
19	90.76(+104)	8.37(-178)	0.73(-77)	0.11(+37)	0.02(+163)
20	95.46(+31)	4.18(+48)	0.33(+77)	0.04(+116)	0.00(+176)
21	88.63(-51)	10.09(-112)	1.13(-167)	0.14(+145)	0.01(+103)
22	87.97(-127)	10.32(+79)	1.42(-58)	0.25(+168)	0.03(+38)
23	96.86(+150)	3.06(-76)	0.06(+79)	0.01(-109)	0.01(+83)
24	96.65(+76)	3.34(+150)	0.01(-94)	0.00(+159)	0.00(-134)
25	97.80(+37)	2.13(+71)	0.07(+86)	0.00(+45)	0.00(+82)
26	97.91(+24)	2.08(+57)	0.01(+9)	0.00(+115)	0.00(-43)
27	73.48(-39)	20.34(-108)	4.83(-161)	1.14(+148)	0.21(+95)
28	78.23(-121)	17.16(+88)	3.85(-52)	0.68(+171)	0.08(+21)
29	76.35(+151)	18.64(+112)	4.07(+70)	0.81(-142)	0.13(-1)
30	74.13(+74)	20.00(+130)	4.57(-165)	10.96(-97)	0.21(-29)
31	83.78(+4)	14.30(-19)	1.65(-32)	0.24(-38)	0.03(-32)
32	92.30(+49)	6.95(-121)	0.65(+164)	0.09(+103)	0.01(+45)
33	94.90(-94)	4.92(+145)	0.17(+30)	0.00(-63)	0.00(+135)
34	95.88(-103)	3.89(+126)	0.23(-19)	0.01(-124)	0.00(+31)

* Ocean gage.

Table 8

Distribution of Wave Energy Throughout the Model, 20-deg Incident Direction, Period = 0.75 sec, Ocean Wave Height = 0.122 ft

Percent of Total Energy and Phase Angle (deg)

Gage	Fundamental Period 0.75 sec	First Harmonic 0.38 sec	Second Harmonic 0.25 sec	Third Harmonic 0.19 sec	Fourth Harmonic 0.15 sec
1*	99.93(+110)	0.02(+102)	0.02(+61)	0.02(+102)	0.00(-180)
2*	99.57(+149)	0.36(-108)	0.05(+23)	0.02(-170)	0.00(-91)
3	98.14(-119)	1.74(+163)	0.10(+86)	0.01(-2)	0.00(-79)
4	99.09(+161)	0.86(-61)	0.04(+64)	0.01(-118)	0.00(+75)
5	97.86(+67)	2.07(+150)	0.07(-113)	0.01(-0)	0.01(+131)
6	98.42(-21)	1.54(-59)	0.03(-114)	0.00(-144)	0.00(+77)
7	99.63(-101)	0.37(+147)	0.00(-105)	0.00(+122)	0.00(+48)
8	97.26(+164)	2.64(-24)	0.10(+148)	0.00(-28)	0.00(-108)
9	98.49(+70)	1.34(+118)	0.14(+172)	0.03(-103)	0.00(-1)
10	99.88(+10)	0.09(+105)	0.02(-135)	0.00(-58)	0.00(-63)
11	97.81(+157)	2.05(-38)	0.13(+148)	0.01(-49)	0.00(+126)
12	98.83(+67)	1.16(+114)	0.01(+125)	0.00(-159)	0.00(-105)
13	97.64(-18)	2.27(-26)	0.09(-28)	0.01(-28)	0.00(+30)
14	97.77(-106)	2.11(+129)	0.10(+1)	0.01(-93)	0.00(+179)
15	99.24(+170)	0.76(-27)	0.01(+123)	0.00(-22)	0.00(+178)
16	97.11(+66)	2.70(+145)	0.17(-139)	0.03(-64)	0.00(+91)
17	97.31(-15)	2.64(-43)	0.05(-65)	0.00(-60)	0.00(-67)
18	99.69(-60)	0.29(-171)	0.02(+24)	0.01(-49)	0.00(-81)
19	95.27(+73)	4.43(+138)	0.27(-148)	0.02(-41)	0.00(-76)
20	97.95(-11)	2.01(-25)	0.03(-14)	0.01(-47)	0.00(+81)
21	96.20(-99)	3.58(+162)	0.20(+72)	0.01(-9)	0.00(-75)
22	96.70(+174)	3.19(-28)	0.10(+132)	0.01(-54)	0.00(+162)
23	97.67(+83)	2.25(+166)	0.08(-100)	0.00(+26)	0.00(+113)
24	96.28(-22)	3.49(-43)	0.20(-61)	0.03(-64)	0.00(-22)
25	97.24(-86)	2.64(+175)	0.12(+72)	0.01(-29)	0.00(-102)
26	98.96(-119)	1.03(+80)	0.01(+86)	0.00(-151)	0.00(+80)
27	91.29(+27)	8.03(+35)	0.62(+54)	0.05(+92)	0.00(+179)
28	91.63(-57)	7.45(-118)	0.80(-172)	0.11(+144)	0.00(+115)
29	90.62(+147)	8.43(+89)	0.75(-92)	0.09(+133)	0.11(+1)
30	92.75(+123)	6.83(-120)	0.39(+2)	0.03(+140)	0.00(-93)
31	89.96(+23)	8.97(+41)	0.94(+67)	0.12(+102)	0.00(+143)
32	93.64(-66)	5.83(-141)	0.48(+147)	0.05(+93)	0.00(+65)
33	96.12(-122)	3.68(+88)	0.19(-50)	0.01(+171)	0.00(+58)
34	98.42(-147)	1.56(+37)	0.02(-157)	0.00(+59)	0.00(-35)

* Ocean gage.

Table 9

Distribution of Wave Energy Throughout the Model, 20-deg Incident Direction, Period = 0.75 sec, Ocean Wave Height = 0.180 ft

Percent of Total Energy and Phase Angle (deg)

Gage	Fundamental Period 0.75 sec	First Harmonic 0.38 sec	Second Harmonic 0.25 sec	Third Harmonic 0.19 sec	Fourth Harmonic 0.15 sec
1*	99.27(+68)	0.63(+70)	0.04(+59)	0.05(-3)	0.01(+49)
2*	96.88(+107)	2.90(-171)	0.18(-54)	0.03(+99)	0.01(-129)
3	98.06(+124)	1.83(-147)	0.11(-66)	0.00(+41)	0.00(+52)
4	96.37(+21)	3.22(+50)	0.34(+101)	0.06(+135)	0.00(+114)
5	97.47(-53)	2.37(-149)	0.16(+131)	0.00(+46)	0.00(-77)
6	99.19(-143)	0.68(+97)	0.09(+49)	0.02(-68)	0.02(-147)
7	95.15(+139)	4.34(-71)	0.45(+86)	0.06(-112)	0.00(+105)
8	94.67(+56)	4.78(+93)	0.50(+144)	0.05(-137)	0.00(-136)
9	97.00(-17)	2.60(-86)	0.36(-125)	0.04(-126)	0.00(-120)
10	99.48(-41)	0.50(-125)	0.02(+124)	0.01(-145)	0.00(+155)
11	97.77(+14)	2.09(+44)	0.12(+103)	0.02(+161)	0.00(-87)
12	93.88(-68)	5.56(-147)	0.52(+141)	0.05(+86)	0.00(-29)
13	98.40(-151)	1.57(+40)	0.02(-168)	0.01(-115)	0.00(+158
14	94.56(+123)	4.95(-99)	0.41(+59)	0.06(-147)	0.00(+63)
15	92.82(+42)	6.44(+73)	0.67(+119)	0.07(+172)	0.01(+174)
16	96.17(-41)	3.52(-100)	0.29(-147)	0.02(-173)	0.00(+63)
17	96.95(-100)	2.75(+108)	0.26(-19)	0.04(-95)	0.00(-176)
18	98.56(-112)	1.39(+106)	0.05(-64)	0.01(+150)	0.00(+9)
19	91.23(-60)	7.86(-125)	0.81(-177)	0.09(+145)	0.00(+60)
20	95.25(-154)	4.59(+47)	0.16(-108)	0.00(+157)	0.00(+176)
21	93.72(+121)	5.70(-111)	0.52(+30)	0.06(+170)	0.00(-107)
22	90.49(+40)	8.23(+62)	1.10(+96)	0.14(+128)	0.03(+133)
23	94.48(-45)	5.16(-113)	0.34(+179)	0.01(+105)	0.01(-6)
24	95.12(-125)	4.54(+86)	0.33(-58)	0.01(-161)	0.00(-87)
25	97.77(-170)	2.09(-21)	0.14(+124)	0.01(-37)	0.00(-172)
26	97.51(-168)	2.32(+12)	0.13(-178)	0.03(+14)	0.01(-139)
27	88.47(-120)	10.33(+105)	1.10(-20)	0.09(-136)	0.01(+60)
28	82.35(+145)	14.75(-78)	2.49(+64)	0.34(-159)	0.08(-37)
29	84.25(+65)	13.37(+109)	2.09(+159)	0.23(-161)	0.06(-139)
30	84.42(-35)	13.26(-75)	1.98(-111)	0.27(-149)	0.07(+154)
31	85.23(-114)	12.69(+130)	1.88(+23)	0.19(-79)	0.02(+138)
32	94.57(-173)	5.08(+6)	0.31(-163)	0.03(+75)	0.01(-33)
33	97.22(+159)	2.65(-78)	0.12(+31)	0.00(+175)	0.00(+26)
34	95.33(+160)	4.46(-57)	0.18(+84)	0.02(-119)	0.01(+89)

* Ocean gage.

Table 10

Distribution of Wave Energy Throughout the Model, 20-deg Incident Direction, Period = 0.75 sec, Ocean Wave Height = 0.245 ft

Percent of Total Energy and Phase Angle (deg)

Gage	Fundamental Period 0.75 sec	First Harmonic 0.38 sec	Second Harmonic 0.25 sec	Third Harmonic 0.19 sec	Fourth Harmonic 0.15 sec
1*	97.71(-79)	1.93(-103)	0.27(-107)	0.07(-127)	0.02(-134)
2*	95.44(-24)	3.74(-79)	0.66(-137)	0.13(+153)	0.03(+111)
3	98.59(+19)	1.40(+12)	0.00(-34)	0.01(-175)	0.00(-100)
4	90.28(-89)	8.62(+177)	0.98(+89)	0.10(-13)	0.03(-126)
5	97.92(+170)	1.99(-9)	0.06(-107)	0.03(+114)	0.00(+30)
6	88.98(+83)	9.50(+165)	1.24(-105)	0.21(-21)	0.07(+48)
7	94.42(+2)	5.10(-18)	0.41(-51)	0.05(-117)	0.02(-141
8	94.81(-84)	4.84(-149)	0.31(+172)	0.03(+129)	0.00(-125)
9	94.37(-167)	5.05(+49)	0.51(-74)	0.07(+155)	0.00(+15)
10	95.39(+139)	3.75(-44)	0.76(+122)	0.09(-80)	0.01(+105)
11	89.71(-92)	8.89(+175)	1.10(+90)	0.22(-6)	0.08(-115)
12	96.33(+167)	3.58(-46)	0.07(+103)	0.02(+81)	0.01(-100)
13	89.92(+75)	8.84(+147)	1.03(-136)	0.16(-62)	0.05(-7)
14	94.47(-18)	5.27(-56)	0.22(-100)	0.04(+124)	0.01(+103)
15	93.30(-103)	6.13(+172)	0.51(+101)	0.06(+36)	0.00(-100)
16	87.51(+171)	10.83(-22)	1.40(+150)	0.17(-48)	0.08(+11)
17	88.53(+101)	9.68(-150)	1.47(-36)	0.27(+75)	0.05(+159)
18	92.30(+63)	6.54(+153)	0.97(-115)	0.17(-28)	0.02(+65)
19	92.08(+172)	7.36(-30)	0.52(+126)	0.03(-102)	0.02(+42)
20	87.04(+76)	11.22(+147)	1.45(-145)	0.20(-80)	0.09(-24)
21	88.57(-25)	10.22(-59)	1.06(-88)	0.11(-124)	0.04(-165)
22	86.40(-122)	12.09(+121)	1.38(+4)	0.11(-120)	0.02(+88)
23	86.02(+160)	12.02(-56)	1.57(+88)	0.33(+115)	0.06(+32)
24	90.69(+69)	8.56(+139)	0.68(-138)	0.04(-48)	0.02(-21)
25	90.50(+27)	8.45(+36)	0.95(+52)	0.09(+72)	0.02(+56)
26	89.11(+4)	8.96(+18)	1.61(+14)	0.29(+18)	0.03(+14)
27	79.53(+104)	16.56(-167)	3.11(-81)	0.57(-4)	0.24(+66)
28	85.79(+2)	12.17(-24)	1.68(-51)	0.30(-106)	0.06(-139)
29	75.67(+88)	18.92(+140)	4.05(+19)	0.95(-114)	0.41(+105)
30	82.85(+159)	14.46(-72)	2.19(+54)	0.41(+160)	0.10(-90)
31	79.36(+71)	17.15(+126)	2.85(+176)	0.48(-144)	0.18(-114)
32	82.51(+10)	14.65(+12)	2.29(+19)	0.43(+25)	0.13(+18)
33	91.50(-17)	7.87(-46)	0.61(-72)	0.02(-65)	0.00(+114)
34	88.99(-17)	9.51(-55)	1.32(-91)	0.17(-117)	0.01(-166)

* Ocean gage.

Table 11

Distribution of Wave Energy Throughout the Model, 20-deg Incident Direction, Period = 1.00 sec, Ocean Wave Height = 0.112 ft

Percent of Total Energy and Phase Angle (deg)

Gage	Fundamental Period 1.00 sec	First Harmonic 0.50 sec	Second Harmonic 0.33 sec	Third Harmonic 0.25 sec	Fourth Harmonic 0.20 sec
1*	99.06(-177)	0.74(+57)	0.20(-104)	0.00(+71)	0.00(+57)
2*	98.31(-154)	1.58(+78)	0.11(-148)	0.01(+86)	0.00(-25)
3	98.57(+170)	1.38(-70)	0.04(+67)	0.00(-123)	0.00(-95)
4	99.49(+109)	0.50(-88)	0.01(+159)	0.00(+24)	0.00(-122)
5	97.40(+55)	2.57(+116)	0.03(+130)	0.00(+67)	0.00(+141)
6	98.95(+2)	0.98(-33)	0.07(-72)	0.00(-73)	0.00(-120)
7	99.77(-57)	0.22(-94)	0.00(-107)	0.00(+164)	0.00(+131)
8	99.08(-112)	0.84(+154)	0.07(+88)	0.01(+25)	0.00(-30)
9	97.80(-158)	2.15(+47)	0.03(+113)	0.01(-76)	0.00(+118)
10	99.41(-172)	0.54(+19)	0.05(-65)	0.01(+146)	0.00(-20)
11	95.33(-16)	4.54(-29)	0.12(-22)	0.01(+45)	0.00(+47)
12	97.14(-65)	2.82(-165)	0.04(+136)	0.00(-142)	0.00(+178)
13	99.53(-122)	0.44(+122)	0.02(+113)	0.01(-0)	0.00(-117)
14	97.05(-177)	2.88(+5)	0.06(-123)	0.01(+130)	0.00(-68)
15	96.99(+122)	2.99(-131)	0.01(-68)	0.00(-46)	0.00(+61)
16	98.88(+71)	1.07(+107)	0.04(+121)	0.00(+151)	0.00(+178)
17	99.55(+34)	0.31(+79)	0.13(-140)	0.01(-112)	0.00(-140)
18	99.33(+21)	0.63(+42)	0.04(+115)	0.00(+172)	0.00(+43)
19	97.58(-179)	2.40(+6)	0.02(+163)	0.01(-95)	0.00(+128)
20	92.19(+131)	7.47(-112)	0.33(+27)	0.01(+130)	0.00(-41)
21	94.65(+76)	5.24(+120)	0.11(+179)	0.01(-166)	0.00(-5)
22	96.85(+13)	3.09(+15)	0.04(-18)	0.01(-61)	0.00(-51)
23	96.87(-47)	2.91(-90)	0.20(-133)	0.02(+114)	0.00(+82)
24	95.20(-97)	4.76(+160)	0.04(+86)	0.00(+95)	0.00(+7)
25	97.88(-127)	2.09(+85)	0.03(-25)	0.00(-79)	0.00(-128)
26	98.14(-132)	1.81(+27)	0.05(+114)	0.00(-74)	0.00(+23)
27	86.53(+40)	11.47(+49)	1.67(+69)	0.28(+95)	0.06(+135)
28	87.48(-12)	11.14(-41)	1.21(-66)	0.15(-83)	0.02(-76)
29	82.13(-136)	15.57(+120)	1.95(+114)	0.31(+42)	0.04(-16)
30	84.25(-132)	13.39(+70)	1.94(-80)	0.36(+131)	0.06(+4)
31	91.61(+171)	7.65(-49)	0.67(+111)	0.06(-82)	0.02(+107)
32	94.48(+127)	5.14(-118)	0.36(-12)	0.01(+89)	0.00(-152)
33	94.73(+103)	5.18(-170)	0.09(-50)	0.00(-154)	0.00(-149)
34	96.77(+98)	3.19(+179)	0.01(+79)	0.03(+171)	0.00(-120)

* Ocean gage.

Table 12

Distribution of Wave Energy Throughout the Model, 20-deg Incident Direction, Period = 1.00 sec, Ocean Wave Height = 0.154 ft

Percent of Total Energy and Phase Angle (deg)

Gage	Fundamental Period 1.00 sec	First Harmonic 0.50 sec	Second Harmonic 0.33 sec	Third Harmonic 0.25 sec	Fourth Harmonic 0.20 sec
1*	96.87(+11)	3.09(+32)	0.01(-124)	0.03(-167)	0.01(+177)
2*	97.32(+36)	2.43(+99)	0.20(+99)	0.03(+151)	0.02(-131)
3	98.84(-8)	1.14(+13)	0.00(-5)	0.01(-144)	0.00(+165)
4	95.11(-67)	4.69(-137)	0.17(+134)	0.02(+68)	0.01(+39)
5	96.96(-121)	2.73(+81)	0.28(-75)	0.03(+144)	0.00(+41)
6	99.61(-173)	0.33(-22)	0.04(-168)	0.02(+15)	0.00(+125)
7	98.01(+129)	1.82(-91)	0.14(+102)	0.02(-89)	0.01(+68)
8	96.51(+74)	3.32(+160)	0.14(-145)	0.02(-86)	0.00(+47)
9	96.17(+31)	3.82(+38)	0.00(+104)	0.00(-80)	0.00(-6)
10	98.94(+19)	1.03(+9)	0.03(+34)	0.00(+150)	0.00(-108)
11	97.01(+169)	2.81(-54)	0.15(+114)	0.02(-50)	0.00(+150)
12	97.44(+114)	2.42(-123)	0.11(+7)	0.02(+145)	0.00(-77)
13	93.71(+59)	5.82(+129)	0.41(-152)	0.04(-63)	0.02(+29)
14	91.82(+7)	7.76(+1)	0.38(-5)	0.03(-12)	0.01(+40)
15	96.50(-54)	3.16(-126)	0.29(+158)	0.05(+94)	0.00(+66)
16	98.63(-104)	1.33(+130)	0.02(-136)	0.01(+106)	0.00(+4)
17	98.51(-139)	1.37(+105)	0.10(-35)	0.02(-177)	0.01(+91)
18	98.00(-148)	1.95(+67)	0.05(-130)	0.00(+71)	0.00(-81)
19	87.69(+3)	11.28(+0)	0.90(+6)	0.11(+31)	0.03(+76)
20	90.00(-48)	9.08(-127)	0.84(+174)	0.08(+121)	0.01(+91)
21	94.78(-107)	5.06(+127)	0.16(+0)	0.00(-101)	0.00(-79)
22	91.33(-167)	7.90(+20)	0.70(-153)	0.07(+41)	0.01(-111)
23	89.84(+135)	9.01(-97)	0.99(+42)	0.14(-170)	0.02(-4)
24	91.14(+87)	7.79(+153)	0.93(-135)	0.13(-53)	0.02(+63)
25	96.92(+60)	2.96(+96)	0.10(+85)	0.02(+97)	0.00(+159)
26	96.79(+58)	3.05(+92)	0.15(+80)	0.01(+66)	0.00(+147)
27	82.30(-144)	14.74(+58)	2.51(-90)	0.40(+128)	0.06(+3)
28	74.67(+165)	19.91(-54)	4.46(+99)	0.84(-103)	0.13(+56)
29	74.71(-88)	19.99(+117)	4.41(-88)	0.80(+4)	0.09(+88)
30	77.16(+43)	17.85(+60)	4.04(+83)	0.79(+109)	0.16(+125)
31	84.00(-14)	13.54(-47)	2.14(-66)	0.28(-77)	0.03(-61)
32	84.02(-54)	13.33(-125)	2.19(+179)	0.38(+128)	0.08(+92)
33	88.28(-72)	10.27(-166)	1.24(+114)	0.17(+39)	0.04(-20)
34	91.48(-74)	8.09(-163)	0.40(+115)	0.02(+48)	0.01(-22)

* Ocean gage.

Table 13

Distribution of Wave Energy Throughout the Model, 20-deg Incident Direction, Period = 1.50 sec, Ocean Wave Height = 0.077 ft

Percent of Total Energy and Phase Angle (deg)

Gage	Fundamental Period 1.50 sec	First Harmonic 0.75 sec	Second Harmonic 0.50 sec	Third Harmonic 0.38 sec	Fourth Harmonic 0.30 sec
1*	98.68(+45)	0.97(-132)	0.15(-38)	0.19(+34)	0.00(-10)
2*	98.85(+59)	1.01(-69)	0.09(+47)	0.01(+157)	0.04(-72)
3	91.28(+175)	8.34(-19)	0.33(+128)	0.05(-179)	0.00(-58)
4	90.32(+142)	9.27(-98)	0.38(-36)	0.03(-84)	0.00(-113)
5	92.05(+108)	7.78(-167)	0.12(-102)	0.05(-10)	0.00(+176)
6	93.43(+81)	6.47(+118)	0.06(-130)	0.02(+134)	0.01(-153)
7	93.79(+48)	6.00(+42)	0.14(+117)	0.04(-111)	0.03(-17)
8	95.70(+15)	3.79(-32)	0.32(+10)	0.16(-18)	0.03(-169)
9	98.82(-4)	1.10(-86)	0.07(+154)	0.01(-112)	0.00(-179)
10	99.18(-11)	0.80(-79)	0.00(+19)	0.01(+45)	0.00(+163)
11	91.70(-71)	7.88(-149)	0.40(-160)	0.01(-27)	0.02(-126)
12	90.74(-105)	8.28(+143)	0.09(+72)	0.04(+110)	0.00(-35)
13	90.93(-139)	8.40(+72)	0.56(-53)	0.12(+170)	0.00(-165)
14	90.22(-170)	9.13(+4)	0.55(-178)	0.09(+10)	0.02(-166)
15	89.52(+158)	9.51(-70)	0.82(+72)	0.07(+136)	0.08(-33)
16	90.07(+127)	9.82(-145)	0.08(-75)	0.02(+111)	0.01(+170)
17	94.89(+110)	4.73(+180)	0.37(-47)	0.01(-6)	0.00(+44)
18	96.08(+112)	3.86(-178)	0.04(-82)	0.01(+102)	0.01(+73)
19	94.16(+54)	5.64(+115)	0.11(+144)	0.05(-87)	0.03(-111)
20	90.67(+23)	9.07(+47)	0.21(+62)	0.04(+23)	0.02(-32)
21	91.95(-16)	7.69(-34)	0.35(-92)	0.00(-5)	0.00(+160)
22	88.48(-48)	10.91(-110)	0.56(-170)	0.05(-176)	0.00(+161)
23	86.68(-82)	12.50(-179)	0.57(+125)	0.16(-0)	0.09(-50)
24	88.54(-107)	10.32(+128)	1.06(+1)	0.57(-62)	0.29(+138)
25	92.99(-120)	6.95(+93)	0.02(-32)	0.03(+41)	0.01(-56)
26	94.38(-119)	5.49(+97)	0.11(-6)	0.02(-169)	0.01(+10)
27	93.45(-165)	5.82(+8)	0.57(+178)	0.15(+78)	0.01(-72)
28	90.99(+159)	7.84(-63)	0.88(+79)	0.27(-126)	0.03(-6)
29	88.58(+120)	8.54(-142)	2.66(-34)	0.18(+74)	0.04(+157)
30	86.21(+87)	11.06(+160)	2.50(-135)	0.19(-62)	0.04(+17)
31	85.17(+57)	13.36(+102)	1.28(+121)	0.14(+162)	0.06(-128)
32	85.93(+38)	12.33(+51)	1.47(+88)	0.26(+127)	0.01(+104)
33	90.25(+29)	8.97(+22)	0.69(+29)	0.09(+78)	0.00(-38)
34	90.83(+27)	8.61(+21)	0.53(+21)	0.03(-3)	0.00(+26)

* Ocean gage.

Table 14

Distribution of Wave Energy Throughout the Model, 20-deg Incident Direction, Period = 1.50 sec, Ocean Wave Height = 0.111 ft

Percent of Total Energy and Phase Angle (deg)

Gage	Fundamental Period 1.50 sec	First Harmonic 0.75 sec	Second Harmonic 0.50 sec	Third Harmonic 0.38 sec	Fourth Harmonic 0.30 sec
1*	96.99(-154)	2.52(-161)	0.40(+55)	0.06(-65)	0.03(+177)
2*	97.55(-139)	1.93(-119)	0.47(+105)	0.05(+2)	0.00(+151)
3	84.22(-22)	14.41(-67)	1.30(-115)	0.06(+124)	0.01(+118)
4	85.16(-57)	14.42(-153)	0.30(+125)	0.08(+40)	0.03(-26)
5	86.80(-87)	12.68(+138)	0.50(+47)	0.01(+138)	0.00(+67)
6	87.21(-119)	11.87(+61)	0.73(-60)	0.16(+176)	0.02(+49)
7	87.95(-152)	10.68(-5)	1.27(-169)	0.07(-12)	0.03(+161)
8	94.15(+177)	5.38(-83)	0.46(+59)	0.00(-105)	0.00(+122)
9	98.79(+156)	1.00(-137)	0.12(+120)	0.07(-21)	0.01(+127)
10	98.90(+150)	1.00(-132)	0.05(+4)	0.05(-176)	0.00(+11)
11	82.66(+86)	16.15(+167)	1.12(-89)	0.05(-55)	0.01(+45)
12	76.94(+54)	20.20(+98)	2.36(+143)	0.32(-159)	0.09(-105)
13	79.42(+20)	17.81(+26)	2.36(+30)	0.33(+23)	0.08(+47)
14	77.50(-12)	20.01(-49)	2.29(-87)	0.19(-96)	0.02(-135)
15	77.99(-43)	20.46(-121)	1.36(-175)	0.16(+119)	0.03(+72)
16	88.53(-68)	10.25(+172)	1.12(+108)	0.09(+40)	0.00(-21)
17	93.01(-83)	6.42(+137)	0.52(+13)	0.04(-94)	0.01(+138)
18	93.57(-87)	6.13(+133)	0.29(+1)	0.00(-131)	0.00(+29)
19	86.74(-154)	11.64(+63)	1.42(-99)	0.17(+88)	0.03(-53)
20	79.36(+175)	17.80(-16)	2.35(+147)	0.42(-27)	0.08(+153)
21	80.85(+138)	15.84(-96)	2.67(+40)	0.54(+169)	0.09(-50)
22	73.87(+107)	20.35(-163)	4.75(-69)	0.86(+37)	0.18(+134)
23	72.27(+79)	22.49(+133)	4.11(-162)	0.92(-98)	0.21(-25)
24	81.15(+56)	17.46(+70)	1.36(+101)	0.28(+130)	0.01(+112)
25	85.88(+44)	12.70(+39)	1.29(+83)	0.12(+109)	0.01(+124)
26	83.75(+44)	14.41(+41)	1.72(+74)	0.11(+75)	0.01(+90)
27	84.51(-13)	12.06(-50)	2.72(-70)	0.54(-97)	0.17(-119)
28	77.52(-48)	16.14(-118)	4.69(+172)	1.30(+110)	0.36(+53)
29	74.19(-88)	19.04(+166)	4.77(+62)	1.54(-49)	0.46(-147)
30	66.54(-121)	23.29(+101)	7.59(-40)	2.05(-172)	0.53(+59)
31	65.34(-145)	25.17(+44)	6.80(-118)	2.04(+82)	0.65(-73)
32	69.88(-166)	20.88(-0)	7.49(+166)	1.35(-18)	0.39(+161)
33	71.98(-175)	23.47(-27)	3.57(+131)	0.78(-65)	0.19(+94)
34	74.98(-175)	21.05(-22)	3.31(+138)	0.58(-57)	0.08(+110)

* Ocean gage.

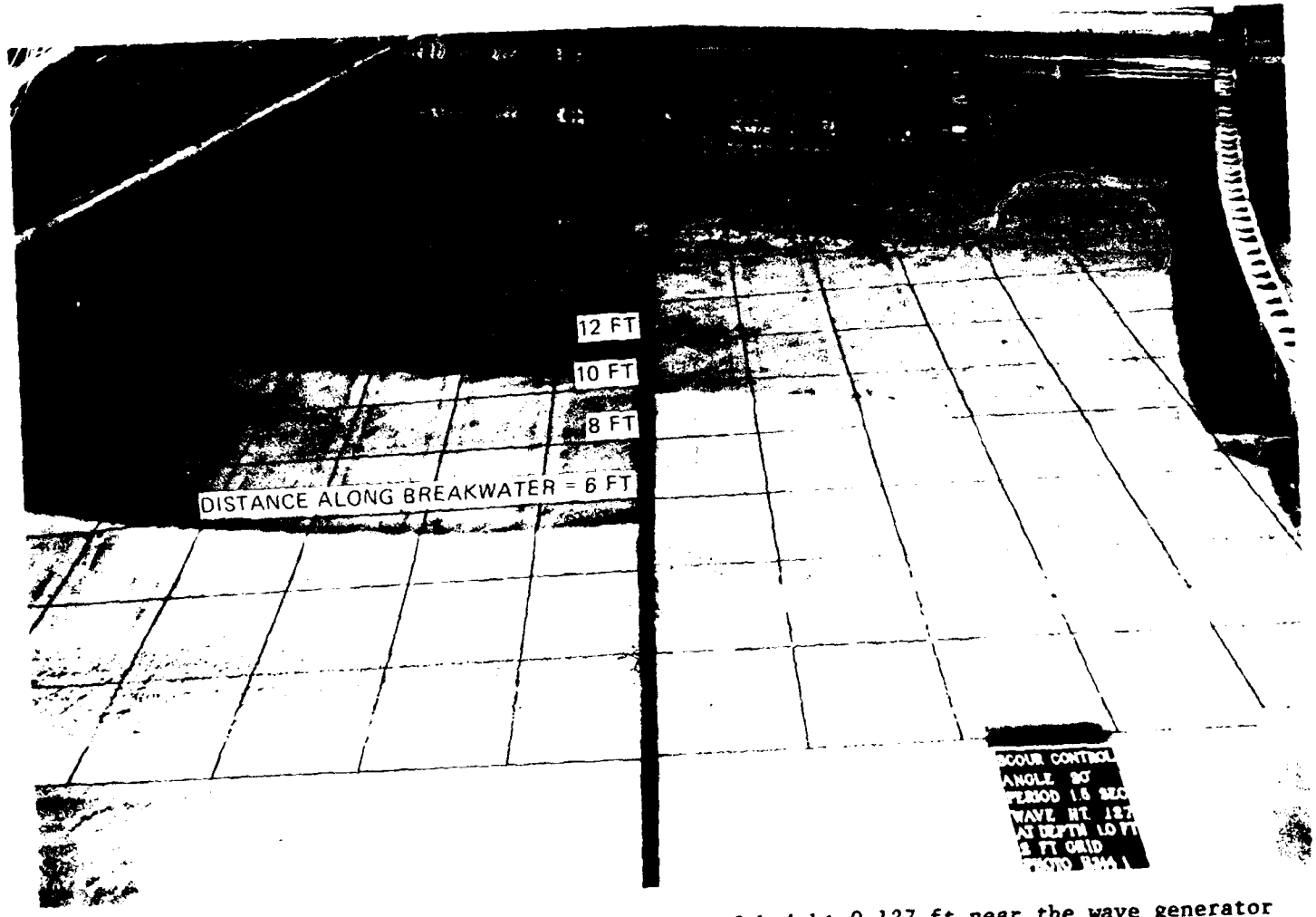

Photo 1. Typical wave pattern for 1.5-sec wave of height 0.127 ft near the wave generator approaching from an incident direction of 20 deg (upwave and downwave region)

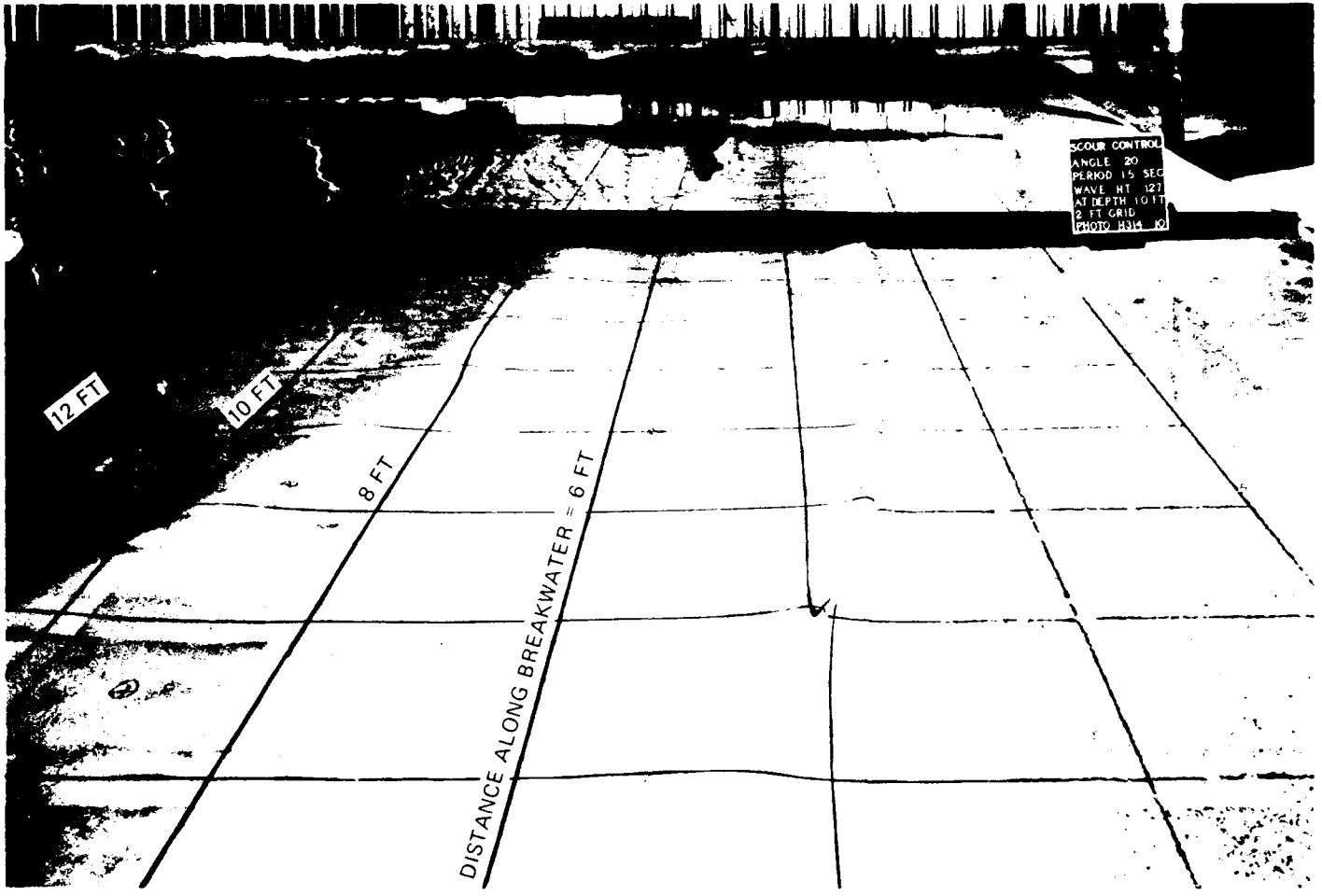

Photo 2. Typical wave pattern for 1.5-sec wave of height 0.127 ft near the wave generator approaching from an incident direction of 20 deg (downwave region)

Photo 3. Typical wave pattern for 1.5-sec wave of height 0.127 ft near the wave generator approaching from an incident direction of 20 deg (upwave region)

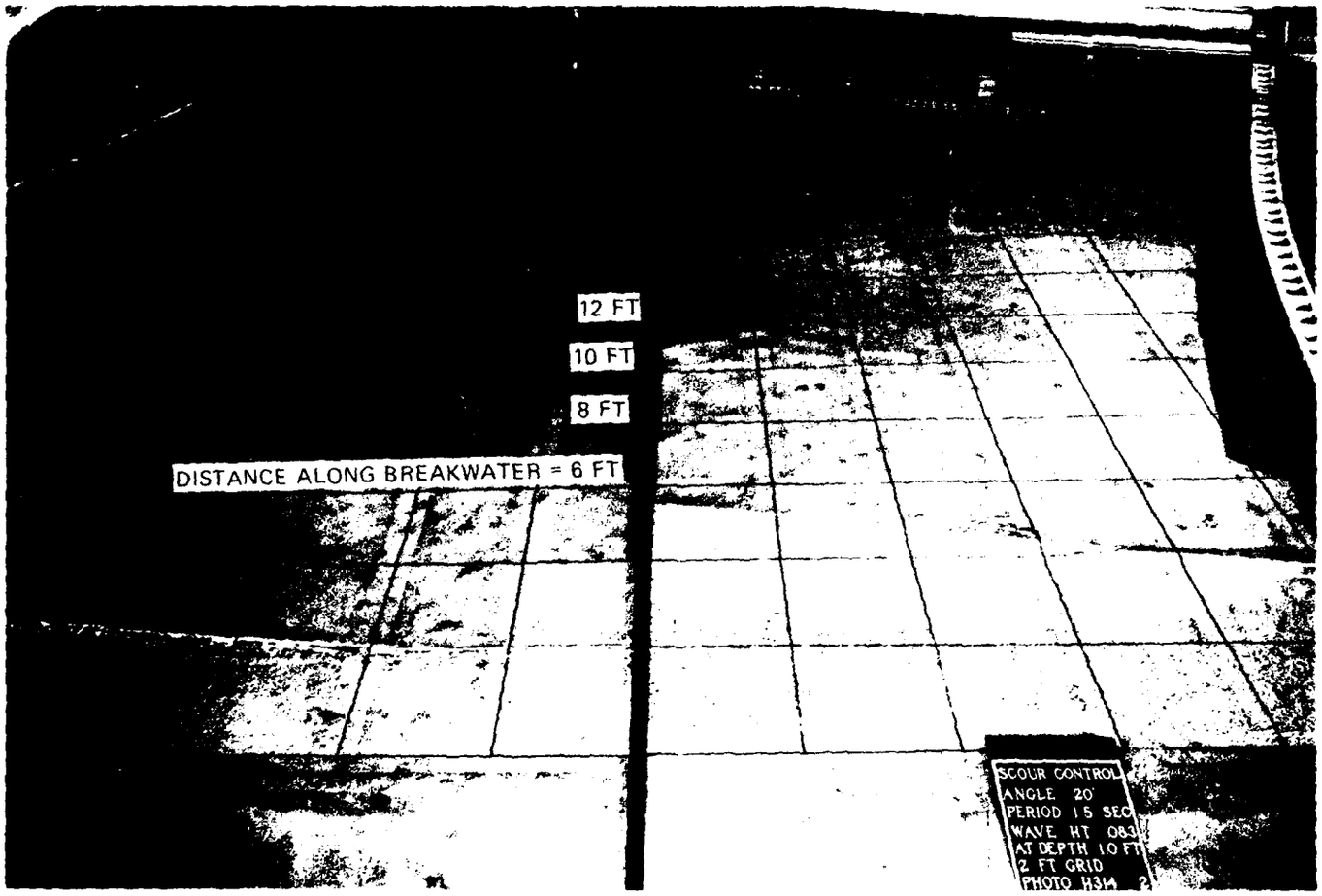

Photo 4. Typical wave pattern for 1.5-sec wave of height 0.083 ft near the wave generator approaching from an incident direction of 20 deg (upwave and downwave region)

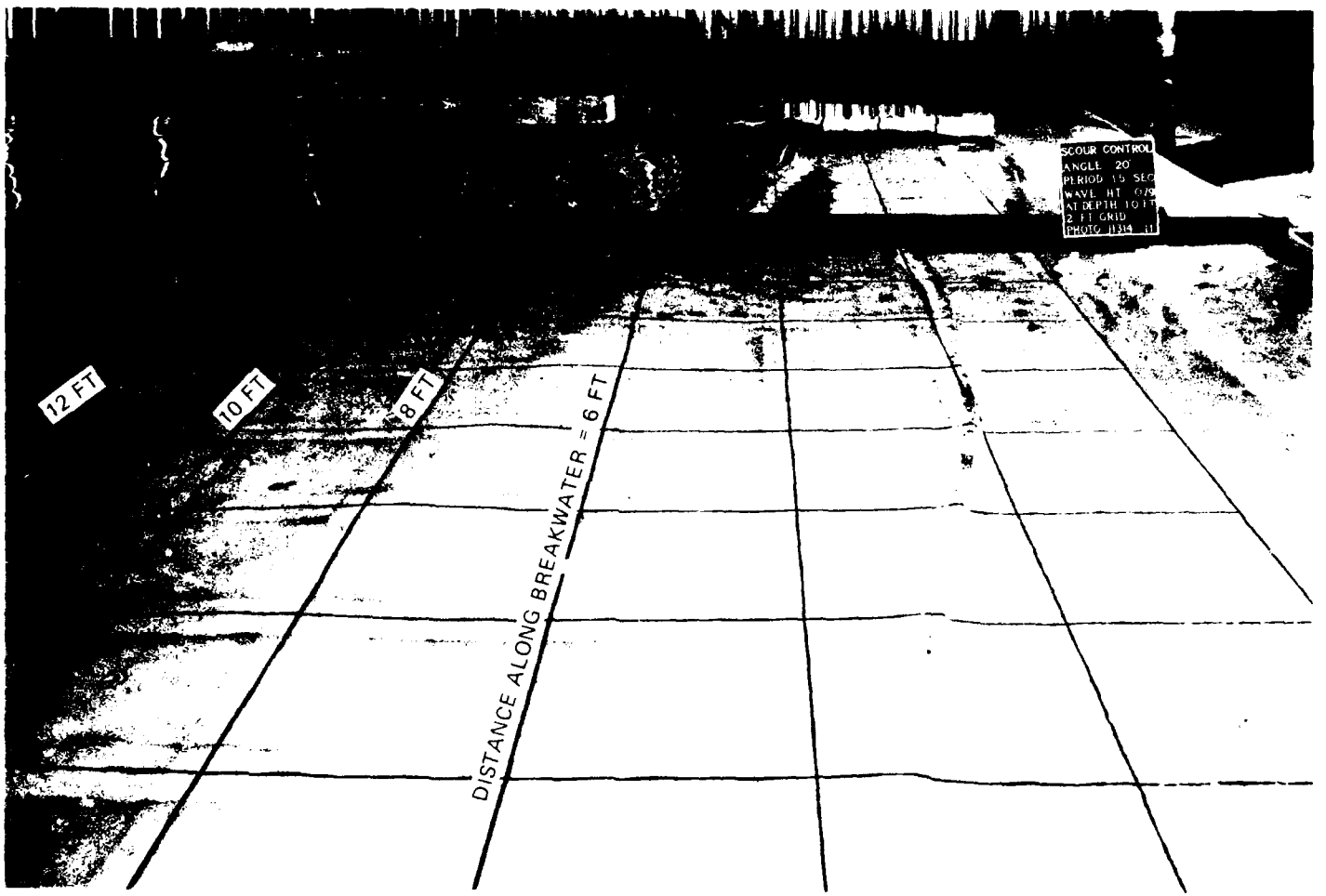

Photo 5. Typical wave pattern for 1.5-sec wave of height 0.079 ft near the wave generator approaching from an incident direction of 20 deg (downwave region)

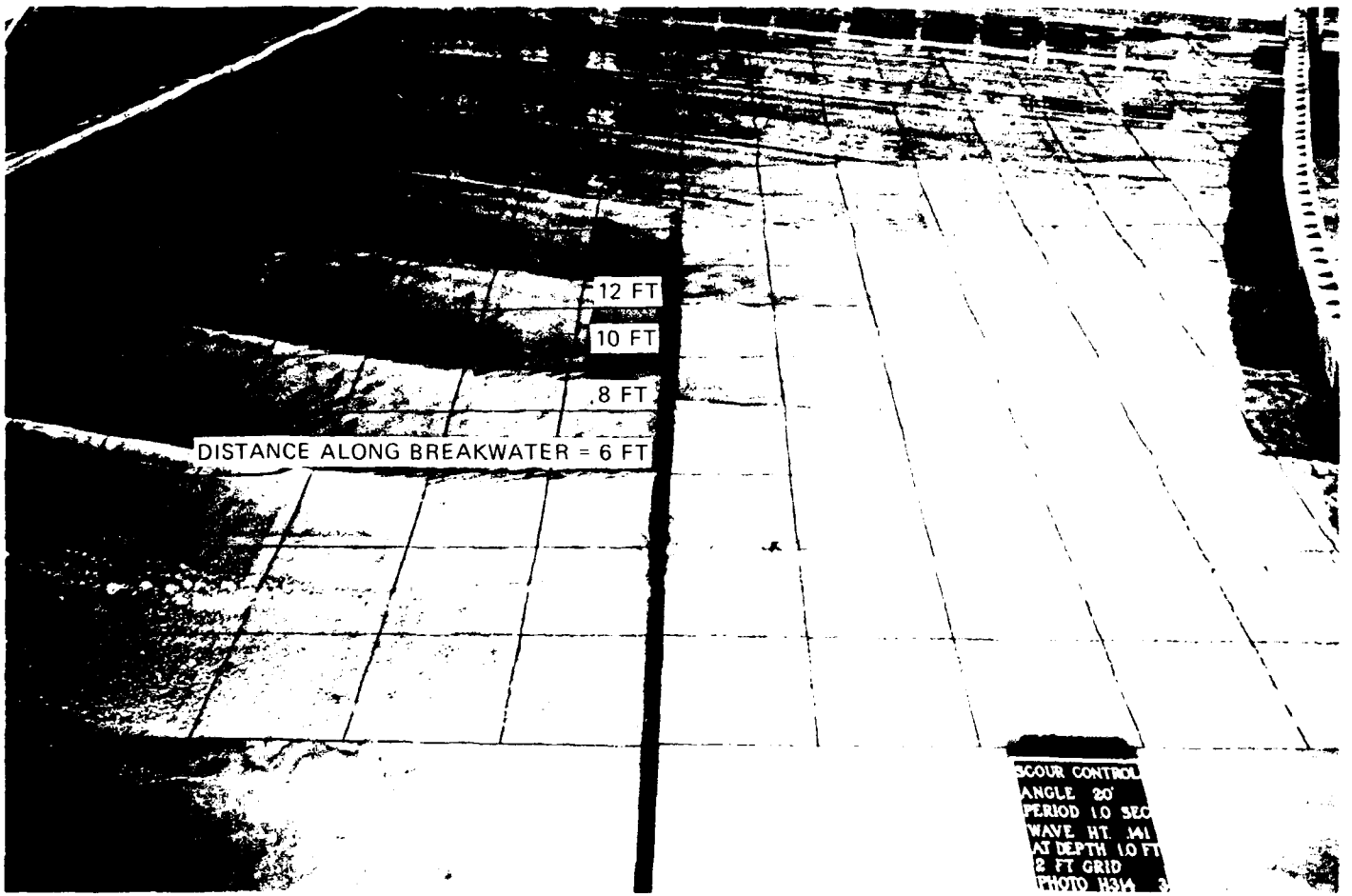

Photo 6. Typical wave pattern for 1.0-sec wave of height 0.141 ft near the wave generator approaching from an incident direction of 20 deg (upwave and downwave region)

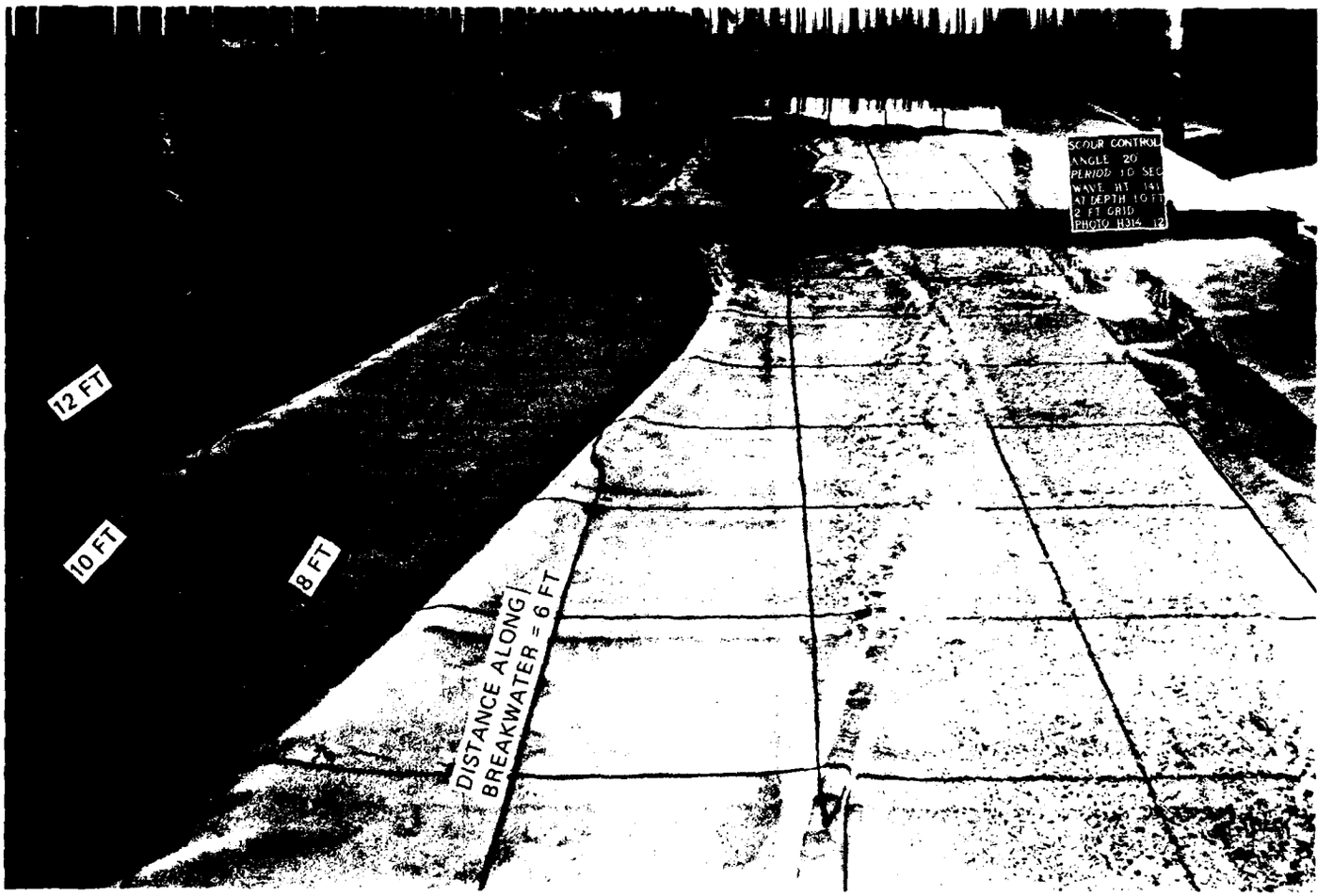

Photo 7. Typical wave pattern for 1.0-sec wave of height 0.141 ft near the wave generator approaching from an incident direction of 20 deg (downwave region)

Photo 8. Typical wave pattern for 1.0-sec wave of height 0.141 ft near the wave generator approaching from an incident direction of 20 deg (upwave region)

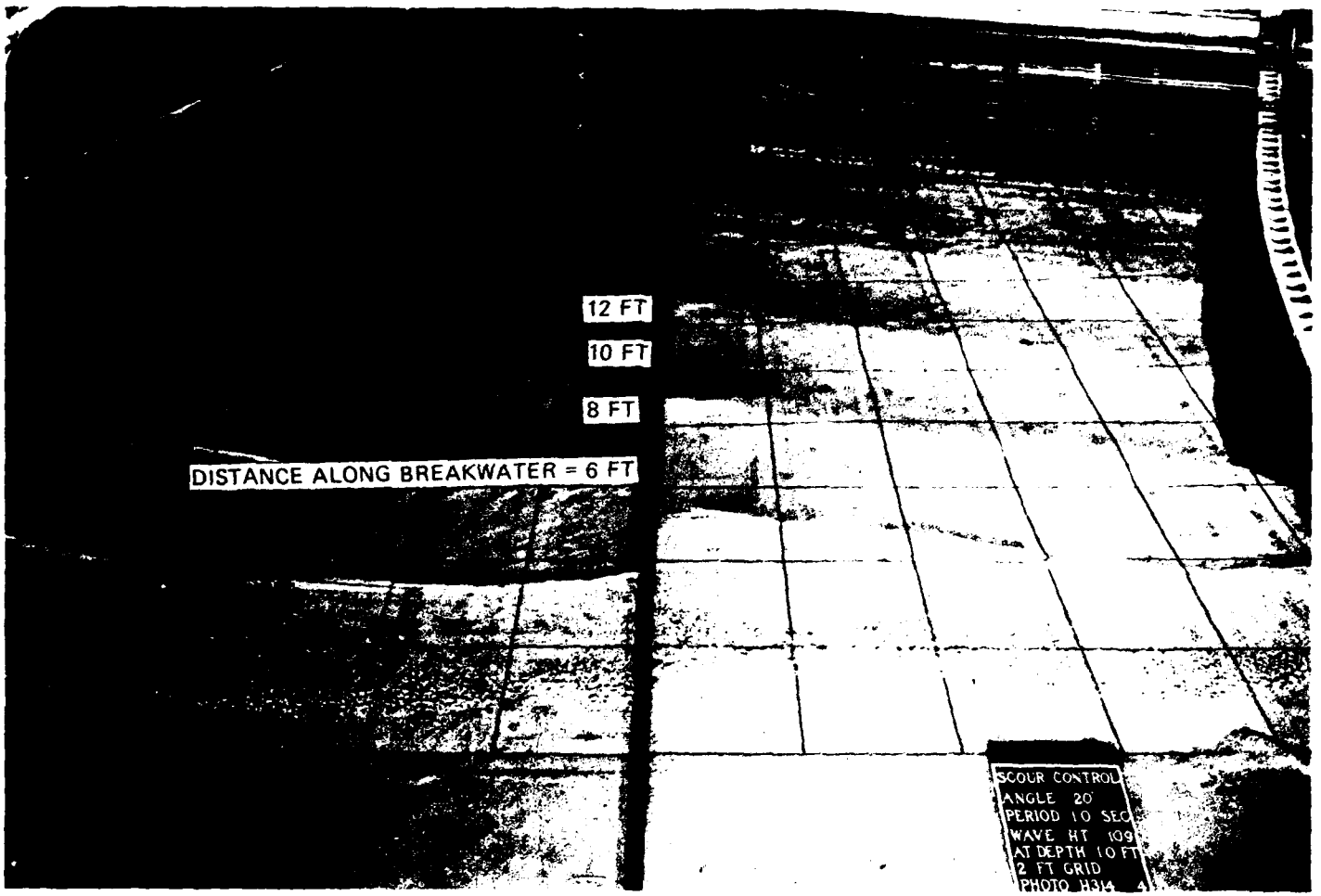

Photo 9. Typical wave pattern for 1.0-sec wave of height 0.109 ft near the wave generator approaching from an incident direction of 20 deg (upwave and downwave region)

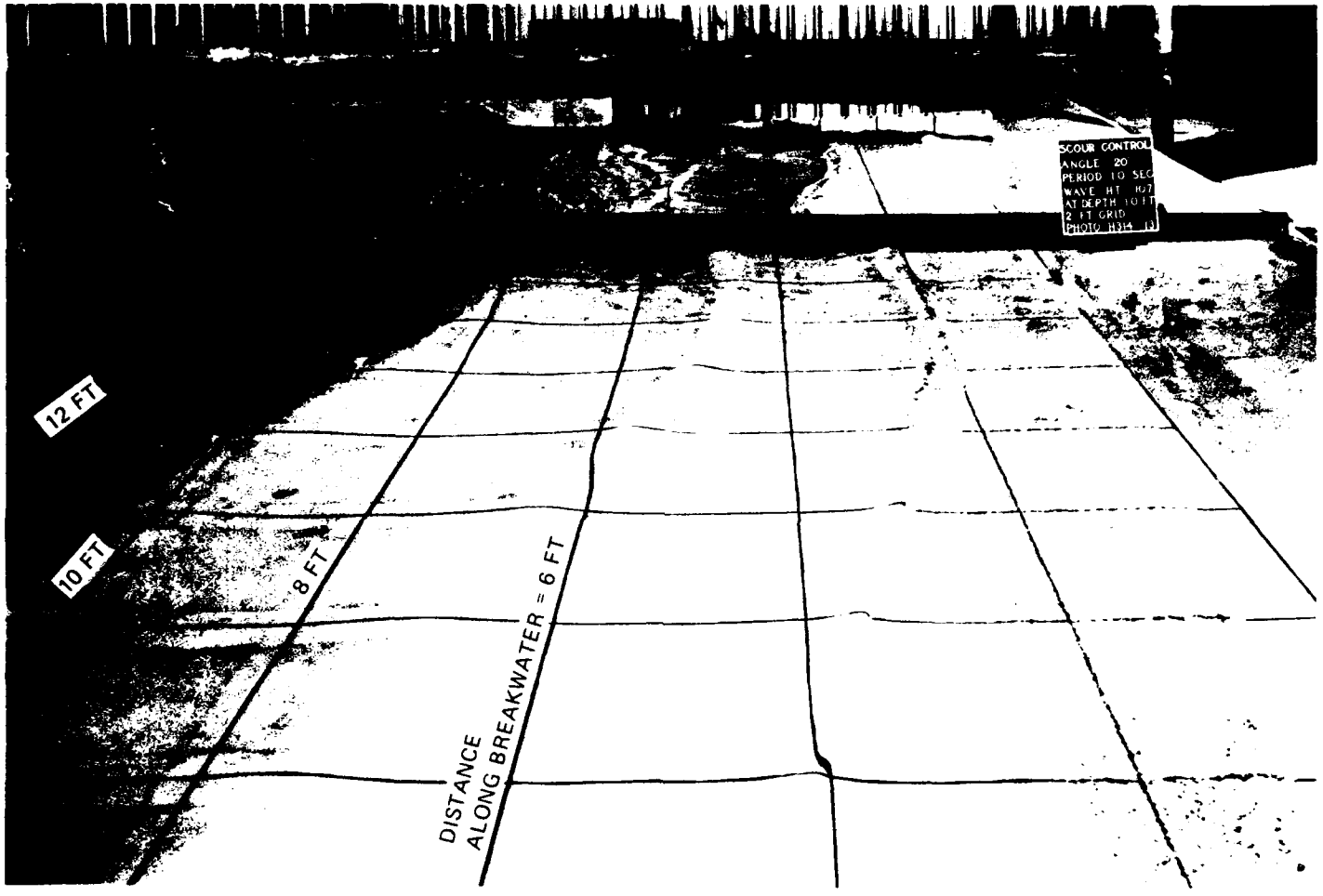

Photo 10. Typical wave pattern for 1.0-sec wave of height 0.107 ft near the wave generator approaching from an incident direction of 20 deg (downwave region)

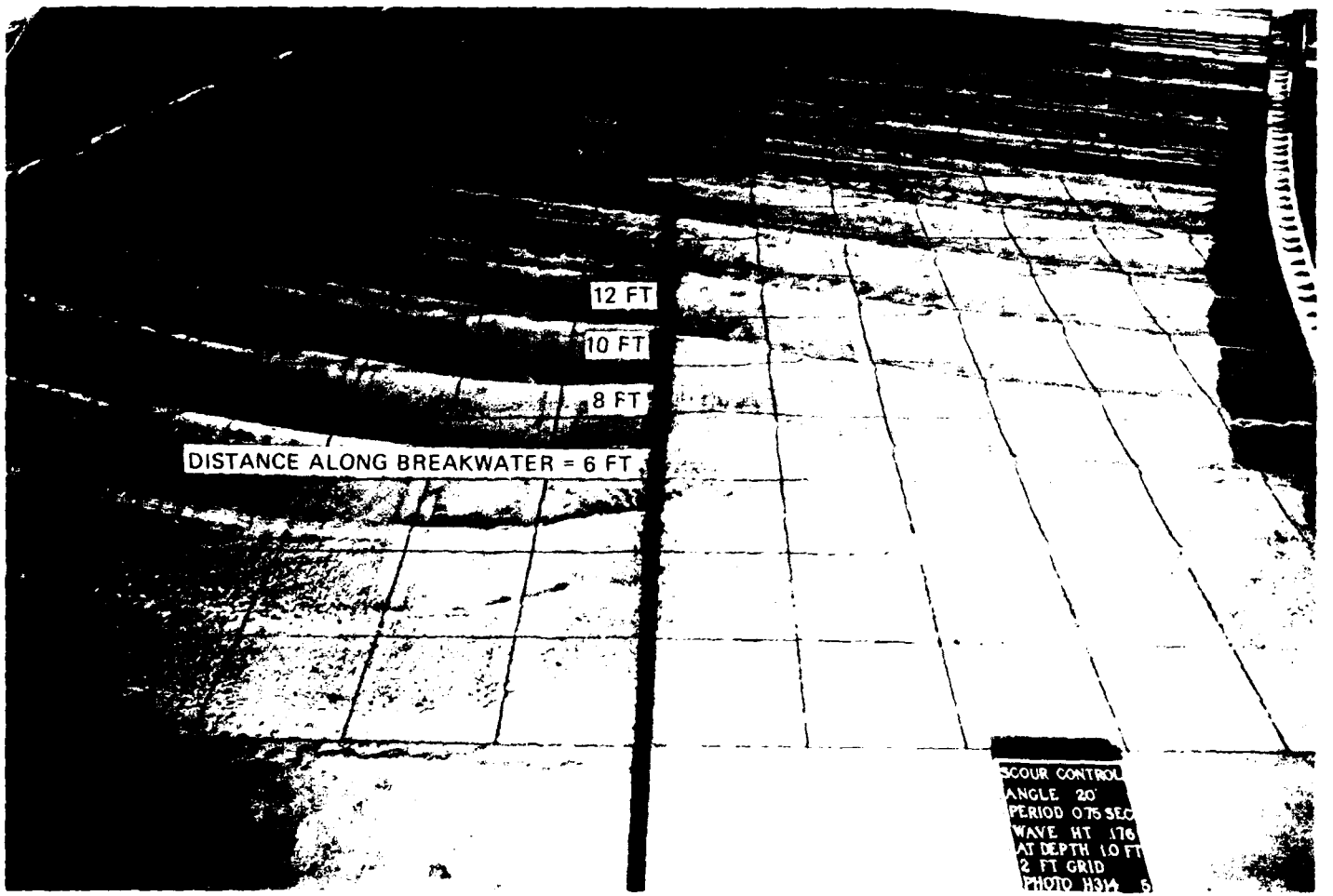

Photo 11. Typical wave pattern for 0.75-sec wave of height 0.176 ft near the wave generator approaching from an incident direction of 20 deg (upwave and downwave region)

Photo 12. Typical wave pattern for 0.75-sec wave of height 0.176 ft near the wave generator approaching from an incident direction of 20 deg (downwave region)

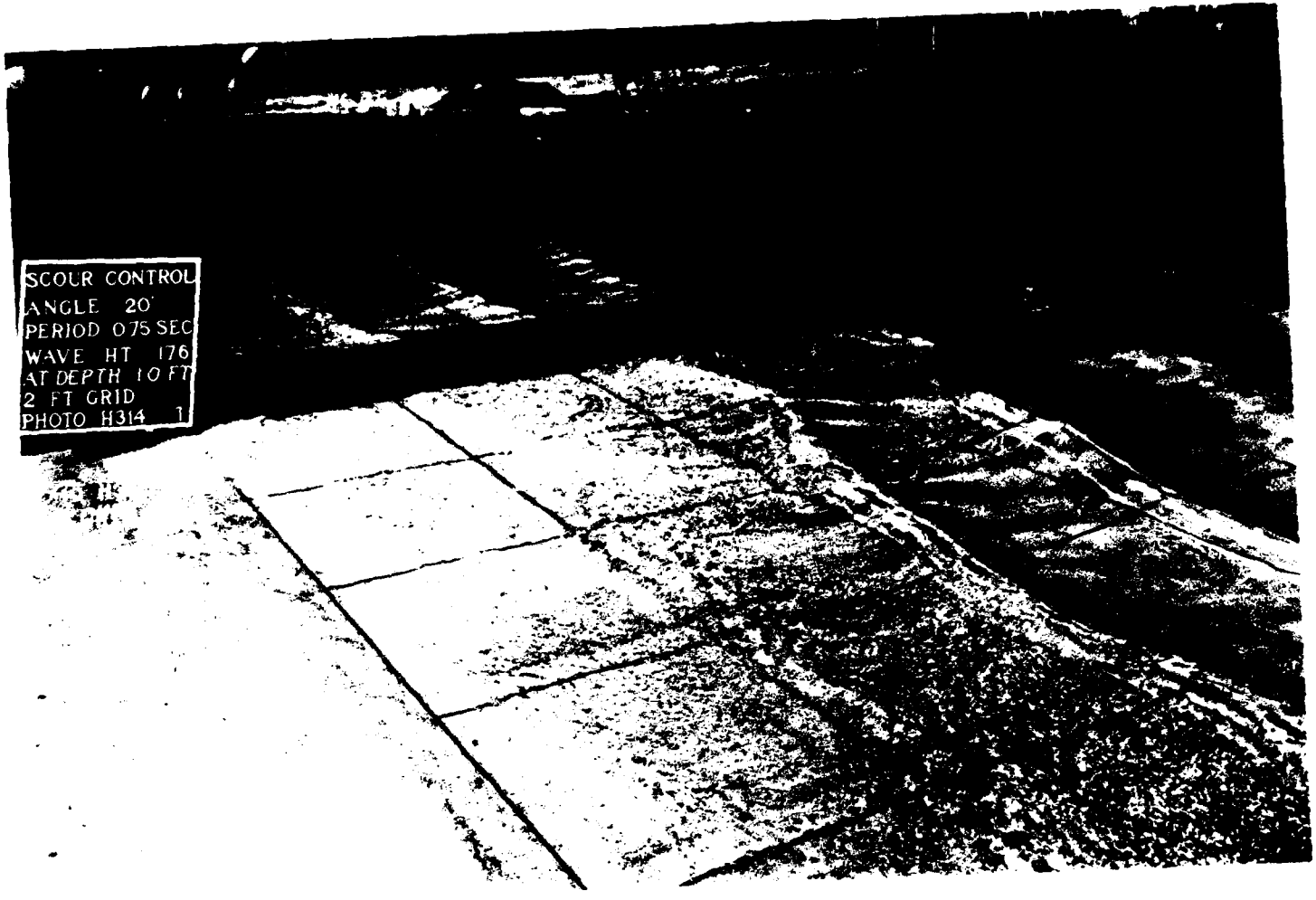

Photo 13. Typical wave pattern for 0.75-sec wave of height 0.176 ft near the wave generator approaching from an incident direction of 20 deg (upwave region)

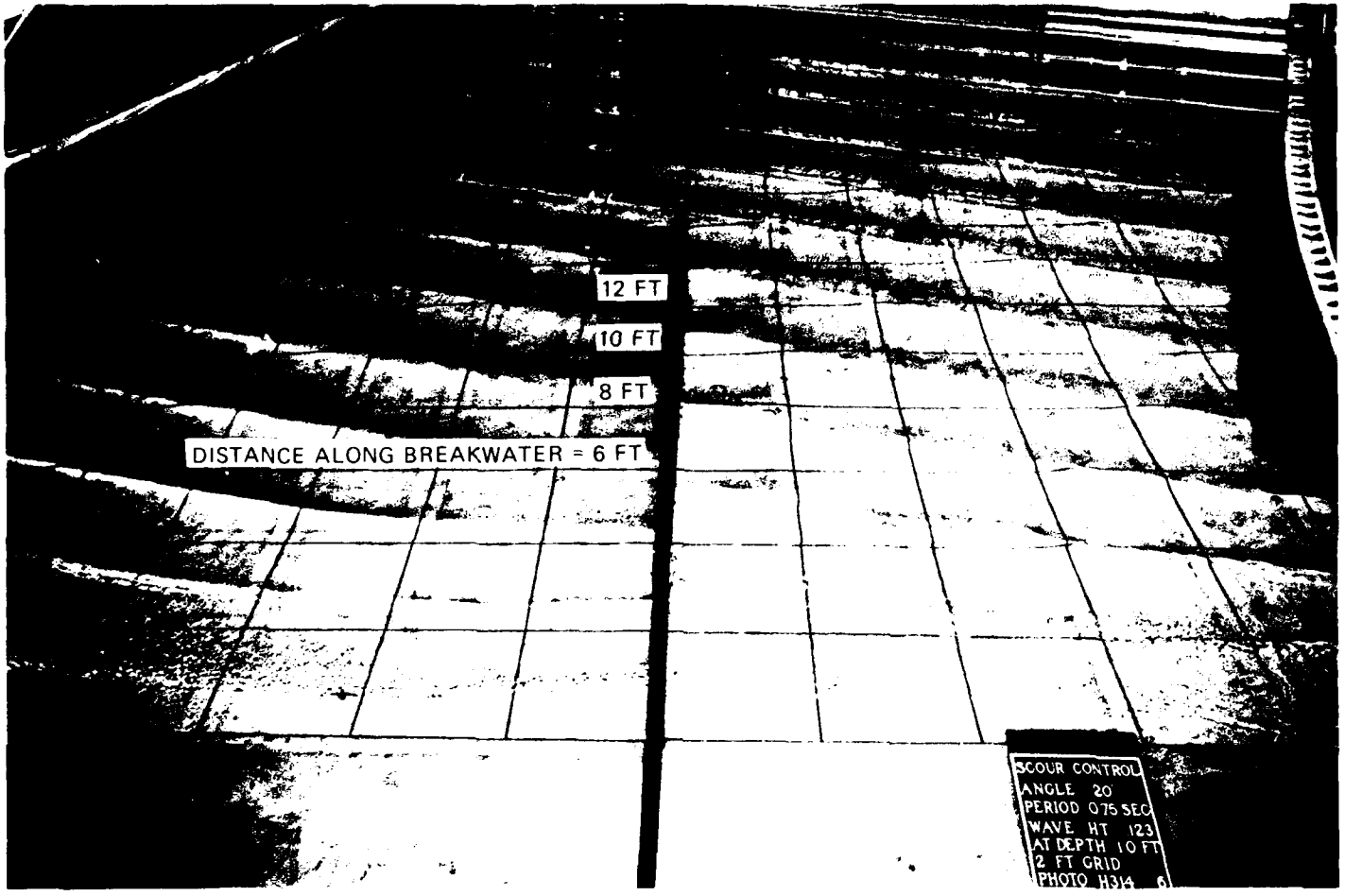

Photo 14. Typical wave pattern for 0.75-sec wave of height 0.123 ft near the wave generator approaching from an incident direction of 20 deg (upwave and downwave region)

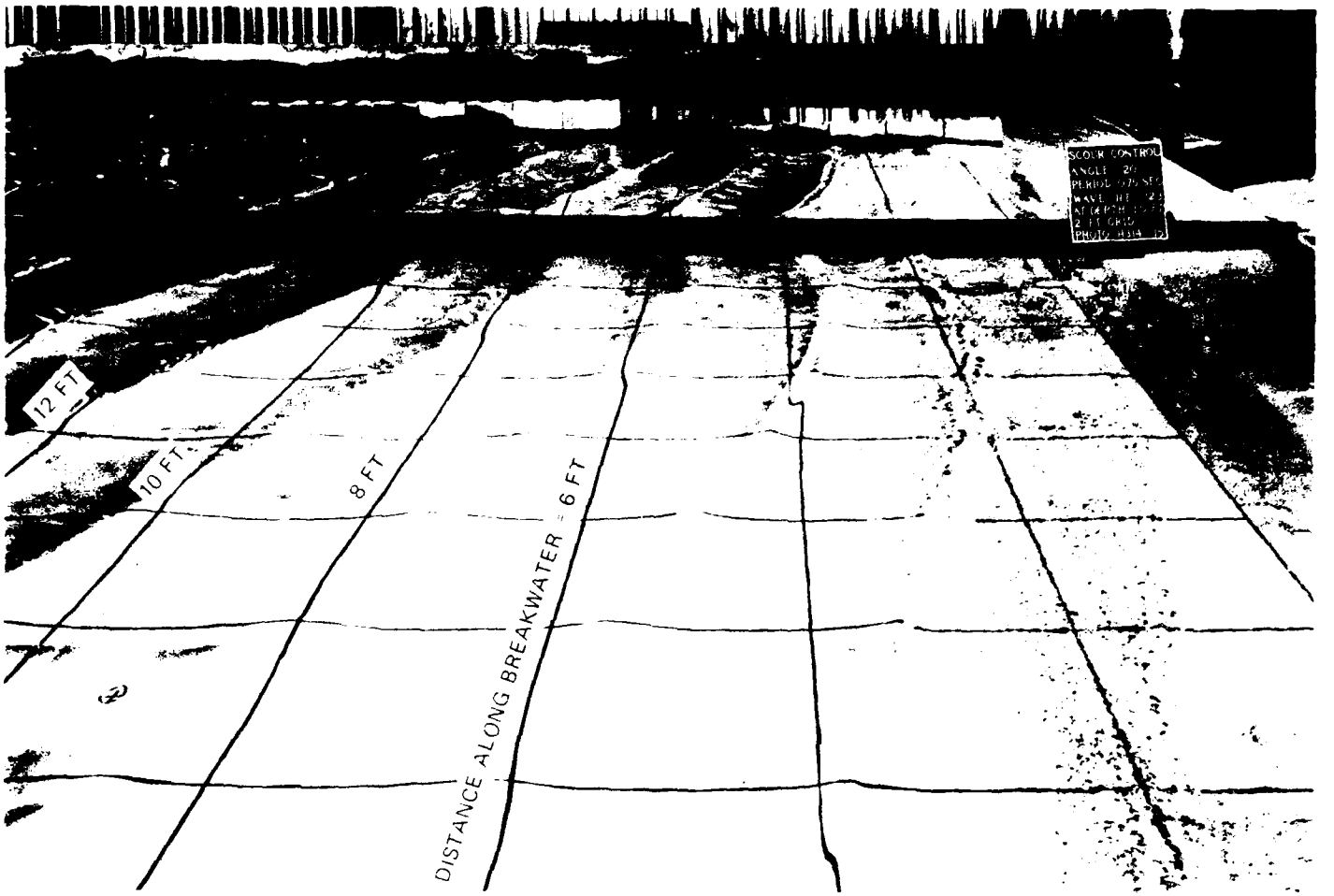

Photo 15. Typical wave pattern for 0.75-sec wave of height 0.123 ft near the wave generator approaching from an incident direction of 20 deg (downwave region)

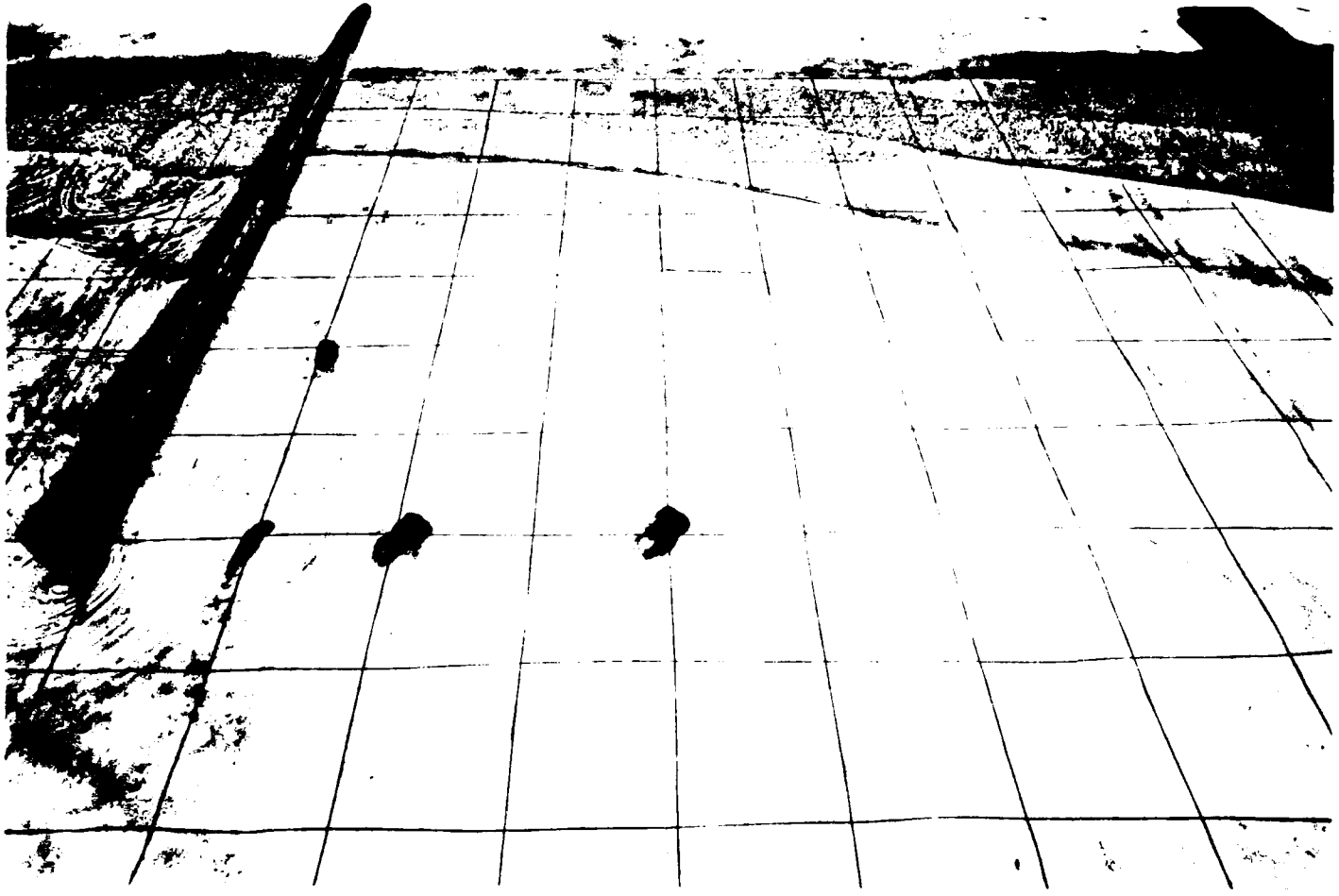

Photo 16. Net dye movement, time after starting generator = 10 sec, wave period = 1.0 sec, wave height near generator = 0.139 ft, angle of incidence = 30 deg

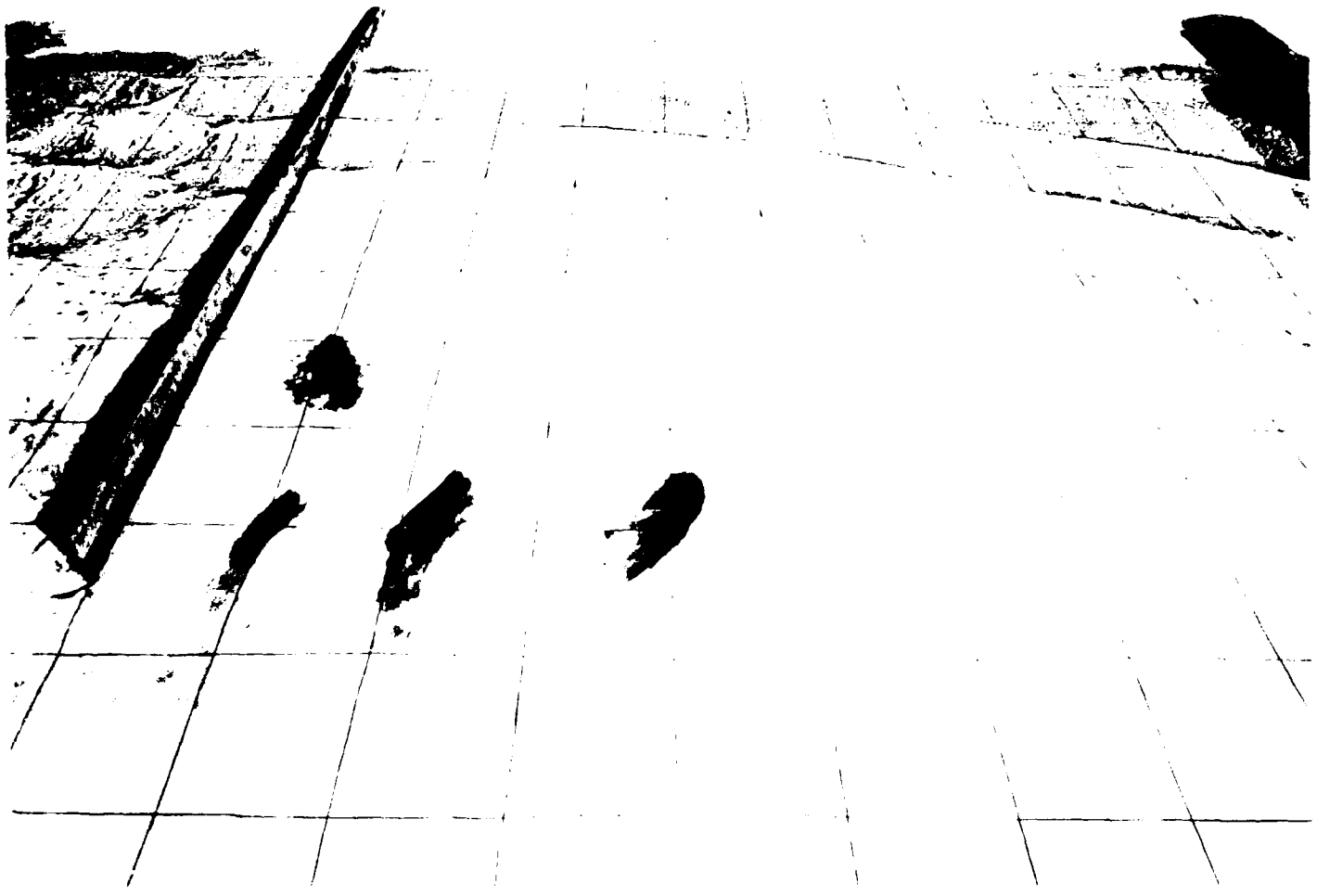

Photo 17. Net dye movement, time after starting generator = 0.5 min, wave period = 1.0 sec, wave height near generator = 0.139 ft, angle of incidence = 30 deg

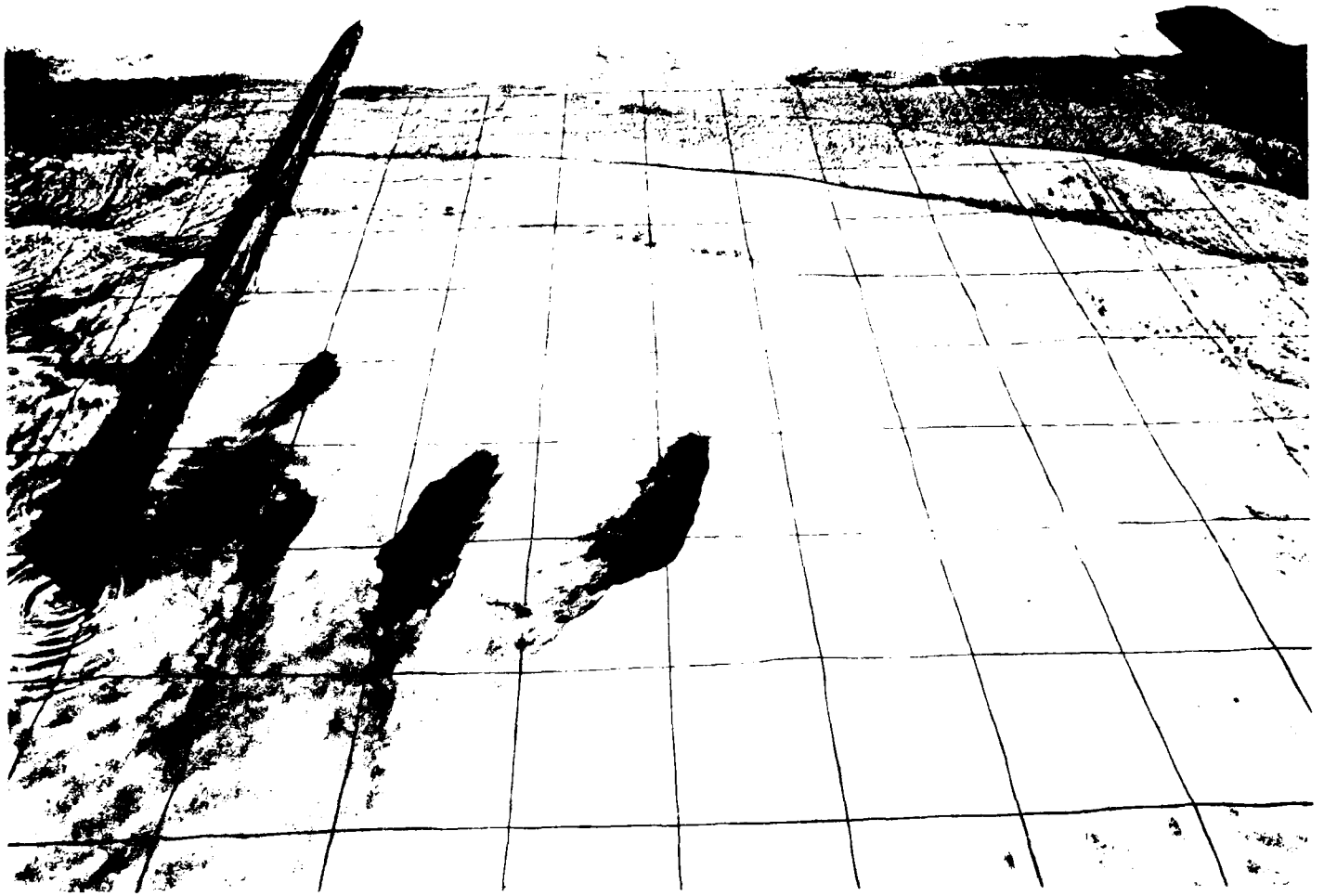

Photo 18. Net dye movement, time after starting generator = 1.0 min, wave period = 1.0 sec, wave height near generator = 0.139 ft, angle of incidence = 30 deg

AD-A092 712 ARMY ENGINEER WATERWAYS EXPERIMENT STATION VICKSBURG--ETC F/G 8/3
EROSION CONTROL OF SCOUR DURING CONSTRUCTION; REPORT 3. EXPERIM--ETC(U)
SEP 80 L Z HALES

UNCLASSIFIED WES/TR/HL-80-3-3 NL

END
DATE FILMED
1-81
DTIC

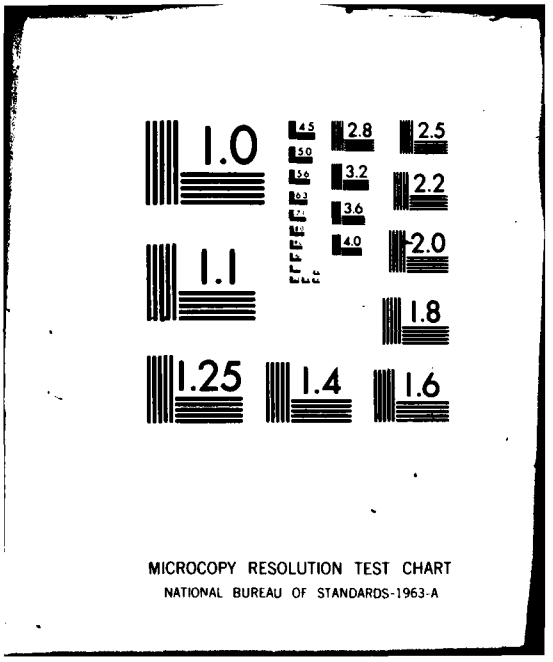
1.0
1.1
1.25
1.4
1.6
1.8
2.0
2.2
2.5
2.8
3.2
3.6
4.0
4.5
5.0
5.6
6.3
MICROCOPY RESOLUTION TEST CHART
NATIONAL BUREAU OF STANDARDS-1963-A

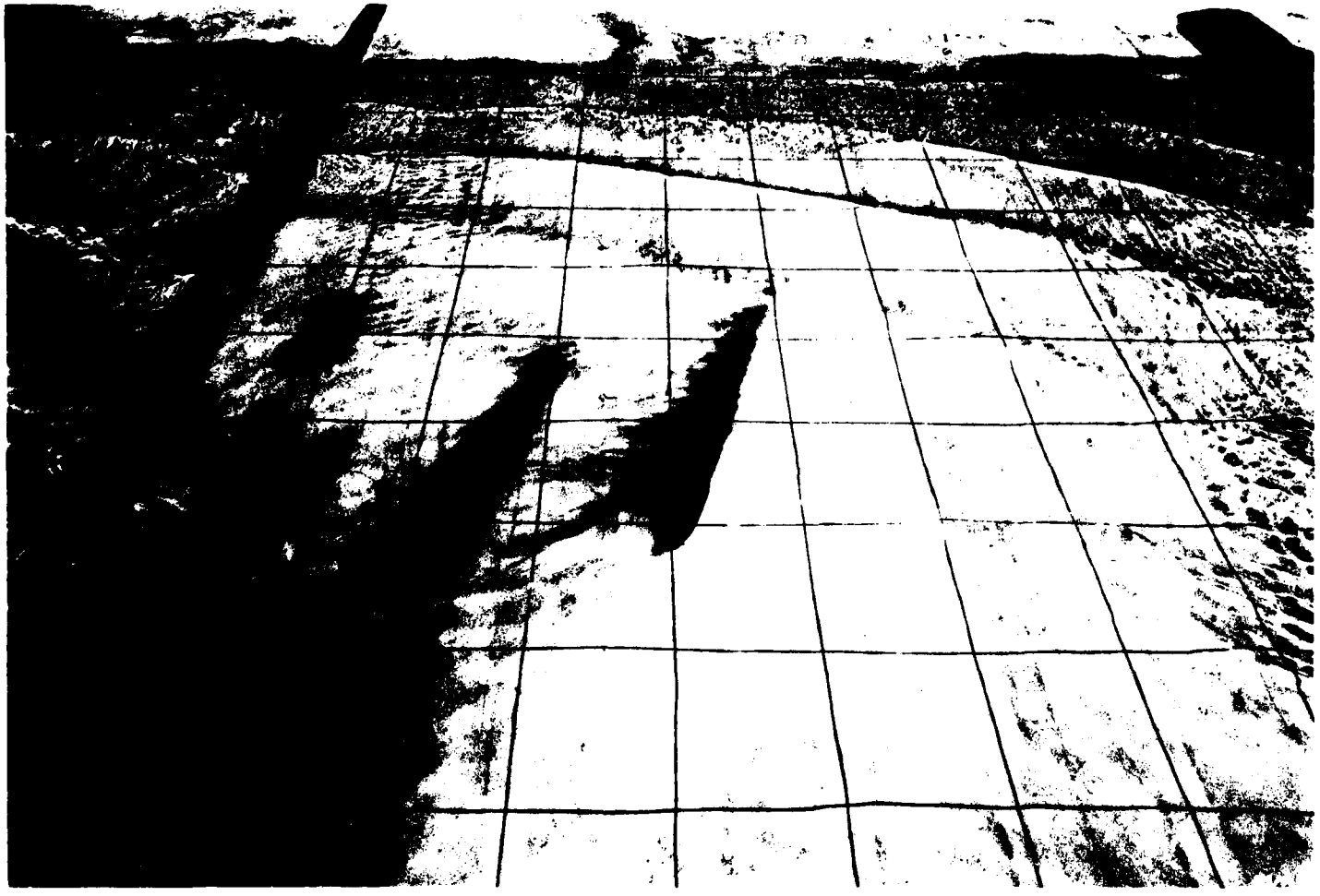

Photo 19. Net dye movement, time after starting generator = 2.0 min, wave period = 1.0 sec, wave height near generator = 0.139 ft, angle of incidence = 30 deg

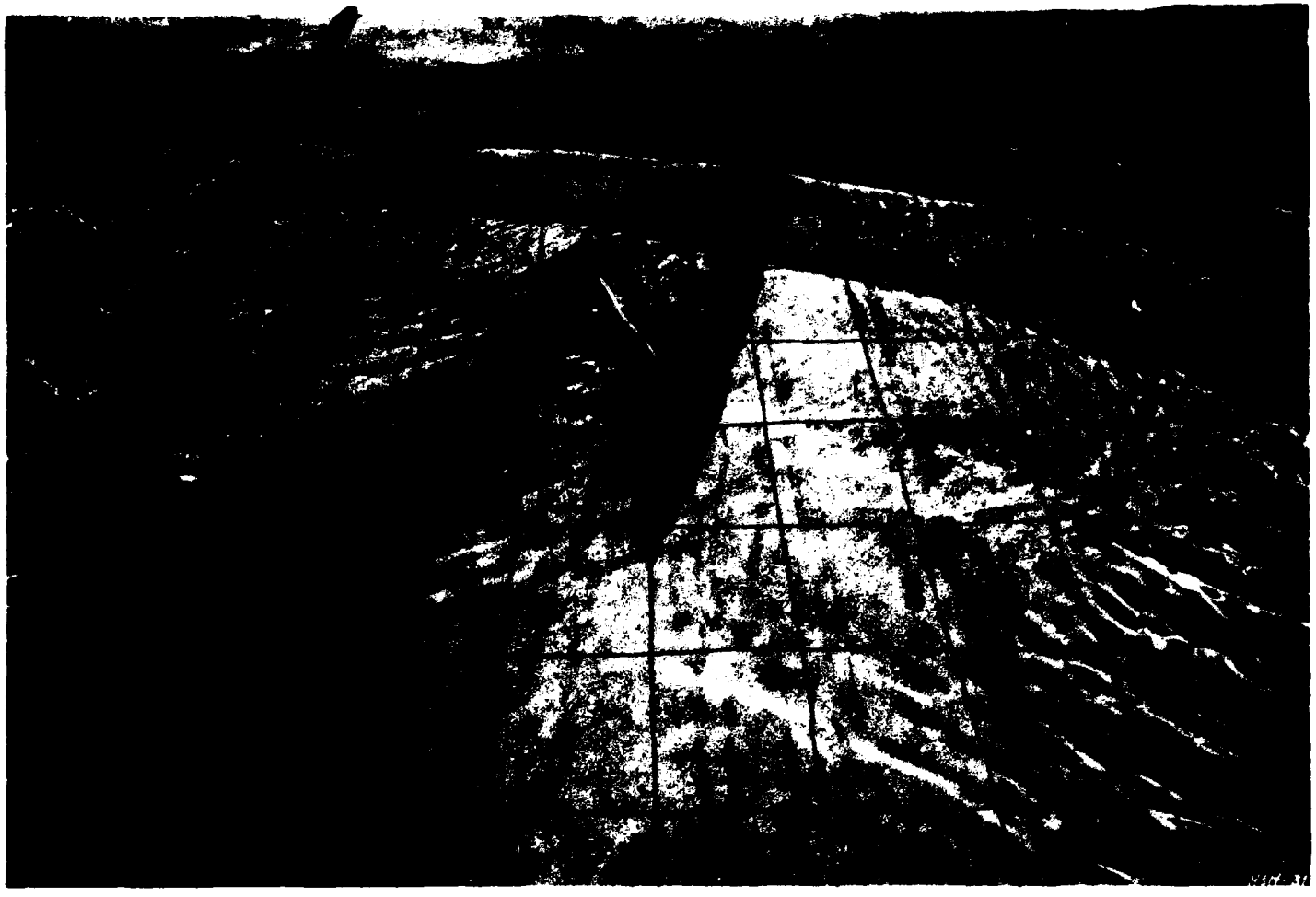

Photo 20. Net dye movement, time after starting generator = 3.0 min, wave period = 1.0 sec, wave height near generator = 0.139 ft, angle of incidence = 30 deg

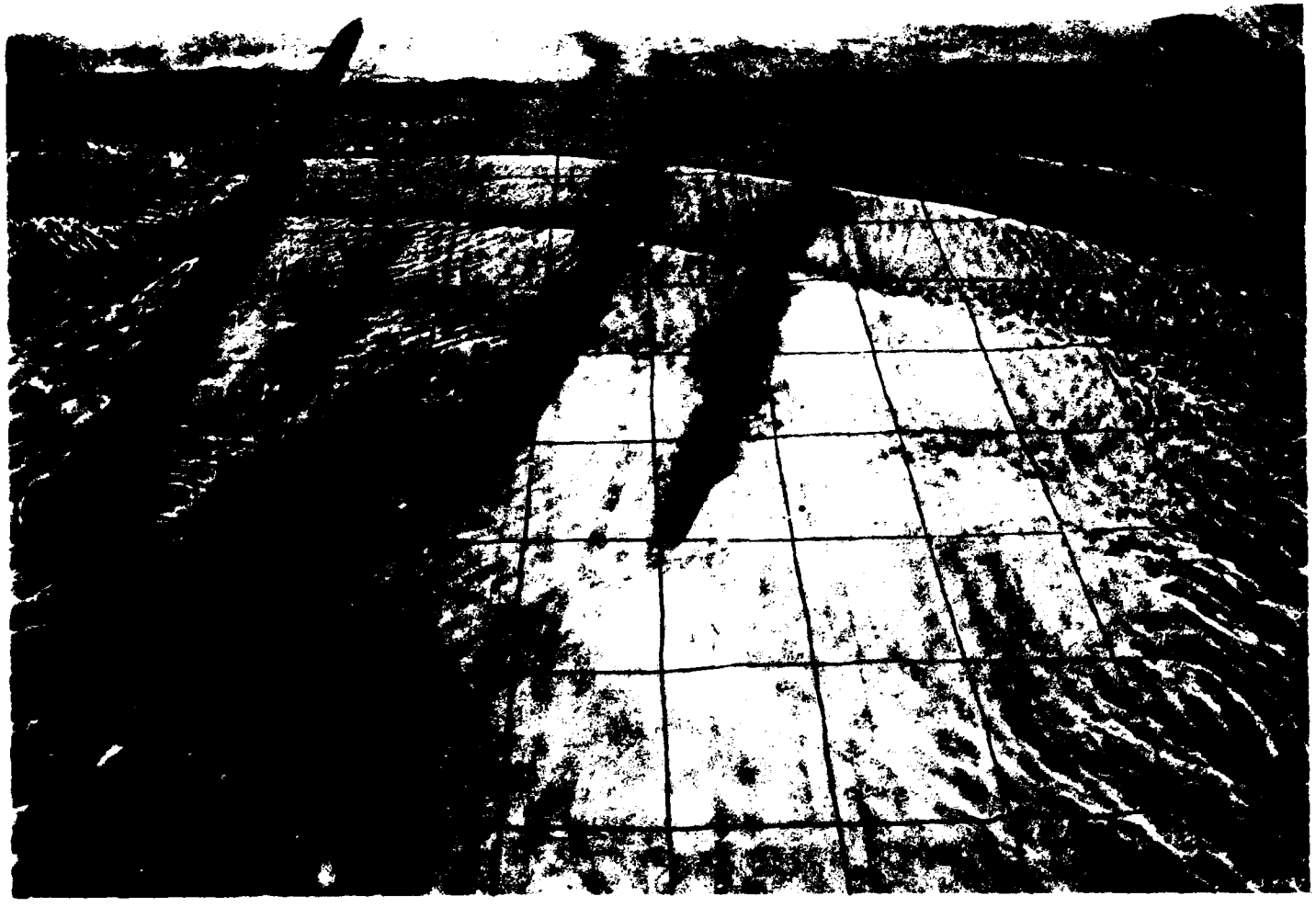

Photo 21. Net dye movement, time after starting generator = 4.0 min, wave period = 1.0 sec, wave height near generator = 0.139 ft, angle of incidence = 30 deg

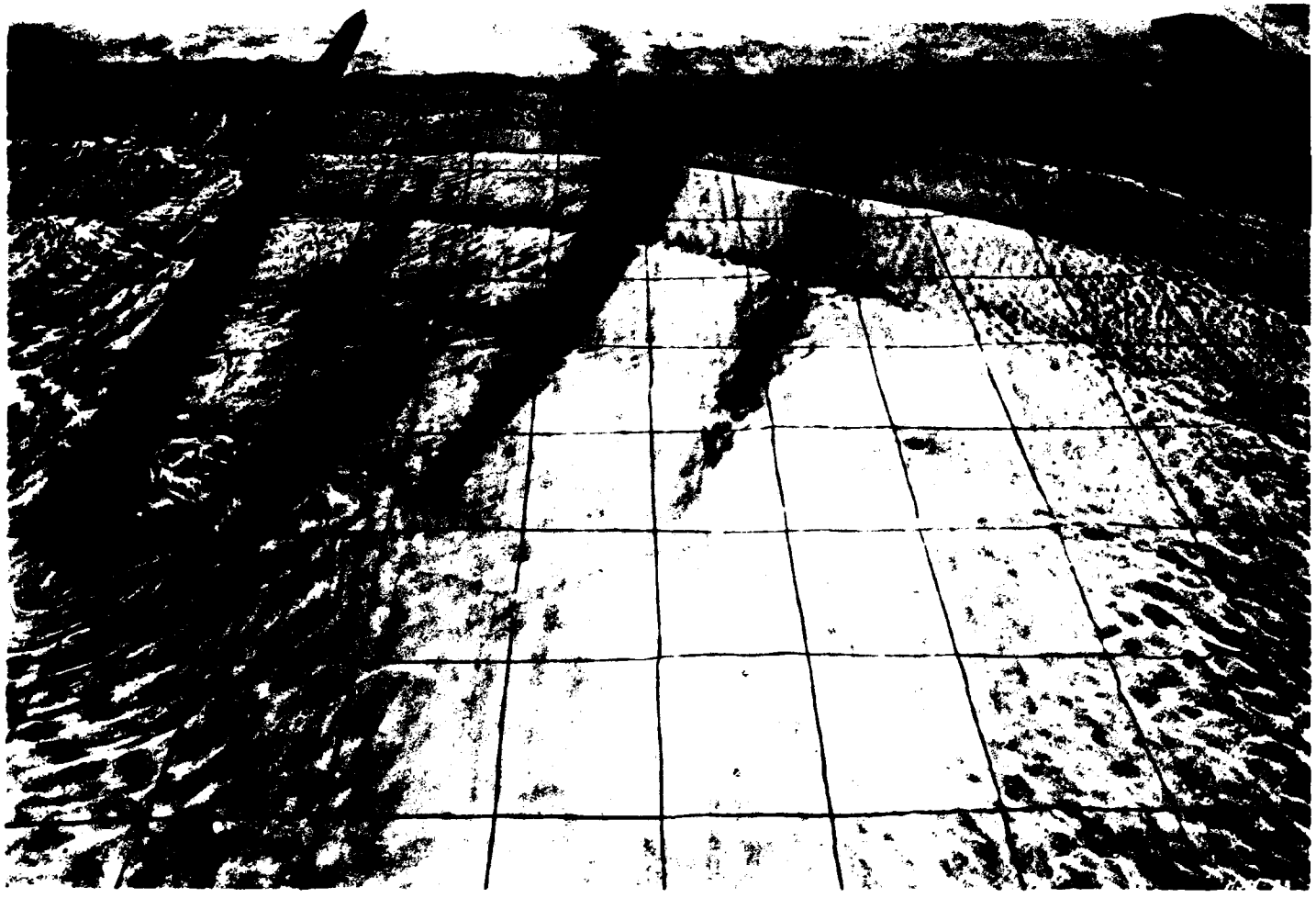

Photo 22. Net dye movement, time after starting generator = 5.0 min, wave period = 1.0 sec, wave height near generator = 0.139 ft, angle of incidence = 30 deg

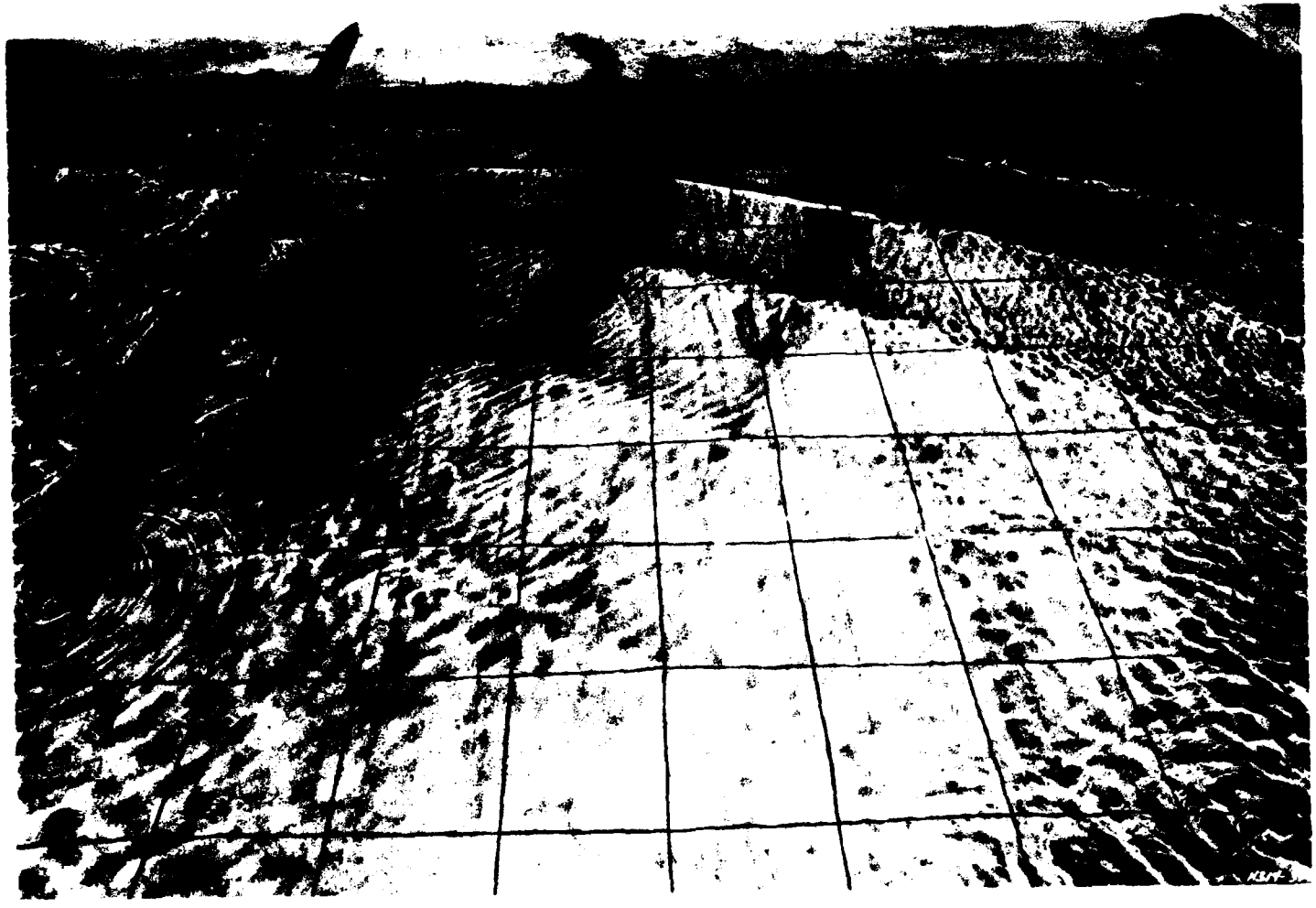

Photo 23. Net dye movement, time after starting generator = 6.0 min, wave period = 1.0 sec, wave height near generator = 0.139 ft, angle of incidence = 30 deg

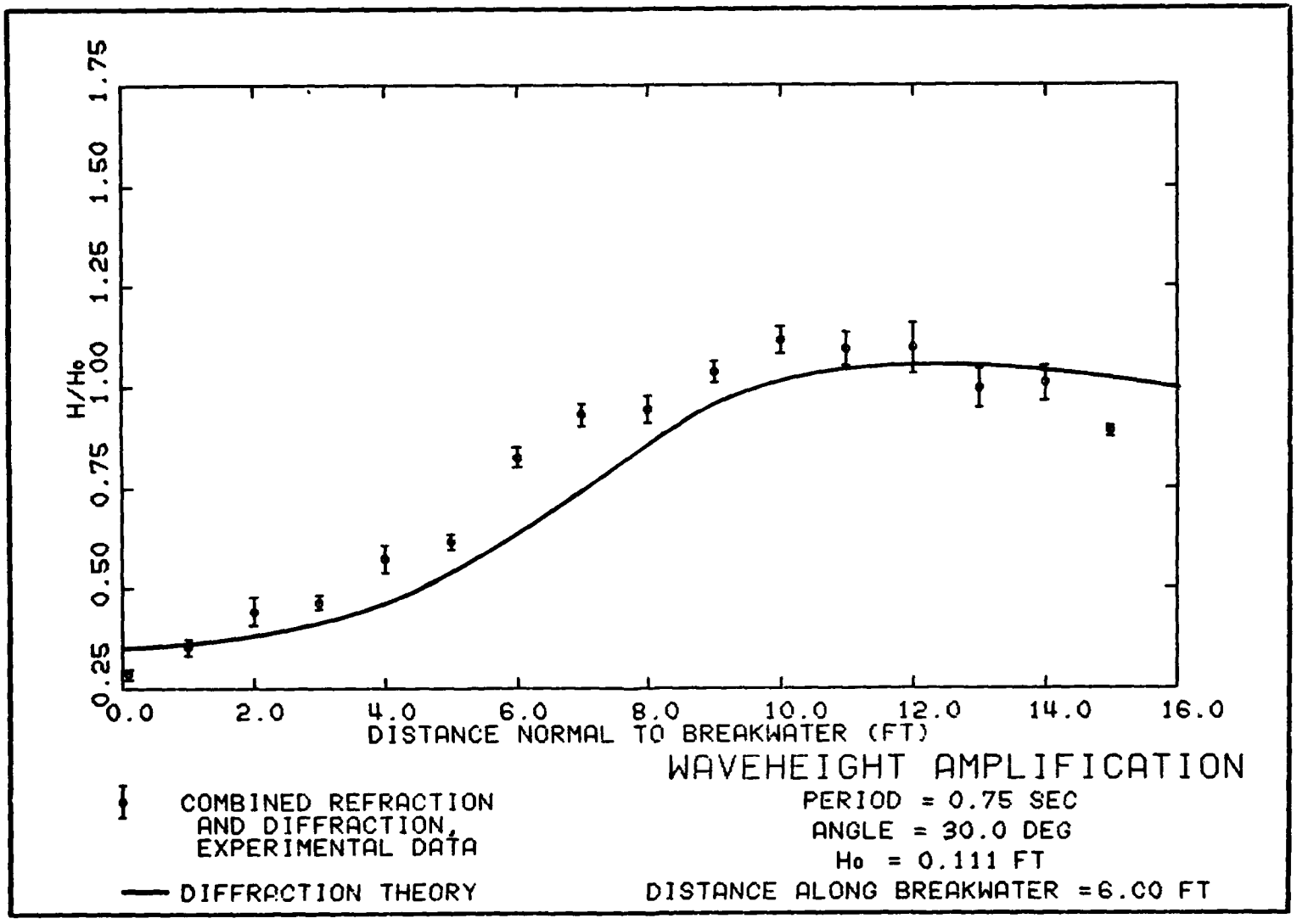
H/Ho
0.25
0.50
0.75
1.00
1.25
1.50
1.75
0.0
2.0
4.0
6.0
8.0
10.0
12.0
14.0
16.0
DISTANCE NORMAL TO BREAKWATER (FT)
WAVEHEIGHT AMPLIFICATION
PERIOD = 0.75 SEC
ANGLE = 30.0 DEG
Ho = 0.111 FT
DISTANCE ALONG BREAKWATER = 6.00 FT
COMBINED REFRACTION AND DIFFRACTION, EXPERIMENTAL DATA
DIFFRACTION THEORY

PLATE 1

PLATE 2

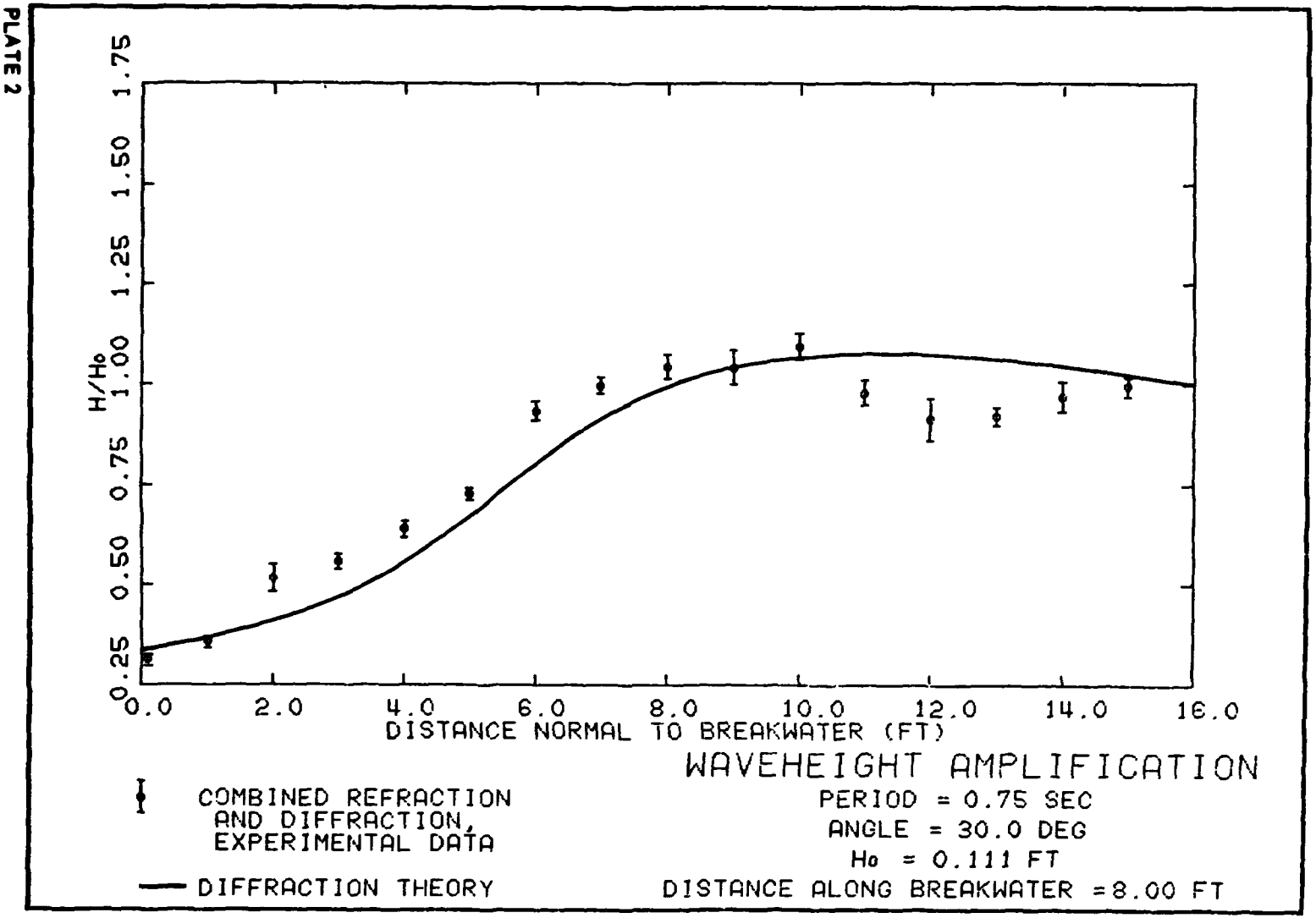
H/Ho
0.25
0.50
0.75
1.00
1.25
1.50
1.75
0.0
2.0
4.0
6.0
8.0
10.0
12.0
14.0
16.0
DISTANCE NORMAL TO BREAKWATER (FT)
WAVEHEIGHT AMPLIFICATION
PERIOD = 0.75 SEC
ANGLE = 30.0 DEG
Ho = 0.111 FT
DISTANCE ALONG BREAKWATER = 8.00 FT
COMBINED REFRACTION AND DIFFRACTION, EXPERIMENTAL DATA
DIFFRACTION THEORY

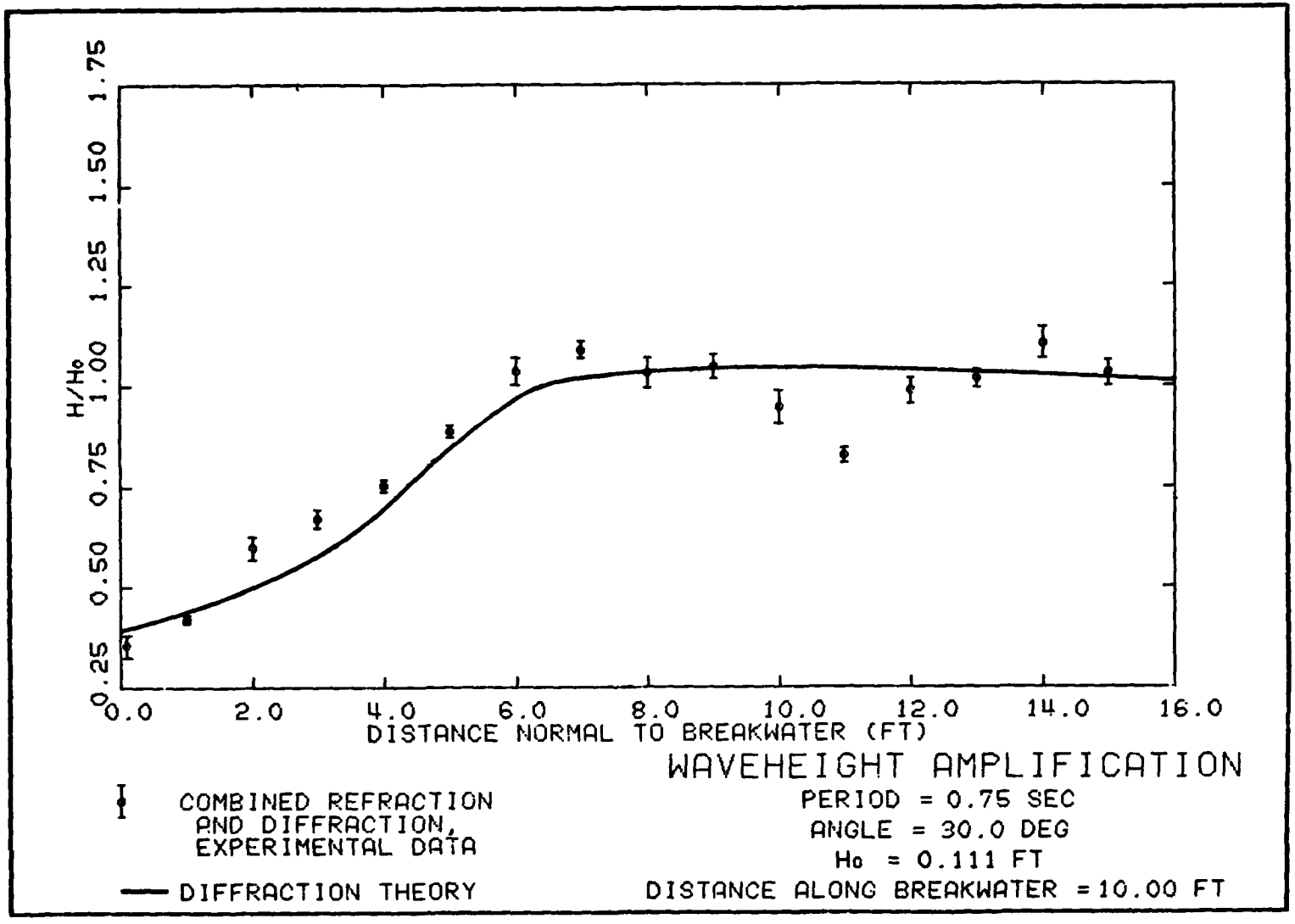
H/Ho
0.25
0.50
0.75
1.00
1.25
1.50
1.75
0.0
2.0
4.0
6.0
8.0
10.0
12.0
14.0
16.0
DISTANCE NORMAL TO BREAKWATER (FT)
WAVEHEIGHT AMPLIFICATION
COMBINED REFRACTION AND DIFFRACTION, EXPERIMENTAL DATA
DIFFRACTION THEORY
PERIOD = 0.75 SEC
ANGLE = 30.0 DEG
Ho = 0.111 FT
DISTANCE ALONG BREAKWATER = 10.00 FT

PLATE 3

PLATE 4

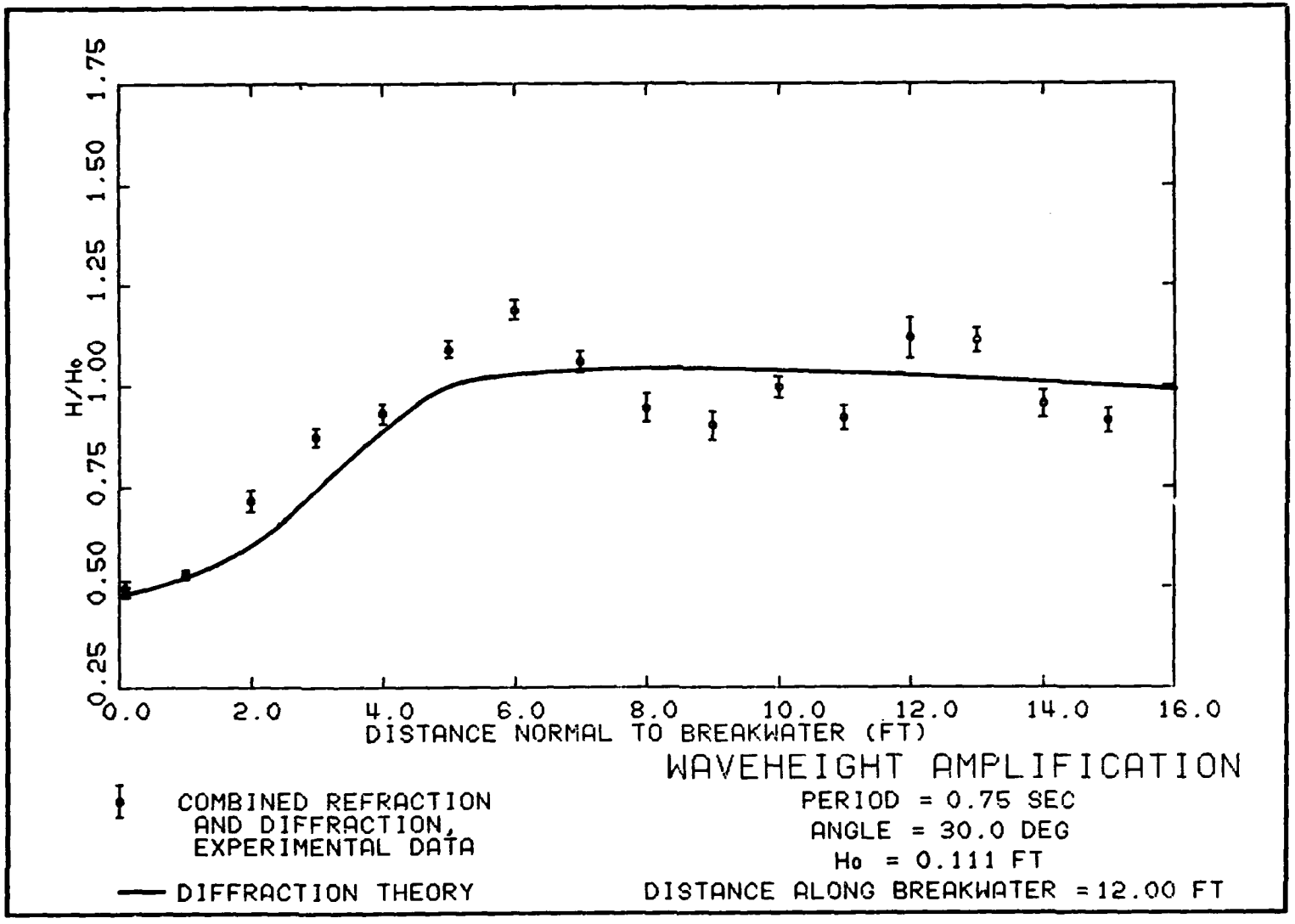
H/Ho
0.25
0.50
0.75
1.00
1.25
1.50
1.75
0.0
2.0
4.0
6.0
8.0
10.0
12.0
14.0
16.0
DISTANCE NORMAL TO BREAKWATER (FT)
WAVEHEIGHT AMPLIFICATION
PERIOD = 0.75 SEC
ANGLE = 30.0 DEG
Ho = 0.111 FT
DISTANCE ALONG BREAKWATER = 12.00 FT
COMBINED REFRACTION AND DIFFRACTION, EXPERIMENTAL DATA
DIFFRACTION THEORY

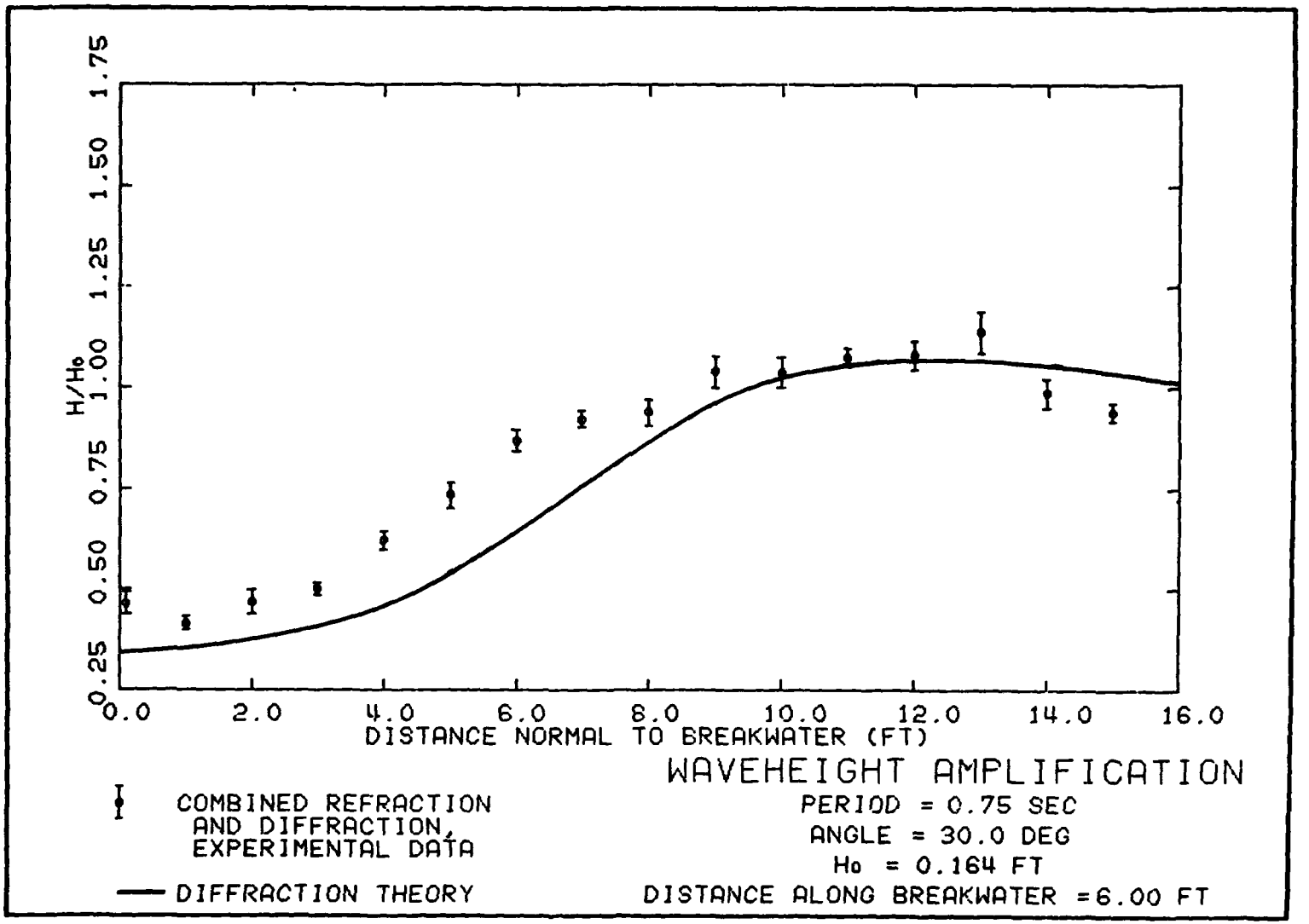
H/Ho
0.25
0.50
0.75
1.00
1.25
1.50
1.75
0.0
2.0
4.0
6.0
8.0
10.0
12.0
14.0
16.0
DISTANCE NORMAL TO BREAKWATER (FT)
WAVEHEIGHT AMPLIFICATION
PERIOD = 0.75 SEC
ANGLE = 30.0 DEG
Ho = 0.164 FT
DISTANCE ALONG BREAKWATER = 6.00 FT
COMBINED REFRACTION AND DIFFRACTION, EXPERIMENTAL DATA
DIFFRACTION THEORY

PLATE 5

PLATE 6

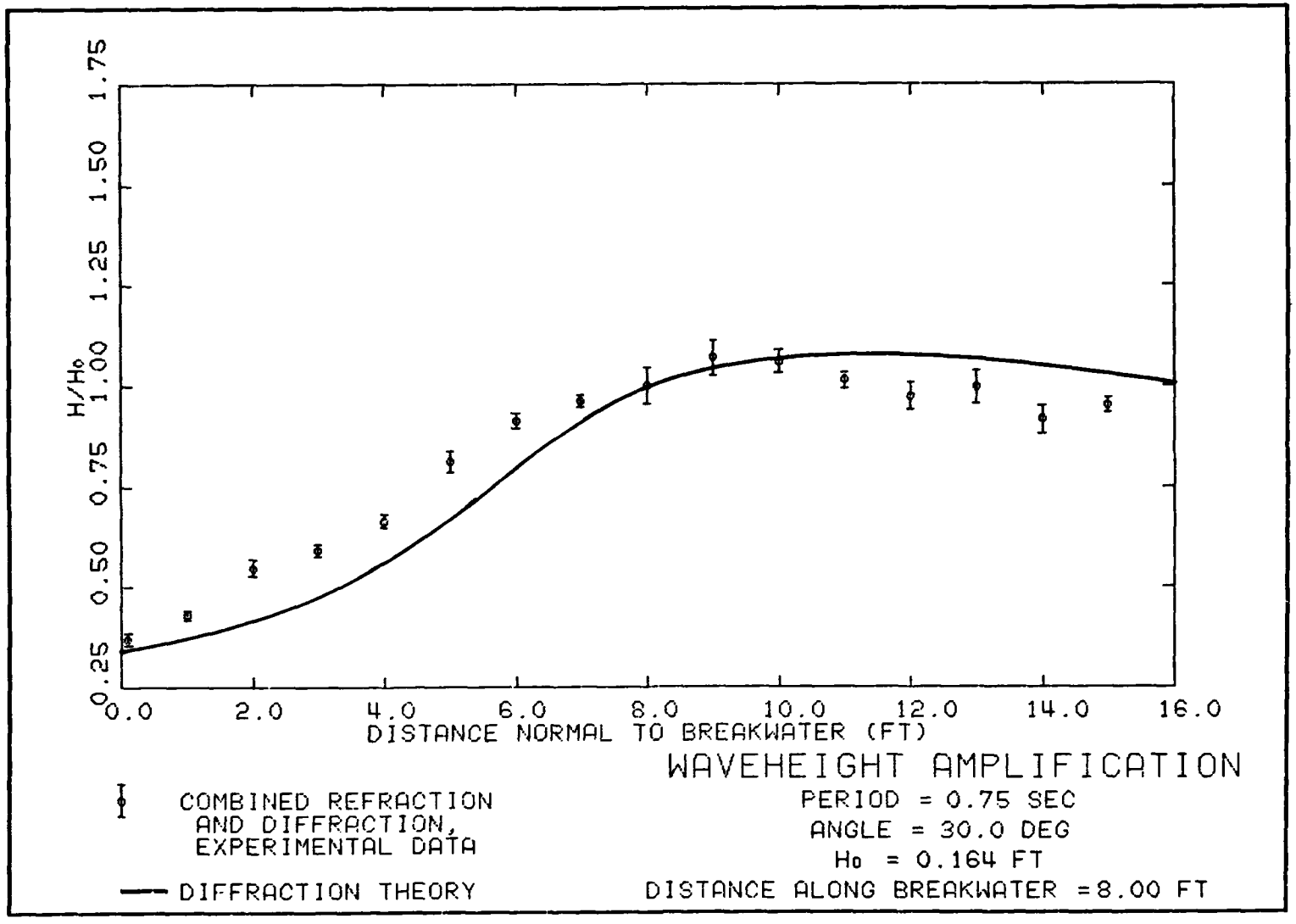
H/H0
0.25
0.50
0.75
1.00
1.25
1.50
1.75
0.0
2.0
4.0
6.0
8.0
10.0
12.0
14.0
16.0
DISTANCE NORMAL TO BREAKWATER (FT)
WAVEHEIGHT AMPLIFICATION
COMBINED REFRACTION AND DIFFRACTION, EXPERIMENTAL DATA
DIFFRACTION THEORY
PERIOD = 0.75 SEC
ANGLE = 30.0 DEG
H0 = 0.164 FT
DISTANCE ALONG BREAKWATER = 8.00 FT

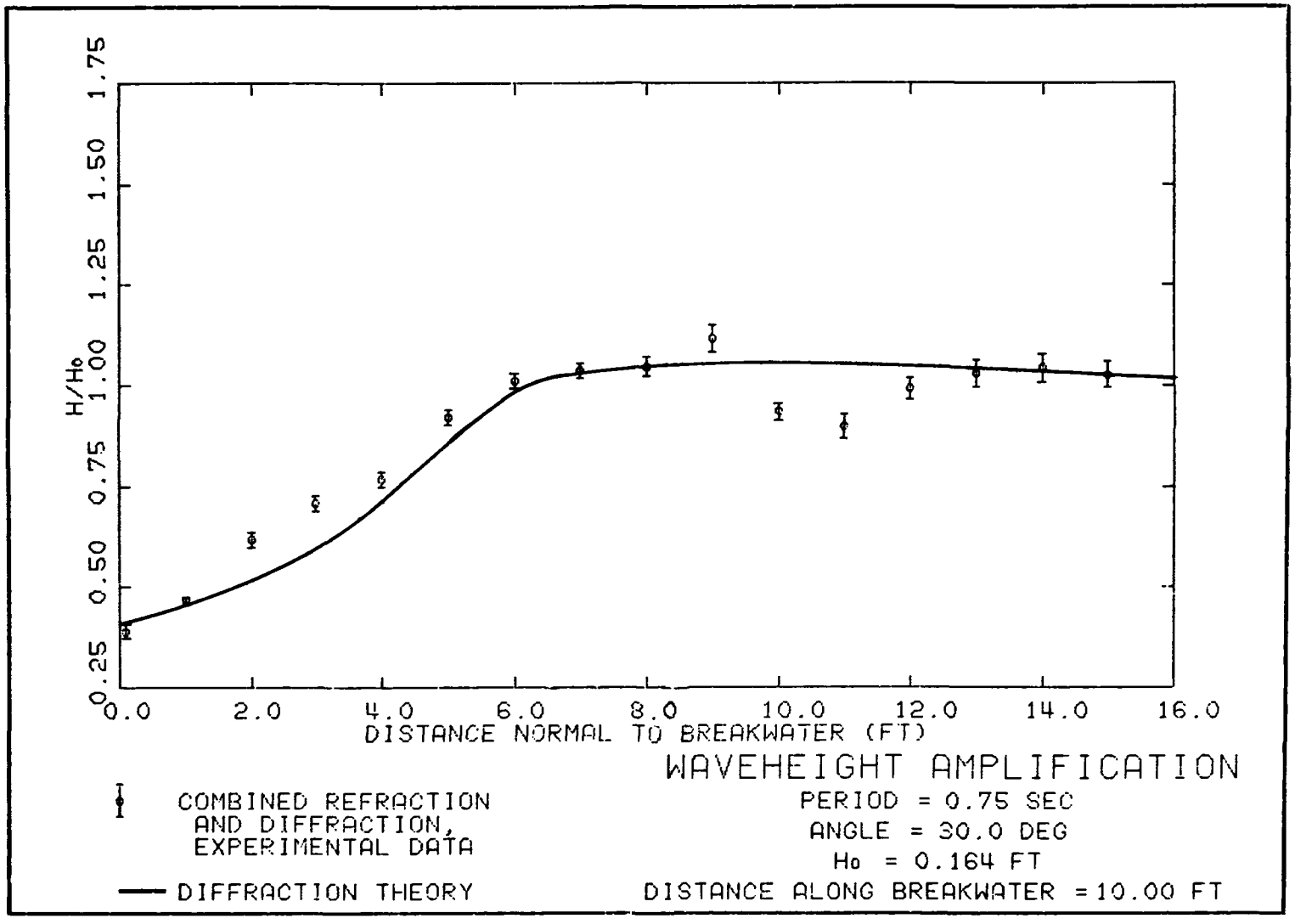
H/Ho
0.25
0.50
0.75
1.00
1.25
1.50
1.75
0.0
2.0
4.0
6.0
8.0
10.0
12.0
14.0
16.0
DISTANCE NORMAL TO BREAKWATER (FT)
WAVEHEIGHT AMPLIFICATION
PERIOD = 0.75 SEC
ANGLE = 30.0 DEG
Ho = 0.164 FT
DISTANCE ALONG BREAKWATER = 10.00 FT
COMBINED REFRACTION AND DIFFRACTION, EXPERIMENTAL DATA
DIFFRACTION THEORY

PLATE 7

PLATE 8

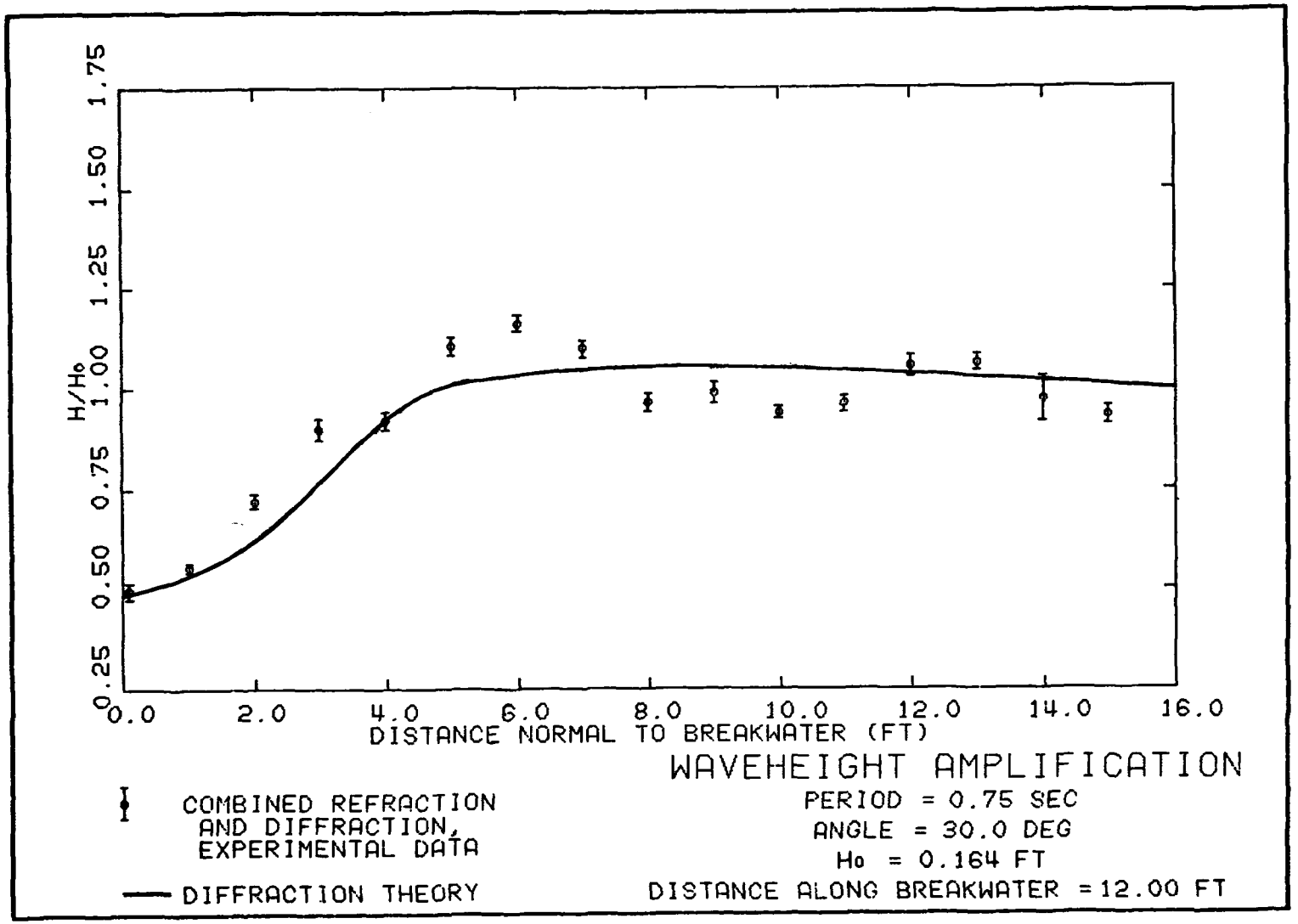
H/Ho
0.25
0.50
0.75
1.00
1.25
1.50
1.75
0.0
2.0
4.0
6.0
8.0
10.0
12.0
14.0
16.0
DISTANCE NORMAL TO BREAKWATER (FT)
WAVEHEIGHT AMPLIFICATION
COMBINED REFRACTION AND DIFFRACTION, EXPERIMENTAL DATA
DIFFRACTION THEORY
PERIOD = 0.75 SEC
ANGLE = 30.0 DEG
Ho = 0.164 FT
DISTANCE ALONG BREAKWATER = 12.00 FT

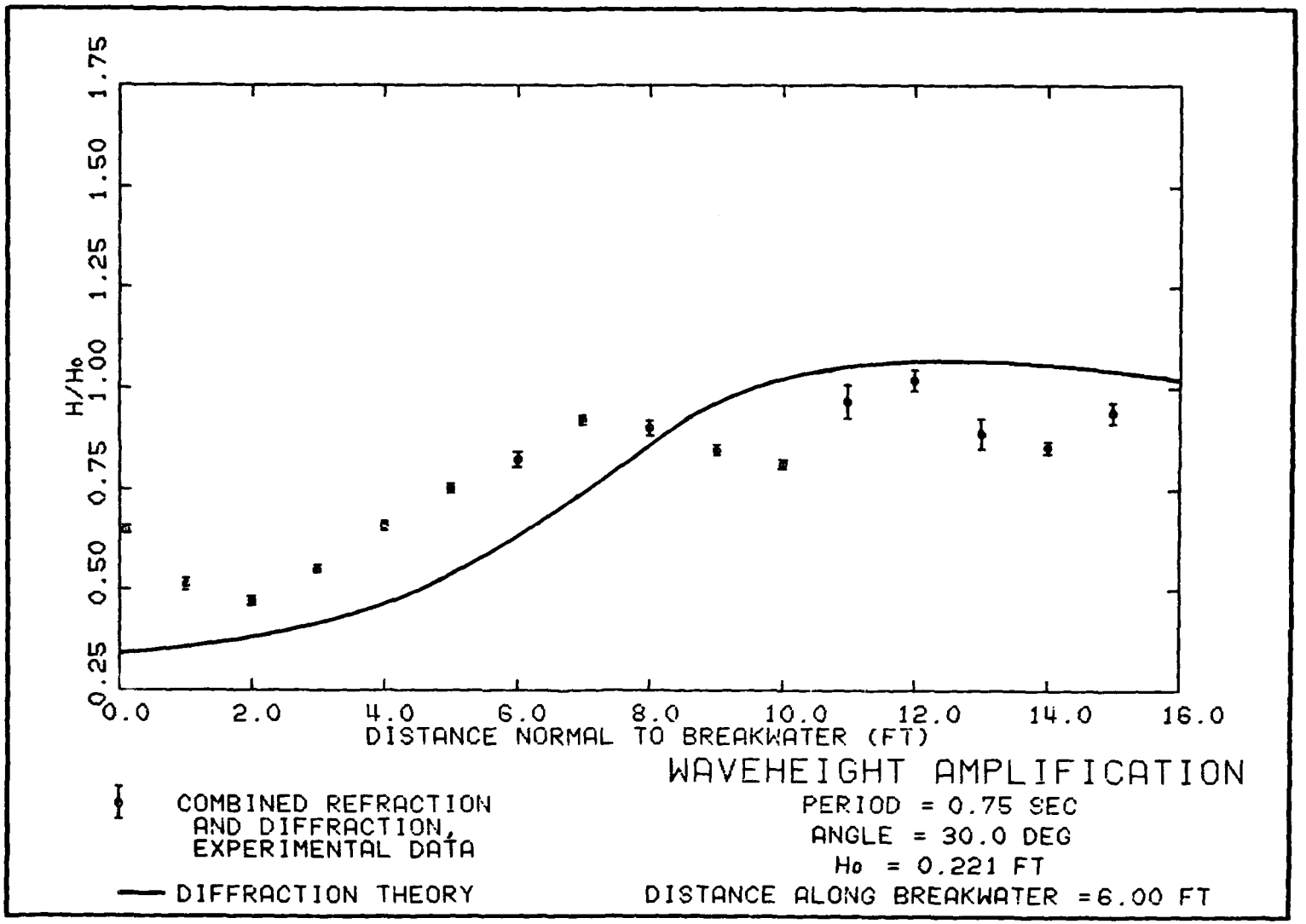
H/Ho
0.25
0.50
0.75
1.00
1.25
1.50
1.75
0.0
2.0
4.0
6.0
8.0
10.0
12.0
14.0
16.0
DISTANCE NORMAL TO BREAKWATER (FT)
WAVEHEIGHT AMPLIFICATION
COMBINED REFRACTION AND DIFFRACTION, EXPERIMENTAL DATA
DIFFRACTION THEORY
PERIOD = 0.75 SEC
ANGLE = 30.0 DEG
Ho = 0.221 FT
DISTANCE ALONG BREAKWATER = 6.00 FT

PLATE 9

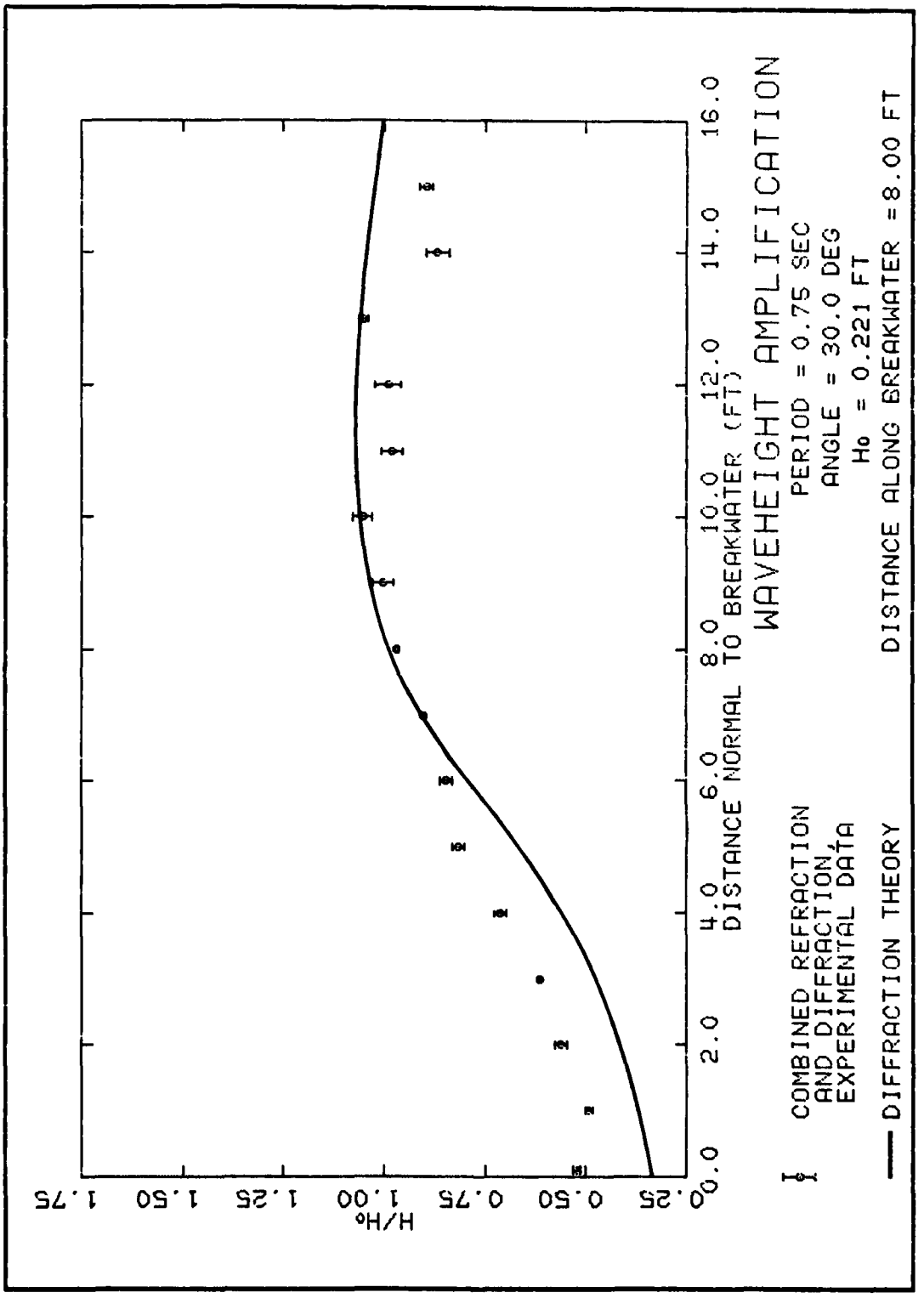
WAVEHEIGHT AMPLIFICATION
PERIOD = 0.75 SEC
ANGLE = 30.0 DEG
Ho = 0.221 FT
DISTANCE ALONG BREAKWATER = 8.00 FT
COMBINED REFRACTION AND DIFFRACTION, EXPERIMENTAL DATA
DIFFRACTION THEORY
H/Ho
0.25
0.50
0.75
1.00
1.25
1.50
1.75
0.0
2.0
4.0
6.0
8.0
10.0
12.0
14.0
16.0
DISTANCE NORMAL TO BREAKWATER (FT)

PLATE 10

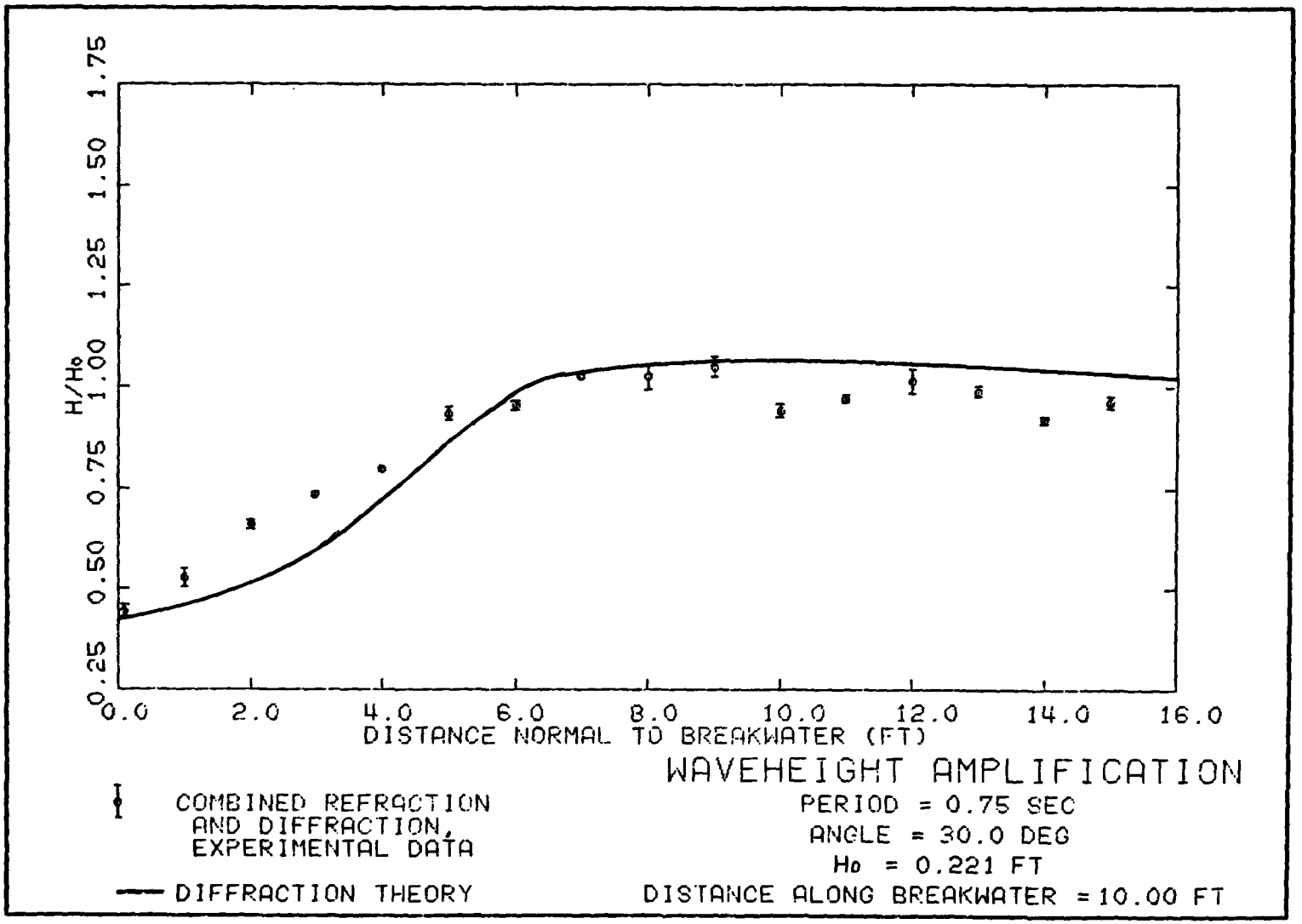
H/Ho
0.25
0.50
0.75
1.00
1.25
1.50
1.75
0.0
2.0
4.0
6.0
8.0
10.0
12.0
14.0
16.0
DISTANCE NORMAL TO BREAKWATER (FT)
WAVEHEIGHT AMPLIFICATION
PERIOD = 0.75 SEC
ANGLE = 30.0 DEG
Ho = 0.221 FT
DISTANCE ALONG BREAKWATER = 10.00 FT
COMBINED REFRACTION AND DIFFRACTION, EXPERIMENTAL DATA
DIFFRACTION THEORY

PLATE 11

PLATE 12

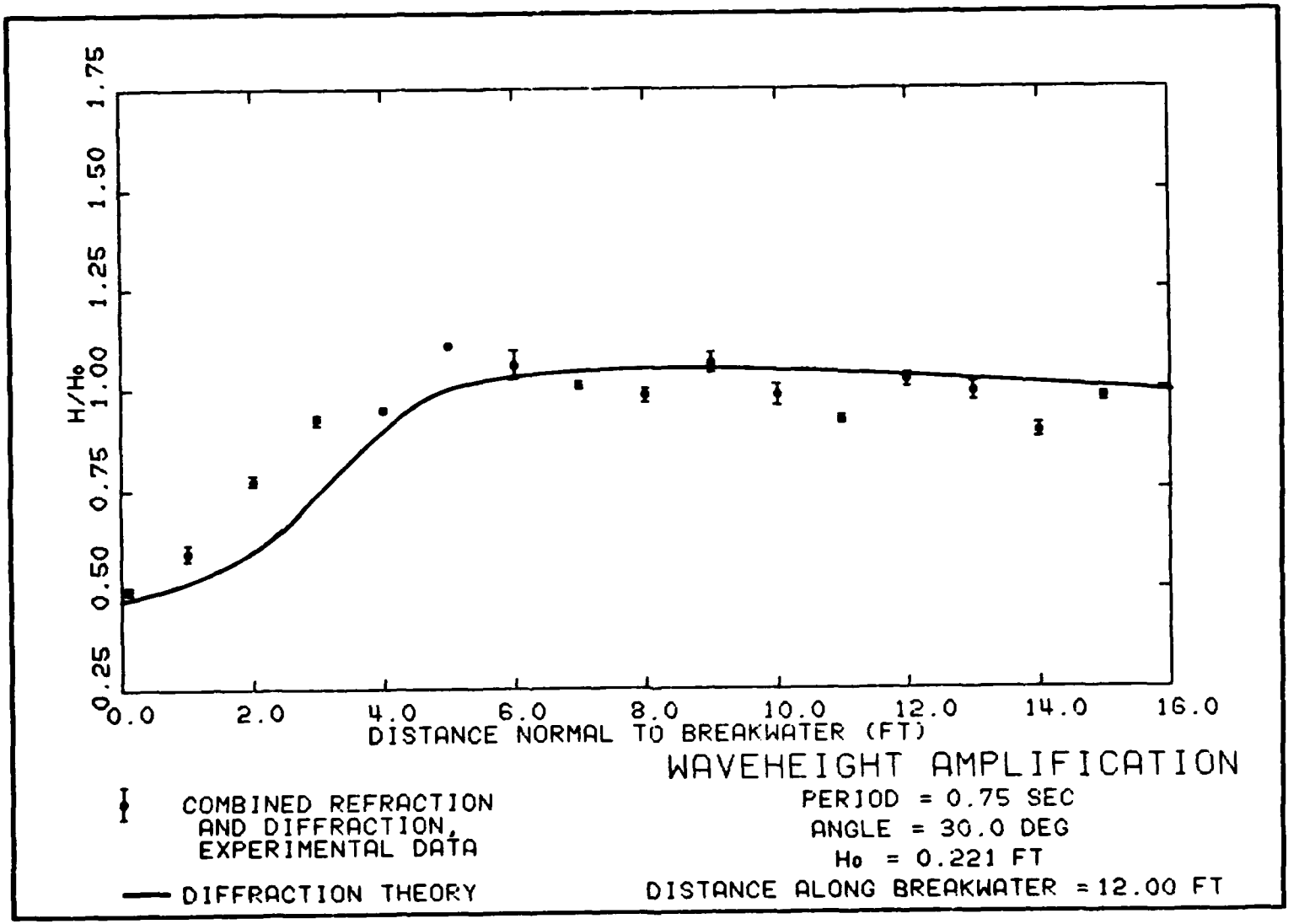
H/Ho
0.25
0.50
0.75
1.00
1.25
1.50
1.75
0.0
2.0
4.0
6.0
8.0
10.0
12.0
14.0
16.0
DISTANCE NORMAL TO BREAKWATER (FT)
WAVEHEIGHT AMPLIFICATION
PERIOD = 0.75 SEC
ANGLE = 30.0 DEG
Ho = 0.221 FT
DISTANCE ALONG BREAKWATER = 12.00 FT
COMBINED REFRACTION AND DIFFRACTION, EXPERIMENTAL DATA
DIFFRACTION THEORY

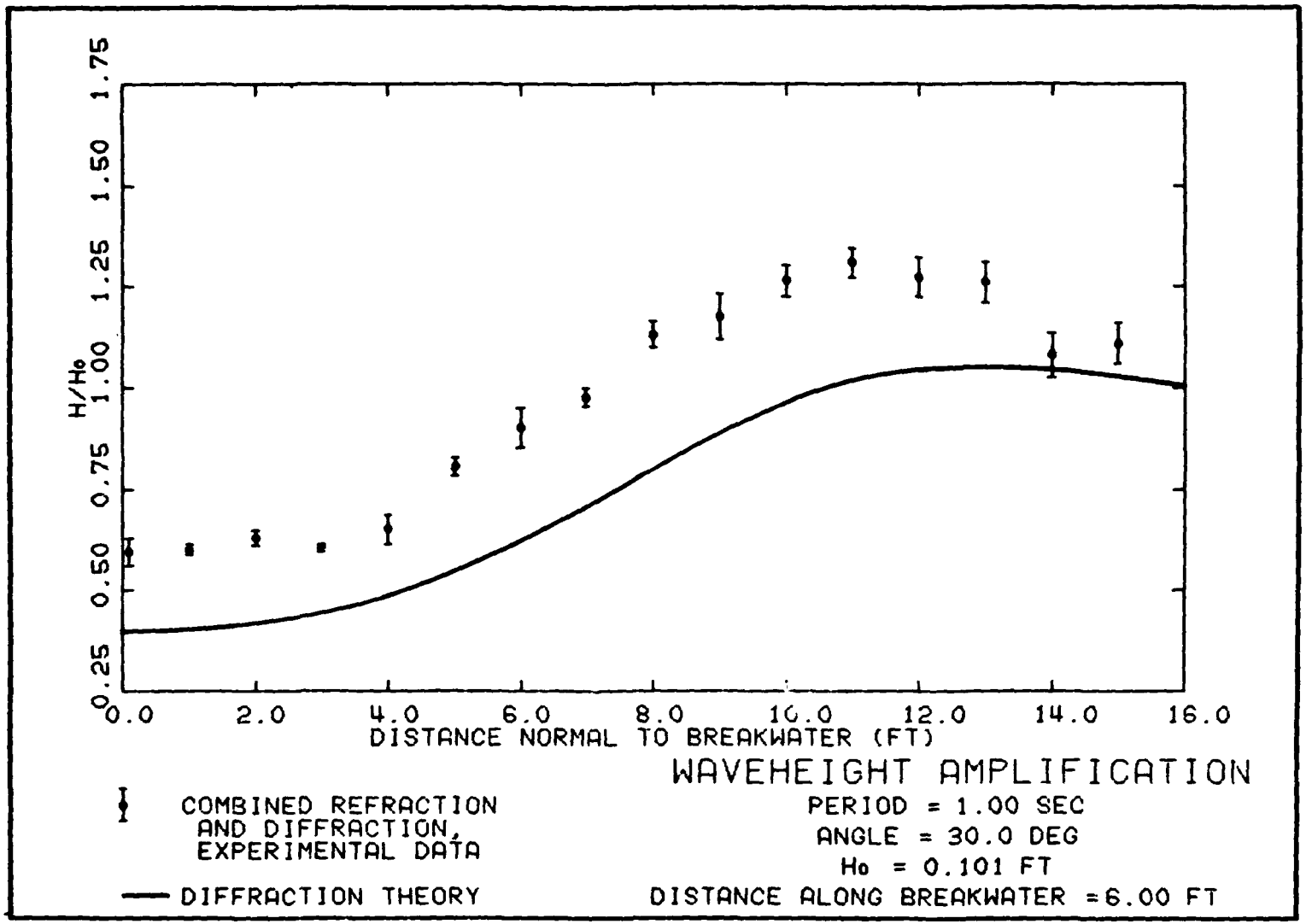
H/Ho
0.25
0.50
0.75
1.00
1.25
1.50
1.75
0.0
2.0
4.0
6.0
8.0
10.0
12.0
14.0
16.0
DISTANCE NORMAL TO BREAKWATER (FT)
WAVEHEIGHT AMPLIFICATION
COMBINED REFRACTION AND DIFFRACTION, EXPERIMENTAL DATA
DIFFRACTION THEORY
PERIOD = 1.00 SEC
ANGLE = 30.0 DEG
Ho = 0.101 FT
DISTANCE ALONG BREAKWATER = 6.00 FT

PLATE 13

PLATE 14

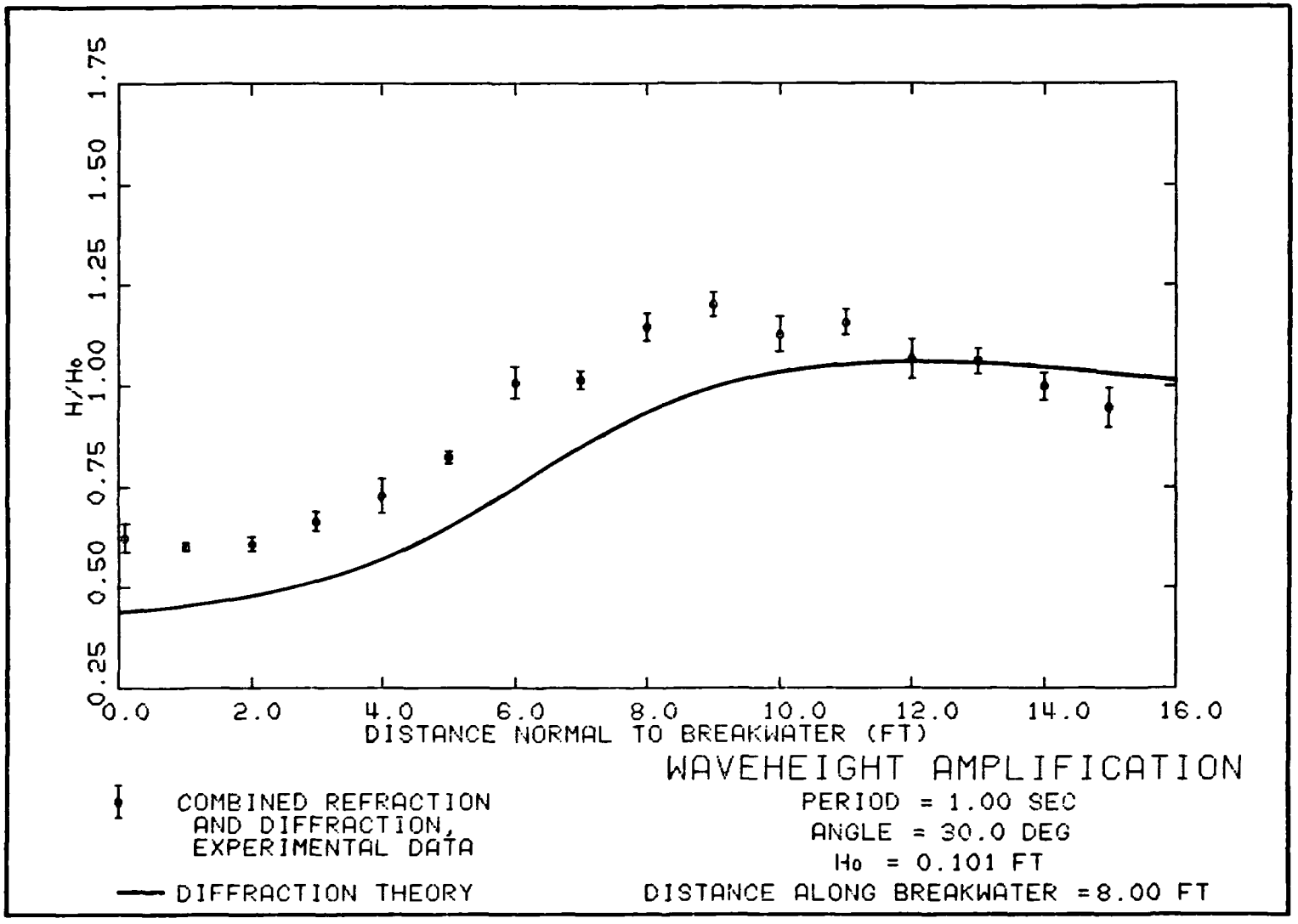
H/Ho
0.25
0.50
0.75
1.00
1.25
1.50
1.75
0.0
2.0
4.0
6.0
8.0
10.0
12.0
14.0
16.0
DISTANCE NORMAL TO BREAKWATER (FT)
WAVEHEIGHT AMPLIFICATION
COMBINED REFRACTION AND DIFFRACTION, EXPERIMENTAL DATA
DIFFRACTION THEORY
PERIOD = 1.00 SEC
ANGLE = 30.0 DEG
Ho = 0.101 FT
DISTANCE ALONG BREAKWATER = 8.00 FT

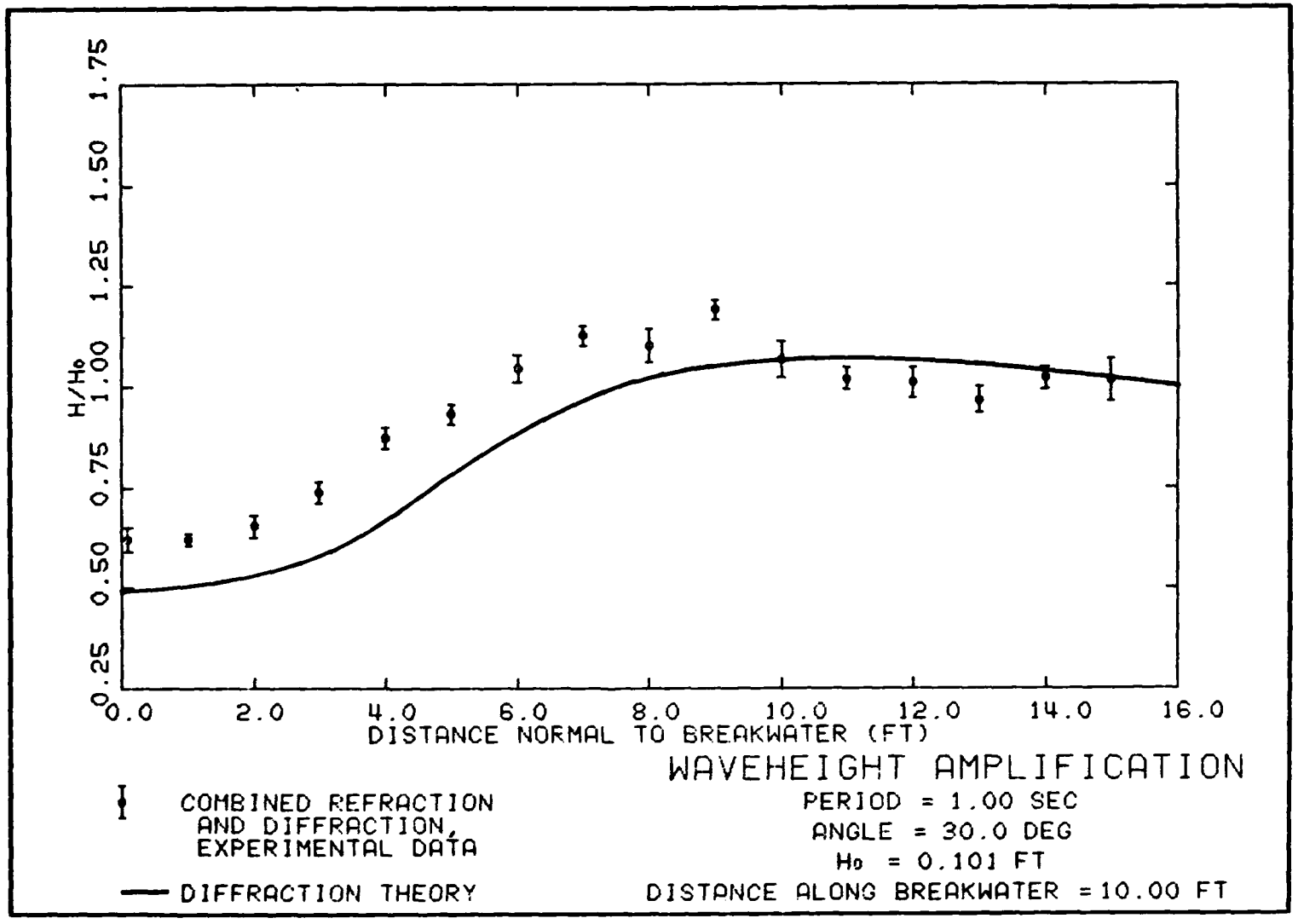
H/Ho
0.25
0.50
0.75
1.00
1.25
1.50
1.75
0.0
2.0
4.0
6.0
8.0
10.0
12.0
14.0
16.0
DISTANCE NORMAL TO BREAKWATER (FT)
WAVEHEIGHT AMPLIFICATION
COMBINED REFRACTION AND DIFFRACTION, EXPERIMENTAL DATA
DIFFRACTION THEORY
PERIOD = 1.00 SEC
ANGLE = 30.0 DEG
Ho = 0.101 FT
DISTANCE ALONG BREAKWATER = 10.00 FT

PLATE 15

PLATE 16

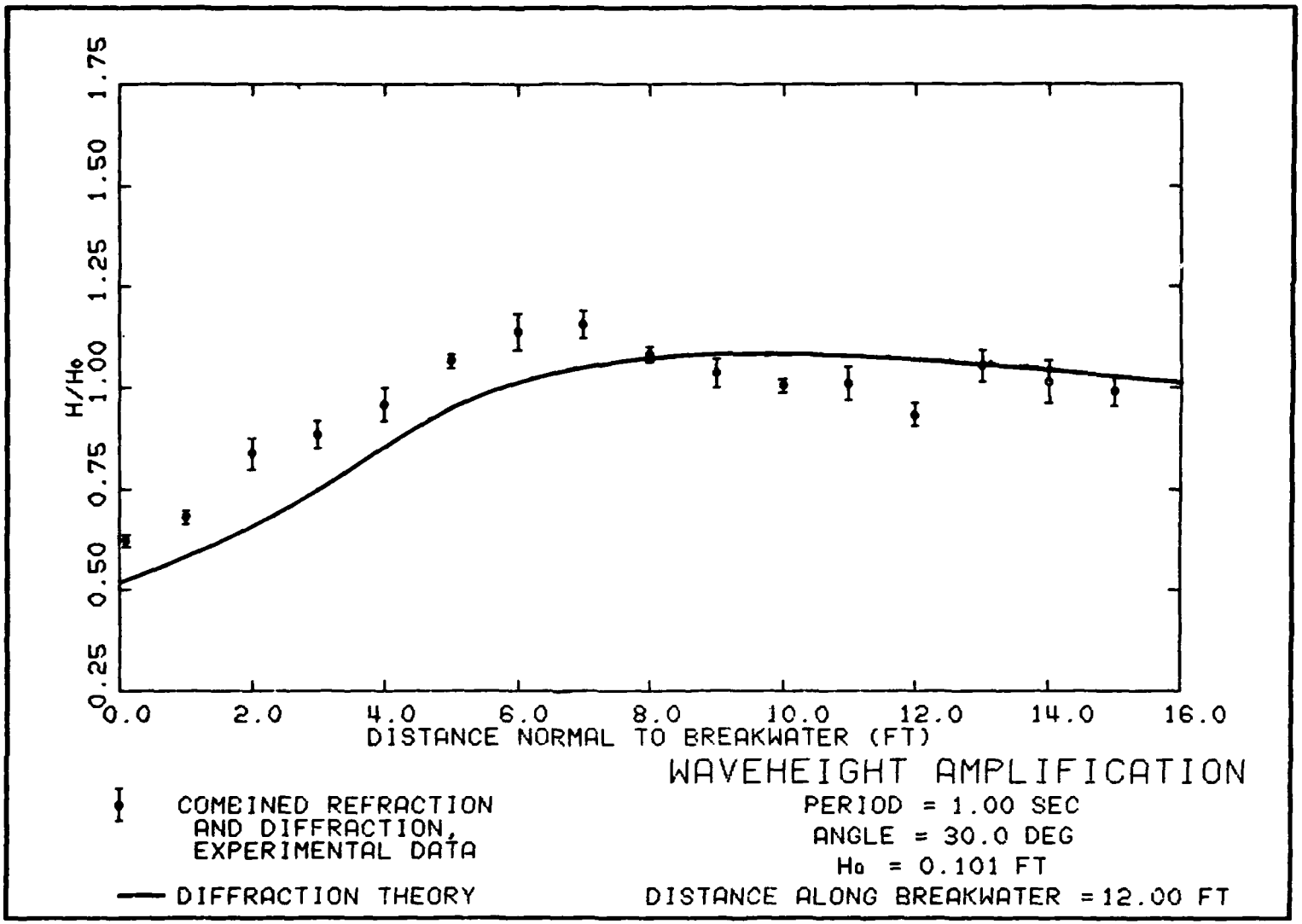
H/Ho
0.25
0.50
0.75
1.00
1.25
1.50
1.75
0.0
2.0
4.0
6.0
8.0
10.0
12.0
14.0
16.0
DISTANCE NORMAL TO BREAKWATER (FT)
WAVEHEIGHT AMPLIFICATION
COMBINED REFRACTION AND DIFFRACTION, EXPERIMENTAL DATA
DIFFRACTION THEORY
PERIOD = 1.00 SEC
ANGLE = 30.0 DEG
Ho = 0.101 FT
DISTANCE ALONG BREAKWATER = 12.00 FT

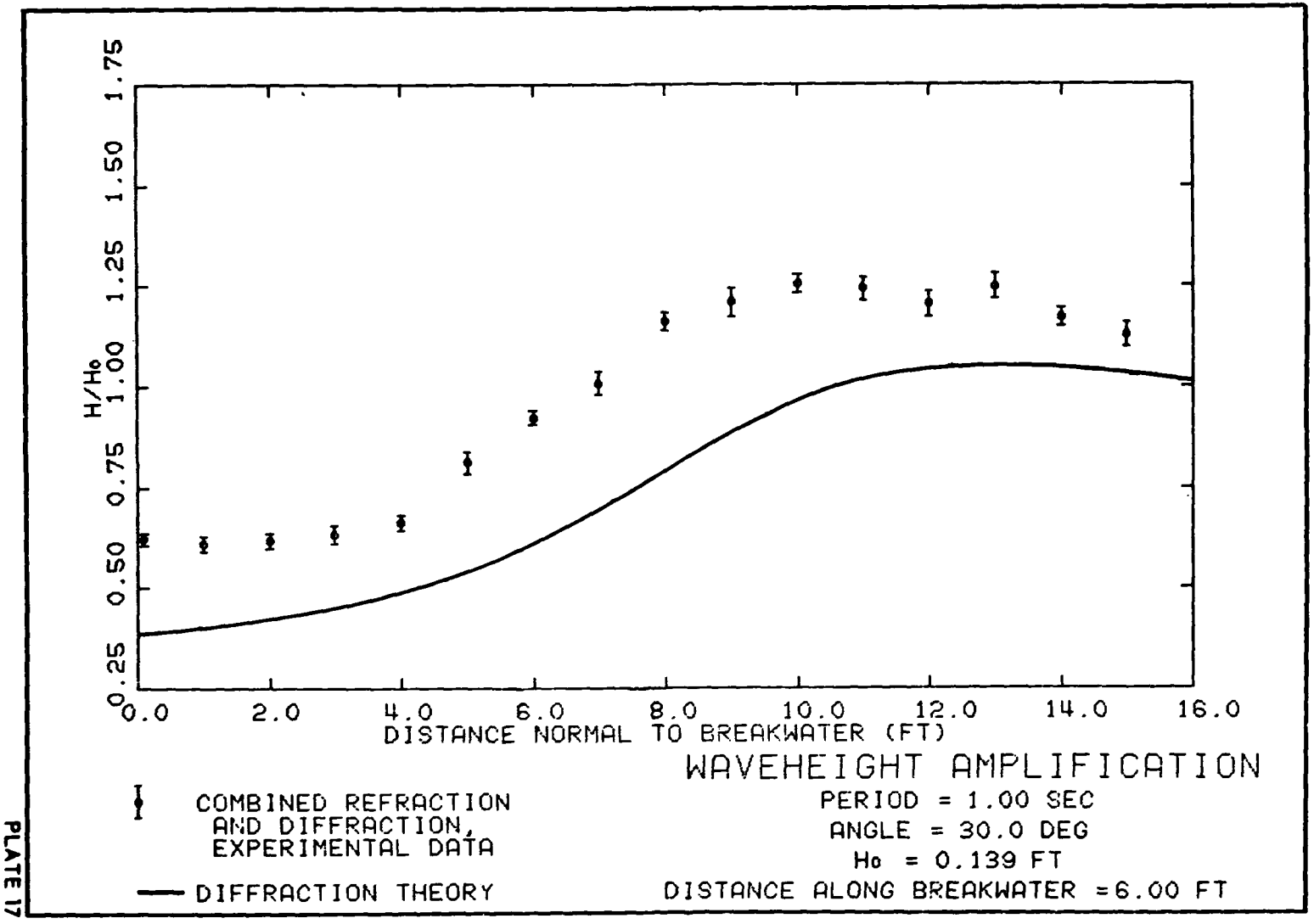
H/Ho
0.25
0.50
0.75
1.00
1.25
1.50
1.75
0.0
2.0
4.0
6.0
8.0
10.0
12.0
14.0
16.0
DISTANCE NORMAL TO BREAKWATER (FT)
WAVEHEIGHT AMPLIFICATION
COMBINED REFRACTION AND DIFFRACTION, EXPERIMENTAL DATA
DIFFRACTION THEORY
PERIOD = 1.00 SEC
ANGLE = 30.0 DEG
Ho = 0.139 FT
DISTANCE ALONG BREAKWATER = 6.00 FT

PLATE 17

PLATE 18

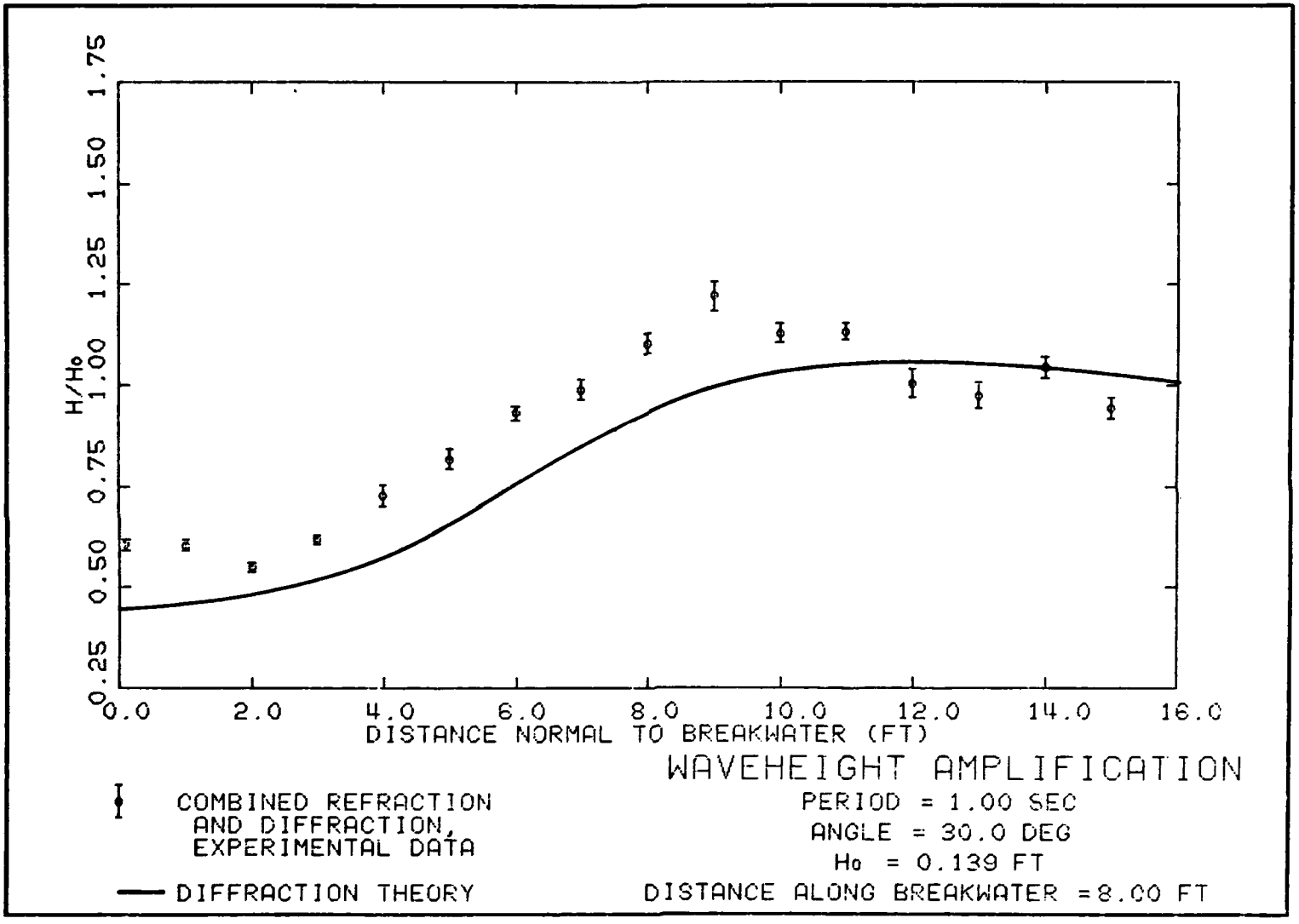
H/Ho
0.25
0.50
0.75
1.00
1.25
1.50
1.75
0.0
2.0
4.0
6.0
8.0
10.0
12.0
14.0
16.0
DISTANCE NORMAL TO BREAKWATER (FT)
WAVEHEIGHT AMPLIFICATION
PERIOD = 1.00 SEC
ANGLE = 30.0 DEG
Ho = 0.139 FT
DISTANCE ALONG BREAKWATER = 8.00 FT
COMBINED REFRACTION AND DIFFRACTION, EXPERIMENTAL DATA
DIFFRACTION THEORY

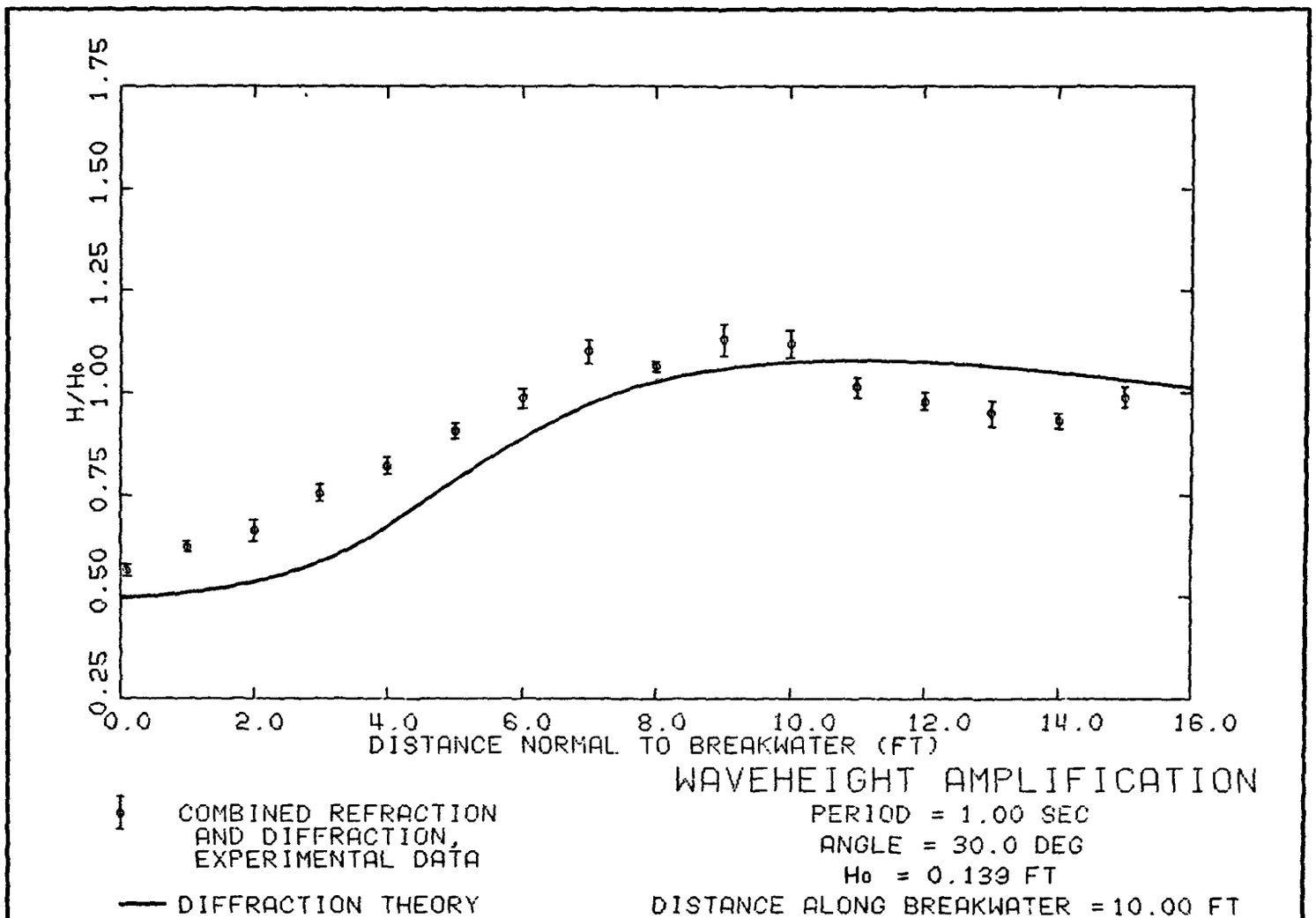
H/Ho
0.25
0.50
0.75
1.00
1.25
1.50
1.75
0.0
2.0
4.0
6.0
8.0
10.0
12.0
14.0
16.0
DISTANCE NORMAL TO BREAKWATER (FT)
WAVEHEIGHT AMPLIFICATION
PERIOD = 1.00 SEC
ANGLE = 30.0 DEG
Ho = 0.139 FT
DISTANCE ALONG BREAKWATER = 10.00 FT
COMBINED REFRACTION AND DIFFRACTION, EXPERIMENTAL DATA
DIFFRACTION THEORY

PLATE 19

PLATE 20

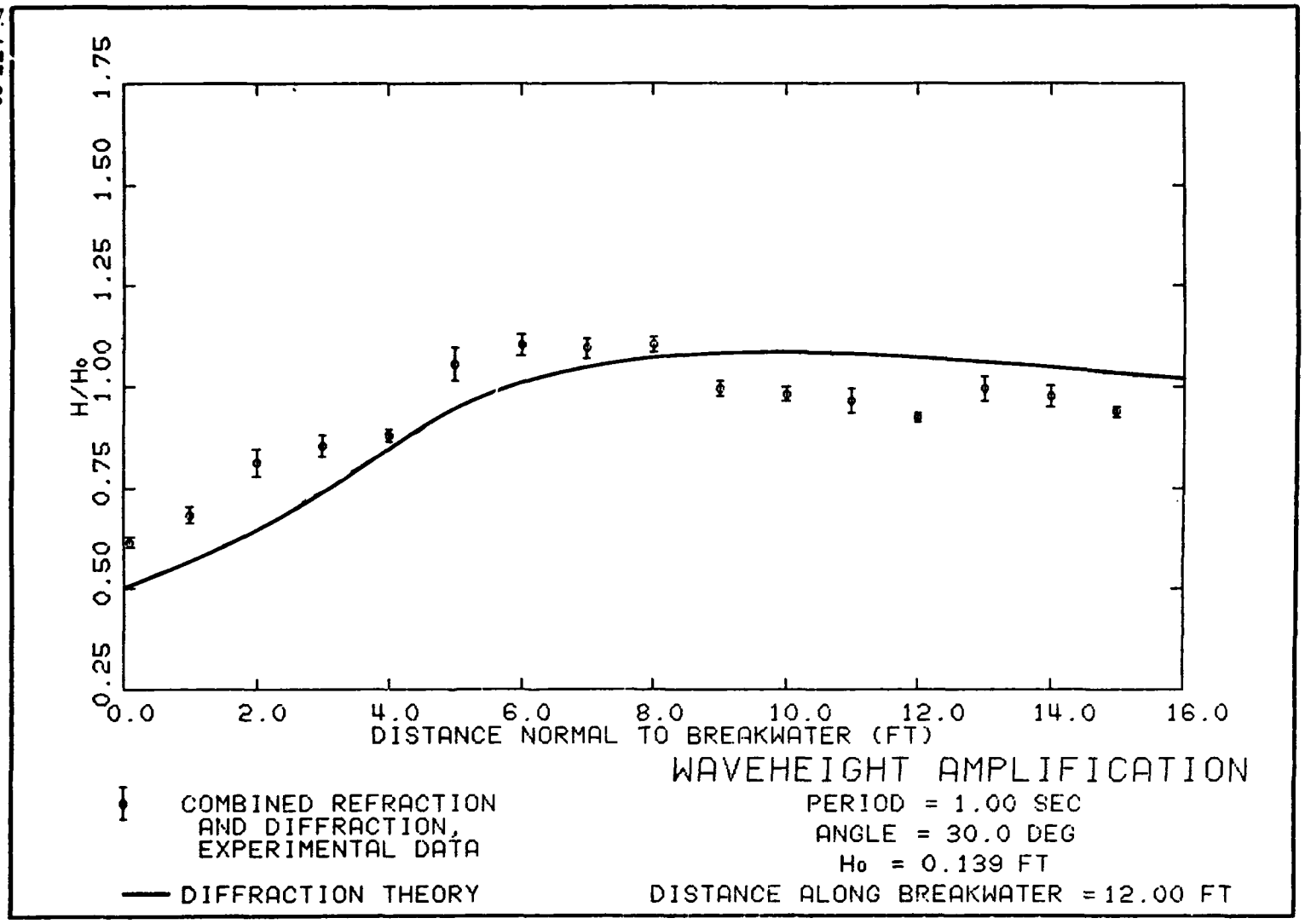
H/Ho
0.25
0.50
0.75
1.00
1.25
1.50
1.75
0.0
2.0
4.0
6.0
8.0
10.0
12.0
14.0
16.0
DISTANCE NORMAL TO BREAKWATER (FT)
WAVEHEIGHT AMPLIFICATION
COMBINED REFRACTION AND DIFFRACTION, EXPERIMENTAL DATA
DIFFRACTION THEORY
PERIOD = 1.00 SEC
ANGLE = 30.0 DEG
Ho = 0.139 FT
DISTANCE ALONG BREAKWATER = 12.00 FT

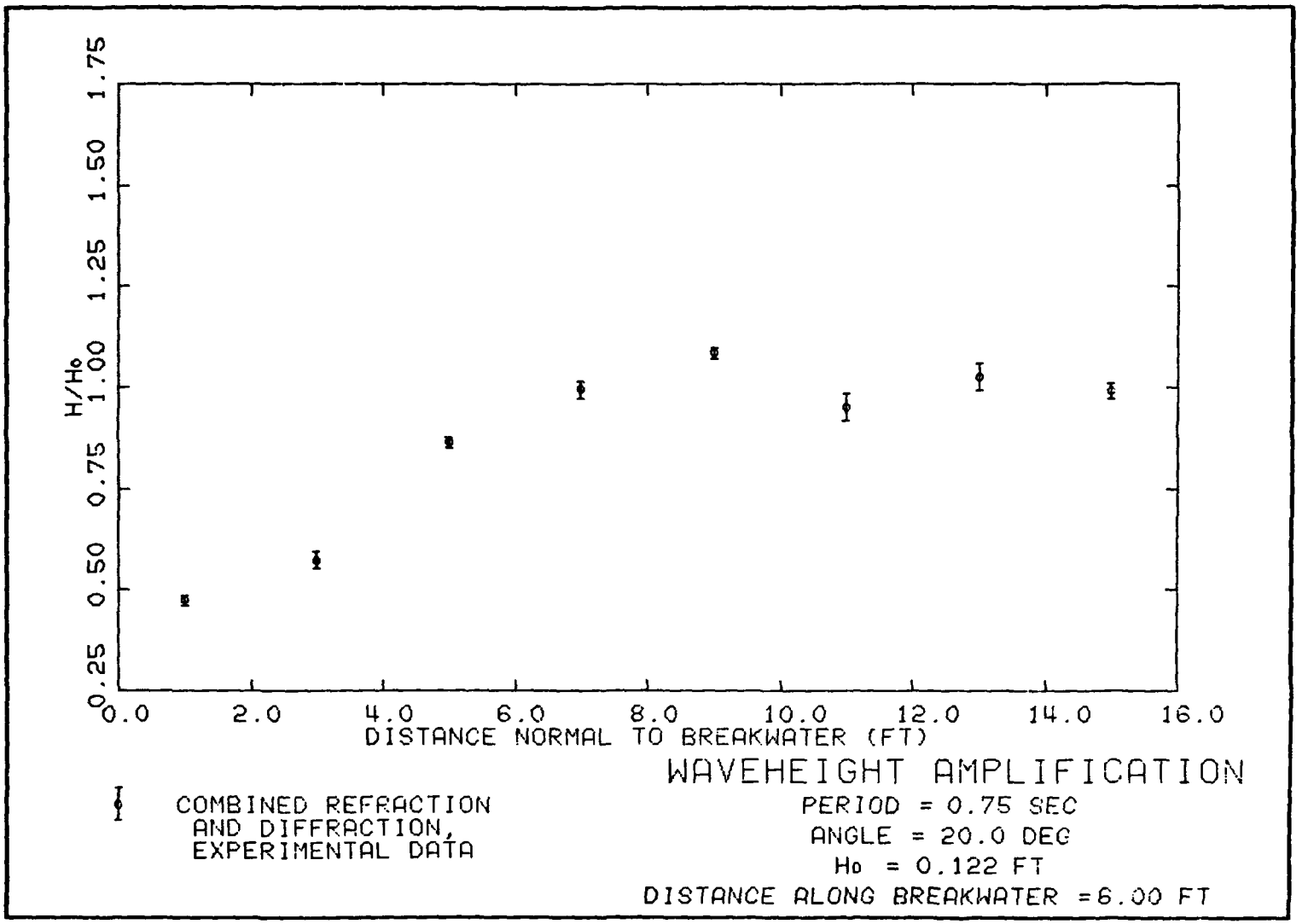
H/Ho
0.25
0.50
0.75
1.00
1.25
1.50
1.75
0.0
2.0
4.0
6.0
8.0
10.0
12.0
14.0
16.0
DISTANCE NORMAL TO BREAKWATER (FT)
WAVEHEIGHT AMPLIFICATION
PERIOD = 0.75 SEC
ANGLE = 20.0 DEG
Ho = 0.122 FT
DISTANCE ALONG BREAKWATER = 6.00 FT
COMBINED REFRACTION
AND DIFFRACTION,
EXPERIMENTAL DATA

PLATE 21

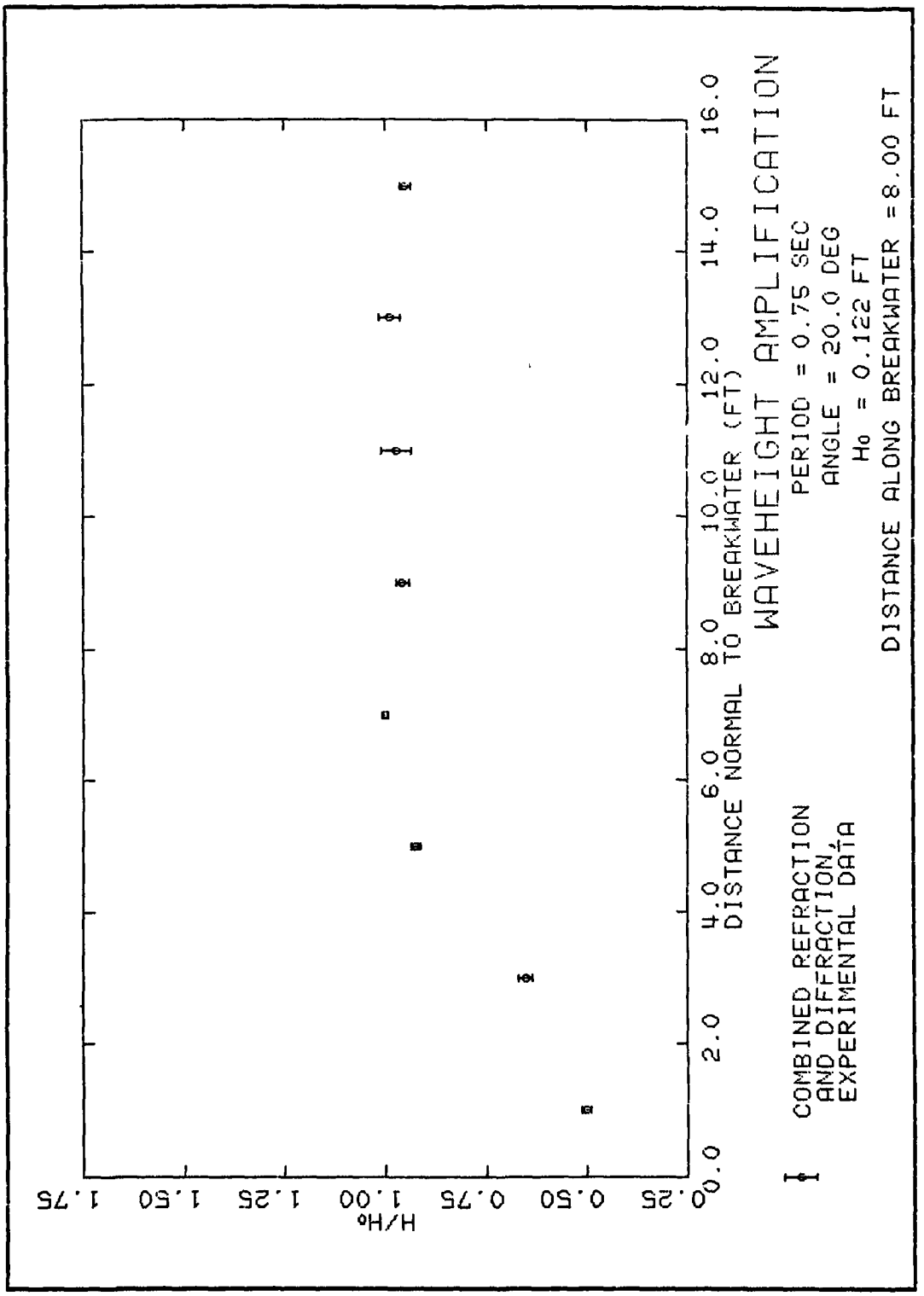
WAVEHEIGHT AMPLIFICATION
PERIOD = 0.75 SEC
ANGLE = 20.0 DEG
H_o = 0.122 FT
DISTANCE ALONG BREAKWATER =8.00 FT
COMBINED REFRACTION AND DIFFRACTION, EXPERIMENTAL DATA
DISTANCE NORMAL TO BREAKWATER (FT)
0.0
2.0
4.0
6.0
8.0
10.0
12.0
14.0
16.0
H/H$_o$
0.25
0.50
0.75
1.00
1.25
1.50
1.75

PLATE 22

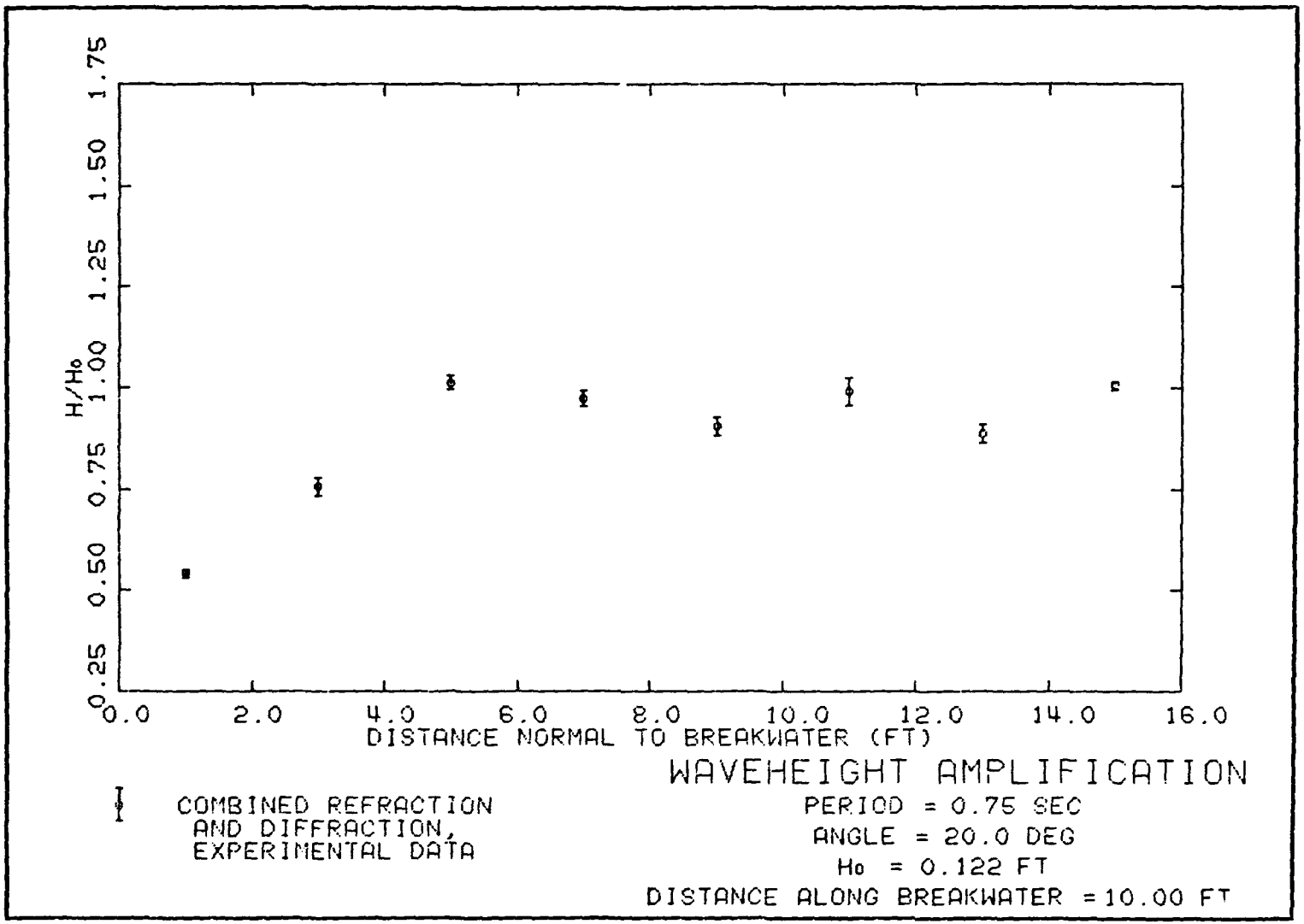
H/Ho
0.25
0.50
0.75
1.00
1.25
1.50
1.75
0.0
2.0
4.0
6.0
8.0
10.0
12.0
14.0
16.0
DISTANCE NORMAL TO BREAKWATER (FT)
COMBINED REFRACTION AND DIFFRACTION, EXPERIMENTAL DATA
WAVEHEIGHT AMPLIFICATION
PERIOD = 0.75 SEC
ANGLE = 20.0 DEG
Ho = 0.122 FT
DISTANCE ALONG BREAKWATER = 10.00 FT

PLATE 23

PLATE 24

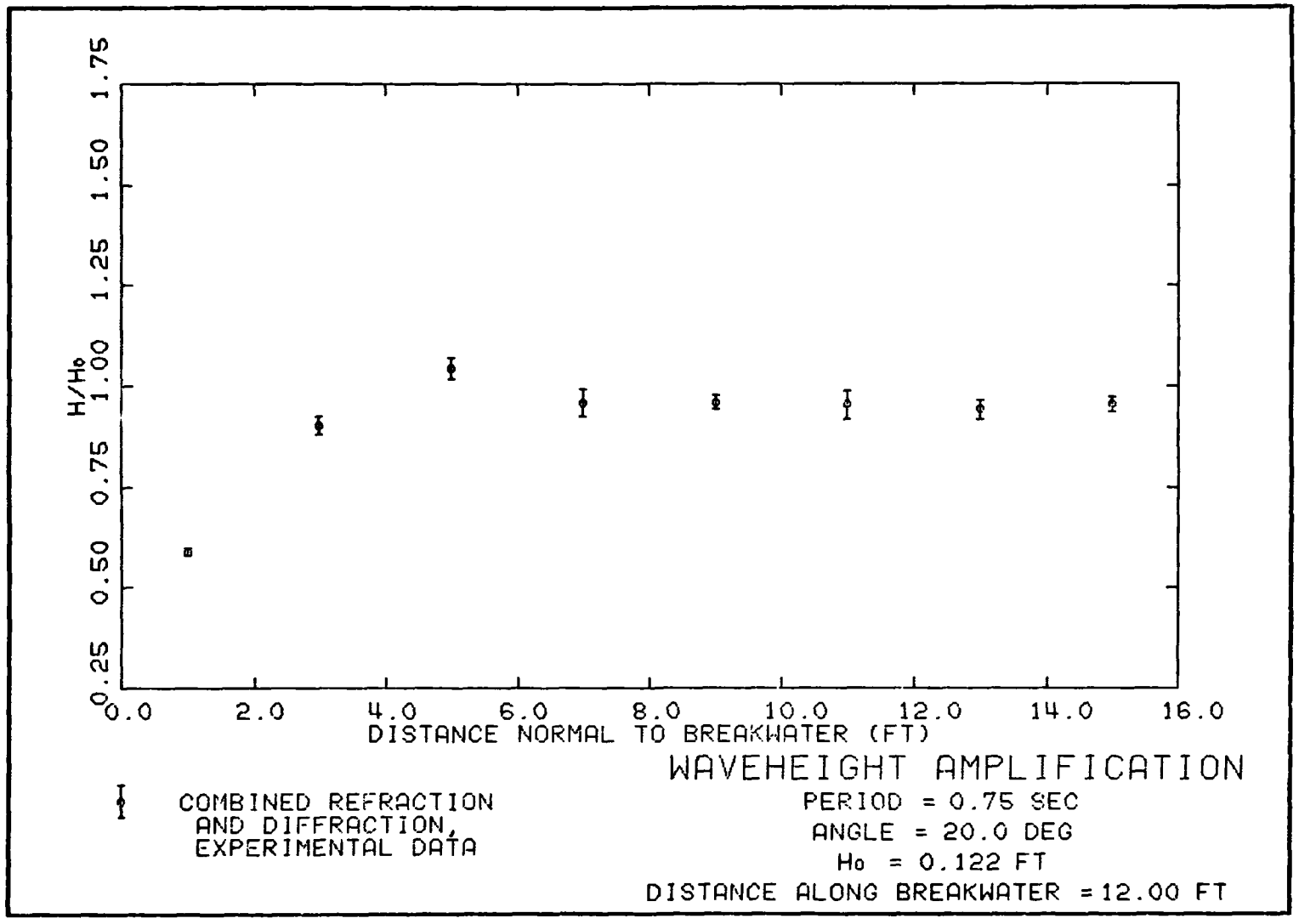
H/Ho
0.25
0.50
0.75
1.00
1.25
1.50
1.75
0.0
2.0
4.0
6.0
8.0
10.0
12.0
14.0
16.0
DISTANCE NORMAL TO BREAKWATER (FT)
COMBINED REFRACTION
AND DIFFRACTION,
EXPERIMENTAL DATA
WAVEHEIGHT AMPLIFICATION
PERIOD = 0.75 SEC
ANGLE = 20.0 DEG
Ho = 0.122 FT
DISTANCE ALONG BREAKWATER = 12.00 FT

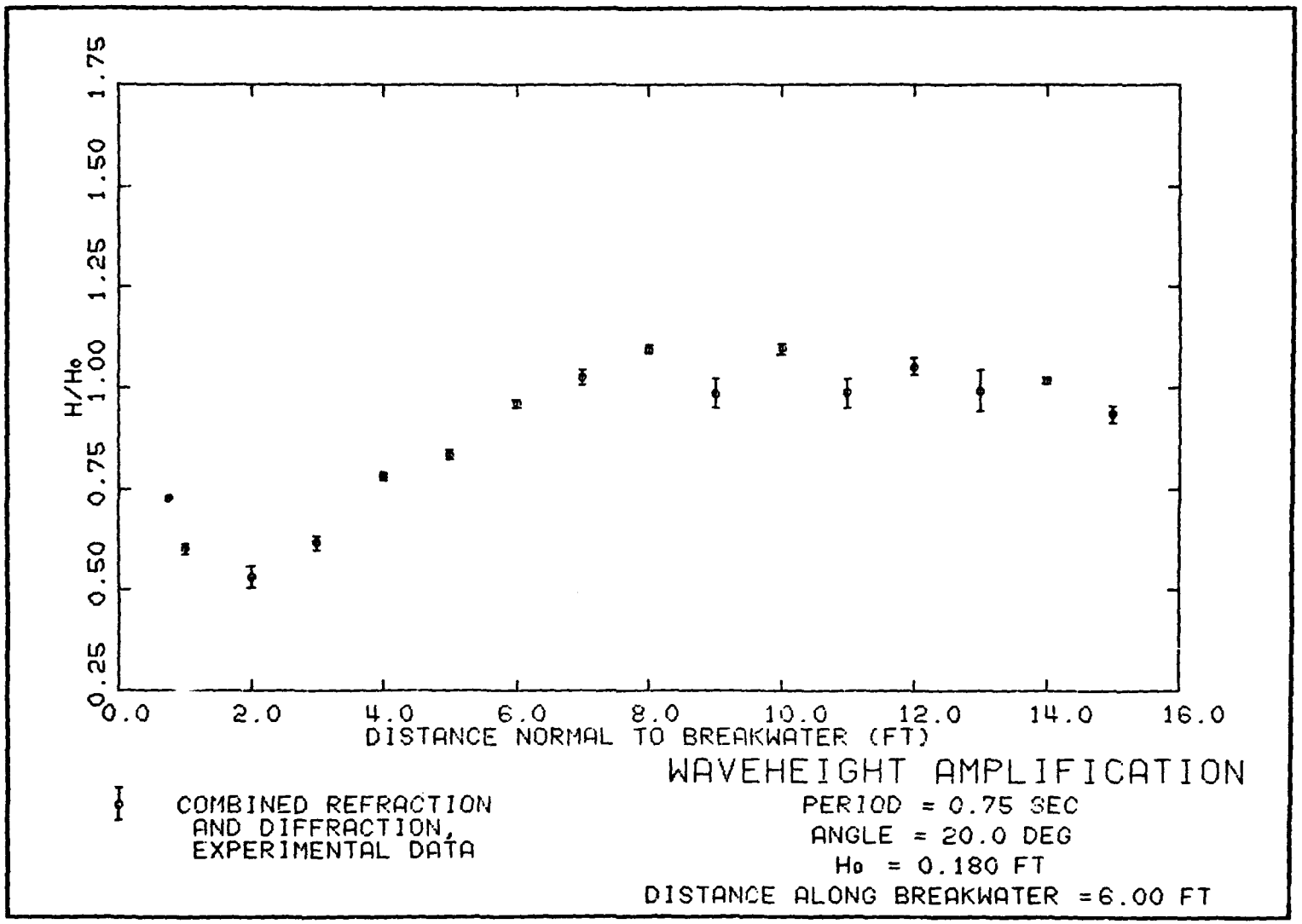
H/Ho
0.25
0.50
0.75
1.00
1.25
1.50
1.75
0.0
2.0
4.0
6.0
8.0
10.0
12.0
14.0
16.0
DISTANCE NORMAL TO BREAKWATER (FT)
WAVEHEIGHT AMPLIFICATION
PERIOD = 0.75 SEC
ANGLE = 20.0 DEG
Ho = 0.180 FT
DISTANCE ALONG BREAKWATER =6.00 FT
COMBINED REFRACTION
AND DIFFRACTION,
EXPERIMENTAL DATA

PLATE 25

PLATE 26

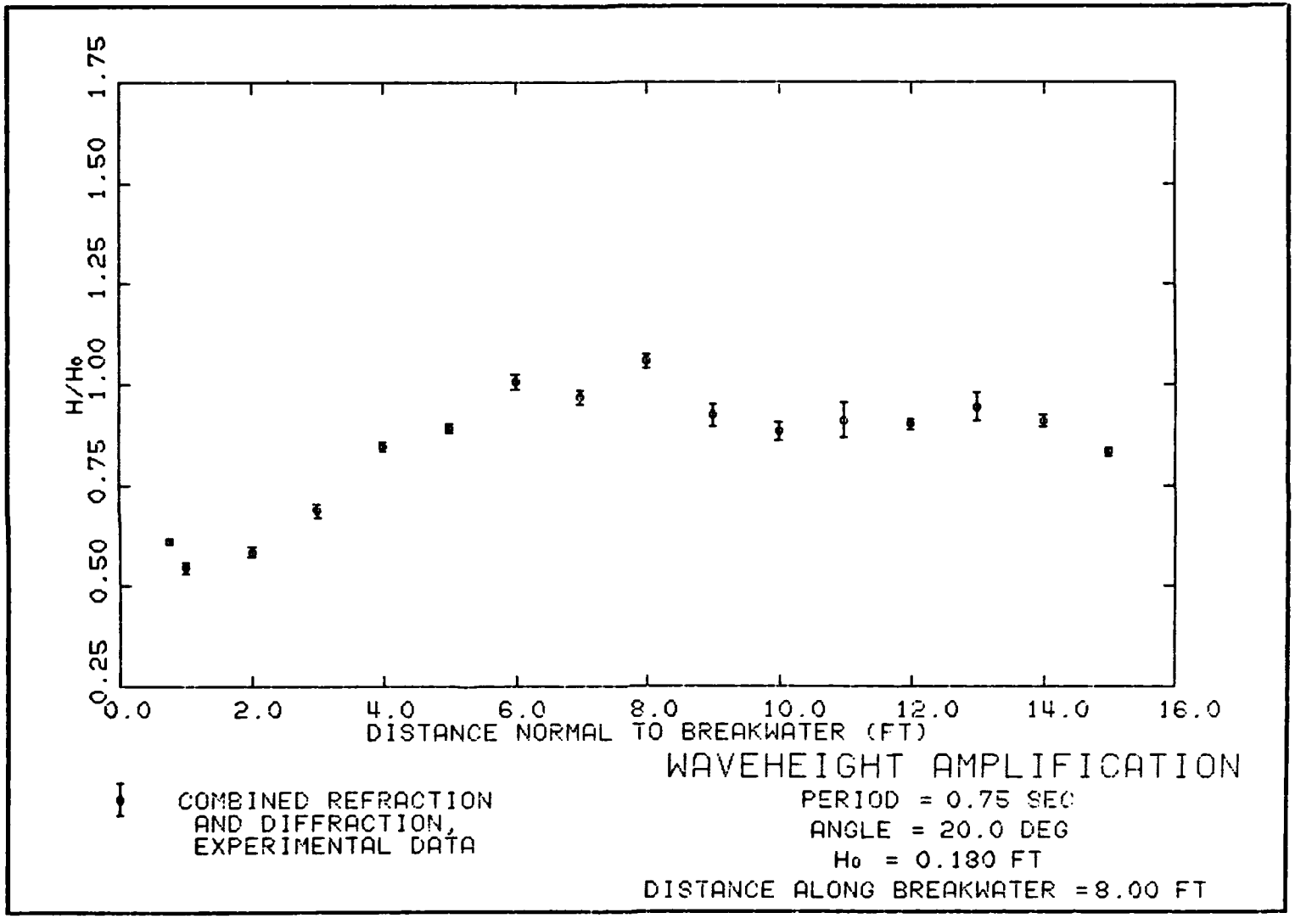
H/Ho
0.25
0.50
0.75
1.00
1.25
1.50
1.75
0.0
2.0
4.0
6.0
8.0
10.0
12.0
14.0
16.0
DISTANCE NORMAL TO BREAKWATER (FT)
WAVEHEIGHT AMPLIFICATION
PERIOD = 0.75 SEC
ANGLE = 20.0 DEG
Ho = 0.180 FT
DISTANCE ALONG BREAKWATER = 8.00 FT
COMBINED REFRACTION
AND DIFFRACTION,
EXPERIMENTAL DATA

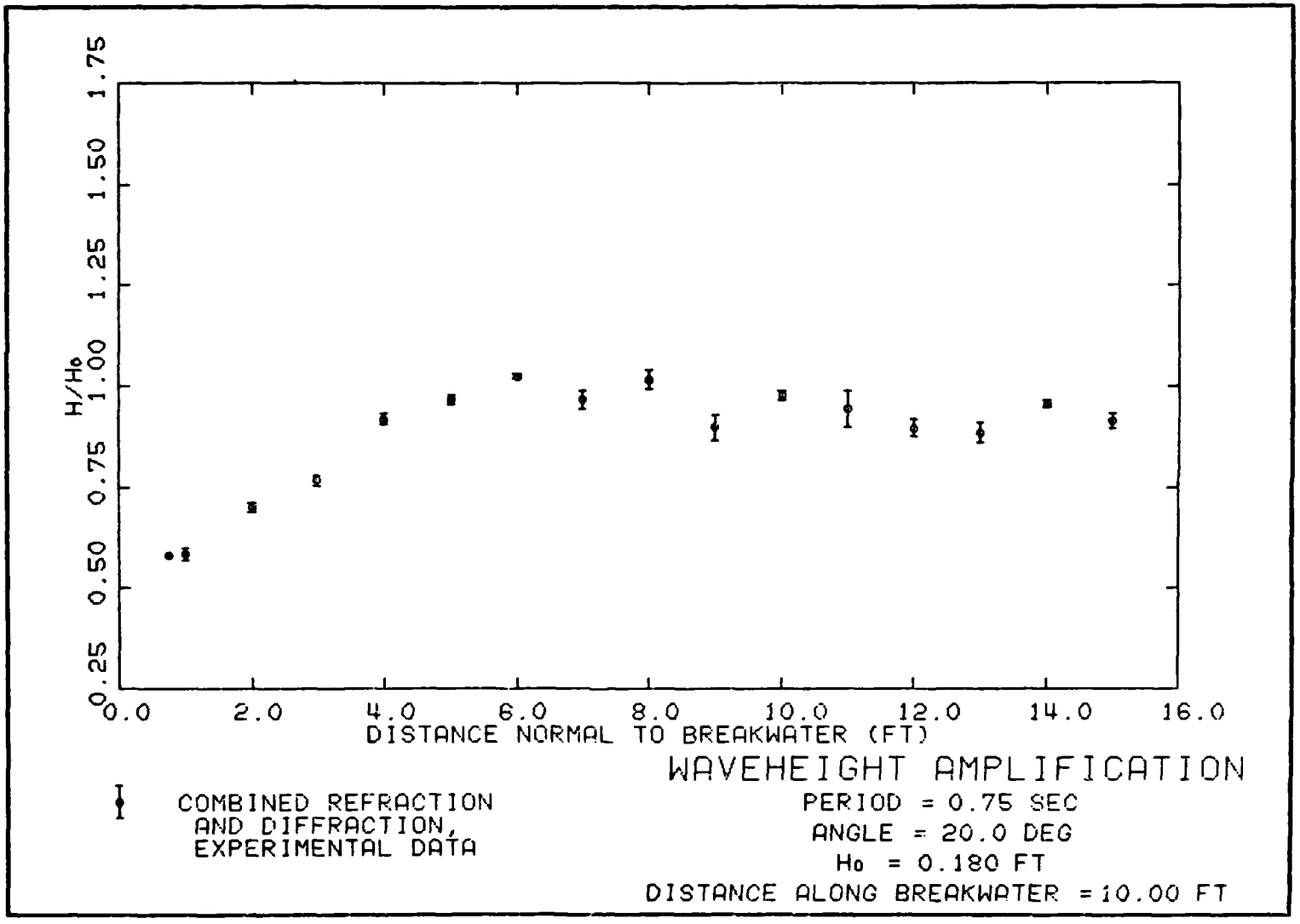
H/Ho
0.25
0.50
0.75
1.00
1.25
1.50
1.75
0.0
2.0
4.0
6.0
8.0
10.0
12.0
14.0
16.0
DISTANCE NORMAL TO BREAKWATER (FT)
WAVEHEIGHT AMPLIFICATION
PERIOD = 0.75 SEC
ANGLE = 20.0 DEG
Ho = 0.180 FT
DISTANCE ALONG BREAKWATER = 10.00 FT
COMBINED REFRACTION
AND DIFFRACTION,
EXPERIMENTAL DATA

PLATE 27

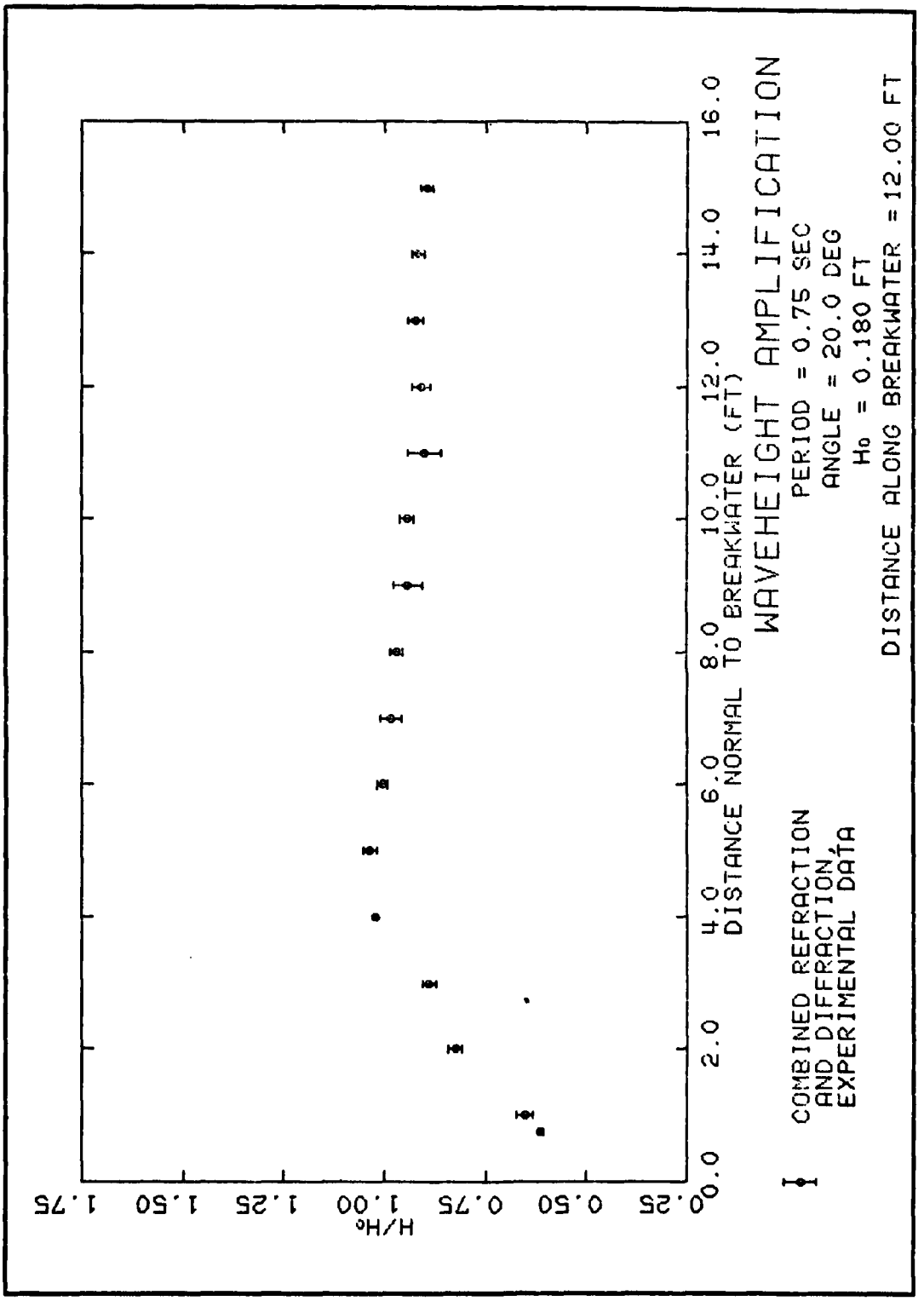
WAVEHEIGHT AMPLIFICATION
PERIOD = 0.75 SEC
ANGLE = 20.0 DEG
H_o = 0.180 FT
DISTANCE ALONG BREAKWATER = 12.00 FT
COMBINED REFRACTION AND DIFFRACTION, EXPERIMENTAL DATA
DISTANCE NORMAL TO BREAKWATER (FT)
0.0
2.0
4.0
6.0
8.0
10.0
12.0
14.0
16.0
H/H_o
0.25
0.50
0.75
1.00
1.25
1.50
1.75

PLATE 28

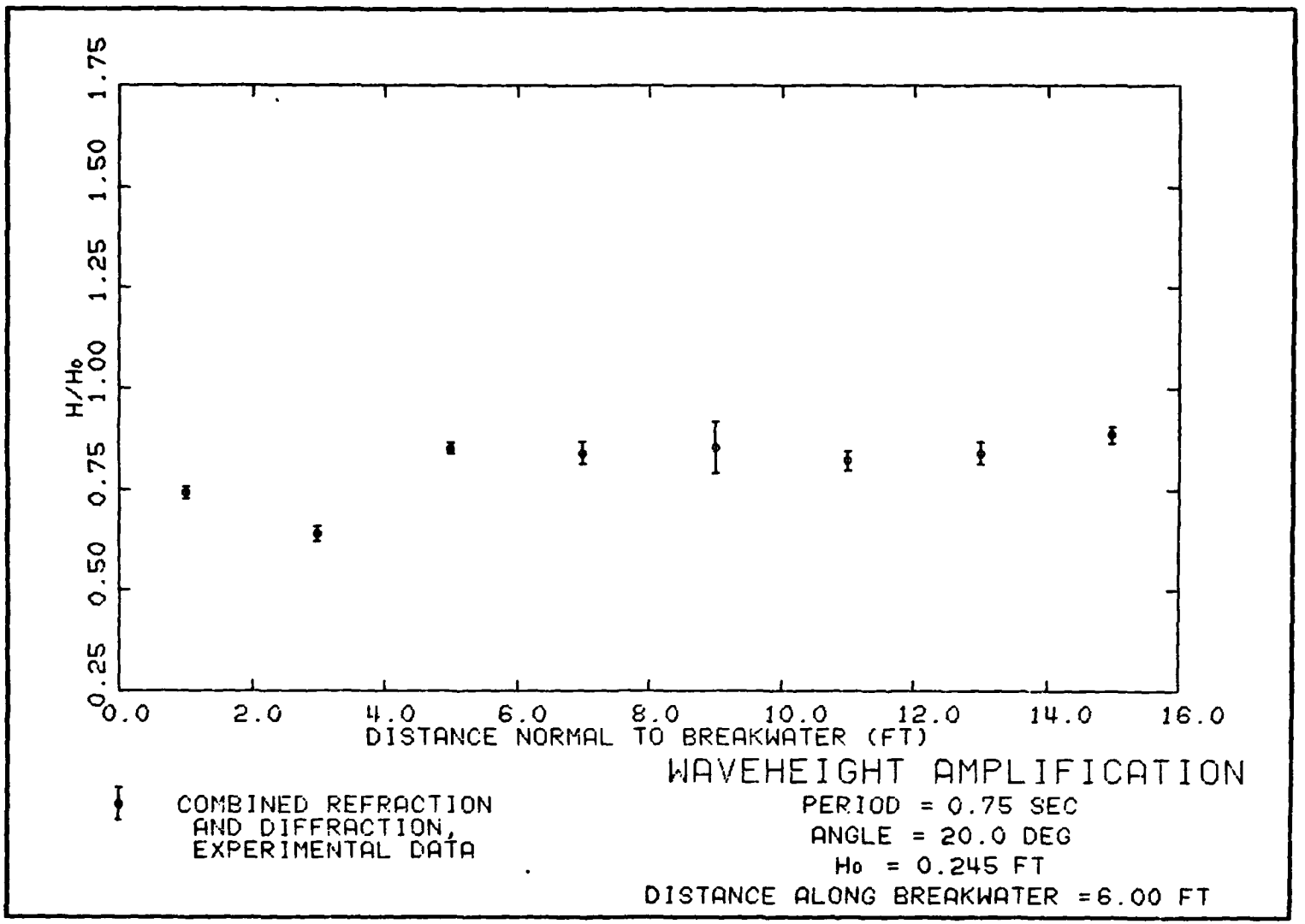
H/Ho
0.25
0.50
0.75
1.00
1.25
1.50
1.75
0.0
2.0
4.0
6.0
8.0
10.0
12.0
14.0
16.0
DISTANCE NORMAL TO BREAKWATER (FT)
COMBINED REFRACTION
AND DIFFRACTION,
EXPERIMENTAL DATA
WAVEHEIGHT AMPLIFICATION
PERIOD = 0.75 SEC
ANGLE = 20.0 DEG
Ho = 0.245 FT
DISTANCE ALONG BREAKWATER =6.00 FT

PLATE 89

PLATE 30

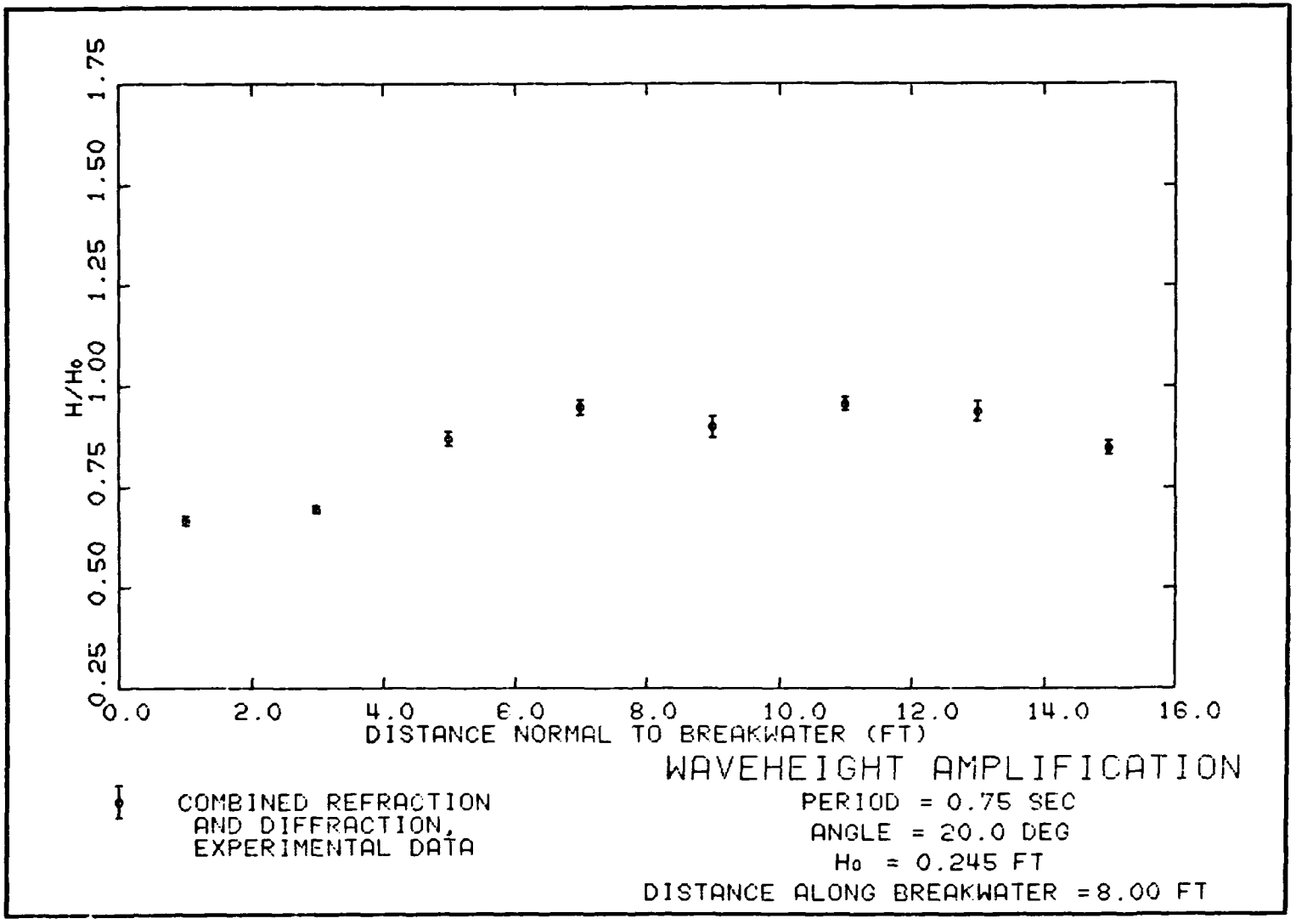
H/Ho
0.25
0.50
0.75
1.00
1.25
1.50
1.75
0.0
2.0
4.0
6.0
8.0
10.0
12.0
14.0
16.0
DISTANCE NORMAL TO BREAKWATER (FT)
WAVEHEIGHT AMPLIFICATION
COMBINED REFRACTION
AND DIFFRACTION,
EXPERIMENTAL DATA
PERIOD = 0.75 SEC
ANGLE = 20.0 DEG
Ho = 0.245 FT
DISTANCE ALONG BREAKWATER =8.00 FT

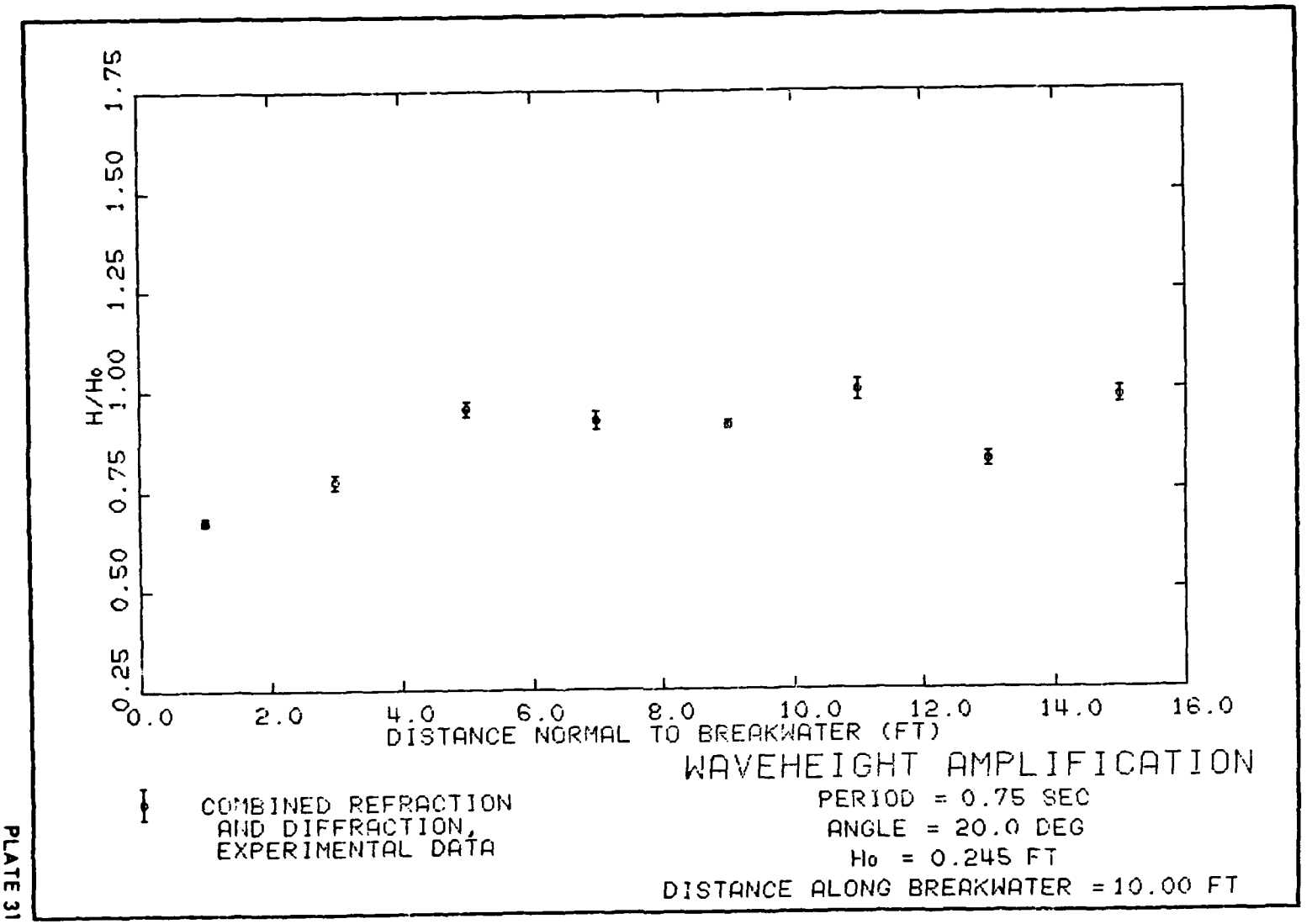
H/Ho
0.25
0.50
0.75
1.00
1.25
1.50
1.75
0.0
2.0
4.0
6.0
8.0
10.0
12.0
14.0
16.0
DISTANCE NORMAL TO BREAKWATER (FT)
WAVEHEIGHT AMPLIFICATION
PERIOD = 0.75 SEC
ANGLE = 20.0 DEG
Ho = 0.245 FT
DISTANCE ALONG BREAKWATER = 10.00 FT
COMBINED REFRACTION
AND DIFFRACTION,
EXPERIMENTAL DATA

PLATE 31

PLATE 32

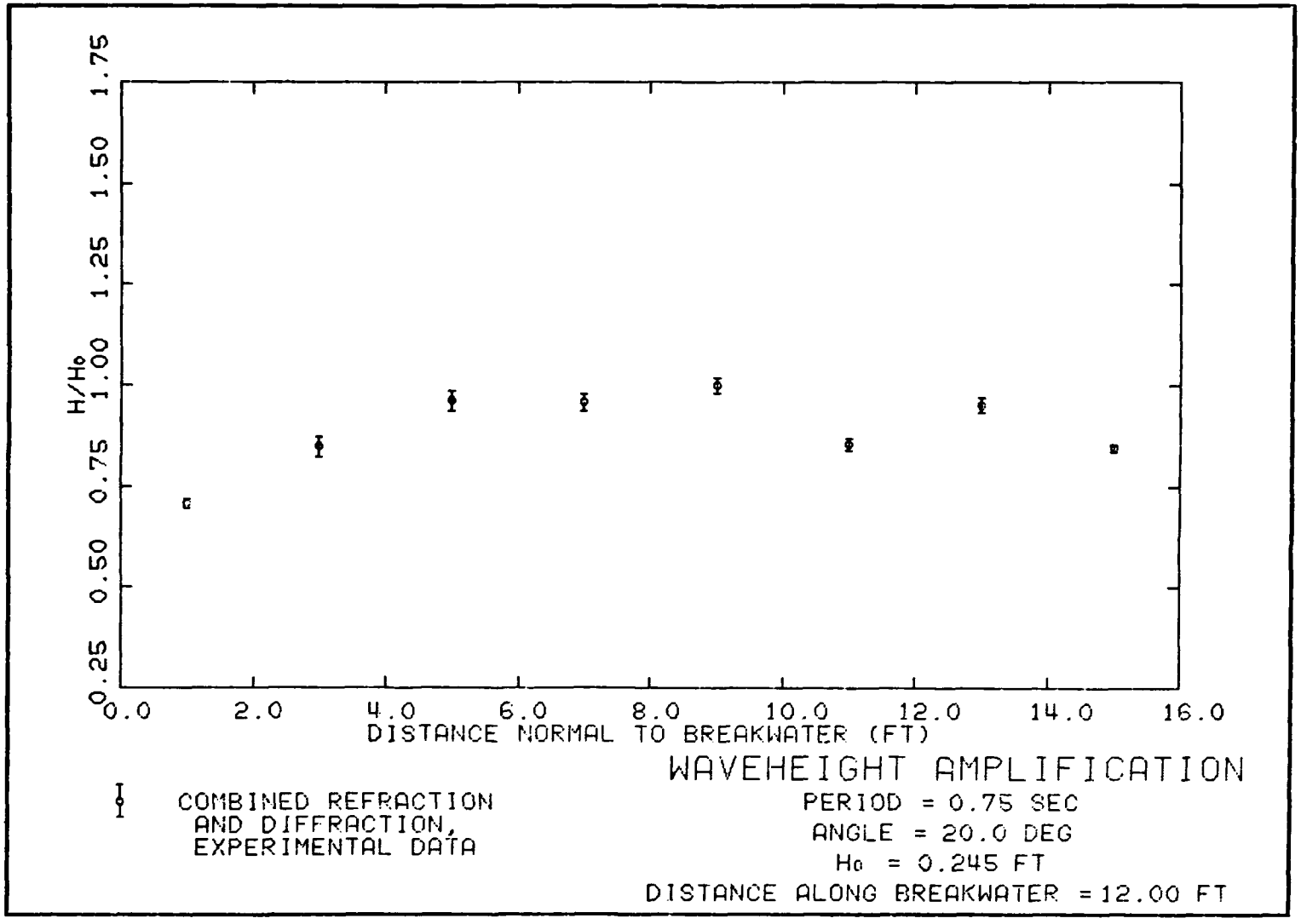
H/Ho
0.25
0.50
0.75
1.00
1.25
1.50
1.75
0.0
2.0
4.0
6.0
8.0
10.0
12.0
14.0
16.0
DISTANCE NORMAL TO BREAKWATER (FT)
COMBINED REFRACTION
AND DIFFRACTION,
EXPERIMENTAL DATA
WAVEHEIGHT AMPLIFICATION
PERIOD = 0.75 SEC
ANGLE = 20.0 DEG
Ho = 0.245 FT
DISTANCE ALONG BREAKWATER = 12.00 FT

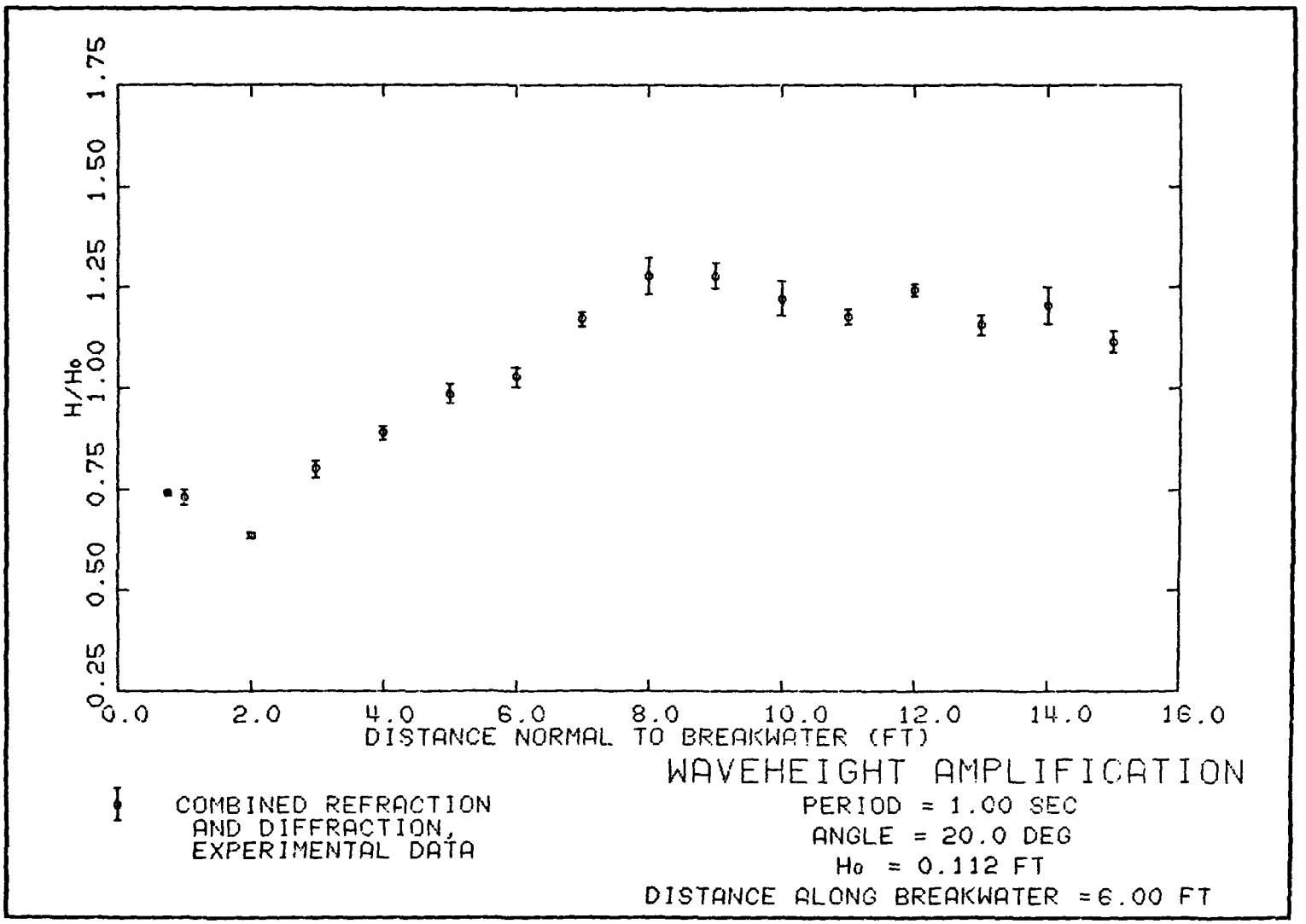
H/Ho
0.25
0.50
0.75
1.00
1.25
1.50
1.75
0.0
2.0
4.0
6.0
8.0
10.0
12.0
14.0
16.0
DISTANCE NORMAL TO BREAKWATER (FT)
WAVEHEIGHT AMPLIFICATION
COMBINED REFRACTION
AND DIFFRACTION,
EXPERIMENTAL DATA
PERIOD = 1.00 SEC
ANGLE = 20.0 DEG
Ho = 0.112 FT
DISTANCE ALONG BREAKWATER = 6.00 FT

PLATE 33

PLATE 34

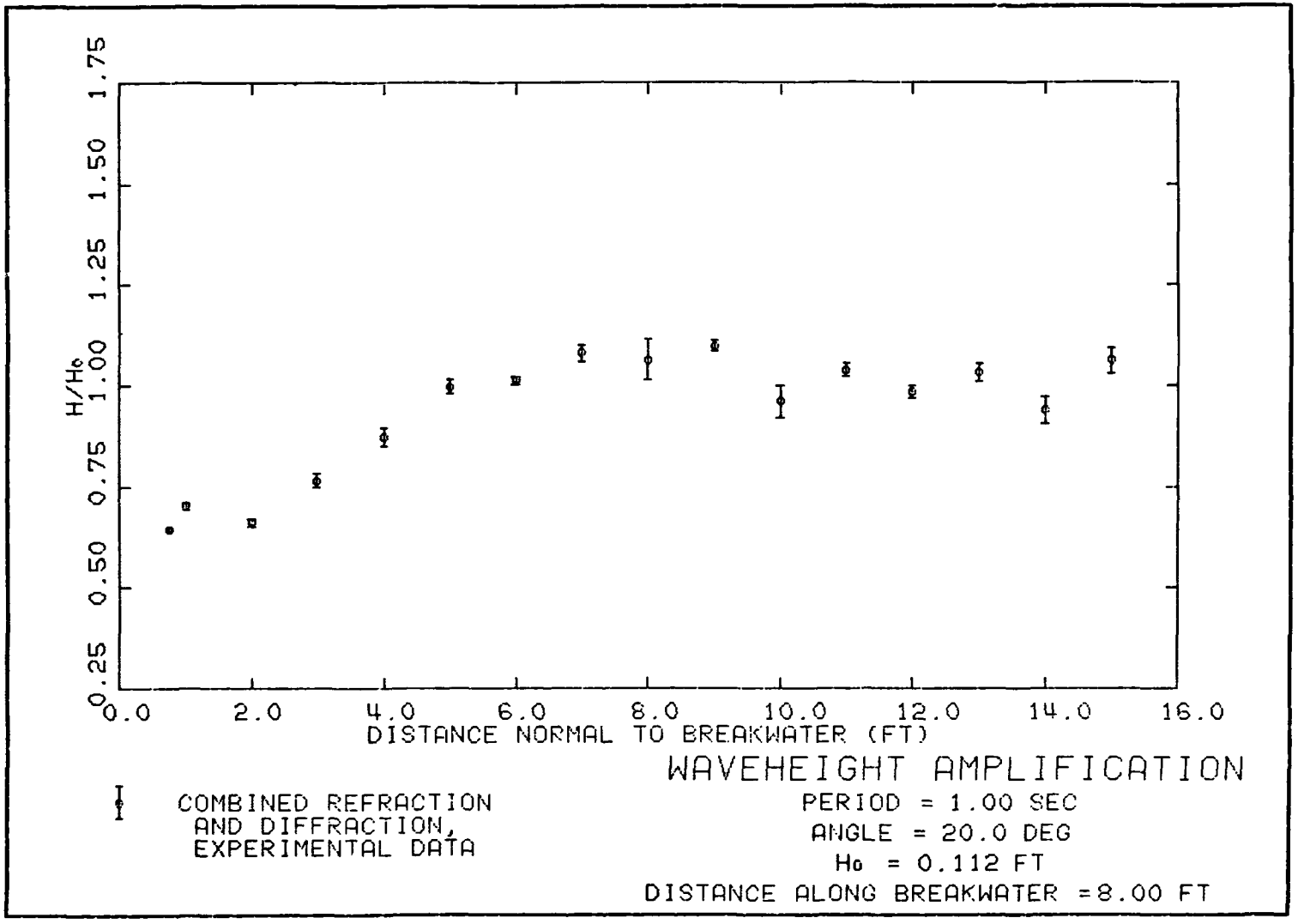
H/Ho
0.25
0.50
0.75
1.00
1.25
1.50
1.75
0.0
2.0
4.0
6.0
8.0
10.0
12.0
14.0
16.0
DISTANCE NORMAL TO BREAKWATER (FT)
COMBINED REFRACTION
AND DIFFRACTION,
EXPERIMENTAL DATA
WAVEHEIGHT AMPLIFICATION
PERIOD = 1.00 SEC
ANGLE = 20.0 DEG
Ho = 0.112 FT
DISTANCE ALONG BREAKWATER =8.00 FT

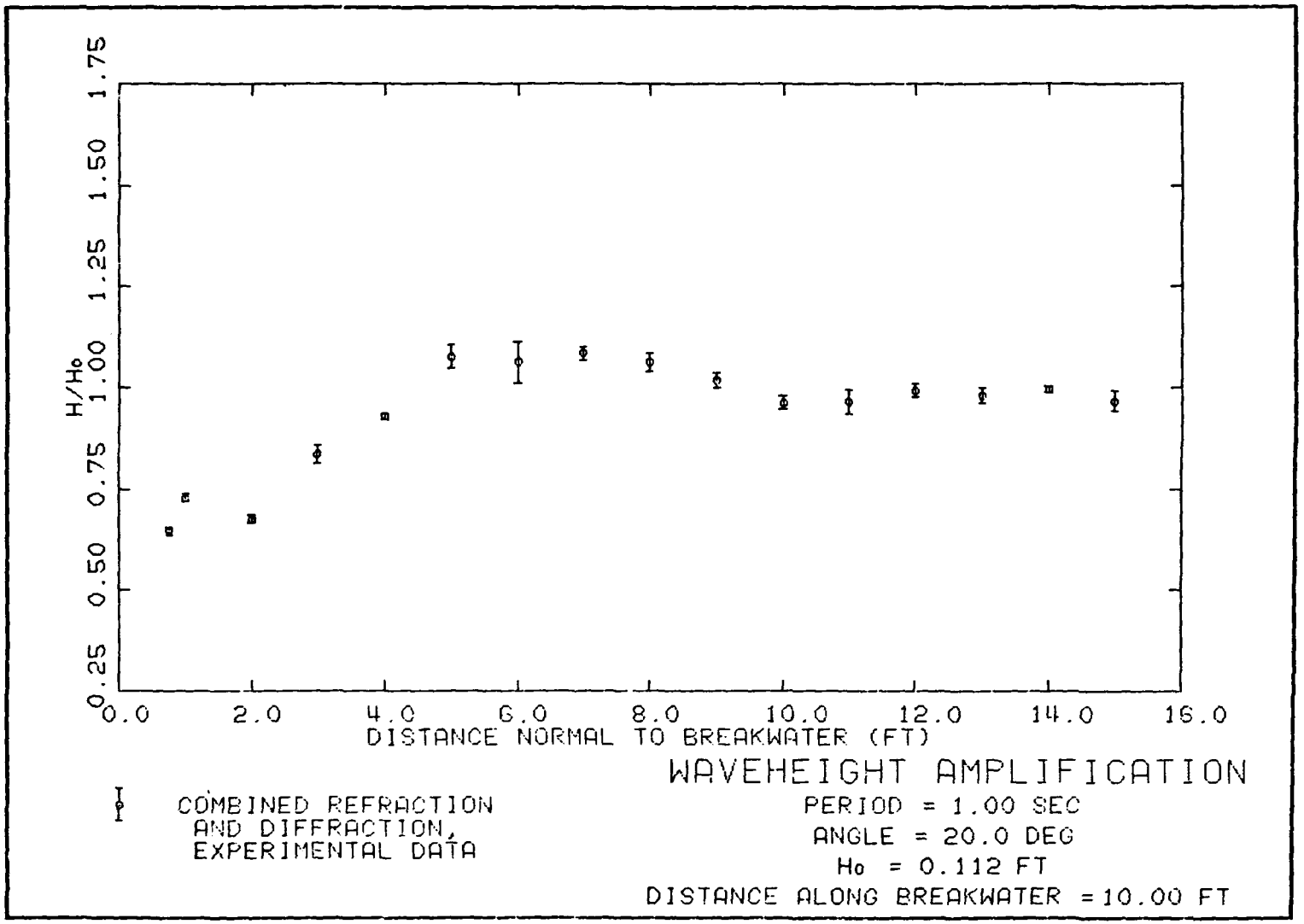
H/Ho
0.25
0.50
0.75
1.00
1.25
1.50
1.75
0.0
2.0
4.0
6.0
8.0
10.0
12.0
14.0
16.0
DISTANCE NORMAL TO BREAKWATER (FT)
WAVEHEIGHT AMPLIFICATION
PERIOD = 1.00 SEC
ANGLE = 20.0 DEG
Ho = 0.112 FT
DISTANCE ALONG BREAKWATER = 10.00 FT
COMBINED REFRACTION
AND DIFFRACTION,
EXPERIMENTAL DATA

PLATE 35

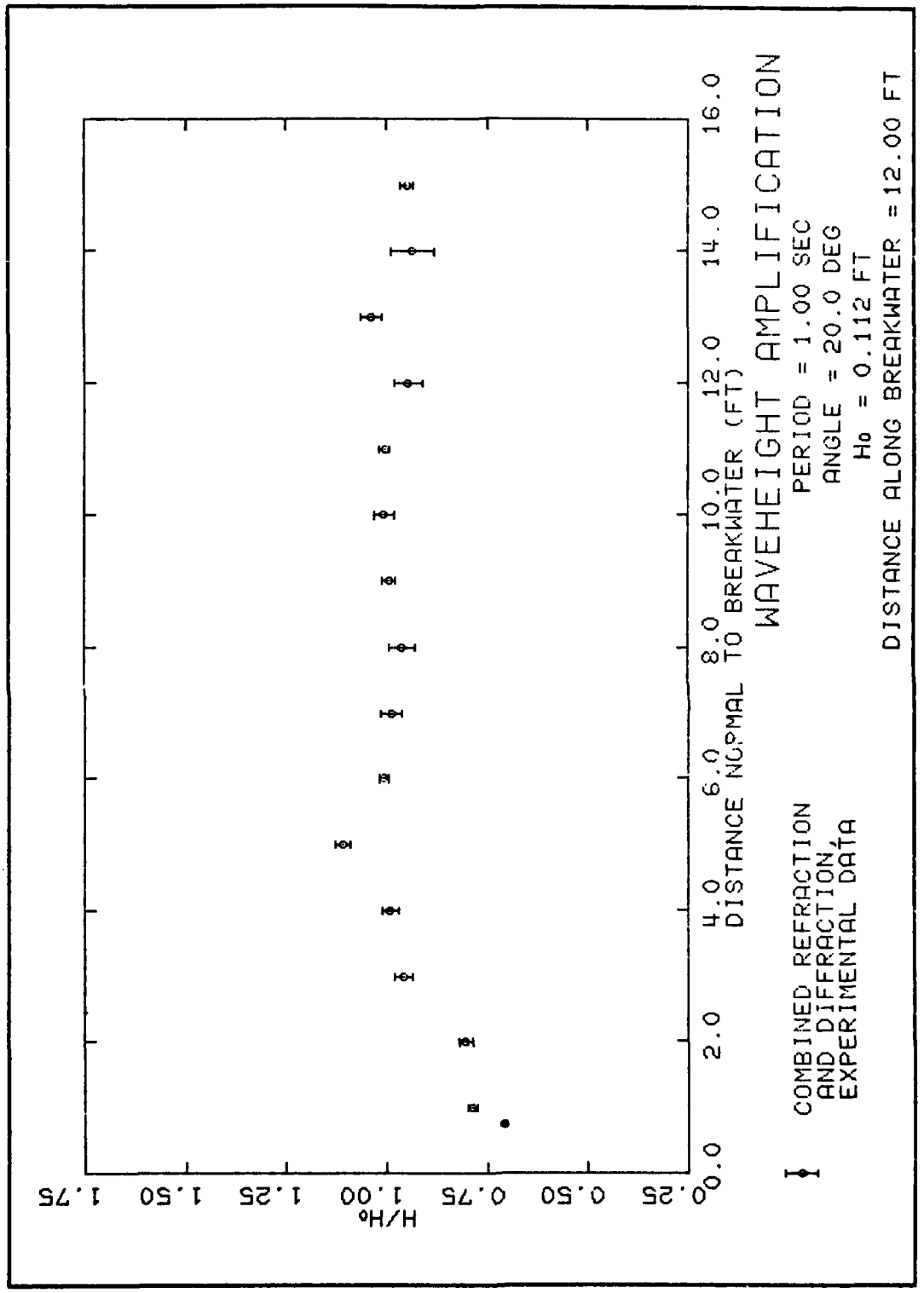
WAVEHEIGHT AMPLIFICATION
PERIOD = 1.00 SEC
ANGLE = 20.0 DEG
Ho = 0.112 FT
DISTANCE ALONG BREAKWATER = 12.00 FT
COMBINED REFRACTION AND DIFFRACTION, EXPERIMENTAL DATA
H/Ho
0.0
0.25
0.50
0.75
1.00
1.25
1.50
1.75
2.0
4.0
6.0
8.0
10.0
12.0
14.0
16.0
DISTANCE NORMAL TO BREAKWATER (FT)

PLATE 36

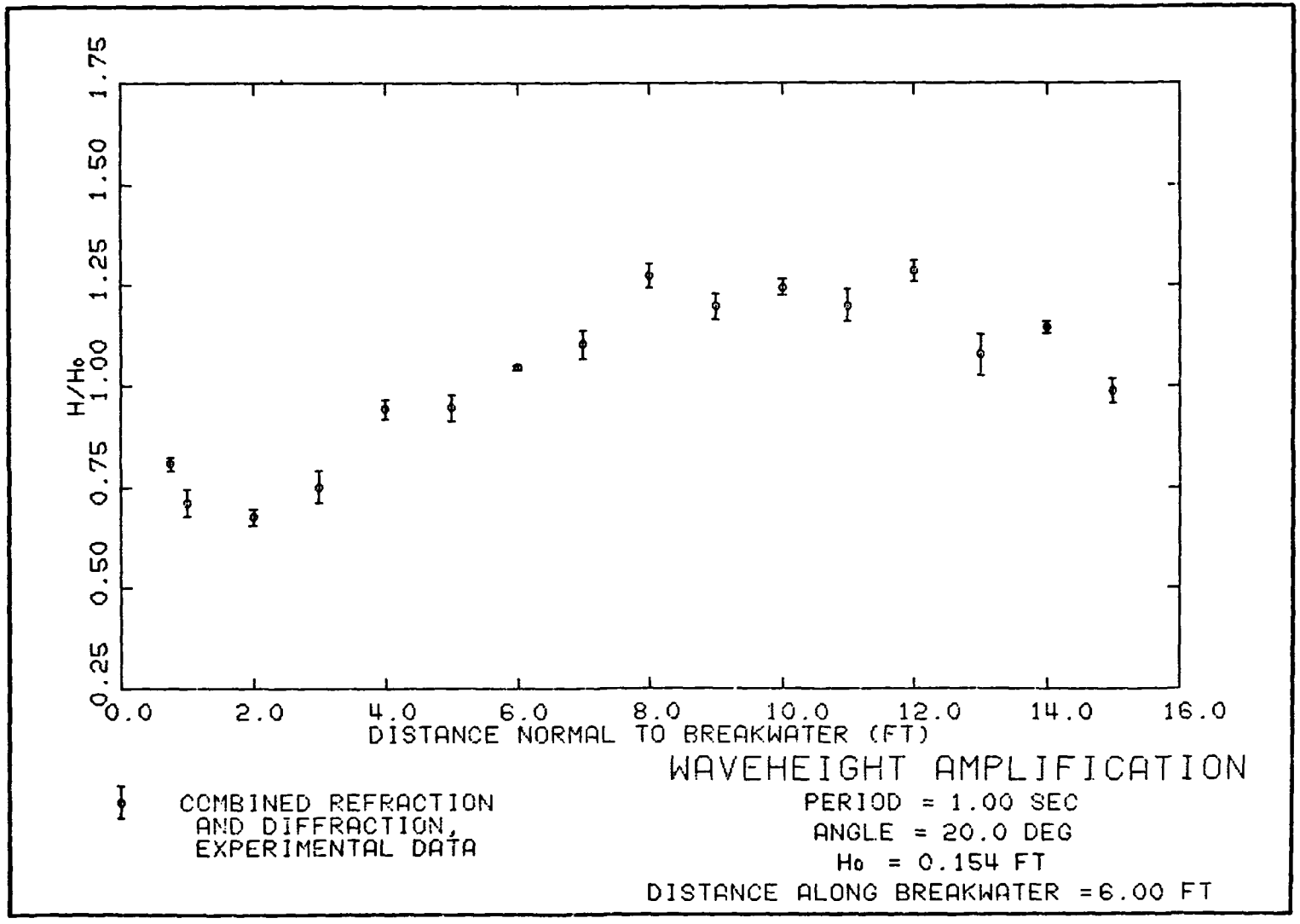
H/Ho
0.25
0.50
0.75
1.00
1.25
1.50
1.75
0.0
2.0
4.0
6.0
8.0
10.0
12.0
14.0
16.0
DISTANCE NORMAL TO BREAKWATER (FT)
WAVEHEIGHT AMPLIFICATION
PERIOD = 1.00 SEC
ANGLE = 20.0 DEG
Ho = 0.154 FT
DISTANCE ALONG BREAKWATER =6.00 FT
COMBINED REFRACTION
AND DIFFRACTION,
EXPERIMENTAL DATA

PLATE 37

PLATE 38

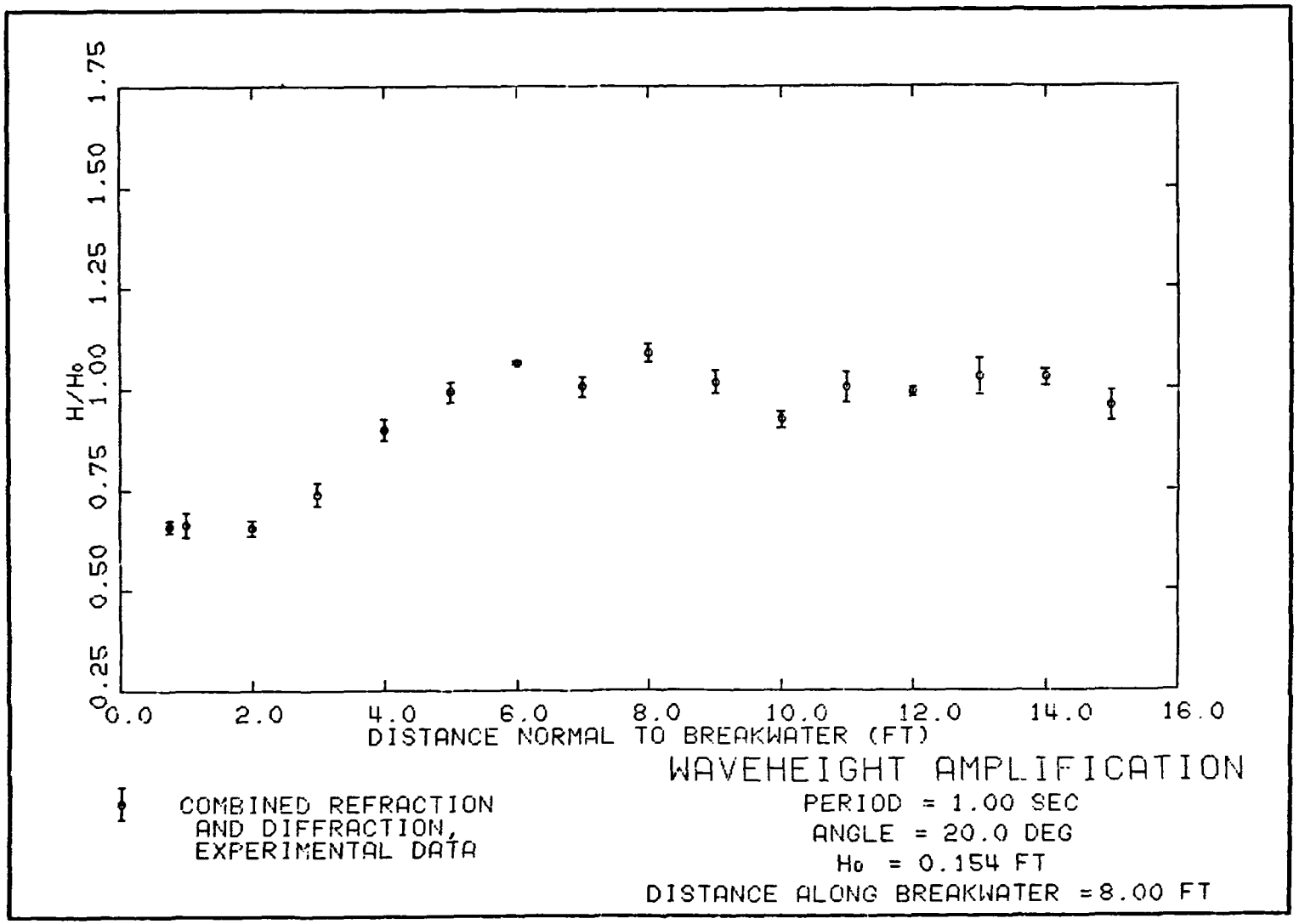
H/Ho
0.25
0.50
0.75
1.00
1.25
1.50
1.75
0.0
2.0
4.0
6.0
8.0
10.0
12.0
14.0
16.0
DISTANCE NORMAL TO BREAKWATER (FT)
WAVEHEIGHT AMPLIFICATION
COMBINED REFRACTION
AND DIFFRACTION,
EXPERIMENTAL DATA
PERIOD = 1.00 SEC
ANGLE = 20.0 DEG
Ho = 0.154 FT
DISTANCE ALONG BREAKWATER =8.00 FT

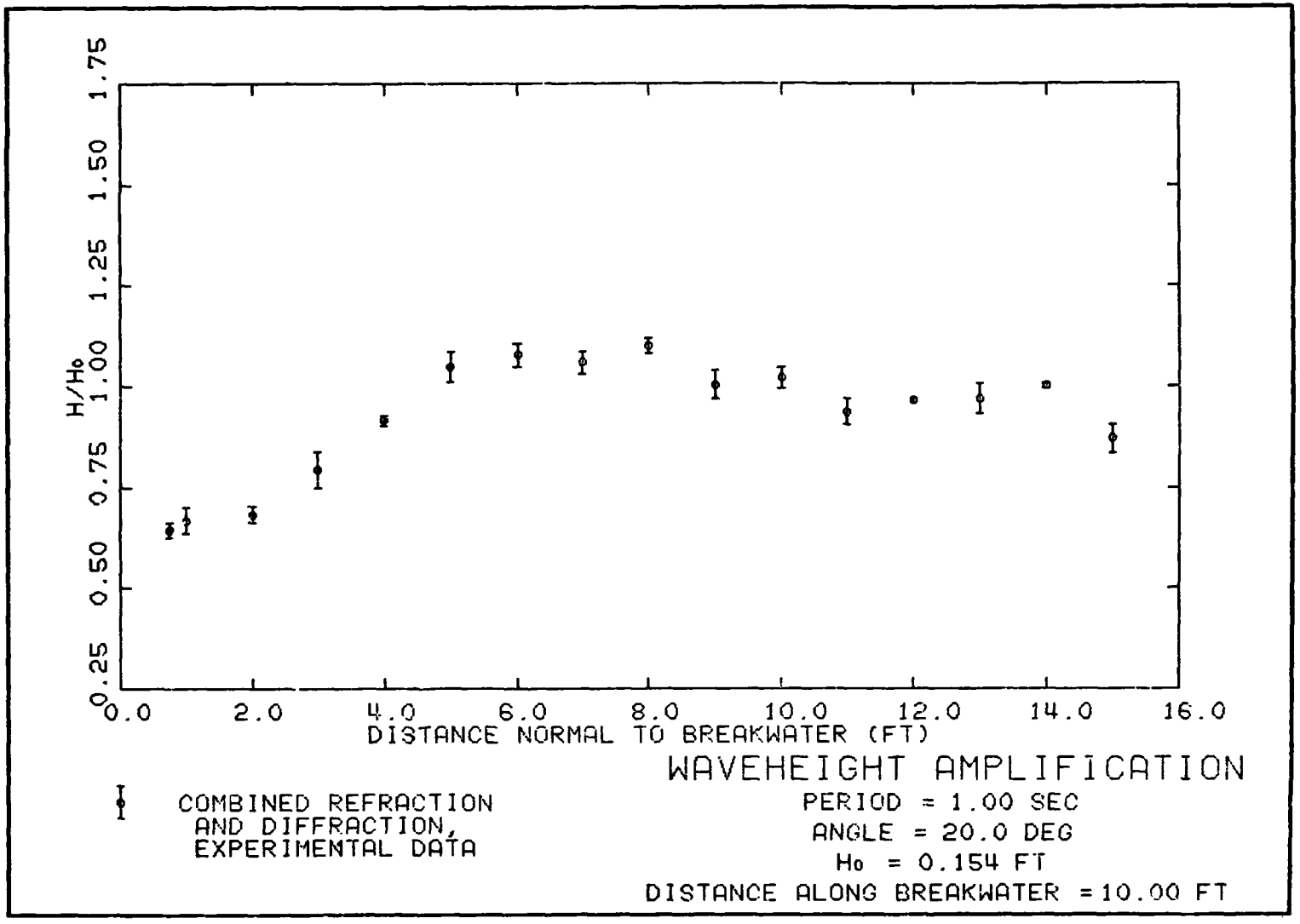
H/Ho
0.25
0.50
0.75
1.00
1.25
1.50
1.75
0.0
2.0
4.0
6.0
8.0
10.0
12.0
14.0
16.0
DISTANCE NORMAL TO BREAKWATER (FT)
WAVEHEIGHT AMPLIFICATION
PERIOD = 1.00 SEC
ANGLE = 20.0 DEG
Ho = 0.154 FT
DISTANCE ALONG BREAKWATER = 10.00 FT
COMBINED REFRACTION
AND DIFFRACTION,
EXPERIMENTAL DATA

PLATE 39

PLATE 40

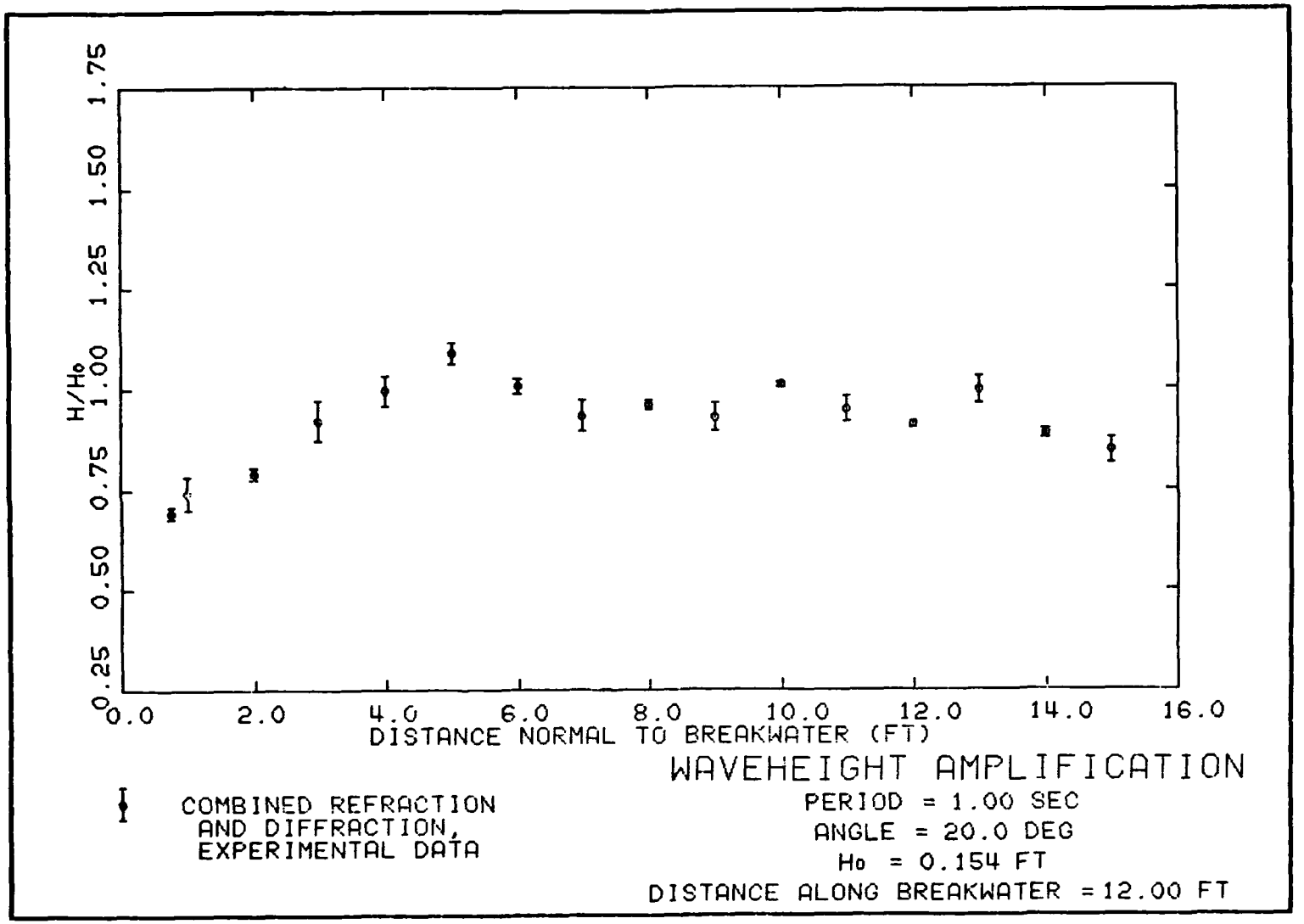
H/Ho
0.25
0.50
0.75
1.00
1.25
1.50
1.75
0.0
2.0
4.0
6.0
8.0
10.0
12.0
14.0
16.0
DISTANCE NORMAL TO BREAKWATER (FT)
COMBINED REFRACTION AND DIFFRACTION, EXPERIMENTAL DATA
WAVEHEIGHT AMPLIFICATION
PERIOD = 1.00 SEC
ANGLE = 20.0 DEG
Ho = 0.154 FT
DISTANCE ALONG BREAKWATER = 12.00 FT

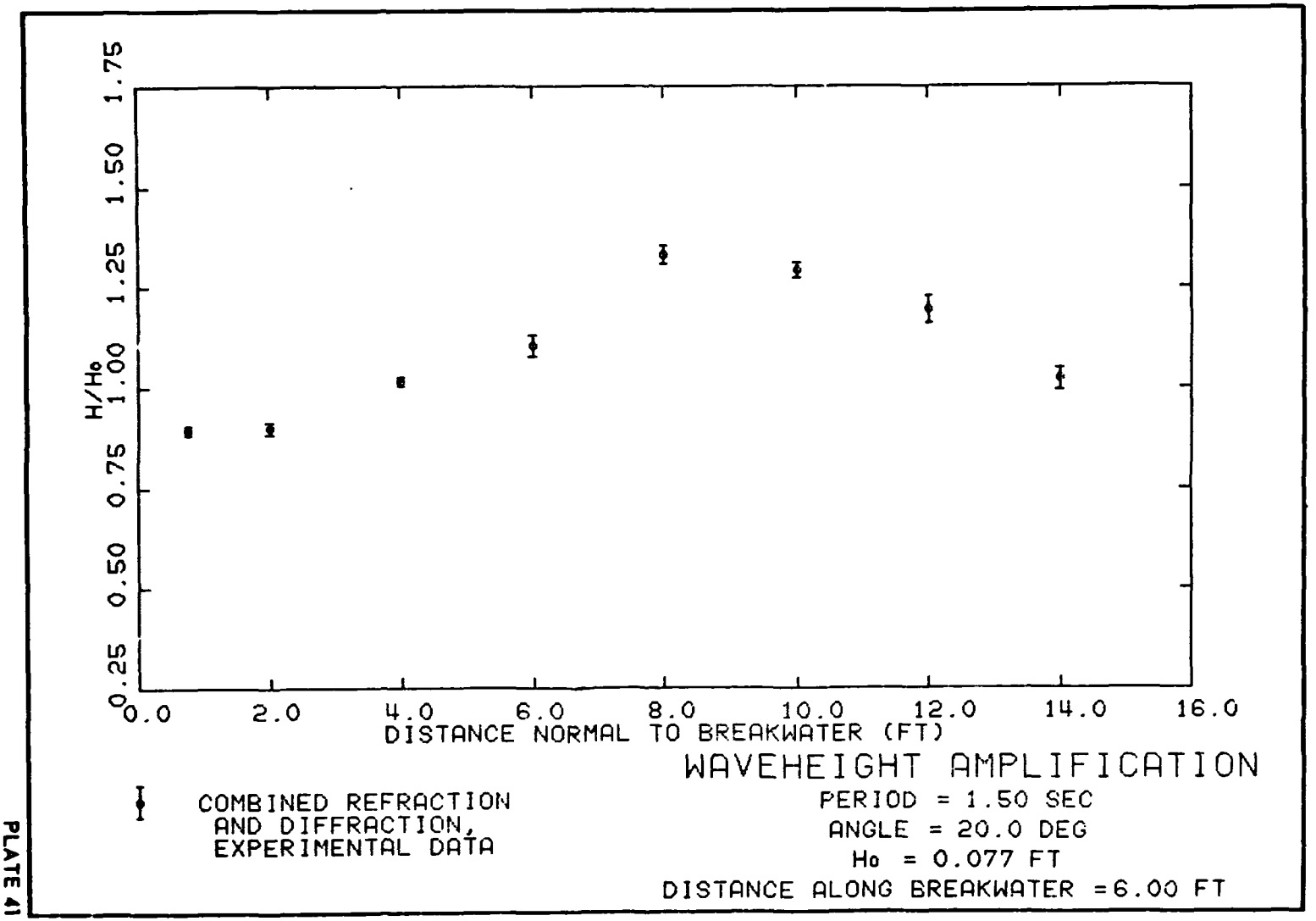
H/Ho
0.25
0.50
0.75
1.00
1.25
1.50
1.75
0.0
2.0
4.0
6.0
8.0
10.0
12.0
14.0
16.0
DISTANCE NORMAL TO BREAKWATER (FT)
WAVEHEIGHT AMPLIFICATION
PERIOD = 1.50 SEC
ANGLE = 20.0 DEG
Ho = 0.077 FT
DISTANCE ALONG BREAKWATER =6.00 FT
COMBINED REFRACTION
AND DIFFRACTION,
EXPERIMENTAL DATA

PLATE 41

PLATE 42

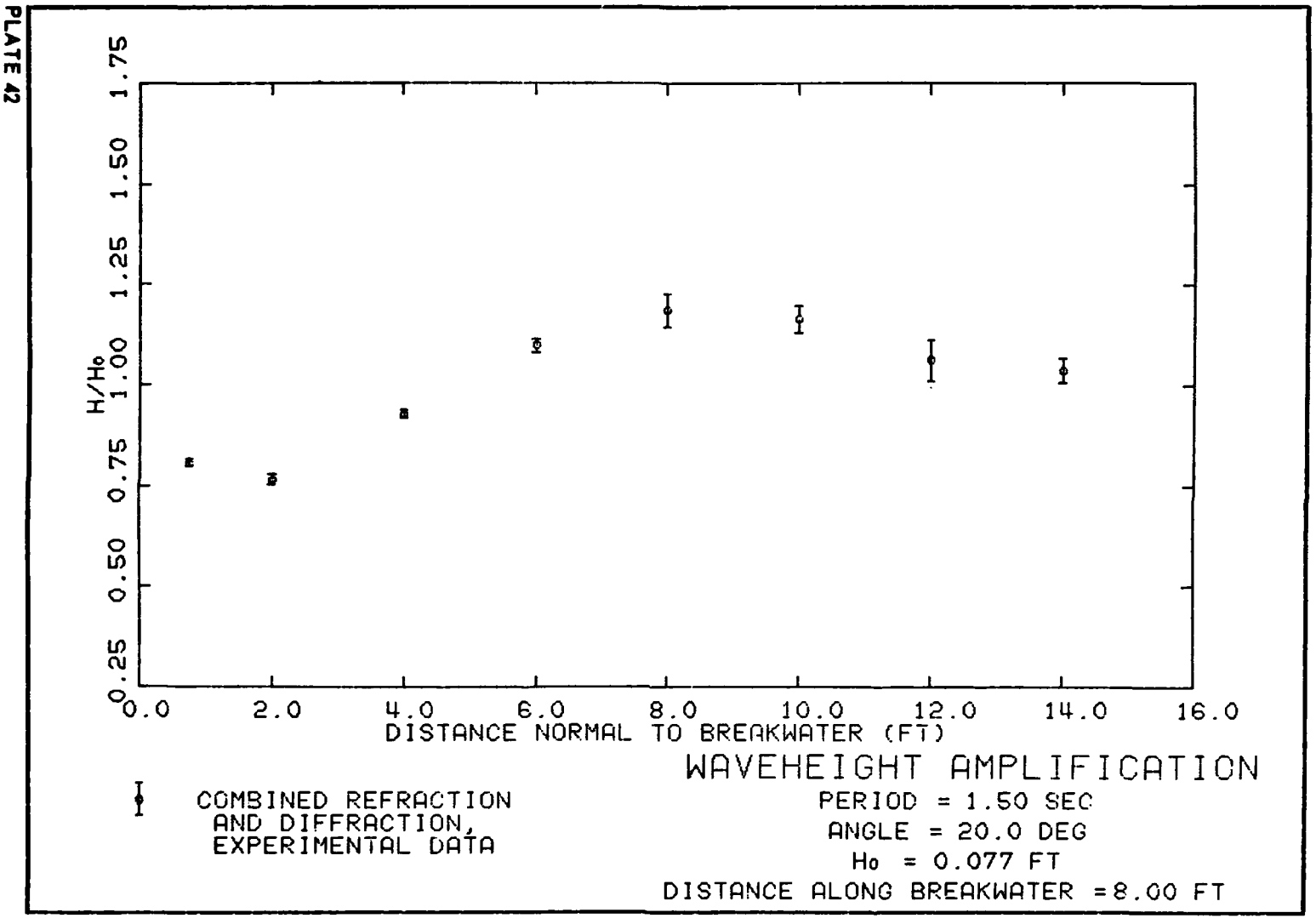
H/Ho
0.25
0.50
0.75
1.00
1.25
1.50
1.75
0.0
2.0
4.0
6.0
8.0
10.0
12.0
14.0
16.0
DISTANCE NORMAL TO BREAKWATER (FT)
COMBINED REFRACTION
AND DIFFRACTION,
EXPERIMENTAL DATA
WAVEHEIGHT AMPLIFICATION
PERIOD = 1.50 SEC
ANGLE = 20.0 DEG
Ho = 0.077 FT
DISTANCE ALONG BREAKWATER =8.00 FT

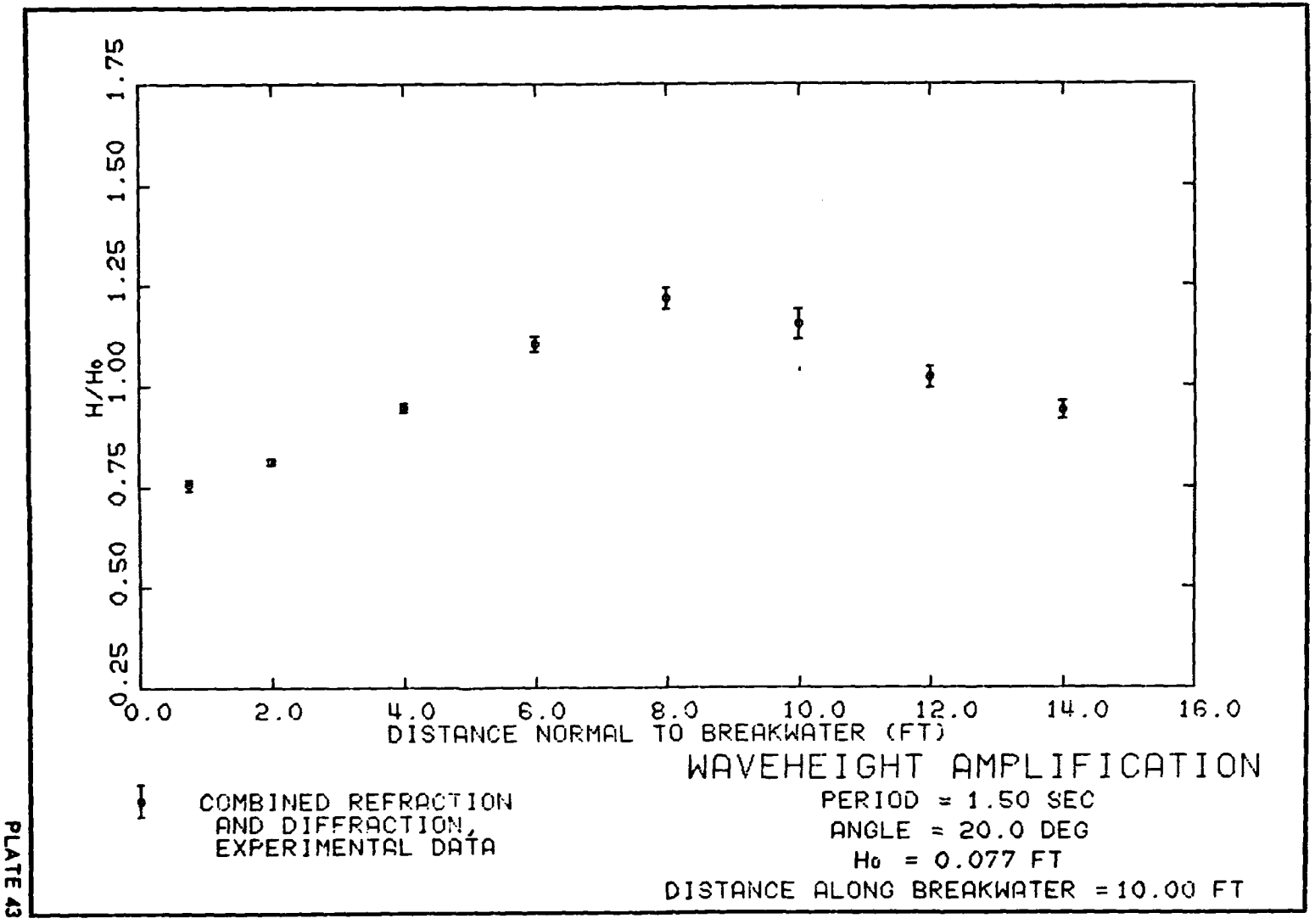
H/Ho
0.25
0.50
0.75
1.00
1.25
1.50
1.75
0.0
2.0
4.0
6.0
8.0
10.0
12.0
14.0
16.0
DISTANCE NORMAL TO BREAKWATER (FT)
WAVEHEIGHT AMPLIFICATION
PERIOD = 1.50 SEC
ANGLE = 20.0 DEG
Ho = 0.077 FT
DISTANCE ALONG BREAKWATER = 10.00 FT
COMBINED REFRACTION
AND DIFFRACTION,
EXPERIMENTAL DATA

PLATE 43

PLATE 44

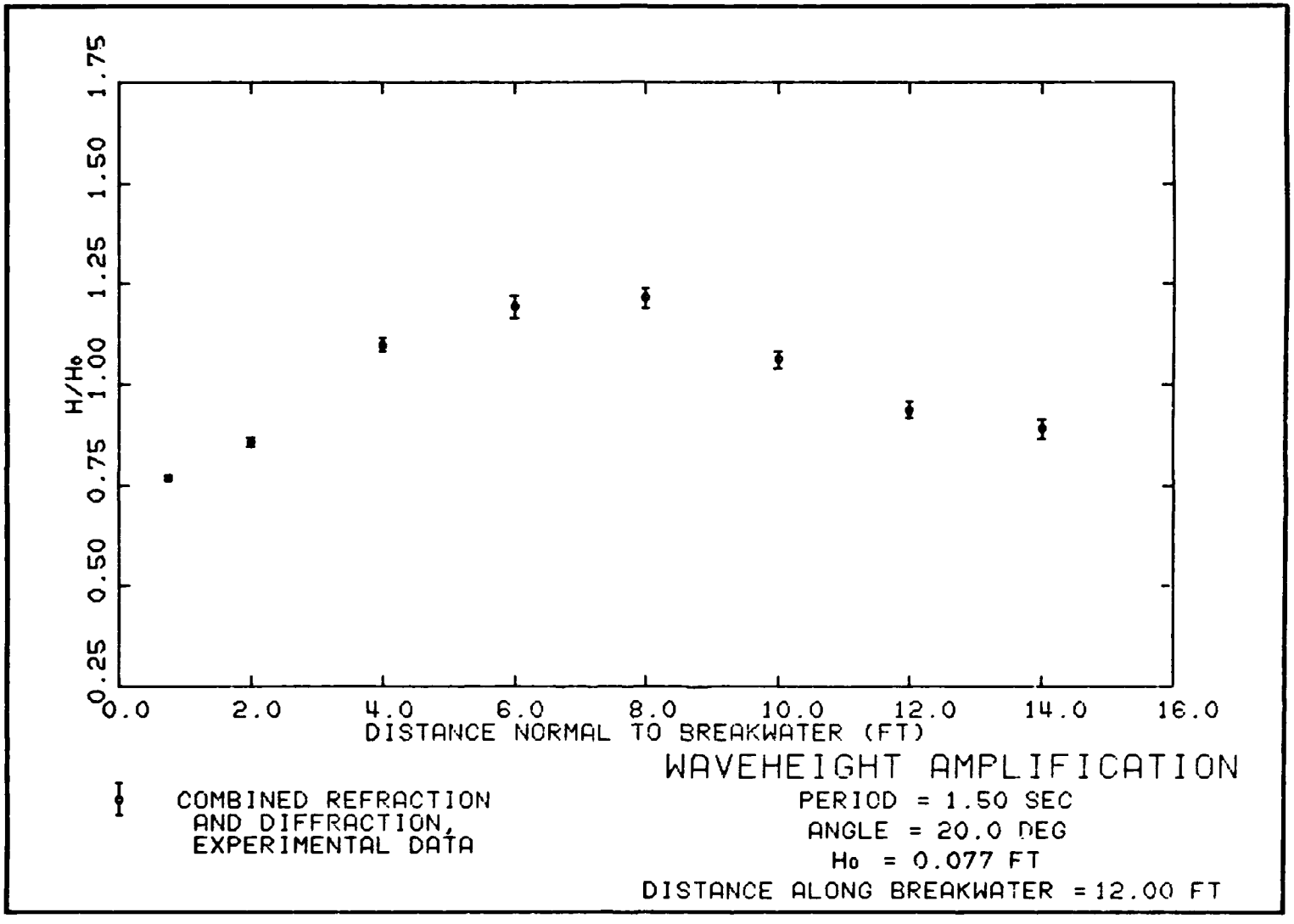
H/Ho
0.25
0.50
0.75
1.00
1.25
1.50
1.75
0.0
2.0
4.0
6.0
8.0
10.0
12.0
14.0
16.0
DISTANCE NORMAL TO BREAKWATER (FT)
WAVEHEIGHT AMPLIFICATION
PERIOD = 1.50 SEC
ANGLE = 20.0 DEG
Ho = 0.077 FT
DISTANCE ALONG BREAKWATER = 12.00 FT
COMBINED REFRACTION
AND DIFFRACTION,
EXPERIMENTAL DATA

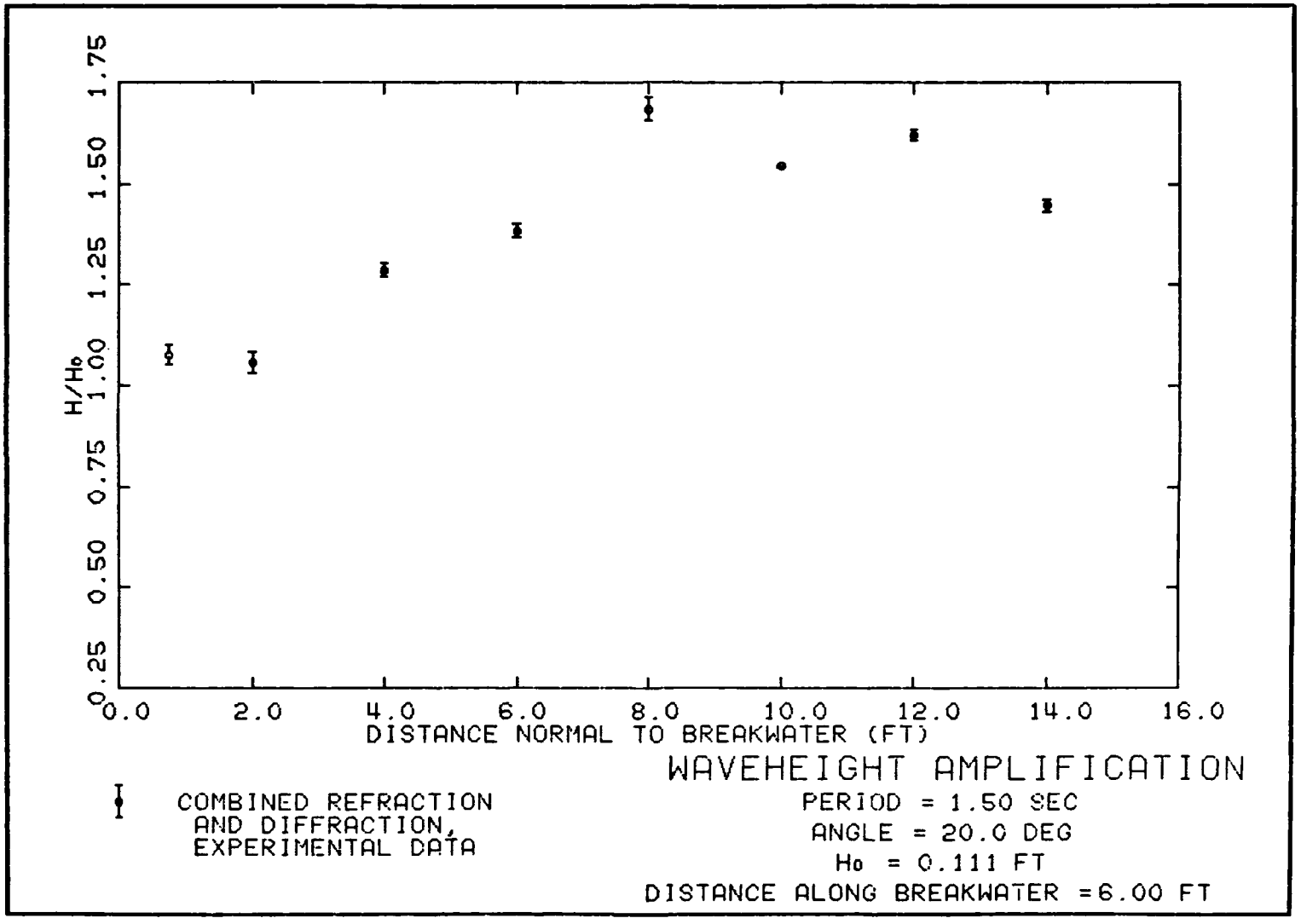
H/Ho
0.25
0.50
0.75
1.00
1.25
1.50
1.75
0.0
2.0
4.0
6.0
8.0
10.0
12.0
14.0
16.0
DISTANCE NORMAL TO BREAKWATER (FT)
WAVEHEIGHT AMPLIFICATION
COMBINED REFRACTION
AND DIFFRACTION,
EXPERIMENTAL DATA
PERIOD = 1.50 SEC
ANGLE = 20.0 DEG
Ho = 0.111 FT
DISTANCE ALONG BREAKWATER = 6.00 FT

PLATE 45

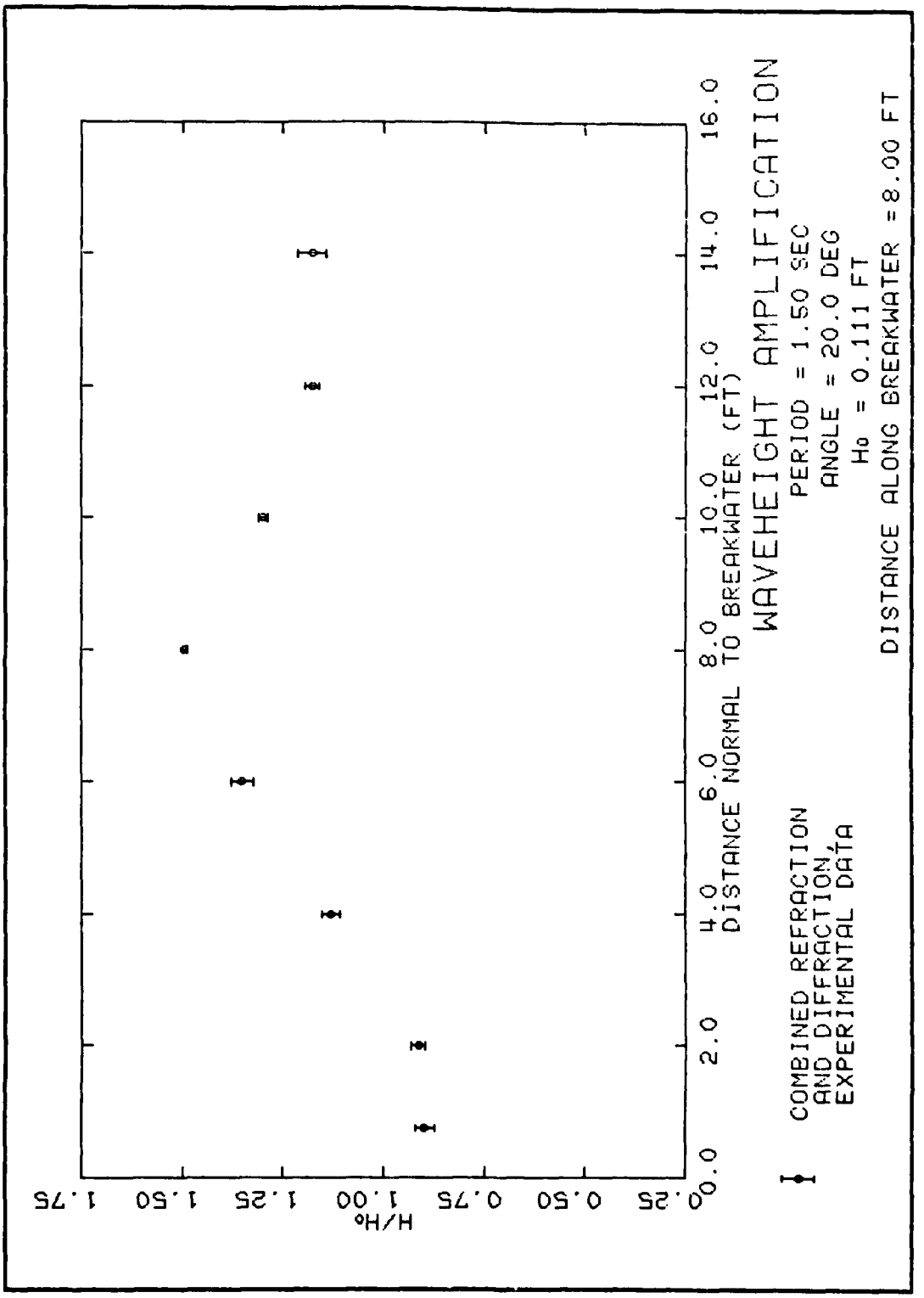
WAVEHEIGHT AMPLIFICATION
PERIOD = 1.50 SEC
ANGLE = 20.0 DEG
Ho = 0.111 FT
DISTANCE ALONG BREAKWATER = 8.00 FT
COMBINED REFRACTION AND DIFFRACTION, EXPERIMENTAL DATA
H/Ho
0.0
0.25
0.50
0.75
1.00
1.25
1.50
1.75
2.0
4.0
6.0
8.0
10.0
12.0
14.0
16.0
DISTANCE NORMAL TO BREAKWATER (FT)

PLATE 46

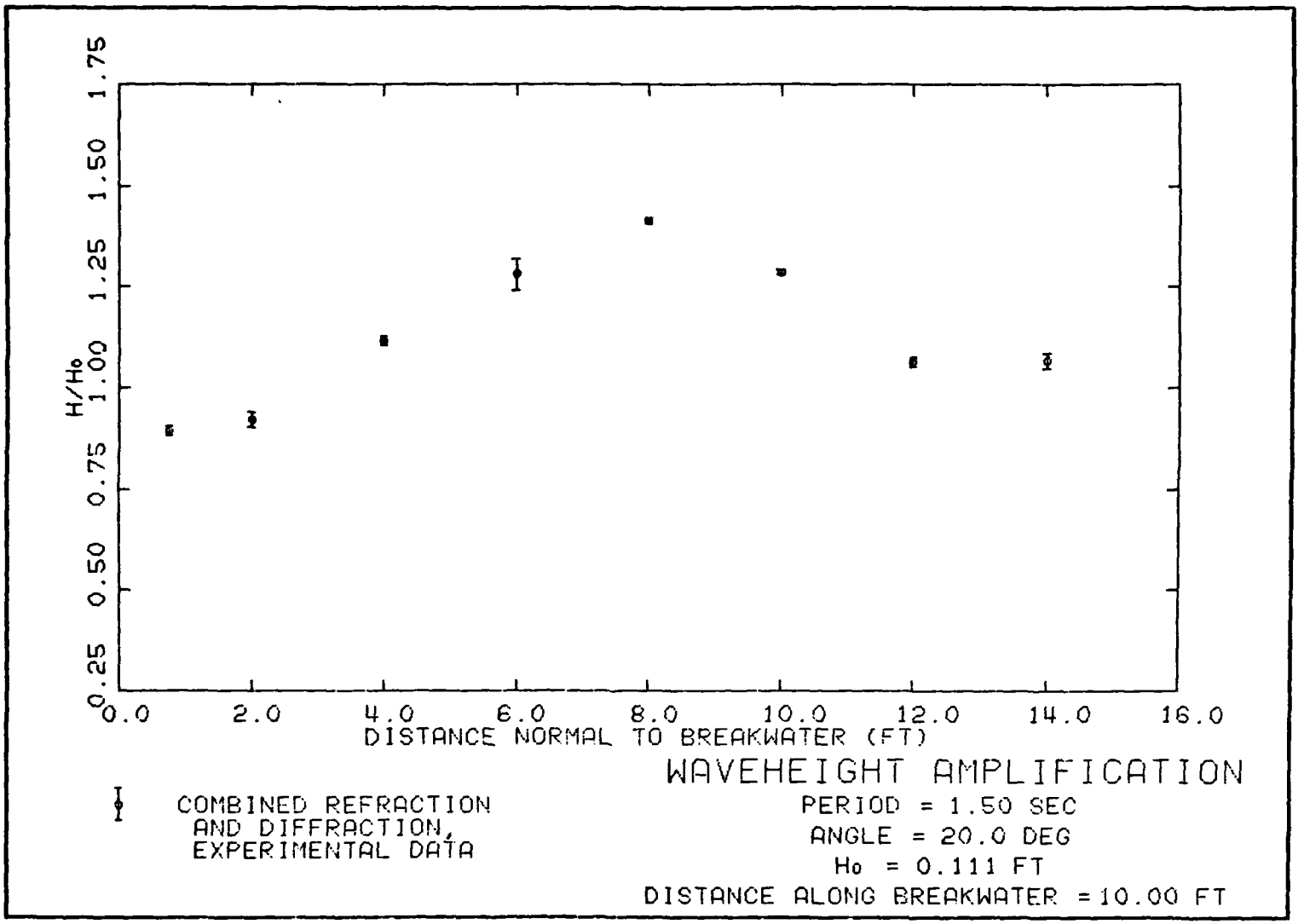
H/Ho
0.25
0.50
0.75
1.00
1.25
1.50
1.75
0.0
2.0
4.0
6.0
8.0
10.0
12.0
14.0
16.0
DISTANCE NORMAL TO BREAKWATER (FT)
COMBINED REFRACTION
AND DIFFRACTION,
EXPERIMENTAL DATA
WAVEHEIGHT AMPLIFICATION
PERIOD = 1.50 SEC
ANGLE = 20.0 DEG
Ho = 0.111 FT
DISTANCE ALONG BREAKWATER = 10.00 FT

PLATE 47

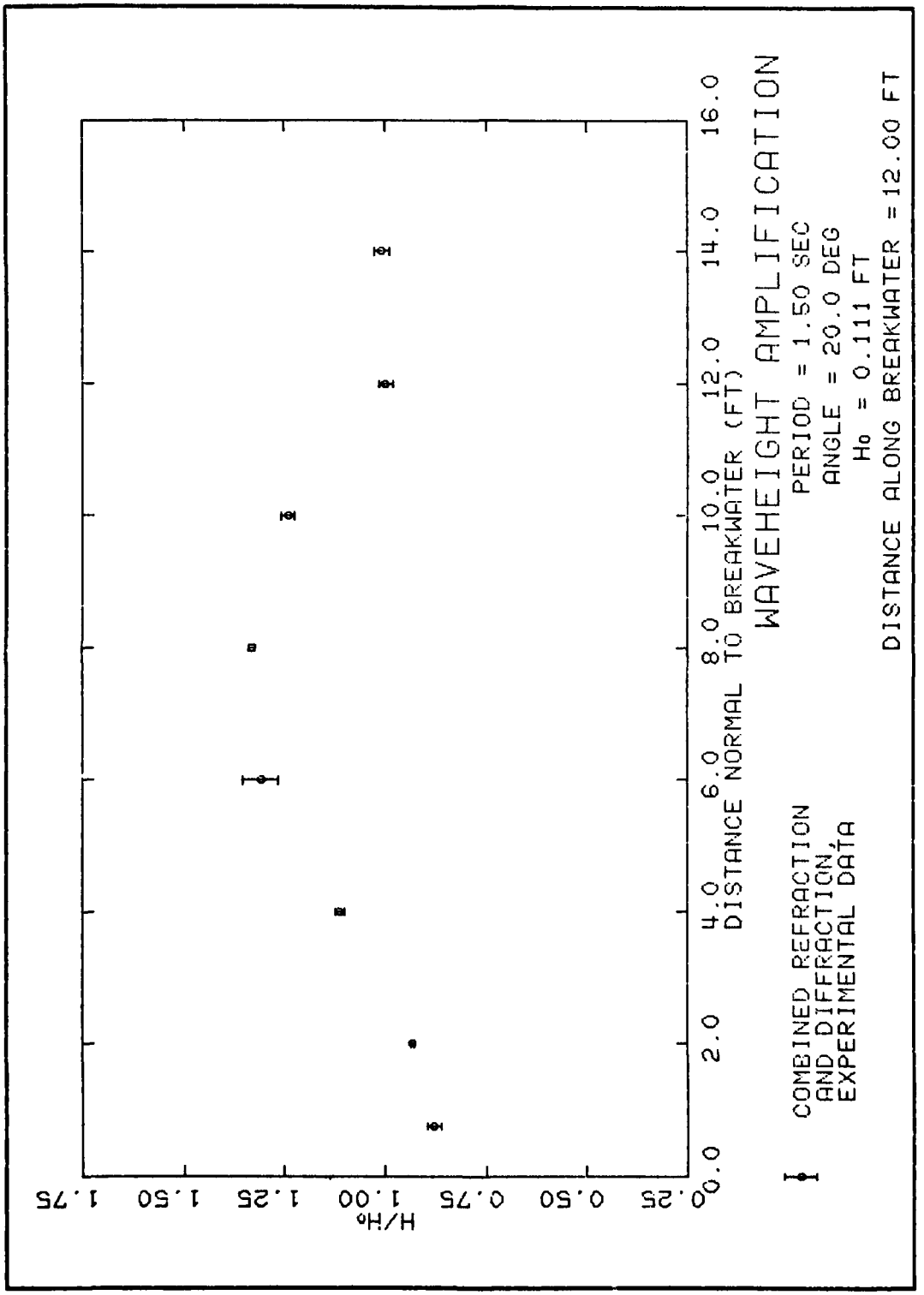
WAVEHEIGHT AMPLIFICATION
PERIOD = 1.50 SEC
ANGLE = 20.0 DEG
H_o = 0.111 FT
DISTANCE ALONG BREAKWATER = 12.00 FT
COMBINED REFRACTION AND DIFFRACTION EXPERIMENTAL DATA
H/H_o
0.0
0.25
0.50
0.75
1.00
1.25
1.50
1.75
2.0
4.0
6.0
8.0
10.0
12.0
14.0
16.0
DISTANCE NORMAL TO BREAKWATER (FT)

PLATE 48

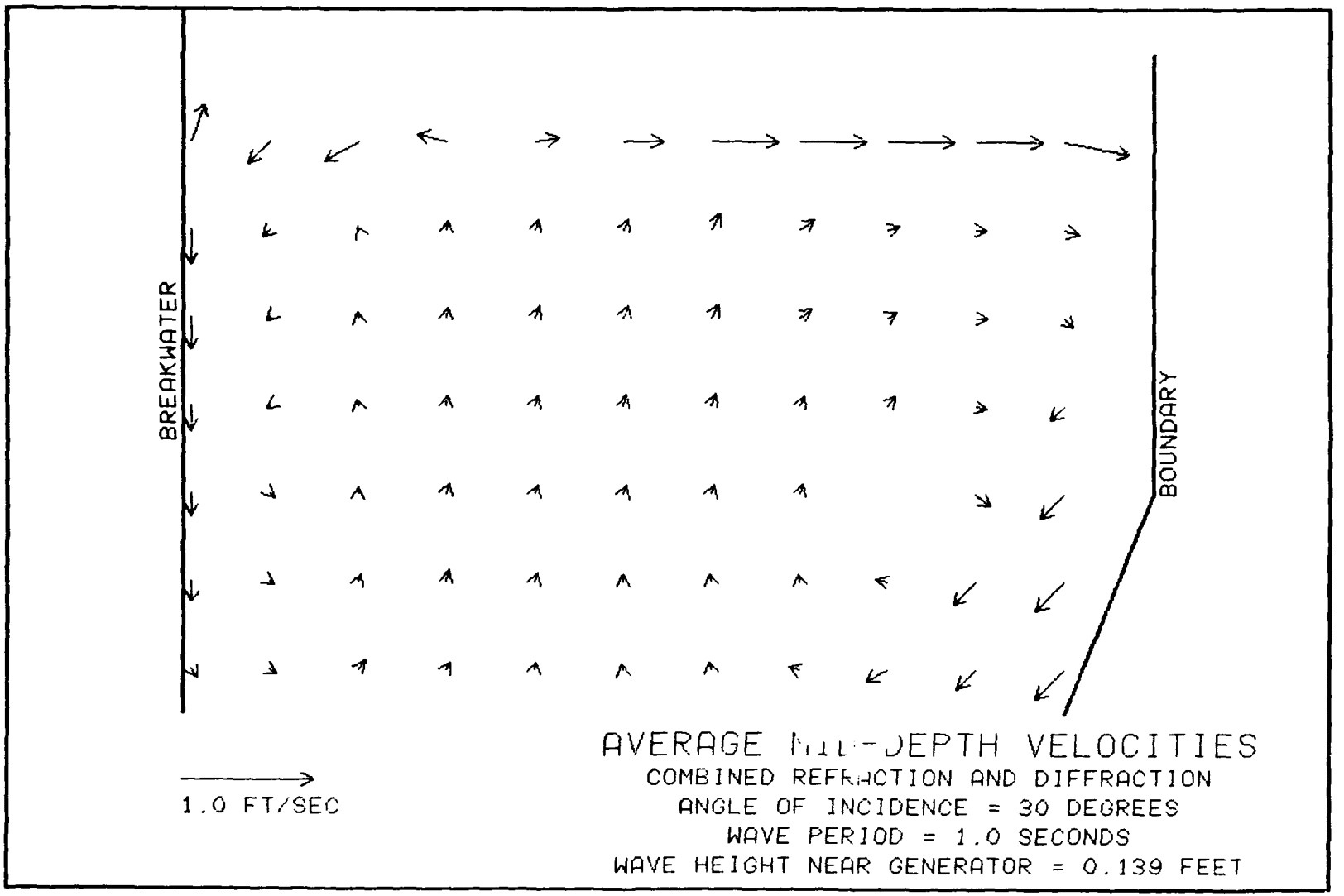

AVERAGE MID-DEPTH VELOCITIES
COMBINED REFRACTION AND DIFFRACTION
ANGLE OF INCIDENCE = 30 DEGREES
WAVE PERIOD = 1.0 SECONDS
WAVE HEIGHT NEAR GENERATOR = 0.139 FEET

PLATE 49

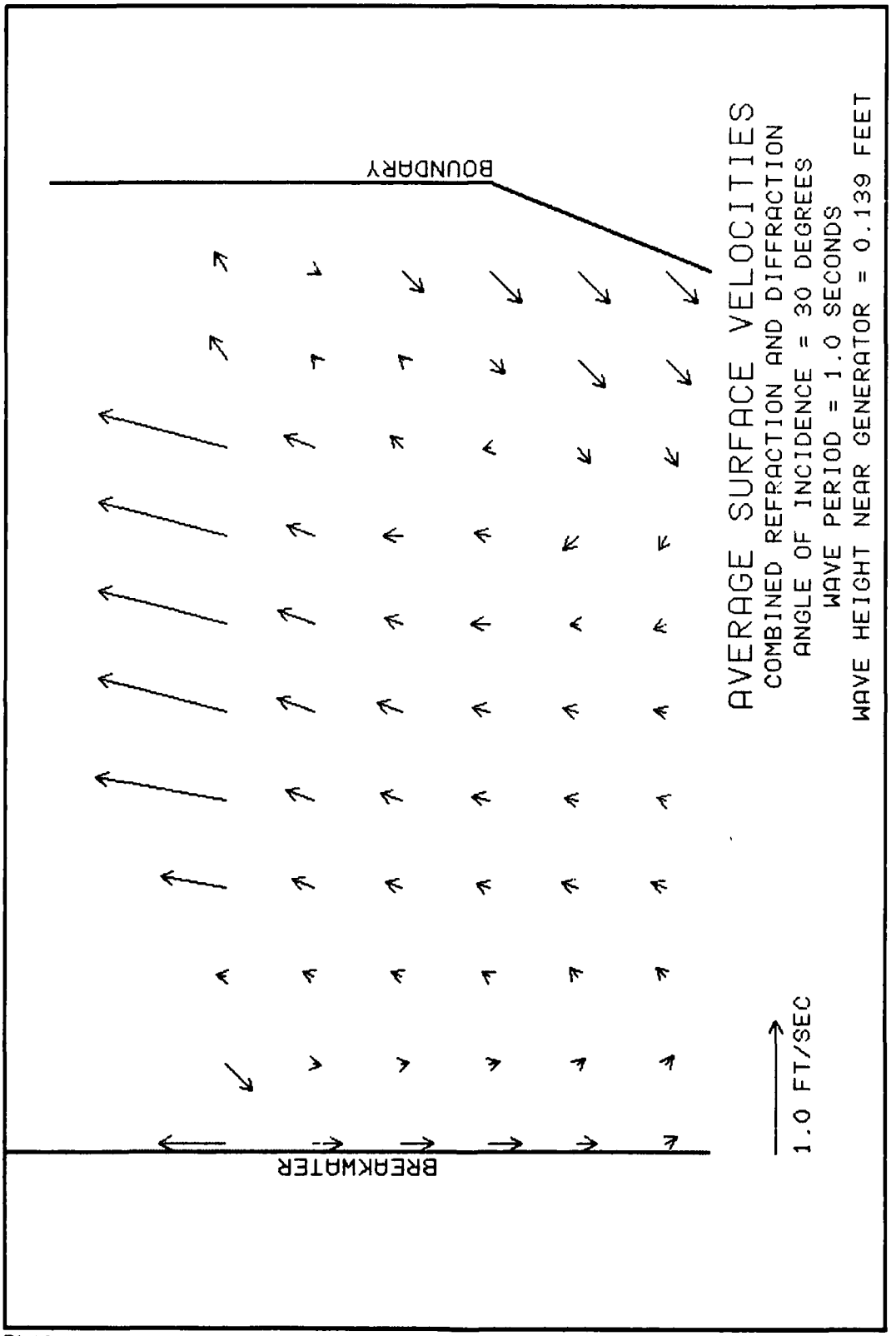
AVERAGE SURFACE VELOCITIES
COMBINED REFRACTION AND DIFFRACTION
ANGLE OF INCIDENCE = 30 DEGREES
WAVE PERIOD = 1.0 SECONDS
WAVE HEIGHT NEAR GENERATOR = 0.139 FEET
1.0 FT/SEC
BOUNDARY
BREAKWATER

PLATE 50

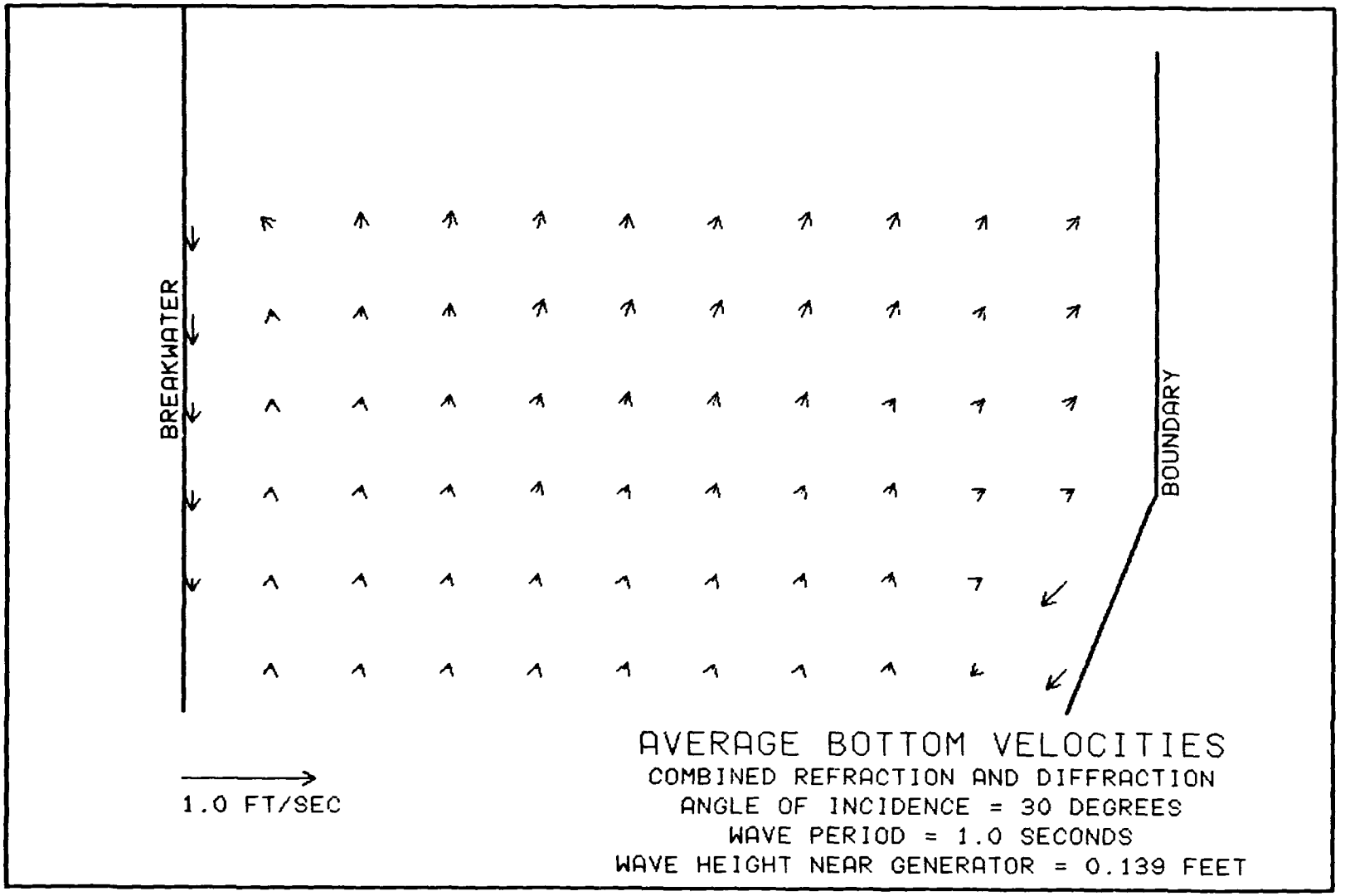

AVERAGE BOTTOM VELOCITIES
COMBINED REFRACTION AND DIFFRACTION
ANGLE OF INCIDENCE = 30 DEGREES
WAVE PERIOD = 1.0 SECONDS
WAVE HEIGHT NEAR GENERATOR = 0.139 FEET

PLATE 51

APPENDIX A: NOTATION

a	Wave amplitude, ft
a_{xx}	Second derivative of wave amplitude in x-direction, 1/ft
a_{yy}	Second derivative of wave amplitude in y-direction, 1/ft
b_1, b_2	Wave ray spacing, ft
c	Wave speed of propagation, ft/sec
c_g	Wave group velocity, ft/sec
C	Friction coefficient, dimensionless
d	Local water depth, ft
d_b	Water depth at breaking, ft
D	Local rate of energy dissipation, lb/ft/sec
e	Base of system of natural logarithms, 2.71828, dimensionless
E_b	Wave energy density at breaking, ft-lb/ft^2
E_o	Wave energy density in deep water, ft-lb/ft^2
F	Mathematical function for wave equation in cylindrical coordinates, dimensionless
F_w	Wave thrust, lb/ft
g	Gravitational constant, ft/sec^2
H	Local wave height, ft
H_b	Wave height at breaking, ft
H_o	Incident wave height, ft
i	$(-1)^{1/2}$, dimensionless
k	Wave number, $2\pi/L$, 1/ft
K_d	Diffraction coefficient, dimensionless
K_r	Refraction coefficient, dimensionless
K_{r-d}	Combined refraction and diffraction coefficient, dimensionless
L	Wavelength, ft
n	Ratio of group velocity to wave velocity, dimensionless
N	Longshore current parameter, dimensionless
P	Rate of wave power transmission, lb/sec
P_{L-H}	Longshore current parameter from Longuet-Higgins, dimensionless
r	Radius in cylindrical coordinates, ft
S	Bottom beach slope, dimensionless

T	Wave period, sec
u	Instantaneous particle velocity
$\vec{u}$	Two-dimensional vector
u_m	Parameter combining breaker wave energy density and local water depth, ft/sec
u_{max}	Maximum wave orbital velocity, ft/sec
u_1, u_2	Diffraction integration limits, dimensionless
V_{ls}	Longshore current velocity, ft/sec
x	Distance offshore, ft
α	Local wave angle with shoreline or breakwater, deg
α_b	Breaker angle of waves with shoreline, deg
α_o	Deepwater wave approach angle, deg
β	Angle between wave ray and breakwater, deg
δ	Defined parameter, $(a_{xx} + a_{yy})/k^2a$, dimensionless
Δb	Wave ray spacing, ft
η	Local water-surface elevation, ft; complex wave amplitude
θ	Direction in cylindrical coordinates, deg
θ_o	Angle between breakwater and undiffracted wave crests beyond breakwater, deg
μ_e	Horizontal eddy viscosity coefficient, lb-sec/ft^2
ρ	Fluid density, lb-sec^2/ft^4
τ	Local shear stress, lb/ft^2
τ_{ls}	Local mean longshore shear stress, lb/ft^2
ϕ	Velocity potential, ft^2/sec
ω	Wave angular frequency, $2\pi/T$, 1/sec
∂	Partial derivative symbol, dimensionless
∇	Horizontal gradient operator, dimensionless

In accordance with letter from DAEN-RDC, DAEN-ASI dated 22 July 1977, Subject: Facsimile Catalog Cards for Laboratory Technical Publications, a facsimile catalog card in Library of Congress MARC format is reproduced below.

Hales, Lyndell Z
Erosion control of scour during construction; Report 3: Experimental measurements of refraction, diffraction, and current patterns near jetties / by Lyndell Z. Hales. Vicksburg, Miss. : U. S. Waterways Experiment Station ; Springfield, Va. : available from National Technical Information Service, 1980.
61, [38] p., [26] leaves of plates : ill. ; 27 cm. (Technical report - U. S. Army Engineer Waterways Experiment Station ; HL-80-3, Report 3)
Prepared for Office, Chief of Engineers, U. S. Army, Washington, D. C.
References: p. 59-61.

1. Construction practices. 2. Erosion control. 3. Harbor structures. 4. Scour. I. United States. Army. Corps of Engineers. II. Series: United States. Waterways Experiment Station, Vicksburg, Miss. Technical report ; HL-80-3, Report 3.
TA7.W34 no.HL-80-3, Report 3